POLITECNICO DI MILANO

Facoltà di Ingegneria dei Processi Industriali
Dipartimento di Chimica, Materiali e Ingegneria Chimica
"Giulio Natta"
Master of Science in Materials Engineering and Nanotechnology

PHOTOVOLTAIC EFFICIENCY AND LONG TERM ENVIRONMENTAL STABILITY OF POLYMER-BASED LUMINESCENT SOLAR CONCENTRATOR DEVICES

Advisor: Prof. Stefano TURRI
Co-advisor: Dott. Gianmarco GRIFFINI

Roberto REGUZZONI
ID 763295

Academic Year 2011-2012

"Il palazzo è un simbolo, come lo è l'atto di distruggerlo. Sono gli uomini che conferiscono potere ai simboli. Da solo un simbolo è privo di significato, ma con un bel numero di persone alle spalle, far saltare un palazzo può cambiare il mondo."
[Cit. V in V per Vendetta]

Table of contents

List of figures

List of tables

Abstract

Thin-film luminescent solar concentrator (LSC) devices were investigated in this thesis. In the first part of this work, an optimization of the photovoltaic (PV) performance of state-of-the-art PMMA-based LSC devices was carried out by studying the effect of organic dye (Lumogen F Red 305, LFR305) concentration, matrix (PMMA) thickness and waveguide aspect ratio on the PV behavior of the LSC. In addition, the effect of the use of white TiO_2-based back reflectors (BR) on LSC PV performance was studied, by varying TiO_2 concentrations and thickness of the BR film. All the fabricated LSC's were also characterized by UV-Vis absorption spectroscopy, fluorescence emission spectroscopy, EQE and gloss measurements.
In the second part of this thesis, alternative crosslinked matrices based on fluoro-polymers were proposed in order to investigate the possibility to fabricate efficient and environmentally stable LSC devices to outperform state-of-the-art PMMA-based LSC devices. Two different polyurethane-based and one melamine-based matrices were studied. The optimization of dye concentration and matrix thickness was carried out on all these new systems, together with UV-Vis absorption spectroscopy, fluorescence emission spectroscopy and EQE tests to characterize the performance of the synthesized matrices.
Finally, all the LSC devices were subjected to UV-A aging tests to highlight the differences in the behavior of the newly synthesized matrices when irradiated with highly energetic photons. In addition, all optimized LSC devices were subjected to weathering tests for up to 1000 hours of continuous light exposure, to highlight the effect of the host matrix system on LSC degradation. Moreover, the effect of long term stabilizers (NOR HALS) was also investigated.
It was found that polyurethane-based crosslinked systems outperformed standard PMMA-based LSC devices in terms of long-term lifetime. Being their efficiency comparable to state-of-the-art PMMA-based LSC's, the new systems proposed in this work may be employed as alternative host matrices to fabricate LSC devices with long-term environmental stability and high PV efficiency.

ESTRATTO IN LINGUA ITALIANA

Efficienza fotovoltaica e stabilità ambientale a lungo termine di concentratori solari luminescenti a base polimerica

Introduzione

Soddisfare la crescente domanda di energia e la riduzione di emissioni nocive conseguenti all'uso dei combustibili fossili rappresentano le sfide energetiche del XXI secolo. Ciò ha creato molto interesse e aspettative nel campo delle energie rinnovabili. Il Sole è una fonte di energia rinnovabile praticamente infinita la cui luce viene convertita in corrente elettrica tramite un dispositivo che sfrutta l'effetto fotovoltaico. Le attuali tecnologie fotovoltaiche sono per lo più basate sul Silicio che implica, tuttavia, elevati costi di produzione e efficienze di foto conversione limitate. I concentratori solari luminescenti (LSC) rappresentano un importante strumento per ridurre i costi legati alla tecnologia fotovoltaica e contestualmente aumentarne le efficienze. In questo lavoro sono stati investigati i concentratori solari luminescenti a film sottile a base organica (OLSC). Essi consistono in un substrato trasparente sopra cui viene deposta una matrice polimerica in cui è contenuto un colorante organico fluorescente. I fotoni incidenti sulla superficie del substrato luminescente vengono assorbiti dalle molecole di colorante organico e riemessi secondo il processo di fluorescenza. I fotoni riemessi viaggiano per riflessione interna totale (TIR) verso il lato del substrato trasparente, dove trova posto una cella fotovoltaica il cui strato attivo è posto contro il substrato. In questo modo il numero di fotoni che arrivano alla cella fotovoltaica sono molto maggiori rispetto al caso in cui la cella sia direttamente esposta alla radiazione incidente. Nell'ambito della ricerca vengono perseguiti due obiettivi: l'ottimizzazione degli attuali dispositivi a film sottile per ottenere efficienze sempre maggiori e l'incremento della stabilità dei dispositivi. In questo lavoro sono stati investigati entrambi gli aspetti. Dapprima è stato ottimizzato un dispositivo con matrice polimerica in poli(metilmetacrilato) (PMMA) che nell'ambito delle matrici rappresenta lo stato dell'arte di questa tecnologia. L'ottimizzazione è stata volta a diversi aspetti, tra cui la determinazione della concentrazione ottimale di colorante organico (Lumogen F Red 305), l'ottimizzazione dello spessore del film luminescente, l'ottimizzazione del rapporto lunghezza/larghezza del substrato (L/W) e l'effetto sulla performance fotovoltaica del concentratore, a seguito dell'uso di Back Reflectors (BR). Per quanto concerne la stabilità dei dispositivi, sono state

sintetizzate matrici alternative basate su fluoro-polimeri ed è stato effettuato uno studio circa l'ottimizzazione di tali matrici in termini di concentrazione di colorante organico e spessore del film luminescente. Infine, tramite test di invecchiamento accelerati è stato possibile investigare la stabilità dei dispositivi basati sulle matrici sintetizzate rispetto ai dispositivi basati sul PMMA.

Parte sperimentale

Per caratterizzare le matrici a di base poliuretano, è stato effettuato il monitoraggio di opportuni picchi IR per diversi tempi di reticolazione. Inoltre per tutte le matrici sono state effettuate prove DSC per verificare che le molecole di colorante fossero ben disciolte e per verificare le temperature di transizione vetrosa. I parametri fotovoltaici di ciascun dispositivo sono stati ottenuti tramite un apparato di test costituito da un simulatore solare ed un multimetro (figura I).

Figura I Simulatore solare (destra) e multimetro digitale (sinistra).

Sono state utilizzate diverse tecniche di caratterizzazione per indagare le ragioni degli andamenti delle performance fotovoltaiche dei dispositivi. Tra queste, la spettroscopia di assorbimento UV-Visibile, la spettroscopia di emissione di fluorescenza e la misura dell'efficienza quantica esterna (EQE) del dispositivo. È stato inoltre utilizzato un profilometro ottico per misurare gli spessori delle matrici proposte. Gli studi degradativi sono stati invece condotti mettendo i dispositivi ottimizzati in weather-o-metro, lasciandoli esposti per circa 1000 ore a una radiazione costante di 1000 W/m^2. Ulteriori test degradativi sui dispositivi LSC ottimizzati sono stati condotti illuminandoli con lampade UV-A e UV-C.

Risultati e discussione

Ottimizzazione di dispositivi LSC a base PMMA

Il dispositivo a base PMMA ha evidenziato un massimo incremento dell'efficienza della cella fotovoltaica (ΔPCE = 33 %) per una concentrazione di colorante pari al 5 % in peso sul peso del PMMA (figura II).

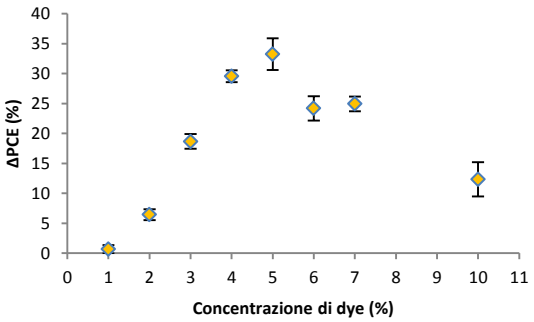

Figura II ΔPCE in funzione della concentrazione di colorante per un dispositivo a base PMMA.

Lo spessore ottimale della matrice è stato individuato in 9 µm poiché per tale spessore si ottiene la massima ΔPCE.
Test spettroscopici confermano che il campione con una concentrazione di colorante pari al 5 % emette maggiormente degli altri campioni a diversa concentrazione, nonostante assorba meno intensamente la luce UV-Visibile.
Il rapporto ottimale L/W della guida d'onda è stato identificato in 0.5. Infatti per questo rapporto il concentratore

solare raggiunge la sua massima efficienza assoluta, $PCE^{LSC.}$. Questo dato è confermato dalla curva EQE per diversi rapporti L/W, che mostra come la EQE del campione a minor rapporto L/W produca percentualmente un maggior numero di cariche elettriche in relazione al numero di fotoni incidenti sulla superficie del dispositivo LSC.

È stato dimostrato che l'uso di BR bianchi a base di TiO_2 ha un effetto positivo sulla prestazione del concentratore solare luminescente. Questo perché il BR riflette la luce trasmessa dal concentratore verso la guida d'onda. All'aumentare dello spessore del BR la prestazione del concentratore aumenta, per via della minor probabilità che ha un fotone di essere trasmesso attraverso il BR. Inoltre all'aumentare della quantità di TiO_2, la performance dell'LSC aumenta. Ciò accade perché una maggior concentrazione di titania causa una diffusione più efficace della luce incidente sulla superficie del BR per via della maggior rugosità superficiale. Questo effetto si traduce in una riduzione del Gloss (capacità di riflessione speculare) della superficie del BR all'aumentare del contenuto di pigmento, TiO_2, come si può evincere da figura III.

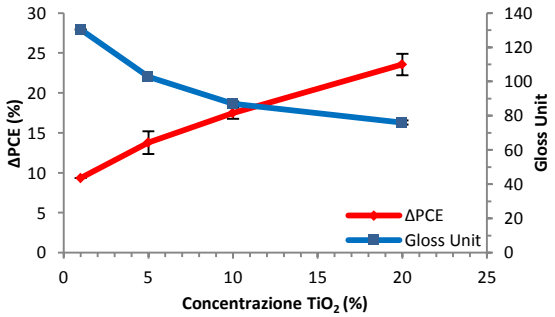

Figura III ΔPCE e G.U. in funzione della concentrazione di TiO_2 per un dato spessore di legante del BR.

Ottimizzazione di dispositivi LSC a base fluoro-polimeri

Sono state studiate diverse matrici con fluoro polimeri per la loro intrinseca stabilità. Un primo tipo di matrice fluorurata reticolata basata sul legame uretanico è quella formata da Lumiflon LF-910 LM e Tolonate HDT-LV2. Il primo è un fluoro-etilen vinil etere (FEVE) prodotto da Asahi Glass Co.LDT mentre il secondo un polisocianato alifatico prodotto da Perstop. I due reagenti danno origine alla matrice per i dispositivi LSC a base LT. La reticolazione tra questi due reagenti è stata verificata tramite il monitoraggio dei picchi IR. In particolare è stata monitorata la scomparsa del picco relativo allo stretching del gruppo isocianurato (-N=C=O con picco di assorbimento IR per 2260 cm^{-1}) che si trova nel Tolonate HDT-LV2. In figura IV sono riportati i picchi del gruppo isocianurato per diversi tempi di reticolazione a 150° C.

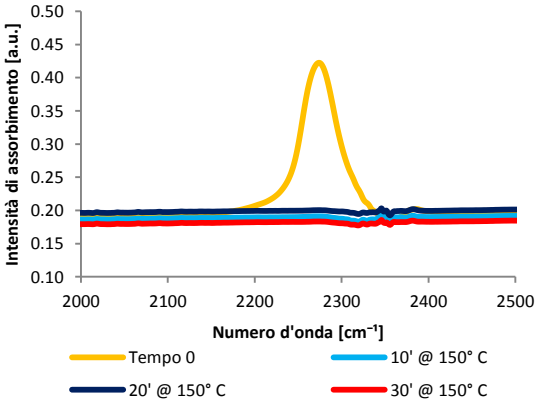

Figura IV Picco IR del gruppo isocianurato per diversi tempi di reticolazione a 150° C.

La temperatura di transizione vetrosa T_g per questa matrice è di circa 40 °C ed stata evidenziata tramite una prova DSC (figura V).

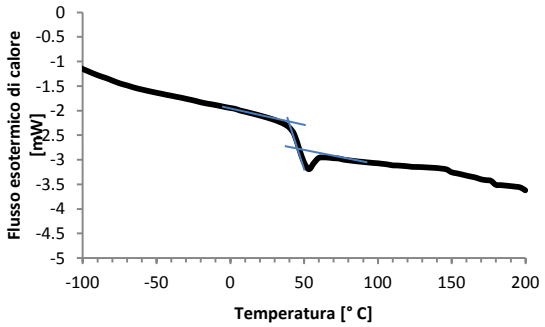

Figura V Curva DSC per la matrice LT reticolata.

Questa matrice ha evidenziato un massimo nella prestazione fotovoltaica su un dispositivo LSC per una concentrazione di colorante organico pari al 4 % in peso rispetto a quello della matrice, e per uno spessore del film luminescente pari a 5 µm.

Una seconda matrice poliuretanica reticolata a partire da Lumiflon LF910 LM e Vestanat T1890/100 è stata studiata (dispositivi LSC a base LV). Il vestanat T1890/100 è un poliisocianato alifatico prodotto da Evonik Industries. La matrice utilizzata ha evidenziato una T_g di 83 °C e massimi nella prestazione fotovoltaica per concentrazioni di colorante del 4 % e spessori della matrice di 6 µm. La spettroscopia di assorbimento UV-Vis ha evidenziato come la matrice non dopata sia trasparente alla luce visibile come si può evincere da figura VI, in accordo con i requisiti fondamentali per una matrice per applicazioni LSC.

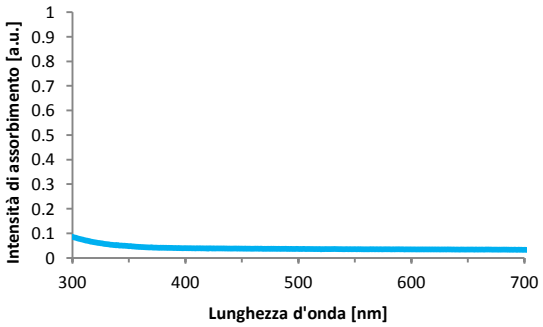

Figura VI Spettro di assorbimento UV-Visibile della matrice LV non dopata.

La caratterizzazione dei dispositivi LSC per diversi spessori della matrice è stata realizzata anche attraverso spettroscopia di emissione di fluorescenza. In figura VII sono riportati gli spettri di emissione per diversi spessori del film LV.

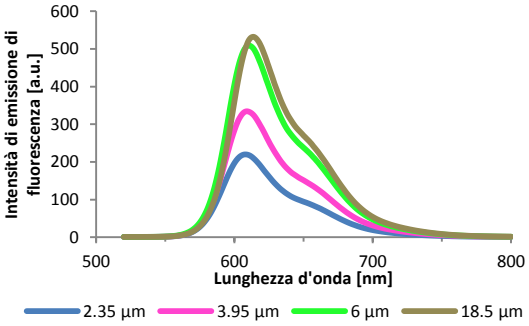

Figure VII Spettri di emissione per diversi spessori del film luminescente LV.

Una terza tipologia di matrice reticolata basata sul legame etere è quella formata a partire da Lumiflon LF-910 LM e Cymel 303 (LSC a base LC). Il Cymel 303 è prodotto da Cytec e la sua struttura chimica è basata su quella della dell'esametossimetilmelamina. Questa matrice è caratterizzata da una T_g di circa 60 °C. I dispositivi LSC a base LC hanno evidenziato il massimo incremento dell'efficienza fotovoltaica della cella per una concentrazione di colorante pari al 4 % e uno spessore della matrice luminescente di 5 µm. La caratterizzazione dei dispositivi per diversi spessori del film luminescente è stata fatta anche attraverso la misura della efficienza quantica esterna EQE (figura VIII).

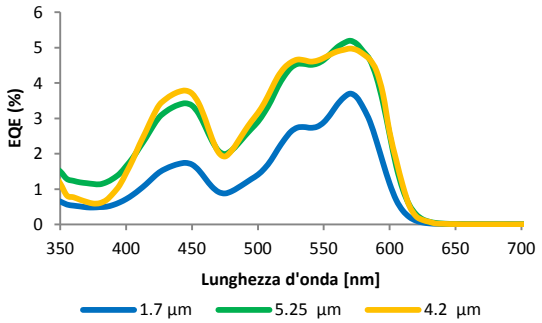

Figura VII Spettri EQE per diversi spessori del film luminescente LC.

Studio della stabilità dei dispositivi ottimizzati per tempi lunghi

Il dispositivo LSC ottimizzato a base PMMA è stato sottoposto a invecchiamento sotto lampada UV-C per un tempo di 5 ore. I parametri fotovoltaici sono stati registrati ogni 30' di esposizione. Il dispositivo ha mostrato un brusco calo nelle prestazioni fotovoltaiche nella prima ora di esposizione, probabilmente per via dell'elevata energia della radiazione incidente che ha effetto sul colorante e sulla matrice polimerica. In figura IX è riportato l'andamento di ΔPCE in funzione del tempo di invecchiamento.

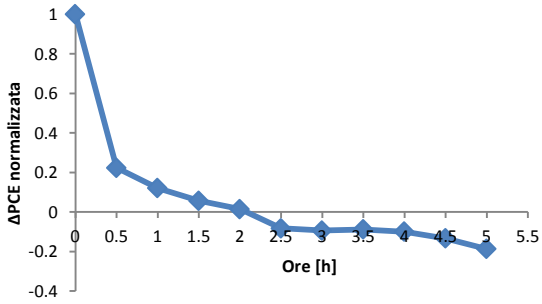

Figura IX ΔPCE in funzione del tempo di esposizione a UV-C per dispositivi a base di PMMA.

Per confrontare la resistenza a degradazione delle matrici sintetizzate rispetto al PMMA, è stato svolto un test di invecchiamento sotto UV-A per tutti i dispositivi ottimizzati. È stato evidenziato che i dispositivi a base PMMA e LC subiscono un calo di prestazione fotovoltaica all'aumentare del tempo di esposizione. I dispositivi a base poliuretanica, LT e LV, evidenziano invece un incremento della prestazione fotovoltaica con l'esposizione a UV-A nei primi momenti dell'irraggiamento seguiti da una sostanziale stabilità della performance, motivo per cui non mostrano sensibili diminuzioni di ΔPCE. Il comportamento di questo tipo di matrici è attualmente sotto investigazione. Test di emissione di fluorescenza evidenziano come l'intensità di emissione di fluorescenza per LT e LV aumenti dopo 30' di esposizione a UV-A, cosa che non si verifica per LC e PMMA. Figura X mostra l'andamento della ΔPCE in funzione del tempo di esposizione per i sistemi citati.

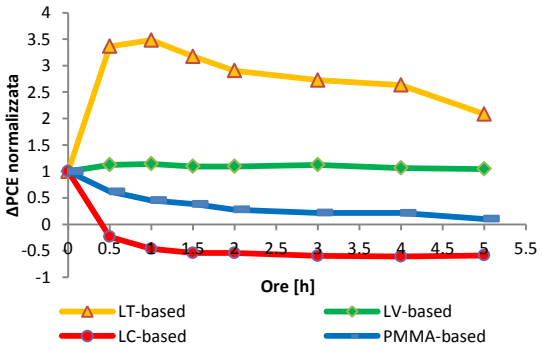

Figura X ΔPCE normalizzata in funzione del tempo di esposizione a UV-A.

Tutti i dispositivi ottimizzati sono stati messi in un weather-o-meter e testati per tempi crescenti di esposizione. Dopo 1000 ore di esposizione continuata, i dispositivi a base PMMA e LC mostrano sensibili diminuzioni della ΔPCE (- 79 %, - 79 % rispetto al valore iniziale rispettivamente) mentre LSC a base LT e LV una diminuzione del 36 % e 49 % rispettivamente, rispetto al valore di ΔPCE iniziale. Nessun dispositivo ha evidenziato una ΔPCE negativa al termine

dell'esposizione: ciò significa che tutti i dispositivi incrementano ancora la prestazione della cella. Tuttavia, i sistemi a base poliuretano sembrano mantenere le proprietà per più tempo. Infine è stato studiato l'effetto di additivi stabilizzati per esposizioni durature (NOR HALS). Gli additivi hanno rallentato la cinetica di degradazione sui dispositivi a base PMMA ma non su quelli a base LC. Per quanto riguarda i dispositivi a base poliuretano, LT e LV, l'effetto degli additivi non sembra essere del tutto chiaro per via dell'iniziale incremento di ΔPCE per esposizione a UV che sembra mascherare il reale andamento della ΔPCE in funzione del tempo.

Conclusioni

È stata effettuata l'ottimizzazione dei dispositivi a base PMMA mediante l'ottimizzazione della concentrazione di colorante (5 %) e dello spessore del film luminescente (9 μm). Anche il rapporto L/W della guida d'onda è stato ottimizzato; a tal proposito si è evidenziato che quello che offre l'efficienza assoluta PCE^{LSC} maggiore è il rapporto 0.5. L'uso di BR si è dimostrato benefico per la prestazione del concentratore. In particolare, un maggiore spessore del film riflettente e una maggiore concentrazione di pigmento bianco (TiO_2) al suo interno incrementano maggiormente la ΔPCE.

Sono inoltre state caratterizzate nuove matrici per applicazioni LSC: due reticolate a base poliuretanica e una reticolata a base etere, tutte contenenti fluoro-polimeri. I dispositivi con queste matrici mostrano performance fotovoltaiche confrontabili con quelle del PMMA. Tutte le matrici sono state ottimizzate in termini di concentrazione di colorante e spessore della matrice.

I sistemi a base poliuretano mostrano una resistenza a degradazione sensibilmente migliore rispetto a quelli a base etere e PMMA.

Foreword

The worldwide use of renewable resources is one of the possible approaches to solve the problems related to the steady increase in energy consumption and to the necessity of reducing the environmental impact of fossil-fuel based energy sources. Despite the multiple efforts in the development of renewable technologies, several limitations on these technologies still exist. Among the possible technologies based on renewable resources, photovoltaics (PV), the conversion of sunlight into electricity, seems to be one of the most promising approaches and significant efforts have been made in research to further develop the weak aspects of such technology. The PV technology is nowadays largely dominated by silicon-based devices which show, however, manufacturing high costs and relatively low power conversion efficiencies. One possible way to reduce the costs and to increase the efficiency of PV devices is the use of organic luminescent solar concentrators (OLSC). The basic idea behind the LSC concept is the replacement of a large expensive solar cell area with an inexpensive polymer-based thin film or plate collector, that enables a large amount of photons to be harvested and redirected towards a small-area PV cell, where the photon-to-charge conversion occurs. In this way, reduction of material cost can be achieved together with optimization of solar cell functioning. OLSC's are promising optical devices which will be used to complement the current photovoltaic technology and for this reason a lot of efforts have been recently made in this research field. However, several issues such as environmental stability and device efficiency are still to be investigated in detail and optimized before commercialization of this technology can be attained.

The work carried out in this thesis mainly concerns two aspects: the analysis and optimization of device parameters of poly(methylmethacrylate)-based LSC's, this material currently representing the state-of-the-art host matrix for LSC applications; the study and optimization of new polymeric matrices for LSC applications in the attempt to improve the environmental stability of LSC devices while maintaining high power conversion efficiency. In the first part of this work, a parametric study on PMMA-based thin film LSC's will be

presented, ultimately aiming at the optimization of photovoltaic performance. In this study several device parameters were analyzed, including dye concentration, polymer-matrix thickness concentration, device aspect ratio (length/width of the plate) and use of white back reflectors on LSC performance,

In the second part of this work new polymeric host matrices for LSC devices based on fluoro-polymers were analyzed due to their potentially improved environmental stability compared to standard PMMA-based devices. A study on each synthesized matrix will be presented, following the optimization of the main LSC device parameters.

Finally, the environmental stability of optimized LSC devices was investigated through a series of accelerated weathering tests on working LSC devices.

In particular, this work is structured as follows:

- *Chapter I: Introduction*

  An overview of the working principles of LSC devices and of the state-of-the art in LSC design will be proposed.
- *Chapter II: OLSC devices: materials and fabrication techniques*

  The focus will be on the materials used to fabricate LSC devices. The technologies used in the fabrication of LSC devices will be shown.
- *Chapter III: Characterization methods*

  The techniques used to characterize the performance of LSC's and their fundamental working principles will be shown.
- *Chapter IV: Results and discussion*

  The PV results and the supporting tests in the characterization of the fabricated LSC's will be shown.
- *Chapter V: Conclusions and future developments*

  The conclusion and the future developments in the LSC research field will be proposed.

I

Introduction

The world's energy system has been giving a lot of advantages and benefits to our society. This kind of policy is however no more sustainable: energy is indeed primarily derived from fossil fuels and oil derivatives but this kind of sources is not infinite and produce a significant amount of harmful emission such as for example carbon dioxide, CO_2. CO_2 is known as the most important greenhouse gas which contributes to global Earth's warming.

Actually the world uses about 10 TW of energy and this figure is expected to increase by 2050 up to 30 TW [1]. In order to fulfill this ever increasing requirement and to control greenhouse gases emission, it is mandatory to turn toward renewable energy sources.

I.1 Solar energy

Solar energy is an example of clean energy because it comes from a renewable source (sun) and its conversion into electricity or heat takes place at zero impact one. The radiative energy output from the sun derives from a nuclear fusion reaction. Each second 6×10^{11} kg of hydrogen are converted in helium with a mass loss, directly proportional to the amount of the energy transformed which is emitted as electromagnetic radiation. The total mass of the sun is about 2×10^{30} kg which leads to the conclusion that the sun can have a reasonably constant radiative energy output for about 10 billion years [2]. Light emitted from the sun strikes the Earth and is attenuated by the atmosphere due to water vapor absorption in infrared (IR), ozone in the ultraviolet (UV) and scattering by dust. The role of atmosphere is quantified by *air mass:* research usually refers to AM1.5 G conditions which describe a situation in which sunlight strikes the Earth at 48° with respect to the normal to the Earth

surface with a power density of 100 mW/cm^2. The term G accounts for both direct and diffuse light [2, 3]. In figure I.1 the sunlight spectrum emission is shown from UV to IR.

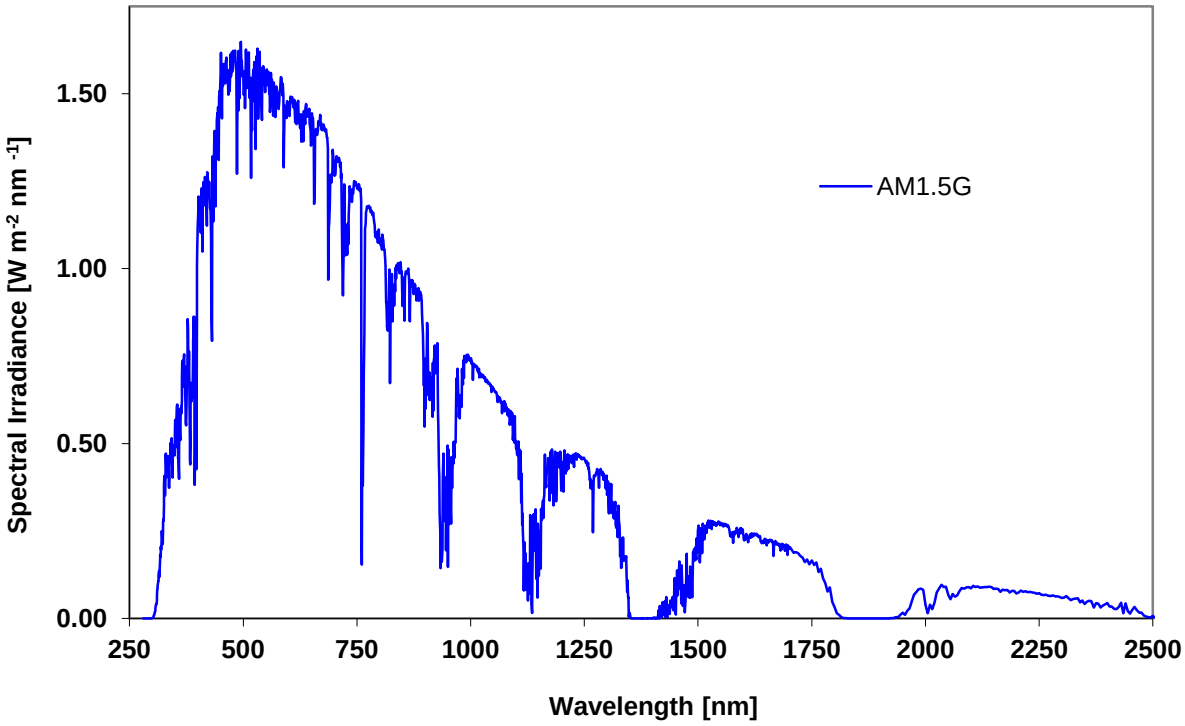

Figure I.1 Sunlight emission spectrum.

Radiation emitted from the sun can be used to generate electricity (photovoltaic effect) or to produce heat (solar thermic). In this work we will focus only on the first effect which is known since the 19th century mainly from the work of Becquerel, which discovered this effect by shining light onto electrolytic cells. This technology is now acquiring interest both for academia and industry, although significant improvements are needed to play an important role in the world's energy supply landscape.

Now a brief review of the physics of photovoltaic cells will be proposed, first of all focusing on p-n junctions.

I.2 P-N junction

As said before, a photovoltaic device transforms an optical input in an electrical output in a two steps process: absorption of light which generates an "electron – hole" pair (usually known as exciton) and separation of the two charges mainly due to the structure of the device, creating an electric current. Its behavior is based on the P-N junction, concept which will be briefly discussed in the following. We usually refers to a silicon P-N junction even if different kinds of semiconductors exist.

Silicon is an element of the IV group and has four valence electrons in the outer shell. It is commonly known as a semiconductor, a material whose conductivity is between 10^4 and 10^{-8} $S.cm^{-1}$ [4]. A semiconductor always presents a little energetic gap between valence and conduction bands. Even if theoretically a pure semiconductor shouldn't have free charges available for electric conduction, electrons could be thermally excited from the valence to the conduction band even at room temperature, leaving a hole in the valence band. Electrons and holes move in opposite direction but both contribute to the current flux. A semiconductor like pure Si which presents only one type of atom is termed intrinsic semiconductor but this kind of structure doesn't find a great field of applications. In order for semiconductors to become more attractive in a technological perspective a doping process is needed. Doping elements have to be added to the structure, thus resulting in a number of potentially interesting properties. A doped semiconductor is also referred to as extrinsic.

We usually define two kinds of doping: a negative one known as N type, and a positive one called P type. The former is obtained by adding pentavalent (phosphorous, arsenic) elements to silicon. We will refer to those dopants as Donor materials. Every silicon atom will bind covalently to four donors and every donor will bind to four silicon atoms: each donor atom will have an excess of one electron which could be easily excited to the conduction band. We will denote by N_D the concentration of donors which is substantially equal to the concentration of free electrons. Instead of doping with pentavalent impurities let us consider now a trivalent doping (e.g. boron): in this case an excess of holes is observed in the valence band and we usually refer to this kind of impurities as acceptors. As with donors, we

will denote the acceptors concentration as N_A, which is equal to the holes concentration in the valence band.

By putting in physical contact a P and an N type semiconductor, we obtain a so called PN junction, a two terminal device whose electronic energy curves are schematically depicted in figure I.2. At the junction there is a tendency for electron (dots) to migrate towards the P side (left) while holes (circles) move to the opposite direction towards the N side (right). Not all electrons and holes have sufficient energy to overcome the energy barrier and most of them are pulled back to the starting zone. This kind of movement is known as diffusion.

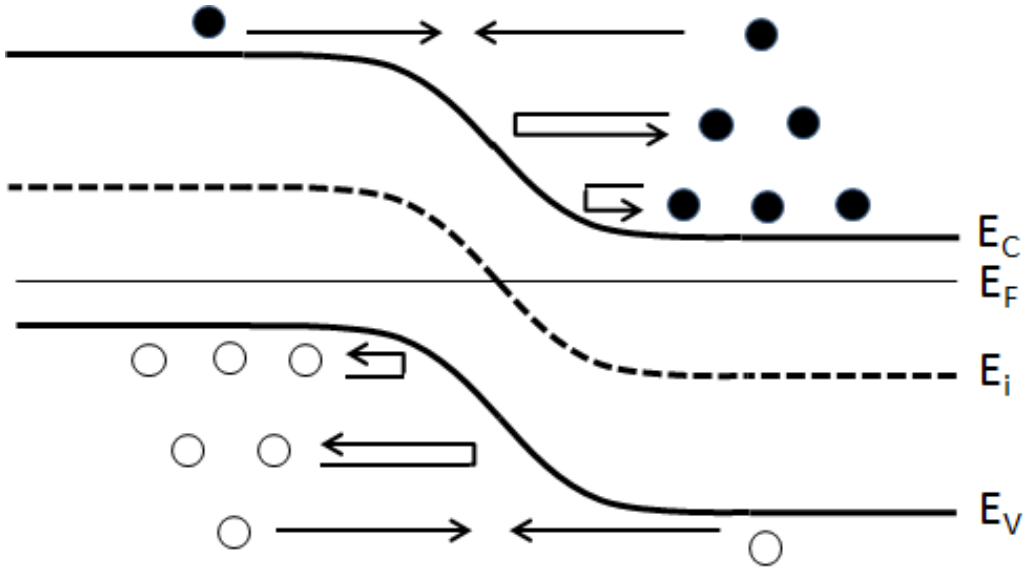

Figure I.2 PN junction energy levels at the equilibrium. Donor is on the right while Acceptor on the left. E_C stands for the energy level of the conduction band, E_V for that of the valence band, E_F indicates the Fermi energy level. E_i is a generic energy level.

As a result, the donor atoms become positively charged while the acceptors become negatively charged thus establishing an electric field: the net positive charges on the N side are prevented from further diffusion and a net negative charges acts in a similar way on the other side of the junction. The final result is a double layer zone better known as depletion zone, a region at the junction which is depleted by mobile conductive charges. The potential

difference set up in the two portions of the device is also known as built in potential [5]. This situation can be observed in figure I.3

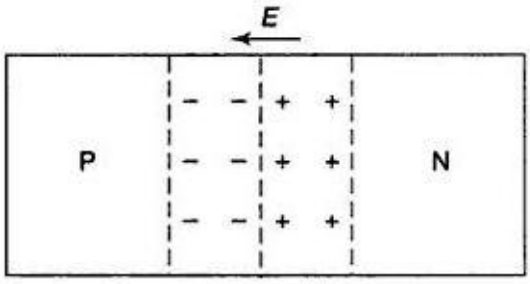

Figure I.3 Depletion zone and built-in potential, E.

In addition to diffusion processes also a drift current is observed, affecting the minority carriers, which give rise to an avalanche flux. Electrons in P side and holes in the N side move towards the opposite side of the junction where they can reach a more advantageous energetic situation. After the diffusion process, no further diffusion is observed and the system is now at equilibrium. The only way of permitting a current flux is by applying a bias. It is possible to apply a forward bias or a reverse one.

The two act in opposite ways: a forward bias is established when the positive pole of the power supply is connected to the P side of the junction and the negative pole to the N side. Consequently, the barrier height is reduced and this allows the current to flow because now more electrons can reach the P side and more holes can reach the N side. What is observed is a net current flux but only for a threshold voltage value which must be higher than the built in potential. Once the threshold voltage has been passed, current starts to rise with an exponential law (figure I.4)

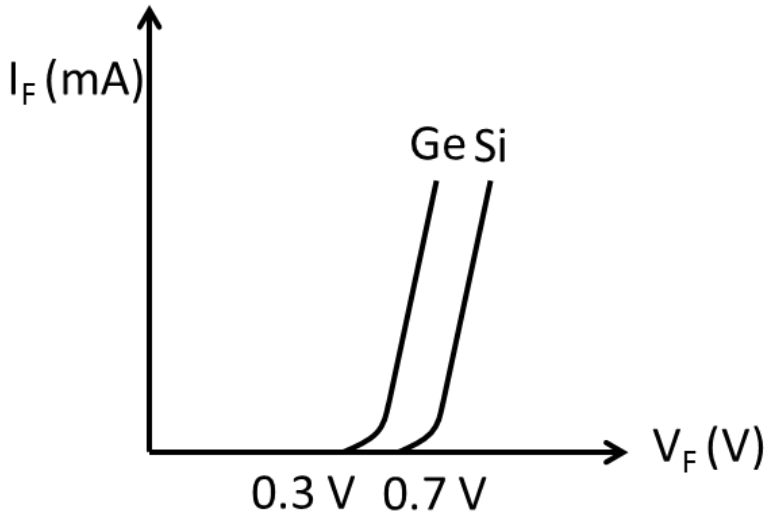

Figure I.4 I-V characteristic and threshold voltage for pure germanium and silicon. I_F and V_F indicate the forward voltage and current.

If the negative and the positive poles of the power supply are connected respectively to the P and the N side of the junction, what is established is a reverse bias. In this case a very little current is observed because the height of the potential barrier is increased allowing only a few electrons and holes to migrate towards the opposite side. In this way a reverse current is observed which goes from the N side to the P side of the junction. Its value is however very low because only few electrons and holes have sufficient energy to overcome the energy barrier. Those carriers which contribute to the drift current are not affected by biasing because they tend to reach a more favorable energetic situation. The reverse current is expected to saturate – become bias independent – once the majority carrier diffusion is reduced to a negligible level at a small reverse bias. Let us indicate with V the voltage applied and with I_0 the saturation reverse current. In this case the overall I-V dependence is given by eq.1:

$$I = I_0\left(e^{qV/KT} - 1\right) \qquad \text{Eq. I.1}$$

where q is the elementary charge of electron, K stands for the Boltzmann's constant and T is the absolute temperature.

The overall I – V characteristic for a PN junction is reported in figure I.5, where the breakdown is also shown, corresponding to a sudden increase in reverse current. Breakdown occurs due to avalanche effect in which thermally generated minority carriers cross the depletion region and acquire sufficient energy to produce new carriers by removing valence electrons from their bonds. Equation I.1 does not take into account this effect.

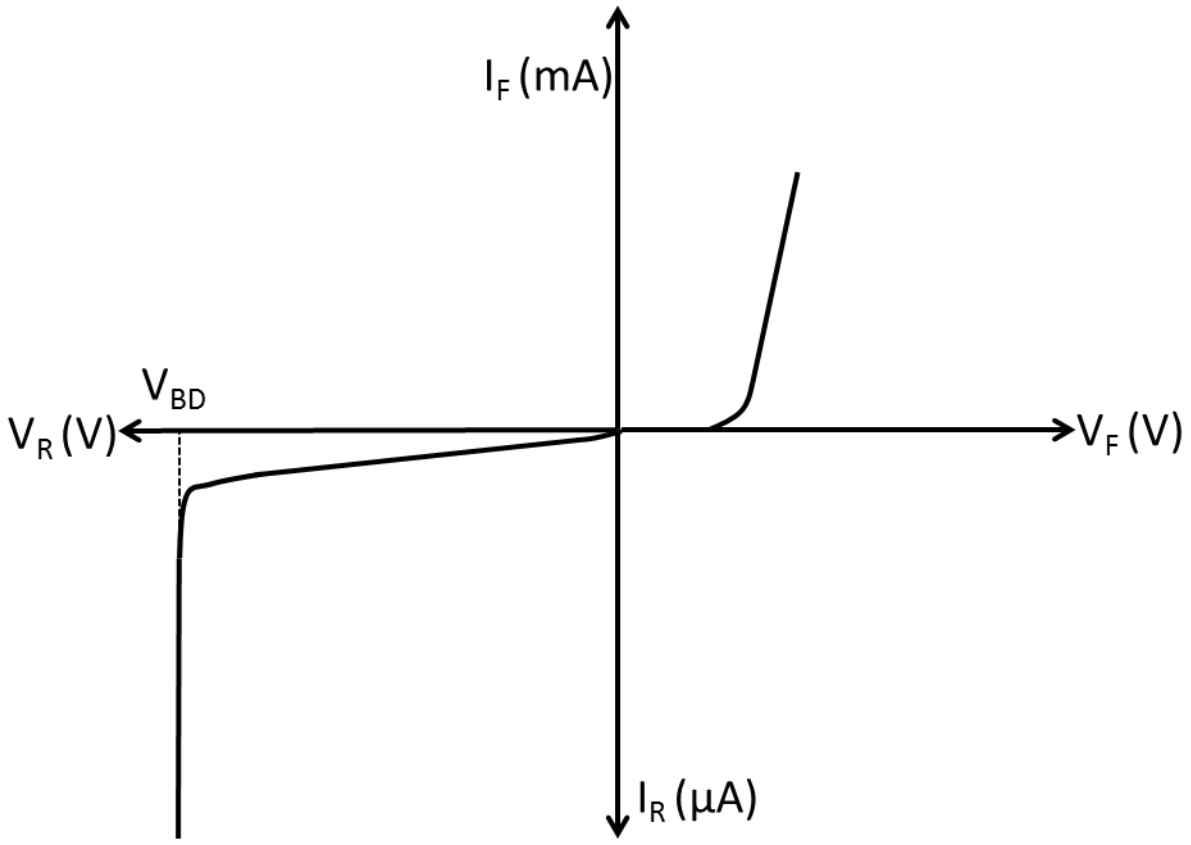

Figure I.5 Complete I-V characteristic for a PN junction. V_{BD} indicates the breakdown voltage. The reverse voltage and current are indicated with the subscript R. V_{BD} stands for breakdawn voltage.

I.3 Photovoltaic cell

A typical Photovoltaic (PV) device is based on the PN junction. When a semiconductor material absorbs photons whose energy is equal or greater than its band gap, an electron hole pair (also called exciton) is formed which implies the promotion of an electron from valence to conduction band, leaving a hole in the valence band. The structure of the device permits the separation of excitons leading to generation of a photocurrent made of minority carriers. Indeed electrons generated in the N part of the junction are negligible compared to the majority carriers while those generated in the P part are larger with respect to minority carriers at equilibrium in the dark as can be seen from figure I.6 [3].

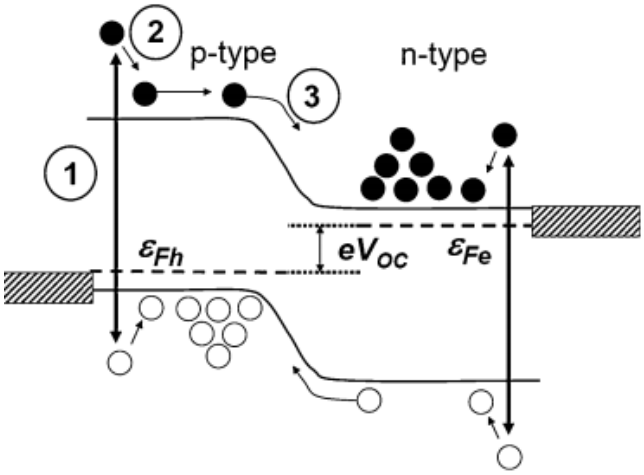

Figure I.6 Schematization of the energy levels in a photovoltaic cell. Minority carriers (electrons on the P-side and holes in the N-side) are responsible for the current flux in a photovoltaic device. Electrons move from the P side to the N side while holes move from the N side to the P side. In the movement, both electrons and holes reach a more favorable energetic situation than the starting one. The picture was taken from [3].

Minority carriers diffuse towards the depletion zone, that is electrons moves from the P side to the N side while holes from the N side to the P side. Once reached the depletion zone, electrons and holes cross this zone thus becoming majority carriers on the opposite side.
It is possible to model a PV device by means of an equivalent circuit such as that shown in figure I.7

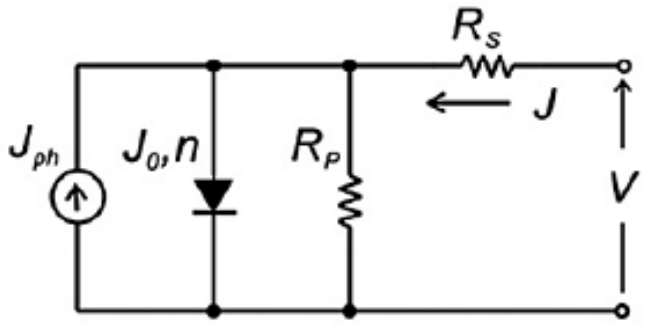

Figure I.7 Model of PV cell by means of an equivalent circuit. The circuit is composed by a current generator which takes into account the photocurrent generated upon illumination J_{ph}, a diode (J_0 and n) to schematize the PN junction and two resistances (R_s and R_p) which represent non ideal processes. The picture was taken from [3].

There are several components in this schematization: a current source which indicates the photocurrent generated upon illumination (J_{ph}), a diode which models the P-N junction and which is characterized by the ideality factor n and by the saturation reverse current density, J_0, which serves as a reminder that a solar cell is simply a diode if stored in the dark. In addition, there are also two resistances: R_s is the series resistance which must be minimized to achieve optimal PV performance and accounts for the resistance of the semiconducting material, the resistance between the semiconductor and the electrodes and the resistance of the electrodes themselves. R_p is the shunt resistance and must be maximized because it represents the loss of carriers via leakage paths caused by the presence of possible defects which can induce recombination of the carriers.

An analytical solution for the equivalent circuit has been proposed as described in equation I.2, also known as Shockley equation [3]:

$$J = \frac{1}{1+\frac{R_S}{R_p}} \left[J_0 \left\{ \exp\left(\frac{V - JR_S A}{nKT/q}\right) - 1 \right\} - \left(J_{ph} - \frac{V}{R_p A} \right) \right] \qquad \text{Eq I.2}$$

where A denotes the area of the cell. Moreover it is possible to derive equations for two important cell paramaters: we will indicate with V_{OC} the open circuit voltage of the cell or

the voltage when there is no current flow (eq. I.3) , and with J_{SC} the short circuit current or the current flux density when there is no voltage applied (eq. I.4)

$$V_{OC} = n\frac{KT}{q}\ln\left(1 + \frac{J_{ph}}{J_0}\right) \qquad \text{Eq I.3}$$

$$J_{sc} = -\frac{1}{1+\frac{R_S}{R_p}}\left\{J_{ph} - J_0\left(\exp\left(\frac{JR_SA}{nKT/q}\right) - 1\right)\right\} \approx -J_{ph} \qquad \text{Eq I.4}$$

The short circuit current is proportional to solar radiation but shows also a little dependence on temperature. On the other hand, the open circuit voltage increases rapidly with illumination until it reaches a nearby saturation value.

The characteristic curve of a photovoltaic cell can be represented as a plot of current density versus voltage. An example of this plot is given in figure I.8

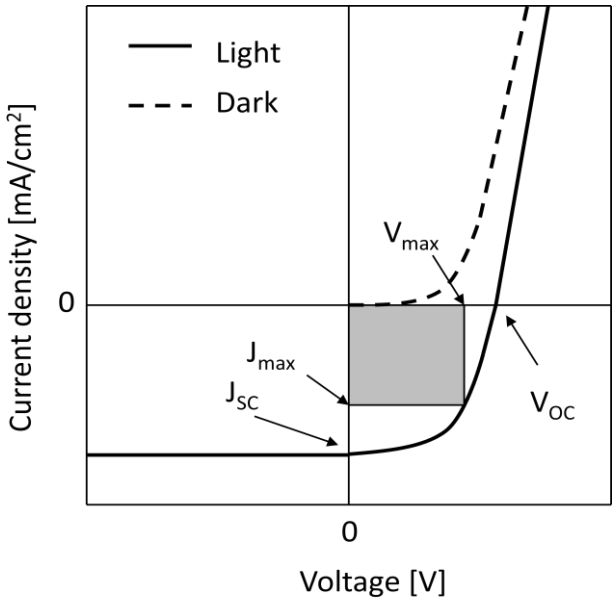

Figure I.8 Characteristic curves for a photovoltaic cell. The dashed line represents the exposure to dark conditions while the solid one models the behavior of the cell upon light exposure. In the figure the main photovoltaic parameters are also indicated.

Obviously the characteristic curve is dependent on the degree of illumination. In the case defined in figure I.8 two typical conditions are represented, one upon illumination and the other in the dark. In this latter case in particular the characteristic curve of the PV device resembles that of a diode. Another important parameter of a photovoltaic device is the fill factor (FF) which is a measure of the quality of the operating diode. Graphically it can be considered as a measure of the sharpness of the curve and it is defined as follows (eq. I.5)

$$FF = \frac{I_{max}V_{max}}{I_{SC}V_{OC}} \qquad \text{Eq. I.5}$$

namely as the ratio between the maximum power output of the cell and the ideal power output; its value is comprised between 0 and 1 but the latter value is in practice impossible to obtain. Typical values of FF for highly performing inorganic photovoltaic cells lie around 0.8 [3].

In order to classify the cell performance, a very useful parameter is the power produced, which is simply the product of current and voltage as can be seen in equation I.6.

$$P = VI \qquad \text{Eq. I.6}$$

Another important parameter is the point of functioning of the PV cell, identified by the maximum power produced (eq. I.7), also reported in figure I.8

$$P_{max} = I_{max}V_{max} \qquad \text{Eq. I.7}$$

The ultimate measure of solar cell performance is the power conversion efficiency (PCE), defined as the ratio between the maximum power produced by the solar cell P_{max} and the incident power density, P_{in} (eq. I.8)

$$PCE = \frac{P_{max}}{P_{in}} = \frac{I_{max}V_{max}}{P_{in}} = FF\frac{I_{SC}V_{OC}}{P_{in}} \qquad \text{Eq. I.8}$$

In the following, the two terms PCE and η will be used interchangeably.

Finally, it is also useful to define quantum efficiencies of the PV device, the first called *external* and the second *internal:* both are related to the number of electrons produced by the device upon illumination. In particular, the former considers all photons incident on the photovoltaic device while the latter only considers photons absorbed by the solar cell, thus omitting those reflected or scattered.

$$EQE = \frac{number\ of\ electrons\ produced\ by\ the\ PV\ cell}{number\ of\ incident\ photons\ on\ the\ device\ surface\ area} \qquad \text{Eq. I.9}$$

$$IQE = \frac{number\ of\ electrons\ produced\ by\ the\ PV\ cell}{number\ of\ \ photons\ absorbed\ by\ the\ device} \qquad \text{Eq. I.10}$$

All the parameters listed so far are considered the key parameters in the characterization of a PV device.

I.4 PV devices: materials and technologies

It is commonly accepted by experts that PV technologies can be divided into three main categories, primarily based on the materials employed to build the device and its fabrication technology [6]. Although nowadays silicon is the most commonly used material for the PV device fabrication, its band gap (1.12 eV at room temperature) is not optimal for photovoltaic solar energy conversion based on a single junction solar cell because it shows a maximum theoretical efficiency of 29 % [7]. In [7] authors showed that the optimal band gap for energy conversion is 1.3 eV which give rise to a maximum theoretical efficiency of 40 %. But the advantage of Si with respect to other technologies is that research in this branch is advanced also due to electronics. Silicon is an indirect semiconductor because the maximum of the valence band and the minimum of the conduction band have not the same crystal momentum. This kind of semiconductors have a peculiar characteristic: their light absorption coefficient are not high. For example, to absorb 90% of light only 1 μm of GaAs (direct semiconductor) is sufficient while for silicon 100 μm are needed to absorb the same amount of light.

The main parameter used to study the technological potential of a specific PV technology on the market is the evaluation of its payback time, or time needed for a device to generate as much energy as that needed to fabricate it.

The first PV generation usually refers to bulky monocrystalline (m-Si) and multicrystalline silicon devices which have led to the most important PV cell efficiencies which are around 20% (with the most powerful cell ever produced has a PCE of 25% [8]). Usually monocrystalline silicon (but also multicrystalline) has a low absorption coefficient with the consequence that silicon wafers thicknesses must be around 200 μm to ensure an acceptable light absorption.

A typical crystalline silicon device structure is shown in figure I.9.

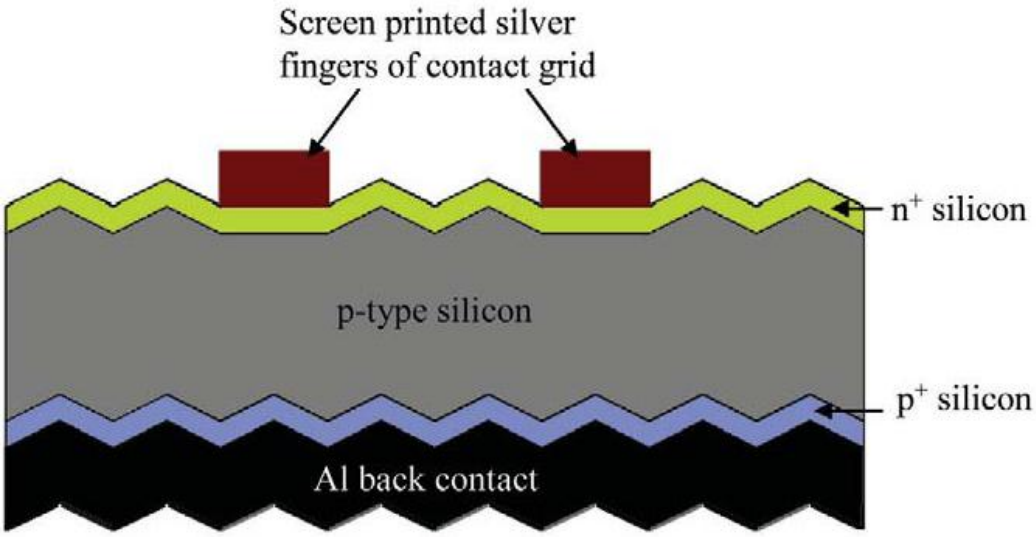

Figure I.9 Typical structure of a crystalline silicon device.

These kind of devices are produced by Czochralski method [9], the same adopted in electronic industry to produce Si wafers. The P-N junction is formed by diffusion of an N type dopant -phosporous- into the wafer as an impurity leading to the n^+ doped emitting layer. Screen printed silver contacts are necessary on the n-type to make the electrical contact. Al paste is used to make contact at the back p type surface. By annealing of Al layer, a p^+ doped region is formed. To optimize incident solar radiation, it is common practice to apply an antireflection coating (typically TiO_2) which minimizes reflected radiation. To complete the device, a SiO_2 layer is placed on the back surface to promote its passivation.

While the high efficiencies are one of the advantages of this kind of technology, the production of monocrystalline silicon solar cells is very expensive and this contributes to limit its diffusion.

To overcome some of the associated problems with crystalline silicon PV cells, new materials and fabrication technologies have been introduced, which led to the second generation of PV cells. One of the major drawback linked to Si-PV was the necessity to reduce costs maintaining approximately the same output. This second generation adopts thin films PVs whose efficiency are lower than monocrystalline silicon but have a lower intrinsic cost.

This branch includes a number of different technologies and materials: amorphous silicon has a predominant role but also the technology based on cadmium telluride is important; in

addition technologies such as that based on Copper Indium Selenide (CIS) and Copper Indium (di)Selenide (CGIS) have shown interesting properties. Amorphous silicon (a-Si) is known since the '60s but only in 1976 a PV cell in a-Si was built. From a physical point of view, the material employed is an alloy of silicon and hydrogen which has not a defined crystalline structure with a long range order. Plasma enhanced chemical vapor deposition (PECVD) is the dominant deposition technique based on SiH_4 precursor gas. Typical deposition temperatures are approximately 500° C which are necessary to be able to incorporate diatomic hydrogen into the film. Hydrogen plays the important role of passivating the dangling bonds that result from the random arrangement of the Si atoms. The optical absorption coefficient of hydrogenated silicon is greater than 10^5 cm^{-1} (quite high) meaning that only few microns of material are needed to absorb most of the incident light.

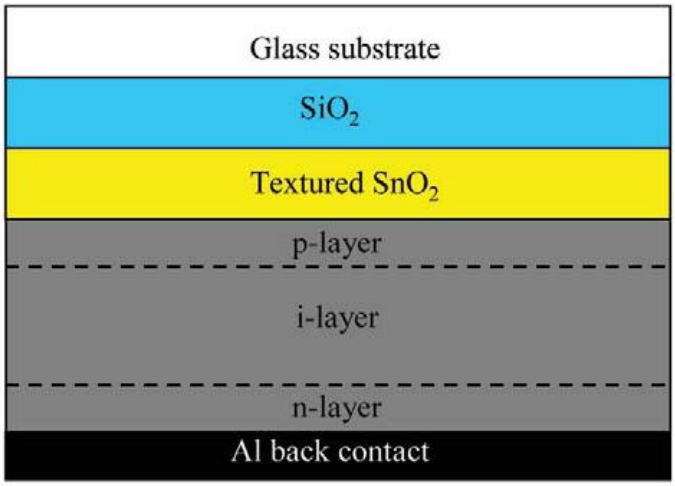

Figure I.10 Typical structure of a device based on amorphous silicon.

A typical structure of a PV device based on a-Si is reported in figure I.10. The manufacturing process can be made either on flexible substrates or on rigid ones. Most of the structures are based on the so called p-i-n structure but this kind of system suffers from degradation problems. This structure is based on the junction between a P doped layer and a N doped layer between which an intrinsic semiconductor layer is placed. The major problem of this kind of technology is degradation induced by illumination in the very first hours of exposure,

whose action directly affects FF and I_{SC} of the PV cell, leading to a reduction in cell performance [4]. The degradation process can be recovered by exposing the cell to a temperature of approximately 160° C. It is possible to absorb the solar spectrum more efficiently and to improve cell stability by using stacks of different p-i-n structures with different energy band gap "I" layers to produce double or triple structures.

Another material used as active layer in thin film technology is cadmium telluride. Devices based on this material present several advantageous properties including an optical band gap close to optimum for solar energy conversion and the capability of the material to tolerate defects and grain boundaries. Moreover the high absorption coefficient requires only few microns of CdTe to absorb most of the incident light. Despite those advantages, problems related to deposition process and toxicity of the components limit diffusion of this technology even if in literature [6] efficiencies up to 16.5% are found.

Polymeric solar cells are one example of third photovoltaic generation. These kinds of PV cells are characterized by a polymeric active layer based on the concept of the bulk heterojunction (BHJ) [3], a blend between a donor polymeric material (usually poly3-hexiltiophene, P3HT) and an acceptor (typically [6,6]-phenyl-C61-butyric acid methyl ester, PCMB). Different techniques can be employed to fabricate organic-based devices on large scale [10], mainly based on roll to roll processes because a typical device is based on a stack of several thin films. A typical organic PV device structure is reported in figure I.11. In this figure electron and hole transporting layers are also depicted. The main difference with respect to inorganic devices is that current flux is generated by majority carriers. Incident light generates excitons, which in an organic PV device play a rather important role. In fact, in order for them to form free charges, separation of the exciton into electron and hole must occur before its quenching. Excitons can be separated only at the interface between donor and acceptor and to promote this separation a bulk heterojunction is built.

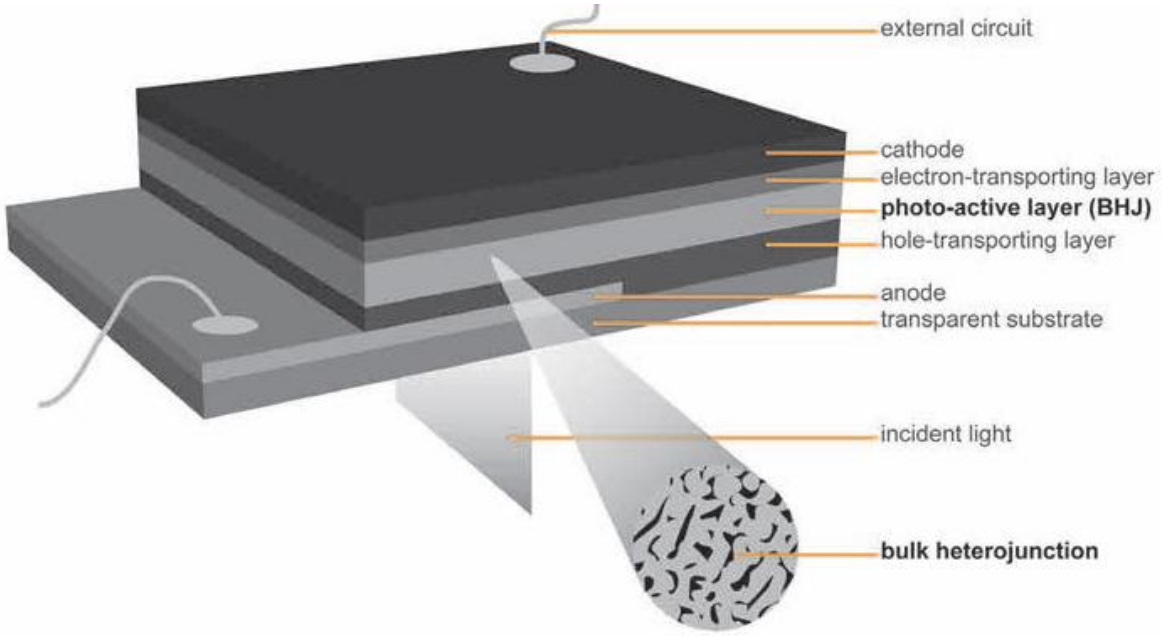

Figure I.11 Typical organic PV device structure. In the picture also the hole and electron transporting layers are depicted

Record efficiencies approaching 8-9 % [11] can be achieved today by polymeric based devices after proper optimization of materials and processing of each layer. It is obvious that these PCE are not comparable to silicon based devices but a great reduction of costs is expected to be achieved by employing polymeric materials. Notwithstanding the number of potential advantages of this technology, several issues are still to be solved, such as for instance the poor environmental stability of the materials used to fabricate this type of PV devices [12 – 14]. This severly limits its diffusion in the market and has motivated the development of a great deal of interesting solutions to overcome or at least partially prevent this problem [14].

The so called dye-sensitized solar cells (DSSC) or Graetzel cells are nowadays the best performing organic-based photovoltaic devices with a PCE of 11% [15]. Light is adsorbed by a dye molecule which is absorbed on a porous film composed by semiconducting metal-oxide nanoparticles immersed in a liquid electrolyte: electrolyte contains a redox couple responsible to the conversion of the oxidized dye to its neutral state. The dye molecule injects an electron into the semiconductor which is responsible for its transport to the anode.

I.5 Imaging light concentrating systems

Despite the significant improvements made during the last thirty years, PV technology still presents some drawbacks which limit its diffusion on the market including the high costs and the intermittence of the solar input. One way to reduce costs is to use concentrator systems by collecting solar radiation over large areas and to redirect it towards small PV active areas. In this approach the high costs are limited because a smaller amount of semiconducting material is used while keeping constant the energetic output because of the increased illumination intensity focused on the cell. We can recognize two main categories of concentrating systems, namely imaging and non-imaging solar concentrators [16].

The first category is also known as concentrated photovoltaic (CPV) which uses a variety of lenses and mirrors of different geometries to achieve the goal. Fresnel lenses are one example but also parabolic dishes are part of this category. This kind of systems presents also some drawbacks including excessive heating of the solar cell which forces the inclusion of an adequate cooling system to prolong solar cell service life. These systems are only able to collect direct radiation omitting the diffused one; a sun tracking system is indeed necessary to reduce the input and also output intermittence. A sun tracking system is usually employed in order to achieve the optimal operating conditions in which the incoming radiation is perpendicular to the active area of the device. In conclusion the whole solar generator area must be continuously adjusted to the actual position of the sun. Tracking systems can utilize either one or two axis: the former affects only one angle and by consequence sun is perpendicular to the PV module only in one plane while the latter affects two angles and sun is always perpendicular to the module [4]. It is customary to divide CPV systems into three main categories principally based on intensity of concentration: low, medium and high concentration.

In the low concentration systems a concentration factor (CF) from 2 to 10 suns (1 CF corresponds to 1 sun or to 1000 W/m^2) is achieved while in a medium systems CF is between 10 and 60 suns. The high concentration systems concentrate light with a CF from 100 to 1000. On the market four main geometries of imaging solar collectors can be found (figure I.12)

- Parabolic trough collectors;
- Heliostat field collectors;
- Linear Fresnel reflectors;
- Parabolic dish collectors

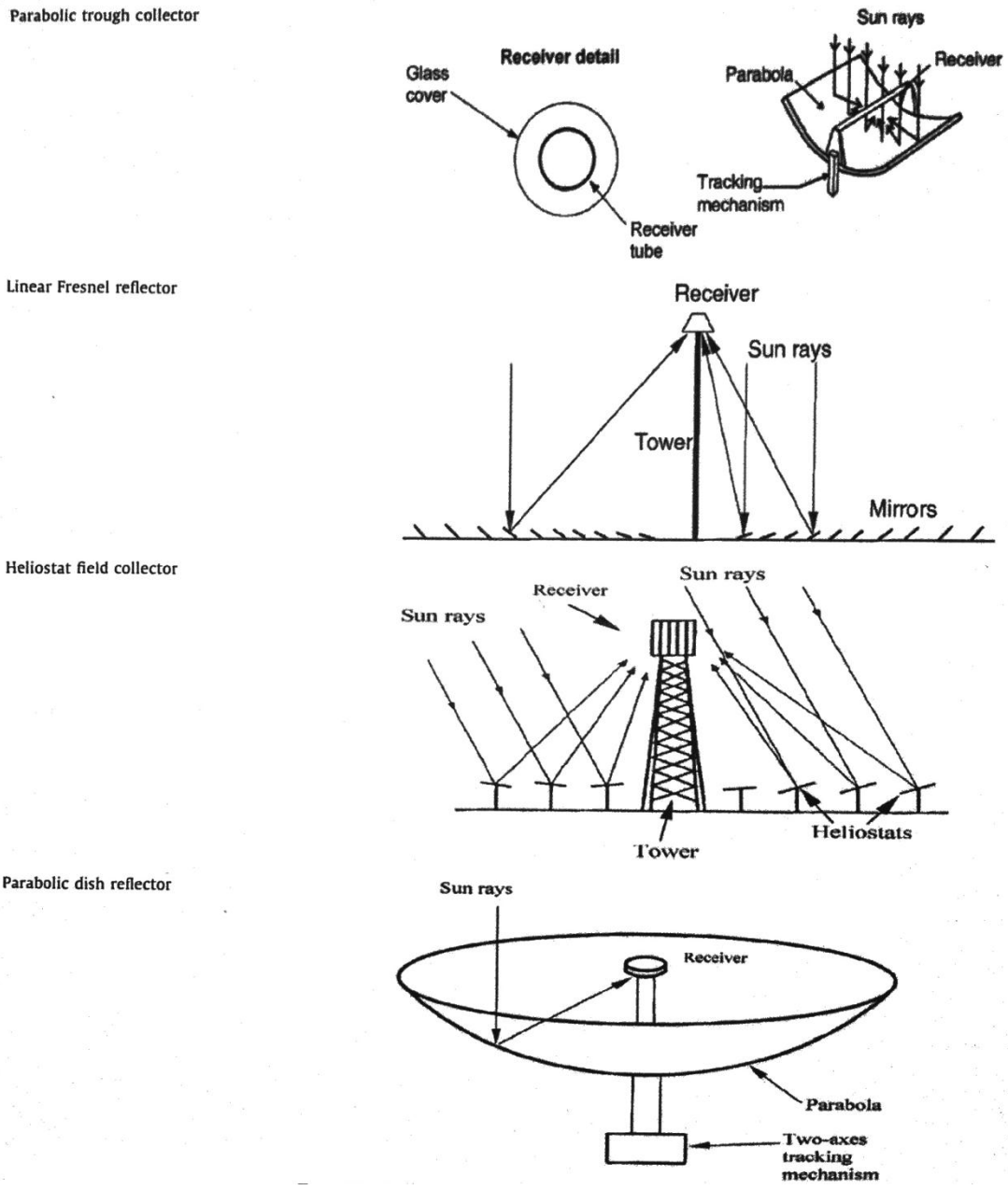

Figure I.12 Types of concentrating photovoltaics devices.

Parabolic trough technology is the most mature concentrated solar power design featuring light structures and relatively high efficiencies [17]; a parabolic trough concentrator is composed by a sheet of reflective material, usually silver acrylic, which is bent into a parabolic shape. Usually this kind of system is mounted on a single axis sun tracking system.

The most recent concentrated solar power (CSP) system to emerge into commercial utility is the heliostat field collector design which features a large array of flat mirrors distributed around a central receiver mounted on a tower. Heliostat field collectors are a powerful tool but their costs are really high leading to a limited use. Each heliostat sits on a two axis tracking mount and has a very high area (up to 150 square meters) and is directed individually to capture direct sunlight and redirect it to the central receiving unit. The immense solar flux reflected towards the receiver yields very high concentration factors (up to 1500 suns) and to temperatures of about 1500°C.

Linear Fresnel (LF) reflectors are quite similar to parabolic trough collector schemes. LF reflectors incorporate long arrays of flat mirrors that concentrate light onto a linear receiver which is mounted on a tower suspended above and along reflector arrays. Mirrors can be mounted on both one or two axis tracking devices. Flatness and elasticity of LF's make their design cheaper than parabolic trough concentrators. Several Fresnel reflectors can be used to approximate a parabolic trough collector shape, with the advantage that the receiver is a separate unit, and does not need to be supported by the tracking device. This makes tracking simpler, accurate and more efficient.

The last type of imaging collector system is based on parabolic dishes which are point focus collectors. They can achieve very high concentration factors reaching up to 1000 suns. The collector type features a large parabolic shaped dish which must track the sun on a two axis tracking system to maintain light convergence at its focal point.

The four main imaging technologies shown must be coupled with sun tracking systems which are difficult to design and need large areas so as to avoid shading effects from neighboring collectors. Another problem with this kind of technology is the high temperature which can be reached on the surface of the PV device. This problem may lead to designing also cooling systems in order to prevent premature degradation of the photovoltaic cell. Moreover

imaging collectors can collect only direct radiation while they completely neglect diffuse radiation.

Non-imaging collectors are based on a different approach which allows also diffused light to be concentrated on small PV areas. This kind of technology is primarily based on Luminescent Solar Concentrators (LSC's) on which research has focused in the past years because of the very interesting perspectives they offer.

I.6 Non-imaging light concentrating systems: Luminescent Solar Concentrators

A Luminescent Solar Concentrator (LSC) consists of a film or a plate of polymeric matrix in which a luminophore has been dissolved or dispersed. The luminophore absorbs light and re-emits it at a longer wavelength as predicted by the fluorescence process. Photons emitted by the luminophore are transported by Total Internal Reflection (TIR) towards the edge where photovoltaic cells are placed. A schematic view of the LSC is reported in figure I.13.

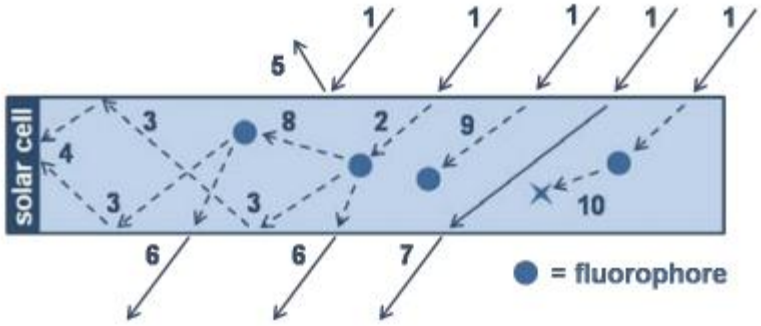

Figure I.13 Schematic lateral view of a LSC. The arrows indicate the movement of photons. 1 represents incident radiation, 2 the movement of the photon within the polymeric matrix, 3 the emitted photon which travels by TIR into the waveguide. 4 indicates the photon which reaches the PV cell placed on the edge of the luminescent plate, 5 shows a possible loss process, the reflection of the incident photon while 6 represents another dissipative process that is the escape of the re-emitted photon from the waveguide through the escape cone. 7 represents the possible transmission of the incident photon. 8 stands for the possible reabsorption of the emitted photon by another dye molecule. 9 shows non radiative fluorescence decay while 10 is representative of the absorption by the polymeric matrix of the emitted photon

The state of the art describes two possible configurations for a LSC: a bulky configuration and a thin film configuration. In the former case we refer to the situation depicted above in figure I.14.b while for thin film LSC we refer to figure I.14a.

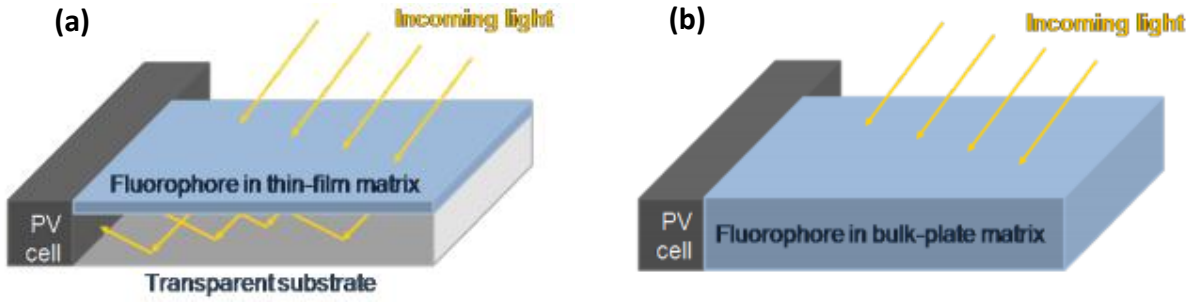

Figure I.14 a) Thin film Luminescent Solar Concentrator; b) Bulky Luminescent Solar Concentrator

In both configurations, a planar arrangement is normally employed. In the bulk plate configuration a plate of transparent host matrix (usually PMMA or PC) is doped with one or more photoluminescent species. Thin film LSC's consist of a transparent carrier matrix doped with dye molecules deposited as a thin film onto a glass or plastic substrate.

Not all the incident light will be absorbed by the luminescent dye because a part will be directly reflected or transmitted due to limited absorption spectrum of the fluorophore. In addition it is not obvious that all the photons absorbed and re-emitted by the dye molecule can reach the PV cell: several dissipative processes have to be taken into account including losses from the escape cone. The portion of the emitted light that is trapped inside the waveguide is determined by the refractive index of the waveguide itself. According to Snell's law, all photons approaching an interface between a material and air at an angle higher than a critical angle will be totally reflected. This critical angle is defined as [18]:

$$\theta_C = \sin^{-1}\left(\frac{1}{n}\right) \qquad \text{Eq. I.11}$$

Where n stands for the refractive index of the substrate.

Using equation I.12 in which L is the percentage of trapped photons and considering a refractive index of the substrate n = 1.5, about 75% of photons emitted will not be lost [18] while remaining 25% will be lost.

$$L = \frac{(n^2 - 1)^{1/2}}{n} \qquad \text{Eq. I.12}$$

Moreover it is possible to estimate reflection from the surface by a Fresnel reflection mechanism using the following relationship [19]:

$$R = \left(\frac{n-1}{n+1}\right)^2 \qquad \text{Eq. I.13}$$

Those photons which are not lost from the escape cone can encounter additional dissipative processes such as, for example, re-absorption by other dye molecules. This phenomenon is expected because of the small Stokes shift[1] between the absorption and emission peak of the dye molecule: this leads to partial overlapping of absorption and emission spectra. The advantage of doped thin films configuration with respect to the bulk configuration one is that the luminescence emitted from the thin film is trapped in the substrate so that parasitic losses due to self-absorption and scattering from impurities can be reduced. For this reason, thin film configuration is often preferred.

Several other dissipative processes can limit LSC efficiency, such as the limited photoluminescence quantum yield of the dye: not all the dye molecules absorb photons and re-emit them with a 100% efficiency. This is due to the presence of non radiative decaying processes such vibrational relaxation that may occur in the dye molecule upon illumination.

The optical efficiency of an LSC can be calculated based on the following equation [17]

$$\eta_{opt} = (1 - R) P_{TIR} \eta_{abs} \eta_{PLQY} \eta_{Stokes} \eta_{TIR} \eta_{host} \eta_{self} \qquad \text{Eq. I.14}$$

[1] The Stokes shift is the difference (in wavelength or frequency units) between positions of the band maxima of the absorption and emission spectra

Where R is the reflection of solar light from the waveguide surface, P_{TIR} is the total internal reflection efficiency, η_{abs} is the absorption of the dye, η_{PLQY} is the photoluminescent quantum yield of the used luminophore, η_{Stokes} is the efficiency of energy transmission due to non-overlapping of absorption and emission spectra, η_{host} is the transport efficiency of the waveguided photons through the waveguide, η_{TIR} is the reflection efficiency of the waveguide determined by the smoothness of the waveguide surface and η_{self} is the transport efficiency of the waveguided photons related to re-absorption of the emitted photons by another luminophore.

The photoluminescence quantum yield can be calculated as reported below (eq. I.15) and is a measure of the probability that an excited molecule emits photons during the photoluminescence mechanism.

$$\eta_{PLQY} = \frac{number\ of\ emitted\ photons}{number\ of\ absorbed\ photons} \qquad \text{Eq. I.15}$$

It seems obvious that a near unity photoluminescence quantum yield is ideal for optimal LSC performance.

Not all the dissipative processes have been reported above: in particular other dissipative phenomena may take place such as, for example, scattering of emitted photons due to impurities (in both matrix and plate) or also absorption by the host matrix which reduces photons to be absorbed.

The parameters which identify LSC performance are the same as for a PV cell, namely $I_{SC,}$ V_{OC}, FF. It is possible to identify two kinds of PCE's, one calculated on cell area (see section I.3) and one defined on plate area. PCE calculated on LSC area will be indicated as LSC efficiency:

$$PCE_{LSC\ area} = \frac{J_{SC}V_{OC}FF}{P_{IN}} \qquad \text{Eq. I.16}$$

Let us now focus our attention on the materials suitable for LSC fabrication.

I.6.1 Luminophores

First of all look at the luminophore usually employed.

Combining the needs for maximum concentration, maximum efficiency and maximum lifetime, the luminophore is the single most important component in the device. An effective luminophore must meet all the following requirements: broad spectral absorption, high absorption efficiency over the whole absorption spectrum, large Stokes shift, high quantum yield, matching the emitted photons to the spectral response of the PV cell (for silicon 1.12 eV) and solubility in the host material. One type of photoluminescent dyes are π conjugated organic molecules in which π electrons are promoted from the ground state to an excited higher energy state. For an organic dye it is possible to theoretically calculate the main absorption wavelength (λ_{abs}) as follows [20]:

$$\lambda_{abs} = \frac{8mC}{h}\frac{L^2}{N+1} \qquad \text{Eq. I.17}$$

when m is electron mass, C is the light speed in vacuum, L is the chain length of the π conjugated plan, h is the Planck's constant and N the number of π electrons. Organic dyes have been investigated as luminophores due to their solubility, high fluorescent yields and large absorption coefficients. The most commonly used dye types for LSCs have traditionally been rhodamines, coumarins and perylene (bisimides) derivatives. Rhodamines are known for their high quantum yields and high molar extinction coefficients but also for their small Stokes shift which leads to significant reabsorption events [18]. The most known rhodamines are Rhodamine 6G, 590, 575 and B but all these dyes experienced a limited photostability with respect to other organic dye molecules like perylenes and some coumarins. Coumarins like Red G, 540A and CRS040 have a reasonably high quantum yield (over 80% for the former and 98% for the two latter).

Perylene and its derivatives are known for their good stability and their use is of practical interest. In addition they are known for their intense fluorescence and large spread between absorption and emission peaks. Debije et al. [19] proposed a new fluorescent dye based on a

perylene perinone which expands the absorption spectrum by approximately 50 nm with respect to the simple perylene.

One of the most limiting factor of organic fluorescent dyes is the overlapping of emission and absorption bands which leads to significant losses of photons. In order to reduce the loss of photons it is possible to use phosphorescent dyes instead of fluorescent. In fact phosphorescent dyes show larger Stokes shift and theoretically allow a reduction of reabsorption losses. Another possibility which is more efficient but more expensive is the use of quantum dots, i.e. nanostructures composed by different semiconductive layers with dimensions in the order of the de Broglie wavelength. One of the main advantages of QD with respect to organic dyes, is the possibility to tune the absorption threshold by a correct choice of the particle diameter [19]: increasing the QD size, the band gap will decrease. QDs are in addition intrinsically more stable than organic dyes and exhibit larger Stokes shift which reduce absorption losses.

Another type of luminophores is rare earth ions due to their good photostablility and the potential for very large Stokes shift. It is possible to increase the absorption spectrumof rare earth ions by employing organic ligands to be coordinated to the ions.

As an alternative to commonly employed luminescent dyes, Mulder et al. [21] proposed an LSC that use phycobilisomes as fluorescent species. Phycobilisomes are large water-soluble pigment-protein complexes that function as light-harvesting devices in red algae and cyanobacteria. They are capable of absorbing light over a broad range of the visible spectrum and concentrating this captured energy at the photosynthetic reaction center. The chromophores are arranged through self-assembly in cascading Förster energy transfer pathways that couple short wavelength chromophores at the edges of the complex to the long wavelength chromophores at the core of the complex. To cast phycobilisomes in solid state waveguides they must be incorporated within a matrix that mimics the native aqueous environment. For this reason thus polyacrylamide was chosen. To increase rigidity of the matrix the water content was reduced. The main advantage shown by phycobilisomes is the reduction of reabsorption losses in LSC by about 50%

Let us now focus on host matrix materials.

I.6.2 Host matrix materials

Another very important part of the LSC is the host matrix whose function is to embed all the luminescent molecules.

The host matrix should exhibit maximum transmission over a broad range of wavelengths and minimal scattering. Accordingly PMMA or PC are generally used as host matrix materials because they are inexpensive, transparent and relatively stable [22]. Even if PMMA is considered one of the best matrices for organic fluorescent dyes because it bears excellent optical properties (index of refraction, n = 1.49), it shows some limitations when dye concentration (e.g. coumarin) is increased considerably: in fact the formation of dimers is observed and in addition these dimers are only weakly fluorescent. For this reason, El-Bashir [23] proposed an alternative nanohybrid matrix based on PMMA/SiO_2 which allows a higher dye concentration; moreover this new matrix has a good stability over light irradiation and exhibits excellent weathering durability.

Other types of matrices have been studied in research. Lim et al. [24] proposed an unsaturated polyester (UP) as a possible alternative host material for LSC. UP's were obtained by polymerization of an unsaturated polyester resin (UP and styrene) with methyl ethyl ketone peroxide as cross-linking agent. The result was a three dimensional network. The cost of UP resin was shown to be lower than PMMA thus making it a potential alternative to PMMA and PC. To enhance host matrix optical properties, a blend between an UP and methylmethacrylate (MMA) [24]. The result was the modification of the chemical structure obtained after polymerization which led to constant index of refraction and optical clarity over a long period of thermal and ultraviolet treatments.

A dye-doped polysiloxane rubber is another possibility as host matrix. It was proposed by Buffa et al. [25]. In fact polysiloxane rubbers are characterized by good transparency, flexibility, mechanical and chemical resistance and by a wide temperature range of stability. In particular, flexibility offers the possibility to integrate LSC in non rigid structures. In this work, the possibility to disperse gold nano-particles in the PS matrix was studied with the aim of enhancing the energy transfer process between the plasmon resonance peak of the Au nano-clusters and the dispersed dye molecules. Despite expectations, gold nano-particles did not show any improvement of the light emitted by the LSC. In addition, it was found that

PS rubber showed the same light collection as PC with the same dye concentration. PS was shown to be a suitable host matrix host matrix for apolar dyes because for polar dye quenching effects were observed.

The demand of environmentally-friendly materials may lead to the discovery and development of sustainable host matrices. Following this input, Fattori et al. [26] proposed a poly-lacticacid (PLA) matrix for LSC purposes. PLA can be stressed or thermally crystallized, impact modifiable, copolymerized and easy processed at a lower cost. PLA is indeed cost-effective and can be considered as a viable alternative to petro-chemical based plastics with the major advantage that at the end of its life-cycle it can be completely degraded to carbon dioxide and water without polluting emissions. PLA was shown to be suitable as matrix material for concentrators because of its high transparency and its refractive index (1.45), which is similar to that of PMMA. The smaller index of refractions lead to a quite insensitive small reduction in maximum light trapped (74% for PMMA with respect to 72% for PLA). It was shown that PLA allows for a higher dye fluorescent quantum yield (35% higher) with respect to PMMA doped with the same dye.

At the state of the art, no studies have been proposed on the use of fluoropolymers in luminescent solar concentrators, although in the PV industry they have been widely used [27] as packaging (backsheets and superstrate) for PV modules. A good package should be durable, chemically and mechanically resistant, electrically insulator and moisture protective: for these reasons, fluoropolymers seem to be the obvious choice. Despite their promising properties were not fully investigated, in literature it is possible to find applications of fluoropolymers in imaging solar concentrators [28]. The most important limitation factor to their large scale usage is probably the high cost.

In the next section the attempts to optimize the luminescent solar concentrators will be shown.

I.6.3 LSC device optimization

In the attempt to increase the performance of LSC's several device improvements have been made [30 – 38].

As already said, reabsorption losses are one of the most limiting factor in LSC technology. One way to solve the problem is the use of patterned thin films [29]. The surface area coverage of the dye molecules is reduced when the dye coating is deposited as line patterns separated by regions of clear waveguide. Decreasing surface area coverage reduces the probability of interaction between re-emitted photons and dye molecules, thereby minimizing reabsorption losses. A schematization of the concept of patterned layers is presented in figure I.15

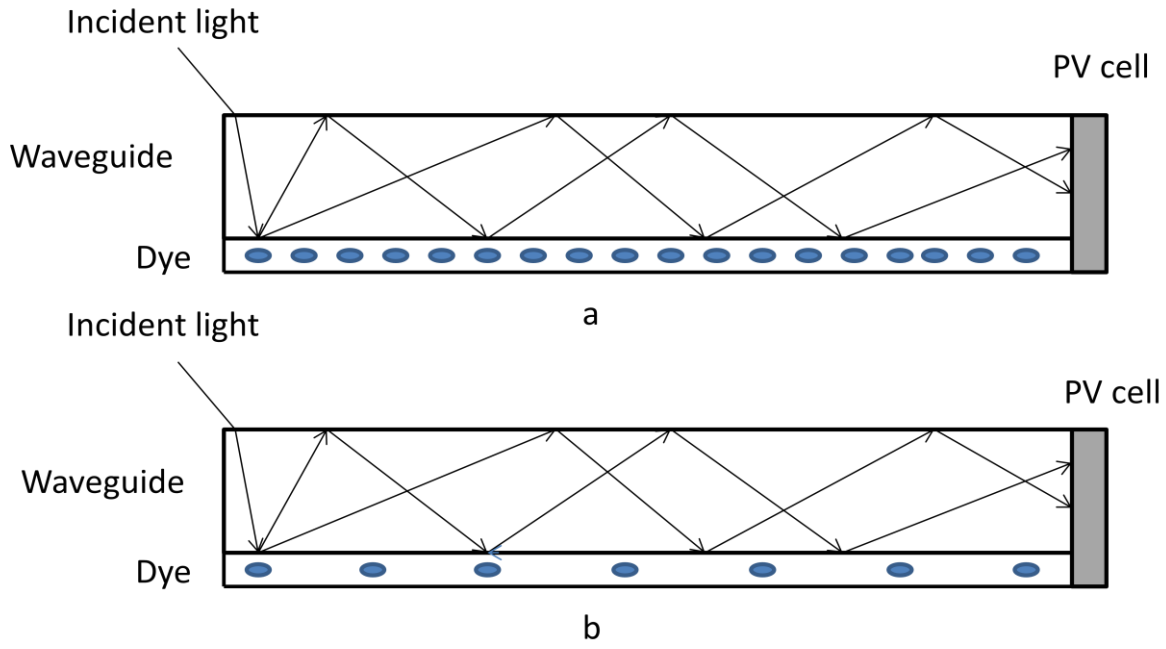

Figure I.15 a) Full area LSC b) Concept of patterned surface. If a pattern surface is considered, during TIR a photon will have a reduced probability to be reabsorbed while if the full area is considered this probability is increased.

Tsoi et al. [29] showed that standard photolithography can be employed to realize the pattern. But a reduction in edge emission has also been observed as the coverage area is gradually reduced because less photons are absorbed and re-emitted. So, despite the efficiency increases as the coverage area is reduced, the amount of absorbed light decreases and similarly the edge emission. In the same paper a study is proposed to determine if dimensional and geometric effects affect edge emission and efficiency. A series of samples consisting of equally spaced lines were prepared and the number of lines was varied. For the same coverage area, a five line patterned film was shown to have the same edge emission of

the ten line sample. A slight difference in relative efficiency (5% improvement for the 10 line samples) was reported due to the greater number of re-encounter events in the 5 lines sample. Tsoi et al. concluded that line width variations have little effect on the edge emission or the efficiency of the LSC system. A similar conclusion was obtained for geometry effects, by preparing a series of samples consisting of squares arranged in rectangular pattern. The area of the pattern was varied as already described.

As a way to increase the overall LSC efficiency, the use of different dyes in the same LSC was investigated [30]. This allows to increase the overall absorption spectrum system leading to the fabrication of an LSC system able to achieve an efficiency of 6.7%. A similar solution was employed by Hernandez-Noyola et al. [31] where a two layers systems was used, one of which constituted by quantum nanocrystals. This is an example of the so called *tandem* structures. To obtain higher power efficiencies, photons first hit by an LSC which can absorb short wavelength photons while long wavelength photons are transmitted and are absorbed by the second LSC. Between the two LSC's layers an air gap is placed thus forming a sequence of high and low index of refraction layers stacked onto each other. The sequence of high and low index of refraction resembles the concept of photonic crystal which is used in [30, 32, 33]. A photonic crystal provides a better confinement of light into the waveguide which results in a higher LSC performance.

Another way to increase the efficiency of a LSC is to attach mirrors on the edges of the luminescent plate [34] thus reducing losses from the escape cone by reflection of the escaped cone photons back to the plate. The use of bottom white back reflectors is a possible alternative to reduce photons escaped from the escape-cone [30] and increasing LSC efficiency by about 35% with respect to a black back reflector. White paints, also commercially available, have been already used in the photovoltaic industry [35, 36] as back coating for antireflection films. These paints are composed by a carrier in which pigments like titanium dioxide TiO_2 are dispersed. In order to characterize the paint it is important to identify the pigment volume concentration, defined as the ratio of the pigment volume to the entire paint volume. Along this lines a study on LSC performance with a white back scatterer and a wavelength selective mirror on top was presented [37]. This selective mirror is composed by a right handed chiral nematic (cholesteric) liquid crystal which is easily

deposited from solution and its aim is to reduce the loss of light through the top surface of the waveguide. An air gap is ensured between the LSC plate and the mirror. The results obtained showed that the cholesteric layer can enhance the light edge output up to 12% and can recover up to 30% of the light normally lost through the escape cone. The advantage of using diffuse back reflectors was also shown in the work by Sloof et al. [38], where a PCE of 7.1% was obtained, resulting in a 20% increase in the measured current.

Research has moved also towards the study of waveguide materials. In particular a study on different waveguide materials was presented by Earp et al. [39]. PMMA (n = 1.49), glass B270 (n = 1.52) two different polycarbonates which differ only in appearance (n = 1.59) and quartz (n = 1.46) were examined. It was concluded that several factors must be taken into account in determining the waveguide material to be used: the refractive index, durability and economic aspects must be considered. From this work quartz was found to be the most suitable material as waveguide.

In the literature there are other additional papers which focus on the maximization of the light output by acting on waveguide length [30, 34] and on dye concentration [40].

I.6.4 LSC degradation

Being composed primarily by organic materials, also LSC suffers from degradation which limit luminescent solar concentrator commercialization on the market. No commercialization will be viable until lifetimes of at least 10 years can be ensured [22]. Photodegradation of both matrix and dye are the most limiting factor for LSC performance [40]. The state of the art of degradation studies is not very developed: indeed very few papers are available in literature [41]. One of them, by R. Kinderman et. al [41], focuses on dyes stability. LSC research began in the 70's but the first results were not very promising due to their poor stability. The stability of the dye can be threaten by several factors including intrinsic instability, reaction with impurities or additives and light induced degradation. The primary visible effect is a reduced absorbance. In one of the first papers focusing on dye stability [41] different types of dyes were subjected to four weeks of continuous exposure and it was found that the most promising fluorescent dye are Lumogen

F series, manufactured by BASF. Residual additives were shown to have a detrimental effect on LSC degradation. Moreover it was suggested that the use of inorganic dyes could increase LSCs lifetime because of their low sensitivity to matrix impurities. An additional study on the effect of degradation was presented by van Sark et al [42]. In this study the samples (LSC doped with Lumogen R305) were illuminated by a sulphur lamp and UV-vis spectra were taken at regular time intervals. It was found that under sulphur lamp the LSC shows a decrease of 20% in EQE but the absorption remained the same. This is an indication that the dyes were absorbing the same amount of light but less re-emitted photons were able to reach the cell because of the increased number of dissipative processes. This was also observed by Seybod et al. [43] for perylene dyes. UltraViolet (UV) radiation is mostly responsible for dye photodegradation but degradation can also be induced also by visible light as in the case of CRS040 dye (a coumarin based one) [44].

LSCs are a really promising technology to reduce costs by keeping constant PV performances, but a significant amount of work still remains to be done especially in the field of stability of materials and devices.

I.7 References

[1] J. Poortmans and V. Arkhimpov, “Thin film solar cells: fabrication, characterization and applications” Ed. Wiley, 2006, pp 97 – 123;

[2] S. M. Sze and Kwok K. Ng, “Physics of semiconductor devices”, 3rd edition, Ed. John Wiley and Sons, 2007 pp 663 – 667;

[3] B. Kippelen and J.L. Bredas, “Organic ptohovoltaics”, Energy and Environmental Science, 2, 2009, pp 251 – 261;

[4] A. Goetzberger and V. U. Hoffmann, “Photovoltaic solar energy generation”, Ed. Springer, 2005 pp 11 – 16;

[5] R. F. Pierret, “Semiconductor device fundamentals”, Ed. Addison-Wesley publishing company, 1996 pp 23 – 149;

[6] R. W. Miles, G. Zoppi and I. Forbes, “Inorganic photovoltaic cells”, Materials Today, 10, 2007, pp 20 – 27;

[7] H. Ehrenreich and J. H. Martin, “Solar photovoltaic energy”, Physics Today, 32, 1979, pp 25 – 32;

[8] J. H. Zhao, A. H. Wang, M. A. Green and F. Ferrazza, “19.8% efficient “honeycomb” textured multicrystalline and 24.4% monocrystalline silicon solar cells”, Applied Physics Letter, 73, 1998, 1991 – 1993;

[9] S. Fransilla, “Introduction to microfabrication”, Ed John Wiley and Sons, 2004, pp 35 – 45;

[10] F. C. Krebs, “Fabrication and processing of polymer solar cells: a review of printing and coating techniques, Solar Energy Materials & Solar Cells, 93, 2009, 394 – 412;

[11] Z. He, C. Zhong, X. Huang, W.Y. Wong, H. Wu, L. Chen, S. SU, and Y. Cao, “Simultaneous enhancement of open-circuit voltage, short-circuit current density, and fill factor in polymer solar cells”, Advanced Materials, 23, 2011, pp. 4636 – 4643;

[12] M. Jørgensen, K. Norrman and F. C. Krebs “Stability/degradation of polymer solar cells, Solar Energy Materials & Solar Cells, 92, 2008, pp 686 – 714;

[13] A. Rivaton, S. Chambon, M. Manceau, J. L. Gardette, N. Lemaitre and S. Guillerez, “Light-induced degradation of the active layer of polymer-based solar cells, Polymer Degradation and Stability, 95, 2009, pp 1 – 7;

[14] G. Griffini, J. D. Douglas, C. Piliego, T. W. Holcombe, S. Turri, J.M. J. Frechet and J. L. Mynar, “Long-term thermal stability of high-efficiency polymer solar cells based on photocrosslinkable donor-acceptor conjugated polymers”, Advanced Materials, 23, 2011, pp 1660 – 1664;

[15] Michael Gratzel, “Photoelectrochemical cells”, Nature, 414, 2001, pp 338 – 344;

[16] G. Smestad, H. Ries, R. Winston and E. Yablonovitch, “The thermodynamic limits of light concentrators”, Solar Energy Materials, 21, 1990, pp 99 – 111;

[17] D. Barlev, R. Vidu and P. Stroeve, “Innovation in concentrated solar power”, Solar Energy Materials & Solar Cells, 95, 2011, pp 2703 – 2725;

[18] M. G. Debije and P. C. Verbunt, “Thirty years of luminescent solar concentrators research: Solar energy for the built environment”, Advanced Energy Materials, 2, 2012, pp 12- 35;

[19] M. G. Debije, P. P. C. Verbunt, P. J. Nadkarni, S. Velate, K. Bhaumik, S. Nedumbamana, B. C. Rowan, B. S. Richards and T. L. Hoeks, “Promising fluorescent dye for solar energy conversion based on a perylene perinone”, Applied Optics, 50, 2011, pp 163 – 169;

[20] M. A. El-Shahawy and A. F. Mansour, “Optical properties of some luminescent solar concentrators”, Journal of Materials Science in Electronics, 7, 1996, pp 171 – 174 ;

[21] C. L. Mulder, L. Theogarajan, M. Currie, J. K. Mapel, M. A. Baldo, M. Vaughn, P. Willard, B. D. Bruce, M. W. Moss, C. E. Clifford, E. McLain and J.P. Mirseman, “Luminescent solar concentrators employing phycobilisomes, Advanced Materials, 21, 2009, 3181 – 3185;

[22] B. C. Rowan, L. R. Wilson and B. S. Richards, “Advanced materials concepts for luminescent solar concentrators, Ieee Journal of Selected Topics in Quantum Electronics, 14, 2008, 1312 – 1322;

[23] S.M. El-Bashir, Photophysical properties of fluorescent PMMA/SiO_2 nanohybrids for solar energy applications, Journal of Luminescence, 132, 2012, pp 1786 – 1791;

[24] Y. S. Lim, C. K. Lo and G. B. The, “Unsaturated polyester resin blended with MMA as potential host matrix for luminescent solar concentrator”, Renewable Energy, 45, 2012, pp 156 – 162;

[25] M. Buffa, S. Carturan, M.G. Debije, A. Quaranta and G. Maggioni, “Dye doped polisiloxane rubbers for luminescent solar concentrator systems, Solar Energy Materials & Solar Cells, 103, 2012, pp 114 – 118;

[26] V. Fattori, M. Melucci, L. Ferrante, M. Zambianchi, I. Manet, W. Oberhauser, G. Giambastiani, M. Frediani, G. Giachi and N. Camaioni, “Poly(lactic acid) as a transparent matrix for luminescent solar concentrators: a renewable material for a renewable energy technology”, Energy & Environmental Science, 4, 2011, pp 2849 – 2853;

[27] M. DeBergalis, “Fluoropolymer films in the photovoltaic industry”, Journal of Fluorine Chemistry, 125, 2004, pp 1255 – 1257;

[28] R. H. French, J. M. Rodriguez-Parada, M. K. Yang, R. A. Derryberry and N. T. Pfeiffenberger, “Optical properties of polymeric materials for concentrator photovoltaic systems”, Solar Energy Materials & Solar Cells, 95, 2011, pp 2077 – 2086;

[29] S. Tsoi, D. J. Broer, C. W. M. Bastiaansen and M. G. Debije, “Patterned dye structures limit reabsorption losses in luminescent solar concentrators”, Optics Express, 18, 2010, pp 536 – 543;

[30] J. C. Goldschmidt, M. Peters, A. Bösch, H. Helmers, F. Dimroth, S. W. Glunz and G. Willeke, “Increasing the efficiency of fluorescent concentrator systems”, Solar Energy Materials & Solar Cells, 93, 2009, pp 176 – 182;

[31] H. Hernandez-Noyola, D. H. Pottersveld, R. J. Kolt and S. B. Darling, “Optimizing luminescent solar concentrator design”, Energy Environmental Science, 5, 2012, 5798 – 5802;

[32] G. Kocher-Oberlehner, M. Bardosova, M. Pemble and B. S. Richards, “Planar photonic solar concentrators for building-integrated photovoltaics”, Solar Energy Materials & Solar Cells, 104, 2012, pp 53 – 57;

[33] Y. F. Xiao, C. L. Zou, Y.W. Hu, Y. li, L. Xiao, F.W. Sun and Q. Gong, “Broadband enhancement of light harvesting in a luminescent solar concentrator, IEEE Journal of Quantum Electronics, 47, 2011, pp 1171 – 1176;

[34] L. H. Slooff, A. R. Burgers and E. Bende, “The luminescent solar concentrator: a parameter study towards maximum efficiency, in Proc. Of SPIE, Photonics for solar energy systems II, 2008, pp 700209-1 – 700209-7;

[35] B. Lipovsek, J. Krc, O. Isabella, M. Zeman and M. Topic, “Analysis of thin-film silicon solar cells with white paint back reflectors”, Physics Status Solid, 7, 2010, pp 1041 – 1044;

[36] o. Berger, D. Inns and A. G. Aberle, “Commercial white paint as back surface reflector for thin-film solar cells, Solar Energy Materials & Solar Cells, 91, 2007, 1215 – 1221;

[37] M. G. Debije, M-P. Van, P. P. C. Verbunt, M. J. Kastelijn, R. H. L. van der Blom, D. J. Broer and C. W. M. Bastiaansen, “Effect on the output of a luminescent solar concentrator on application of organic wavelength-selective mirrors”, Applied Optics, 49, 2010, pp 745 – 751;

[38] L. H. Sloof, E. E. Bende, A. R. Burgers, T. Budel, M. Pravettoni, R. P. Kenny, E. D. Dunlop and A. Buchtemann, “A luminescent solar concentrator with 7.1% power conversion efficiency”, Physic Status Solid, 2, 2008, pp 257 – 259;

[39] A. A. Earp, G. B. Smith, P. D. Swift and J. Franklin, “Maximising the light output of a luminescent solar concentrator”, Solar Energy, 76, 2004, pp 655 – 667;

[40] C. Haines, M. Chen and K. P. Ghiggino, “The effect of perylene diimide aggregation on the light collection efficiency of luminescence concentrators”, Solar Energy Materials & Solar Cells, 105, 2012, pp 287 – 292;

[41] R- Kinderman, L. H. Sloof, A. R. Burgers, N. J. Bakker, A. Butchemann, R. Danz and J. A. M. van Roosmalen, “I-V performance and stability study of dyes for luminescent plate concentrators, Journal of Solar Energy Engineering, 129, 2007, pp 277 – 282;

[42] W. G. J. H. M. van Sark, K. W. J. Barnham, L. H. Sloof, A. J. Chatten, A. Butchemann, A. Meyer, S. J. McCormack, R. Koole, D. J. Farrell, R. Bose, E. E. Bende, E. R. Burgers, T. Budel, J. Quilitz, M. Kennedy, T. Meyer, C. De Mello Donega, A. Meijerink and D. Vanmaekelbergh, “Luminescent solar concentrators – A review of recent results”, Oprics Express, 16, 2008, pp 21773 – 21792;

[43] G. Seybod and G. Wagenblast, “New perylene and violanthrone dyestuffs for fluorescent collectors”, Dyes Pigments, 11, 1989, pp 303 – 317.

II

OLSC devices: materials and fabrication techniques

In this chapter the reader will find an overview of the materials used in this work to fabricate organic luminescent solar concentrators but also the fabrication technologies used. The processes which lead to LSC building will be shown, from solution preparation to deposition techniques, including PV cells bonding.

II.1 Materials

II.1.1 Lumogen F Red 305

Lumogen F Red 305 (LFR305) is a perylene-based red fluorescent dye produced by BASF. LFR305 molecular formula is shown in figure II.1.

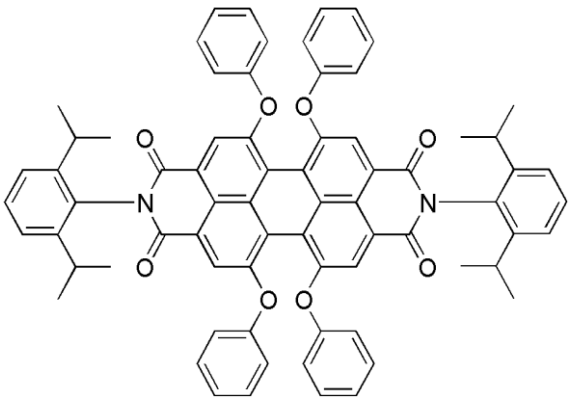

Figure II.1 Molecular formula of Lumogen F Red 305.

LFR305it is constituted by a perylene core and six lateral substituents including four aromatic rings linked to the core by carbon-oxygen-carbon single bonds. Aromatic rings with isopropyl groups as lateral substituents are the two remaining substitutents that are attached to the central core by nitrogen-carbon bonds. The physical form of LFR305 is that of a reddish powder which is largely soluble in aromatic solvents but also in polar ones. It can be easily incorporated in polymeric matrices like poly(methylmethacrylate), poly(styrene), poly(carbonate) or poly(ethylenetherephthalate) which make Lumogen F Red305 a perfect dye for LSC purposes.

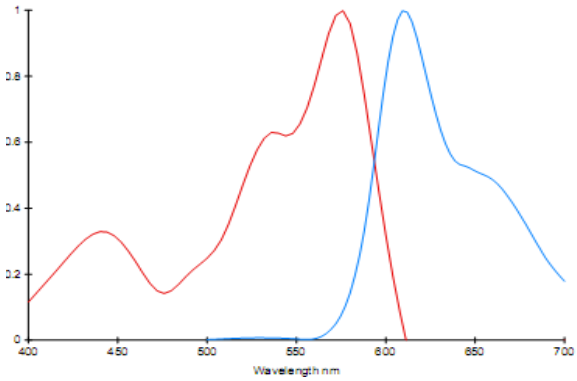

Figure II.2 The absorption spectrum of Lumogen F Red 305 Is depicted in red. Emission spectrum is represented in blue. Both refers to dye dissolved in liquid solution of CH_2Cl_2.

Figure II.2 presents the absorption (red) and emission (blue) spectra of this perylene-based dye in solution. Absorption peak is at 578 nm while the emission one is at 613 nm. The reported spectra are relative to the UV-visible region (380 nm – 760 nm). LFR305 has a fundamental physical characteristic, its high quantum yield: as indicated in the product datasheet, it is higher than 90%.

II.1.2 Poly(methylmethacrylate)

Poly(methylmethacrylate) also known by the acronym PMMA is a thermoplastic polymer, largely used in optics due to its high transparency. Like a glassy polymer PMMA has a glass transition temperature in the range 105 – 120°C. Figure II.3 shows the molecular formula of the repeating unit which gives rise to poly(methylmethacrylate). PMMA is solid at room temperature but if it is put in contact with chlorinated or aromatic compounds it rapidly dissolves thus showing good solubility in this kind of solvents. As mentioned above, PMMA is

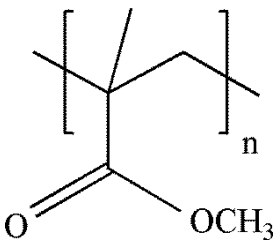

Figure II.3 Monomeric repeating unit of Poly (methylmethacrylate).

optically transparent in the visible region of the spectrum and has a refractive index of about 1.5.

The main advantage in using PMMA usage is the low costs. However also mechanical and chemical resistances make PMMA the preferred polymer as host matrix.

II.1.3 Lumiflon LF-910LM

Lumiflon LF-910LM produced by ASAHI GLASS CO.LDT is already known as fluoroethylene vinylether (FEVE) copolymer. LF-910LM is a reactive polymer whose backbone is partially fluorinated while the lateral substituents are some oxydrilic groups. LF-910LM presents other lateral substituents whose nature is not disclosed but their function is to increase transparency, flexibility, crosslinkability and pigment compatibility. Figure II.4 presents the simplified molecular formula of Lumiflon LF-910LM. As indicated in the datasheet, OH value for LF-910LM is around 100 (mg KOH)/(g polymer). At room temperature LF-910 is a viscous liquid characterized by a yellowish color. Lumiflon is diluted with xylene as solvent: the ratio between LF-910LM and xylene is approximately 2:1 by weight. Generally it shows good solubility in chlorinated and aromatic hydrocarbons.

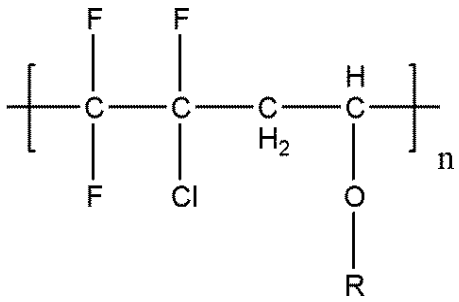

Figure II.4 Monomeric repeating unit of Lumiflon LF-910. R stands for laterals substituents whose nature is not disclosed. The only information available is that R contributes to increase some properties like transparency, flexibility, crosslinkability and pigment compatibility.

Lumiflon LF-910LM is recommended for applications in which long-lasting weatherability have a predominant role (e.g. aerospace applications). LF-910LM cannot be used but must be subjected to crosslinking: several crosslinking agents can be used as can be seen in the following sections.

II.1.4 Tolonate HDT-LV2

Tolonate HDT-LV2 is a solvent free low viscosity aliphatic polyisocianate based on Hexamethylene Diisocianate cyclic trimer (HDI isocyanurate). It is produced by PERSTOP and is typically used as cross-linker of hydroxylated polymers in the preparation of two component polyurethane systems showing excellent outdoor durability and mechanical properties. It is soluble in esters, ketones and aromatic hydrocarbons. In the pristine state it has about 23% of NCO substituents by weight. Figure II.5 presents the molecular formula of the basic unit of Tolonate HDT-LV2.

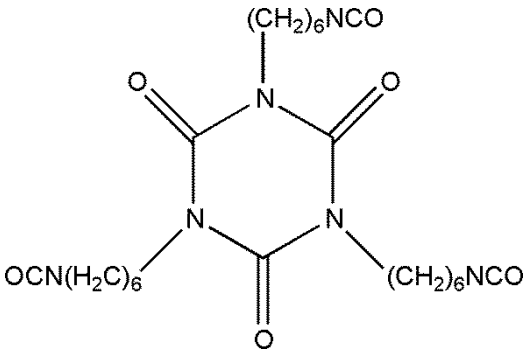

Figure II.5 Molecular formula of the hexamethylene diisocianate cyclic trimer.

II.1.5 Vestanat T1890/100

Vestanat T1890/100 supplied by EVONIK INDUSTRIES is a cycloaliphatic polyisocianate based on isophorone diisocyanate. Figure II.6 shows the structure of Vestanat T1890/100. The basic unit of Vestanat T1890/100 is the isocyanurate ring with an average NCO functionality between 3 and 4. NCO content is 17% and is quite lower than Tolonate HDT-LV2. Vestanat T1890/100 has especially been developed as an isocyanate crosslinking agent for coatings or adhesives and is supplied as pellets. This cross-linker agent is soluble in all types of conventional non-protic solvents like ketones, esters, aromatics and chlorinated hydrocarbons.

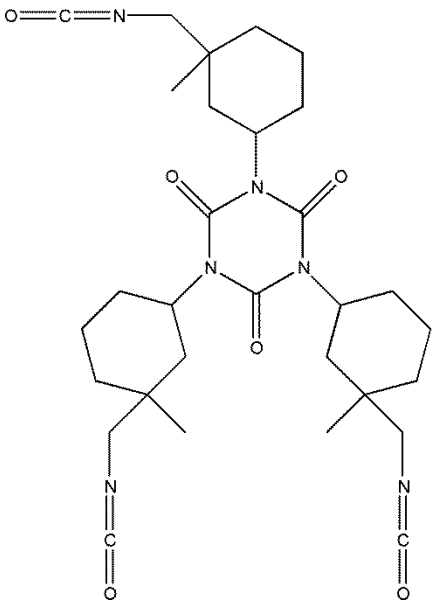

Figure II.6 Molecular formula of the basic unit of Vestantat T1890/100, the cyclic trimer of the isophorone diisocyanate.

II.1.6 Cymel 303

Cymel 303 supplied by CYTEC is a versatile crosslinking agent based on hexamethoxymethylmelamine (HMMM, shown in figure II.7). This kind of crosslinking agent can be used in crosslinking of both waterbone and organo-soluble polymers, containing carboxyl, hydroxyl or amide groups such as epoxy resins and polyesters. It is soluble in most commonly used organic solvents like aromatic hydrocarbon, alcohols, ketones and ester but has a very low solubility in water. At room temperature Cymel 303 appears as a transparent and solvent-free viscous liquid.

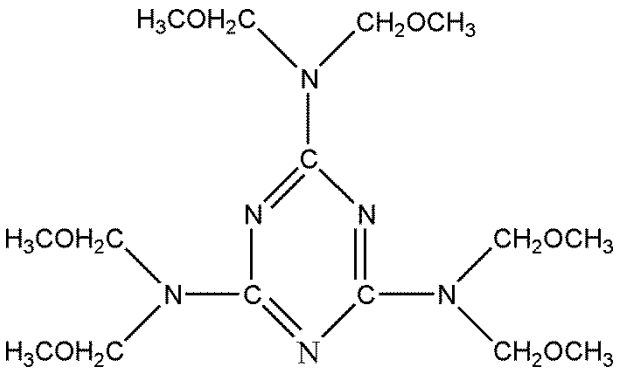

Figure II.7 Molecular structure of hexamethoxymethylmelamine (HMMM).

II.1.7 Hindered Amine Light Stabilizer (HALS)

Degradation upon light exposure is one of the main limitations of polymers for outdoor applications. To mitigate and prevent the effect of light induced degradation, several attempts have been made including the use of stabilizing additives like hindered amine light stabilizers (HALS). These kinds of compounds are based on tetramethyl piperidine derivatives and are excellent alkyl radical scavengers.

In general all the polymers contain or form a certain amount of hydroperoxide groups (P-OOH, where P stands for the alkyl chain) due to the processing step or to thermo-oxidative degradation [1]. The hydroperoxide species absorbs in the UV, resulting in the generation of radicals and their successive propagation. P-OOH is indeed unstable and lead to OH^* radical formation. The operating mechanism of HALS can be explained by the reaction of alkyl radicals with the active species nitroxy radicals, NO^*, thus giving the aminoether species

(NOR). The aminoether terminates peroxy radicals and generates the nitroxyl specie (NO^*). HALS perform a catalytic action but not a sacrificial one because at the end of the cycle the additive is regenerated. This supports the use of HALS in long term stabilization strategies. It can be said that conventional HALS need an activation step which in turn is the formation of the NOR species. The schematic functioning of HALS is reported in figure II.8.

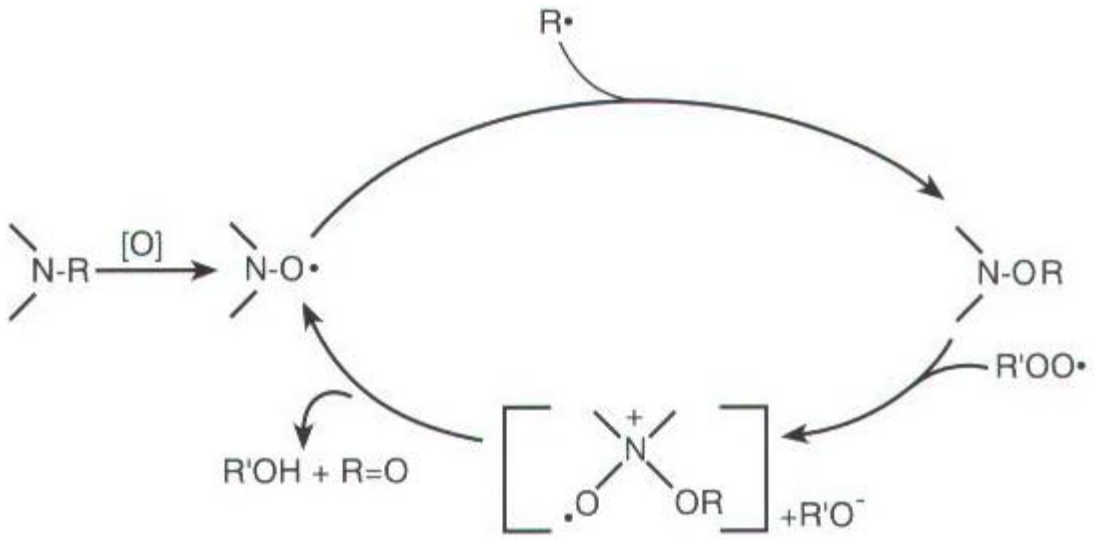

Figure II.8 Schematic functioning mechanism of HALS.

In this work two kinds of HALS have been used: Ciba Tinuvin 292 and Ciba Tinuvin 123.

II.1.7.1 Ciba Tinuvin 292

Ciba Tinuvin 292 is a liquid hindered amine light stabilizer especially developed for coatings.

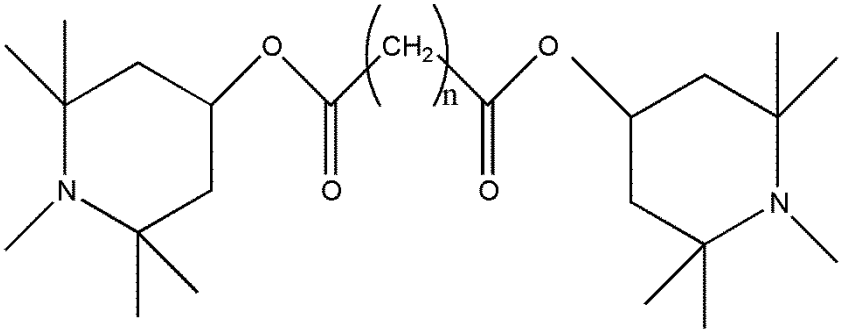

Figure II.9 Molecular formula of Ciba Tinuvin 292. This kind of HALS operates as the conventional theory predicts.

Tinuvin 292 active substance is a mixture and its molecular formula is reported in figure II.9. It is soluble in solvents like xylene, chloroform but not in water. Tinuvin 292 is recommended in coating application, industrial topcoats and radiation curable coatings. Tinuvin 292 operates as the conventional theory predicts (see the previous paragraph) and indeed needs an activation step.

II.1.7.2 Ciba Tinuvin 123

Ciba Tinuvin 123 is a liquid HALS based on aminoether functionality (the molecular formula is reported in figure II.10).

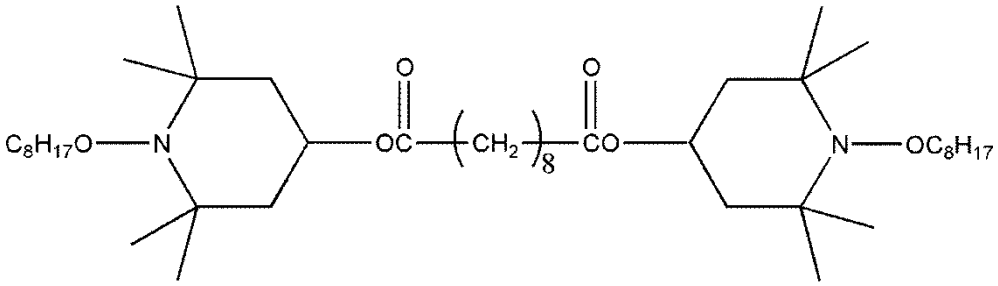

Figure II.10 Molecular formula of Ciba Tinuvin 123

Tinuvin 123 is a free radical scavenger based on a NOR functional group: theory suggests that the hindered amine oxidizes to form nitroxyl radicals (NO^*) which in turn react with the free radicals (R^*) generated during photooxidation of the coating to form an aminoether (NOR), a non-radical species. This kind of HALS does not need the activation step as the conventional ones because the molecule directly incorporates the NOR active specie.

II.1.8 PE 399 Krystalflex

PE 399 Krystalflex by HUNTSMAN INTERNATIONAL LLC is a thermoplastic polyurethane (TPU) adhesive that becomes soft and processable when heated and hard when cooled. Krystalflex appears as a transparent film with good adhesion properties if heated. In the present work

we have used Krystalflex to bond the PV cell to the edge of the glass substrate in the organic luminescent solar concentrators (OLSC) fabrication. The characteristic which identifies Krystalflex as a good bonding agent is the refractive index which is very close to that of glass: Krystalflex has an index of refraction of about 1.5 which allows the quasi-perfect continuity in the refraction index by passing from the glass plate to the PV cell. This is a fundamental characteristic because an higher loss of photons would occur at increasing refraction index differences caused by light scattering.

II.1.9 Ti-pure R-706

Ti-pure R-706 is a rutile titanium dioxide pigment whose color is white. For this reason Ti-pure R-706 could be used in reflective coatings also for its excellent high gloss, good durability and excellent dispersibility. This kind of pigment can be easily dispersed in organic matrices like poly(methilmethacrylate) and poly(carbonate). Titanium dioxide is used in reflective coatings as exemplified by the enormous number of papers available in literature also for its exceptional durability properties.

II.2 LSC devices fabrication

This paragraph is an overview of the techniques used in the fabrication of organic luminescent solar concentrators, including the white back reflectors. All the basic information about the instrumentation will be given but also techniques used in order to complete the LSC fabrication will be introduced.

II.2.1 OLSC fabrication

Several steps are necessary to fabricate a complete LSC: in this section all the passages are shown.

II.2.1.1 Solution preparation

To prepare luminescent solar concentrators with PMMA as host matrix a pre-determined amount of PMMA was put into a flask with chloroform as solvent. The ratio in weight between PMMA and chloroform has a specific value as will be illustrated in the next chapter. Moreover, we also put a precise amount of Lumogen F Red 305: this quantity is calculated from the PMMA weight and must fulfill a precise ratio in weight. Once all the reagents have been put into the flask with a magnetic stirrer, the container is closed and is left under magnetic stirring for three hours.

For LSC's with fluorinated polymers as host matrices, the process is quite similar to that used for PMMA but with some difference. To have a fluorinated host matrix with Lumiflon LF-910FM we have to use a crosslinking agent (Cymel, Vestanat or Tolonate). For this reason, a given quantity of Lumiflon, the chosen crosslinking agent at a given ratio with respect to the fluorinated polymer, chloroform as solvent and a pre-determined quantity of dye are put all together in the batch. The solution obtained is put under magnetic stirring for three hours. In addition, for the systems containing crosslinking agents, it is convenient to prepare another solution which contains a catalyst to get a complete crosslinked structure in a reduced time. For Tolonate and Vestanat the catalyst employed is di-*n*-butyltin dilaurate 95%, while for Cymel the catalyst is toluene-4 sulfonic acid monohydrate. Di-*n*-butyltin dilaurate 95% is dissolved in chloroform while toluene-4 sulfonic acid monohydrate is dissolved in toluene. The amount of catalyst which is used to promote crosslinking is 1% in weight with respect to the total solid weight content present in the solution. Catalysts are added to the flask containing solutions just before the deposition process (see next section) and solutions are left under magnetic stirring for an additional minute to allow complete mixing after which the deposition process takes place.

II.2.1.2 Thin film deposition technique: spin-coating

Fluorescent thin films have to be deposited on top of a glass substrate. In this work we use a glass substrate whose width is constant (25 mm) while length can be varied from 12.5 mm to

75 mm. Before film deposition, glass substrates are cleaned with acetone and a sheet of paper to ensure an optical transparency.

Spin-coating permits to realize coating of various thicknesses depending on several variables. Among these, the most useful process parameters are percentage of solid with respect to solvent, surface tension of the liquid solution, rotational speed time. This is a two step process: deposition of solution and then spinning around the axes perpendicular to the substrate surface area.

The glass substrate is attached to the spin-coater by vacuum via a vacuum pump. An excess amount of solution is withdrawn from the flask and then poured on top of the glass substrate. Once this step is completed, the rotational step can be initiated. The substrate which will be put in rotation will experience a centrifugal force which spreads the solution on the whole substrate surface and eventually off its edges. High number of rotations per minute (rpm) will cause a thinner coating while a low rpm causes a thicker film. Substrate thickness is not affected only by rotational speed but also by duration of the rotation: a longer spinning time creates thinner films while a shorter one creates thicker films. In addition, viscosity of the solution plays an important role. It is clear that a highly viscous solution can be spinned with difficulty while a less viscous one is deposited with less difficulty. An empirical law has been proposed [2] where the thickness of the deposited film can be estimated by:

$$d = k\omega^{\alpha} \qquad \text{Eq.1}$$

Where d is thin film thickness, ω is angular velocity, k and α are empirical constants related to the physical properties of the solvent, solute and substrate. Speed and duration of the rotation are adjusted in order to obtain the desired thickness of the film and complete the evaporation of the solvent. Film thickness is a balance between two forces: the force applied to shear the liquid towards the edge of the substrate and the drying rate which affects the viscosity of the solution. In particular, as the solvent dries out, the viscosity of the solution increases until the radial force of the spin process can no longer appreciably move the

compound over the surface. At this point, the film thickness will not decrease significantly with increased spin time.

The substrate always exerts an acceleration which contributes in determining the coated film properties. The solution begins to dry during the first part of the spin cycle, therefore controlling the acceleration is a crucial point. Typically about 50% of the solvent evaporates in the first few seconds of the process.

In this work 1200 rpm for 40 seconds are used in order to deposit luminescent thin films.

II.2.1.3 Crosslinking

This process is crucial only for fluoropolymer-based host matrices. Once the deposition process is completed, luminescent solar concentrators with Lumiflon LF-910LM must be subjected to a thermal treatment in order to allow the crosslinking process to complete. Therefore all the fluorinated matrix LSC's are inserted in an oven where the temperature is set at 150° C and left there for 30 minutes. This optimal crosslinking time was identified on the basis of a series of preliminary Infrared spectroscopy tests which will be explained in the next chapter.

II.2.1.4 PV cell – LSC bonding

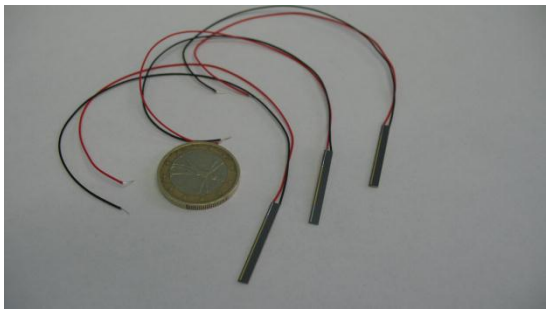

Figure II.11 Silonex SLSD-71N4 solar cells.

In this work we used Silonex SLSD-71N4 solar cells (figure II.11). The bonding process, the one which comprises the attachment of the Silicon PV cell to the edge of the Luminescent plate, is really crucial in order to get the maximum performance of the LSC plate. Probably the bonding process is the most important and critical in the whole fabrication process. As stated previously, we make use of PE 399 Krystalflex as bonding agent. First of all a thin piece of Krystalflex is placed on the silicon photovoltaic cell while this is placed on a heated plate. To favor the bonding process, and

allow the Krystalflex to soften, the temperature is maintained at 140° C. Once the Krystalflex adheres to the cell it is possible to attach the LSC plate taking particular care in ensuring that the concentrator plate edge overlaps only with the cell active area. To achieve good bonding, the excess of PE 399 Krystalflex is removed by making use of a spatula. When the bonding agent cools down, it becomes hard and the PV attachment process is complete.

II.2.2 White back reflectors fabrication

White bottom reflectors are good tools to increase the overall performance of LSCs because they can reflect light which is transmitted through the luminescent plate and redirect it towards the waveguide. Moreover they are able to redirect also light which escapes from the waveguide via the escape cone.

The back reflectors we built are constituted by a white thin film deposited by means of spin-coating technique on top of a transparent glass substrate. PMMA was used as host matrix while the white pigment was Ti-Pure R706. As mentioned above this is constituted mainly by titanium dioxide which is the pigment giving the characteristic white color. PMMA and a specific amount of titanium dioxide are dissolved in a flask with chloroform and allowed to magnetically stirr for two hours. Then the solution is sonicated for one hour to better disperse the titanium dioxide particles to minimize aggregate formation. When the sonication step is complete, the spin-coating process can be performed. The spinning step is, at all extents, analogous to that described in the previous section but in this case the spinning speed is 600 rpm to favor the formation of a thicker film. Neither additional crosslinking processes nor any another treatment is required to complete the white back reflector fabrication process.

During the optimization of white back reflectors we tried to disperse some SiO_2 in the PMMA-TiO_2-$CHCl_3$ system to increase the surface roughness of the back reflectors. The fabrication step is nearly the same except that SiO_2 is added to the solution once the sonication step is finished. The solution which contains PMMA, TiO_2, chloroform and SiO_2 is left under magnetic stirring for an additional time of 15 minutes.

II.3 References

[1] A. Landuzzi, “Stabilizzanti UV”, in Additivi per Materiali Polimerici, Atti del XXIV Convegno Scuola AIM Mario Farina, 2002, pp. 145 – 173;

[2] F. C. Krebs, “Fabrication and processing of polymer solar cells: A review of printing and coating techniques”, Solar Energy Materials & Solar Cells, 93, 2009, pp. 394 – 412.

III
Experimental characterization methods

It is important not only to evaluate the performance of LSC in terms of PCE but also to give some additional information about e.g. the loss mechanisms. In this chapter the reader will find descriptions of all characterization methods used to evaluate the prepared LSC's. Moreover techniques to characterize back reflectors will also be discussed.

III.1 Fluorescence spectroscopy

III.1.1 Electronic transitions

An electronic transition consists of the promotion of an electron from an orbital of a molecule in the ground state to an unoccupied orbital in an excited state by absorption of a photon [1]. The photon which gives origin to the electronic transition has an energy equal or greater than the band gap between the ground state energy level and the excited state. Several transitions can occur, depending on the energy levels available. In absorption and fluorescence spectroscopy two important types of orbitals are considered: the Highest Occupied Molecular Orbital (HOMO) and the Lowest Unoccupied Molecular Orbital (LUMO). In the transition between two energy levels, the electron maintains, in principle, its spin unchanged so that the total quantum number remains equal to zero. Because the multiplicities of both the ground and the excited states are equal to 1 (the multiplicities of an energy level is determined by M which is defined as M = 2S +1 with S = $\sum_i s_i$, total spin number), both are called singlet states.

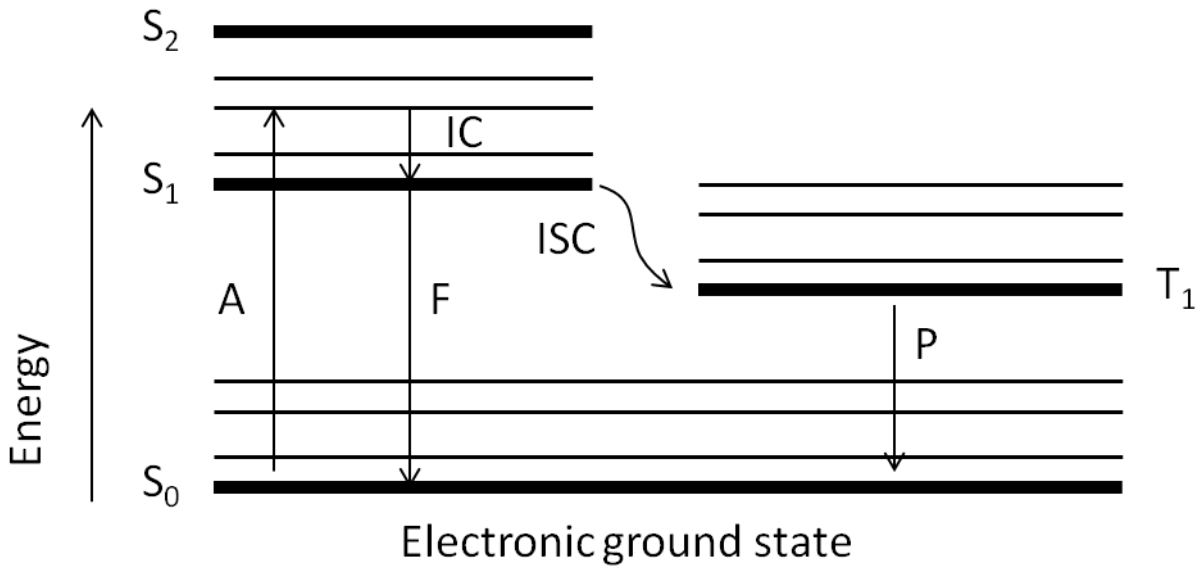

Figure III.1 Perrin – Jablonski diagram. S_0 stands for the electronic ground state. This is a singlet state. S_1 represents the first singlet excited energy level. T_1 is the first triplet excited energy state. A denotes the absorption of a photon, IC the internal conversion process which is non radiative and thus implies the dissipation of a certain amount of energy. F is representative of the fluorescence process which occurs from an excited singlet state to another singlet state. ISC represents the inter system crossing that is the passage of the excited molecule from an excited singlet state to an excited triplet state. P stands for phosphorescence and is always a de-excitation from a triplet state to a singlet state.

The corresponding transition is called singlet – singlet transition and is denoted by S: usually a subscript is also reported which denotes the energy level e.g. 0 stands for the ground state, 1 for the first excited state and so on. If during transition an electron undergoes on change of spin, the multiplicity changes from 1 to 3, giving rise to a triplet state which corresponds to three states of equal energy. The triplet state has a lower energy than the singlet state with the same configuration. The triplet state is denoted by T with a subscript as for the singlet state.

After the absorption event, the excited electrons can undergo several de-excitation processes which are represented in figure III.1 on the Perrin-Jablonski diagram.

Each singlet or triplet state has a certain number of vibrational sub-energy levels: photons absorbed can promote electrons directly into those vibrational energy levels. Every time an electron reaches a vibrational level, it will rapidly decay to the lowest vibrational level of the excited state via vibrational relaxation. The direct de-excitation to the ground state can occur either by non radiative processes or by emission of photons. De-excitation from singlet

state by emission of photons is named fluorescence (time scale of 10^{-9} seconds). In certain cases, electrons can pass from a singlet state to a triplet one even if this transition is in principle forbidden. This process is called inter system crossing. Once the electron is in the triplet state, it can experience de-excitation by photon emission (and this process is known as phosphorescence with a time scale of 10^{-7} seconds) or can reach the ground state by non radiative processes. Because of the high amount of energy lost in the transition between a singlet and a triplet state, phosphorescence occurs at longer wavelengths than fluorescence and the result is a smaller overlap between absorption and emission spectra.

III.1.2 Fluorescence Spectrofluorometres

Instruments for measuring fluorescence and phosphorescence spectra are usually similar between each other and are normally defined with the general term of luminescence spectrometers. With most spectrofluorometers is possible to record both excitation and emission spectra. An emission spectrum represents the wavelength distribution of an emission measured at a single constant excitation wavelength. Conversely, an excitation spectrum is the dependence of emission intensity, measured at a single emission wavelength, upon scanning the excitation wavelength [2].

The instrument consists of several parts of which the most important are a UV-Visible

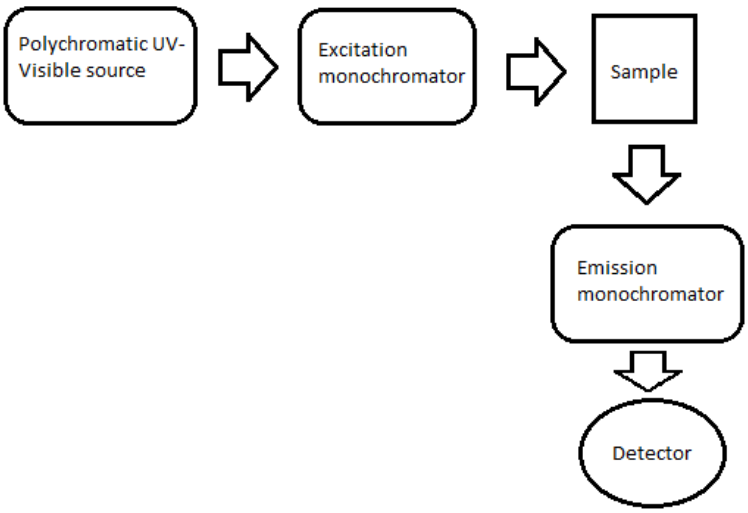

Figure III.2 General schematization of a fluorescence spectrofluorometer.

wavelength source, an excitation wavelength selector, a sample chamber and a detector. A generalized schematization of a fluorescence spectrofluorometer is reported in figure III.2.
Light emitted from an appropriate source passes through a monochromator where the unwanted wavelenghts are removed. Light then hits the sample which fluoresces (or phosphoresces) and emits radiation at different wavelengths which are registered by a detector. Generally spectrofluorometer are single beam instruments but they may also be two-beams. One beam is focused on the sample to be examined, the other on a reference fluorophore.
In this work, fluorescence spectra were recorded on a Jasco FP-6600 Spectrofluorometer. Samples were placed at 30° with respect to the excitation beam. In this way only the emitted light is detected, thus excluding the reflected component.
The set up parameters were:

- Excitation wavelength: 445 nm;
- Scan start: 520 nm;
- Scan end: 800 nm;
- Wavelength stop filter on the emitter side: 420 nm;
- Wavelength stop filter on the collector side: 515 nm;
- Sensitivity: low;
- Data pitch: 1 nm;
- Excitation band width: 5 nm;
- Emission band width: 6 nm;
- Scanning speed: 200 nm/min.

Let us now consider more in detail each component of a typical spectrofluorometer.

III.1.2.1 UV-Visible light source

Typically high pressure xenon lamps (Xe) are the most versatile light sources and are predominantly used in the spectrofluorimeter. This lamp provides a polychromatic light output approximately from 250 nm to 700 nm as a result of recombination of electrons with ionized Xe atoms. These ions are generated by collision of Xe atom with the electron that

flow across the arc: the recombination events generate photons. A special housing is designed to control the highly pressurized xenon gas (even 10 atm) in order to prevent explosions. The housing thus protects the user from the lamp. However the housing has an additional role, which is the collection and collimation of lamp output which is then focused into the entrance slit of the monochromator.

III.1.2.2 Monochromator

Light emitted from the source must be focused on the sample: the light beam has to be collimated and must be monochromatic. To this end, a series of mirrors collimate light and force it to pass through a slit whose width determines the resolution. A larger width yields an increased signal level but also a higher signal-to-noise ratios while a smaller slit width increases resolution, limiting light intensity. Figure III.3 schematically depicts the most common monochromator, Czerny – Turner. Monochromators are used to disperse polychromatic or white light into various colors or wavelengths. The spectrofluorometer is equipped with two monochromators, the first one which serves as excitation wavelength selector and the second one which is used as emission wavelength selector.

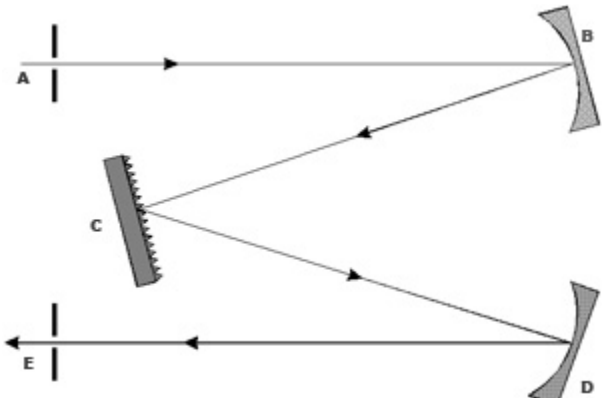

Figure III.3 Czerny-Turner monochromator.

Monochromators in most spectrofluorometers use diffraction gratings which serve as diffractive devices. However an alternative solution is the use of prisms or optical filters to be used for the same purpose as gratings. Sometimes both optical filters and monochromators are used to compensate the non ideal behavior of monochromators. A large variety of filters is available and their function is to transmit only incident wavelengths above a certain value, stopping all the others.

III.1.2.3 Detector

For fluorescence spectroscopy purposes a photomultiplier tube (PMT) is the ideal choice as photodetector. In practice, PMT are current sources: a photocathode which consists of a thin metallic film is connected to a series of dynodes (electrodes) with increasingly high potential. Incident photons coming from the illuminated sample cause electrons of the active film to be ejected as primary electrons from the surface; subsequently, primary electrons accelerate towards the first dynode. The impact between the electron and the dynode surface leads to emission of several secondary electrons which hit the second dynode surface causing emission of additional electrons. This cascade process permits to greatly amplify the input photons signal.

Obviously, only light entering the PMT can generate photocurrent.

III.2 UV-Visible spectroscopy

As discussed in the previous section, UV-Visible light absorption causes an electronic transition from an energetic ground state to an excited state. In particular, UV-Visible light causes electronic and vibrational excitations. By means of UV-Vis absorption spectroscopy it is possible to determine when a sample absorbs light and with which intensity. The output of a UV-Vis spectrophotometer is a plot of the absorbance or transmittance as a function of the incident wavelength. The fundamental difference between fluorescence and UV-Vis spectroscopy is that in the former case the de-excitation process is detected while in the latter only the excitation is considered.

The UV-Vis spectral region extends from 190 nm to 400 nm (UV range) and from 400 nm to 780 nm (visible range).

In this work, UV-Visible spectroscopy analysis were performed by means of a Jasco V-570 UV-VIS-Near spectrophotometer. The set up parameter were:

- Format: absorbance;
- Response: medium;
- Bandwidth: 5 nm;

- Start: 300 nm;
- End: 700 nm;
- Data pitch: 1 nm;
- Scan speed: 100 nm/min.

The extent at which a medium absorbs light is expressed by the Lambert-Beer law which will be briefly recalled in the next paragraph.

III.2.1 Lambert-Beer Law

The efficiency of light absorption at a wavelength λ by an absorbing medium is characterized by the absorbance *A(λ)* or by transmittance *T(λ)*. Transmittance and absorbance are defined as:

$$A(\lambda) = \log\left(\frac{I_\lambda^0}{I_\lambda}\right) = -\log T(\lambda) \qquad \text{Eq. III.1}$$

$$T(\lambda) = \left(\frac{I_\lambda^0}{I_\lambda}\right) \qquad \text{Eq. III.2}$$

Where I_λ^0 and I_λ are the light intensities of the beams entering and leaving the absorbing medium respectively. Usually absorbance follows a simple linear law, the Lambert-Beer law, which is written as follows:

$$A(\lambda) = \log\left(\frac{I_\lambda^0}{I_\lambda}\right) = \varepsilon(\lambda) l c \qquad \text{Eq. III.3}$$

$\varepsilon(\lambda)$ is the molar extinction coefficient (also known as the molar absorption coefficient), *l* is the optical path of the incoming light and *c* the concentration of the absorbing species. The molar absorption coefficient expresses the ability of a molecule to absorb light. It is important to notice that the Lambert-Beer law is valid for a generic absorbing medium. Thus this law will be recalled in the following also when Infrared spectroscopy will be introduced.

III.2.2 UV-Vis spectrophotometers

Generally, to obtain complete spectra in the UV-Vis range, dual beam dispersive scanning instruments or dispersive multi-channel instruments are employed. A spectrophotometer which allows to measure simultaneously the absorption spectra of a sample and reference is known as double-beam instrument. A UV-Vis scanning spectrophotometers consists of a light source, a monochromator, a chopper to generate two beams as well as to recombine them, a sample and a reference compartment and a detector [3]. A block diagram of a typical double beam spectrophotometer is reported in figure III.4.

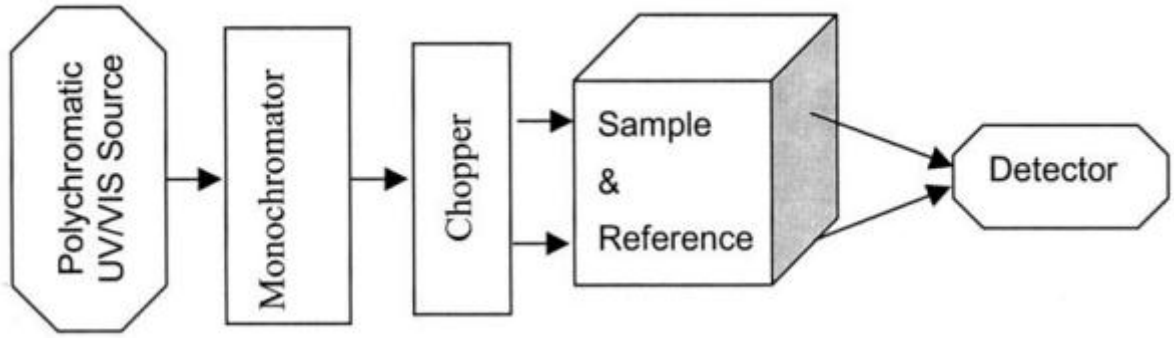

Figure III.4 Block diagram of a spectrophotometer. It consists of a polychromatic UV-Vis source whose light passes through a monochromator. Light which passes the monochromator is then redirected towards a chopper which generates two beams. One of the produced beam is incident on the sample while the other on the reference.

The working principle of UV-Vis absorption spectroscopy is similar to fluorescence spectroscopy.

The most commonly used light sources are deuterium lamps, halogen lamps and those based on a tungsten filament. Deuterium lamps are used in the region from 180 nm to 350 nm: an electric discharge passing through the deuterium gas excites the deuterium atoms which lose their energy as radiation. On the other hand tungsten filament and halogen lamps are used in the region from 330 nm to 900 nm. However if light source covering the entire UV-Vis range is required a complete range light source is required, xenon arc lamps can be used whose emission is from 175 nm to 1000 nm.

Monochromators (described in section III.1.3.2) are a really important part of the instrument because they permit to separate light of a defined wavelength from other wavelengths.

Sometimes it is possible to find UV-Vis spectrophotometer equipped with prism monochromator. Figure III.5 shows a prism monochromator.

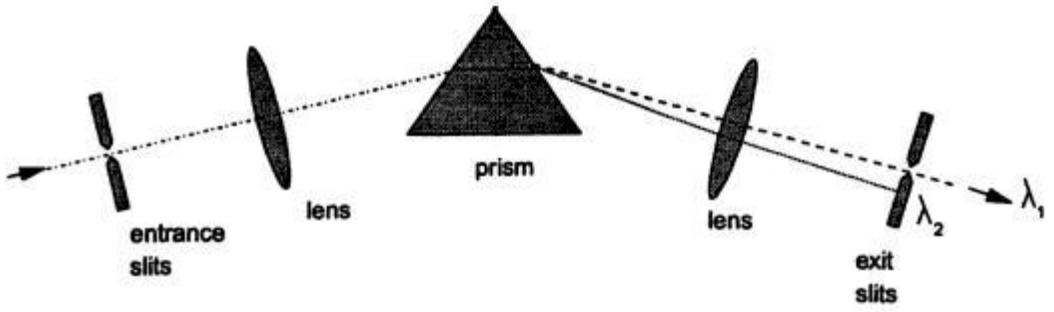

Figure III.5 Schematic view of a prism monochromator.

Light emitted from the light source enters in the monochromator from a slit and is focused by a lenses system on a prism. By exploiting the dependence of the index of refraction wavelength, white light will be diffracted in different directions. Shorter wavelengths are dispersed more strongly than longer wavelengths. Exiting light is focused by a second system of lenses on the exit slit where only a portion of wavelengths will be stopped while the remaining will pass. By acting on slits and lenses, it is possible to selet which wavelengths are allowed to pass. A description of detectors used in UV-Vis spectroscopy was presented in section III.1.2.3

III.3 Infrared Spectroscopy

Absorption of a photon by a molecule causes an electronic transition from ground state to excited states. Depending on the energy of light absorbed and the chemical nature of the absorbing species, excited states may differ significantly in nature. Upon absorption of an infrared photon, a molecule passes from the vibrational ground state to an excited vibrational state.

Due to the longer wavelengths used compared to the UV-Visible spectroscopy, in infrared spectroscopy it is common practice to use wavenumbers instead of wavelengths, defined as eq. III.4

$$\nu\ [cm^{-1}] = \frac{10000}{\lambda\ [\mu m]} \qquad \text{Eq. III.4}$$

where λ is the wavelength expressed in μm. IUPAC recommendations suggest that in a IR spectrum the values of wavenumber axis decrease from left to right while absorbance (or transmittance) is reported on the y-axis.

The infrared electromagnetic spectrum extends from 800 nm (12500 cm^{-1}) to 1mm (10 cm^{-1}). The mid - infrared (MIR) part of the IR spectrum is composed by all the wavelengths from λ = 2.5 µm (4000 cm^{-1}) to 25 µm (400 cm^{-1}). It is surrounded by the far-IR (FIR) that extends from 25 µm (400 cm^{-1}) to 1 mm (10 cm^{-1}). However the very important part of the IR spectrum is the near-infrared (NIR) who extends from 800 nm (12500 cm^{-1}) to λ =2.5 µm (4000 cm^{-1}).

III.3.1 Principles: molecular vibrations

The absorption of IR photons by a covalent bond causes the molecule to pass in higher energy state. A molecule absorbs IR radiation when one of its bonds vibrates at the same frequency as the incident electromagnetic radiation. As a result of the absorption event, the molecule vibrates at an increased amplitude. Clearly, the absorbed frequencies depends on several factors including for example atomic masses involved in the bond and the strength of the bond. Not all molecules can absorb IR radiation. In fact the condition for a bond vibration to be IR active is a change in molecular dipole moment µ during vibration resulting from photons absorption. This condition is expressed by equation III.5 where q stands for the normal coordinate describing the collective motion of atoms in a normal vibration. μ_0 represents the dipole moment calculated for q equal to zero.

$$\mu_j = \mu_0 + \left(\frac{\delta\mu}{\delta q_j}\right) q_j + \frac{1}{2}\left(\frac{\delta^2\mu}{\delta {q_j}^2}\right) q_j^2 \qquad \text{Eq. III.5}$$

The common molecular vibrations involved in IR absorbtion are stretching and deformation of the covalent bonds. These are called vibrational modes. Stretching is a change in length of the bond, resulting in a change of atomic distances. Deformation vibrations, instead, are related to modification of bond angles or change in the position of a group of atoms with respect to the rest of the molecule. Deformation (or bending) vibrations are subdivided in scissoring, rocking, wagging and twisting.

In figure III.6 some of the principal vibration modes are reported.

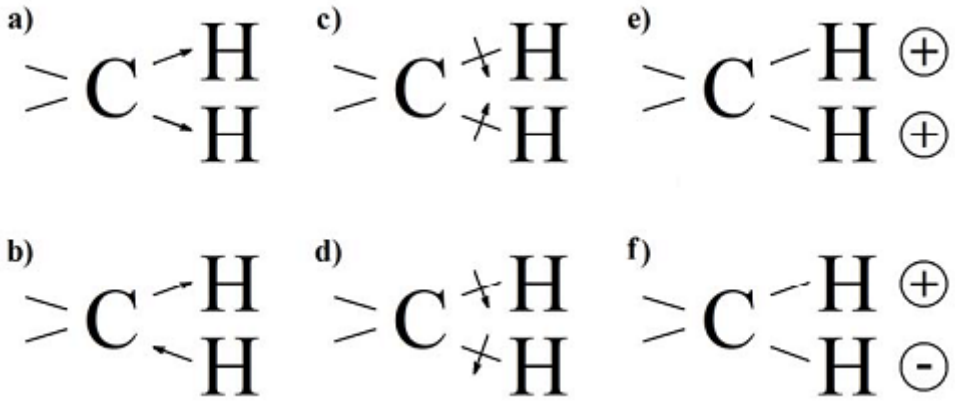

Figure III.6 Principal modes of vibration between a carbon atom and a hydrogen atom in alkanes. a) symmetrical stretching, b) asymmetrical stretching, c) scissoring, d) rocking, e) wagging, f) twisting.

Again, one can set an additional division in symmetric and asymmetrical modes of vibration. By looking at the figure, the molecule experiences symmetric stretching of its bonds when both the hydrogen atoms are coming closer to the central carbon atom. On the other hand, asymmetric stretching takes place when the hydrogen atoms move in opposite direction with respect to each other (e.g. one is coming closer, the other farther). Bending can be in plane or out of plane: the former is a change of bond angles in the plane of the molecule while the latter regards bending outside the plane of the molecule.

III.3.2 Qualitative analysis

The concept of characteristic vibrations is used for qualitative analysis of polyatomic molecules. It is important to underline how IR spectroscopy is not focused on the determination of a complete structure of a generic compound. It is rather focused on the determination of the presence of certain molecular groups.

The radiation absorbed by the sample has the same frequency and is constant for a given set of atoms and chemical bonds: thus the absorption spectrum is a physical property of the molecule. Given the constituents and the configuration, it is possible to predict the principal absorption bands by energetic considerations. In the literature there exist several databases on IR spectra identification which permit a relatively easy group identification and spectra explanation. However the assignment of molecular groups to peaks is never trivial: sometimes overtone bands are added to fundamental vibration bands, or intermolecular interactions (like hydrogen bonding) can cause additional bands. Two main approaches can be followed to assign specific molecular species. The most conventional and most used is the use of databases which permit to interpret a spectrum in a relatively easy way. Typically, if the database is electronic and if the substance is not reported in the database, the computer lists a series of known spectra matching closely that examined.

The other way of proceeding is by evaluating the characteristic or group frequencies. It is worth noting that not all the vibrations exhibit characteristic frequencies. In aliphatic compounds, for example, vibrational frequencies of the various C-C backbone bonds are very much coupled to each other and they depend on the chemical group attached to the aliphatic backbone. Certain functional groups such as $–CH_3$, -C=O, $-NH_2$ and –OH act as separate groups than the rest of the molecule they are included in. The result is the possibility to recognize directly these groups because they have characteristic absorption frequencies. For practical evaluations, the IR spectrum is normally divided into three regions. The first region extends from 4000 to 1400 cm^{-1} and comprises the stretching vibrations involving movements of light atoms (molar mass lower than 20 g mol^{-1}). –OH and –NH stretching bands are in this part of the spectrum, located in the region between 3700 and 2500 cm^{-1}. Organic compounds always have –C-H species whose stretching vibration is located in the region from 3300 to 2800 cm^{-1}. Triple bonds such as C≡C, C≡N or N≡N show

stretching vibrations in the region between 2700 and 1850 cm^{-1}. Other double bonded chemical groups such as C=O show absorption peaks in the region 1950 – 1450 cm^{-1}.

The second important region is that encompassing the 1400 and 1900 cm^{-1} range. This particular region is called *fingerprint* region. Many chemical groups with single bonds have group frequencies in this region. Spectra in this region are very difficult to interpret because these vibrations couple very strongly to each other and particular bands can hardly be attributed to a single molecular group. Typically, if two spectra show the same behavior in this region, than they are assigned to the same substance.

The last region is that from 900 cm^{-1} to 400 cm^{-1}. Some characteristic vibrations of aromatic compounds fall in this region: these bands are due to aromatic C-H out of plane bending vibrations. If in the spectrum no bands are present in the region 900 - 650 cm^{-1}, then it can be said that aromatic compounds are absent. Even though we will not discuss about quantitative measurements in IR spectra interpretation, it should be said that Lambert-Beer law is still valid for this kind of spectroscopic characterization technique.

III.3.3 Fourier transform infrared spectrometer

The Fourier Transform Infrared Spectrometer (FTIR) is the instrument that is currently used for IR analysis. FTIR spectroscopy is based on the idea of interference of radiations between two beams to yield an interferogram. FTIR spectrometers cannot be built as double-beam instruments: they acquire single channel spectra of sample and reference, and their ratio is calculated afterwards. This instrument is constituted by an IR source, an interferometer and a detector. The actual instrument is based on the Michelson interferometer. A schematic diagram of FTIR spectrometer is reported in figure III.7.

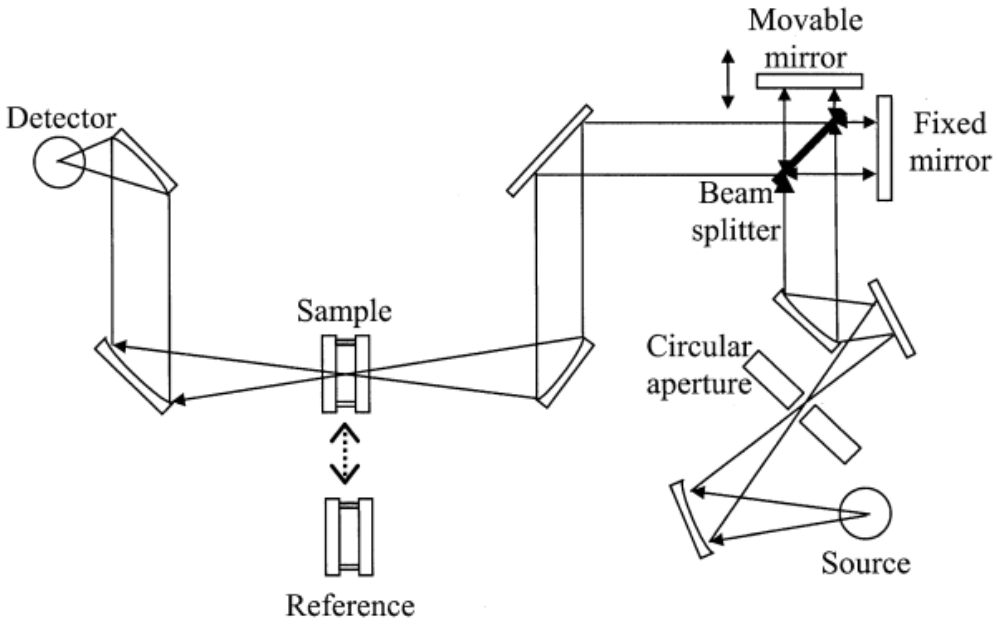

Figure III.7 Schematic diagram of FTIR spectrometer.

All the spectra reported in this work were recorded by means of a Nicolet 760 –FTIR Spectrometer.

Transmission mode was used for thin films deposited onto CaF_2 supports for monitoring the crosslinking reaction. The transmission mode parameters set up were:

- Number of scans: 32;
- Resolution: 2 cm^{-1};
- Y axis: absorbance;
- X axis: wavenumber (cm^{-1});
- First X value: 400 cm^{-1};
- Last X value: 4000 cm^{-1};
- H_2O correction;

The same parameters were used in the collection of background spectra.

III.3.3.1 IR light source

The most common sources of IR radiations are Nernst glowers, globars and heated wires. The Nernst glower is in the form of a cylindrical rod or tube composed by a mixture of certain oxides (e.g. zirconium oxide, yttrium oxide) and operates at temperature of 2000° C. At room temperature this mix of materials is insulating and so a Nernst glower requires an initial external heating. This obsolete device was replaced by a globar and because globars are made of silicon carbide, they do not require initial heating. Globars normally operate at about 1100° C.

Once all of these sources are heated by an adequate current flux, they emit radiation with a spectral matching similar to that of a black body.

III.3.3.2 The Michelson interferometer

The interferometer is the heart of the IR spectrometer. From the wave-optics it is known that if two beams of light with the same phase and wavelength are brought together, they reinforce each other and continue their path. Viceversa, if the two beams are out of phase, destructive interference takes place. The effect of destructive interference is maximum when the two beams are out of phase by 180°. This phenomenon is exploited in the Michelson interferometer.

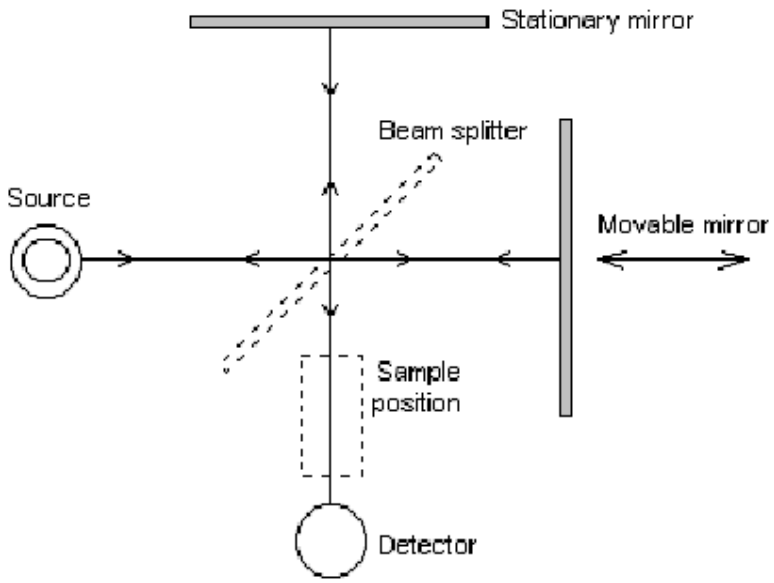

Figure III.8 Schematic representation of a Michelson Interferometer.

The Michelson interferometer basically consists of a beamsplitter and two flat mirrors. A sketch of the interferometer we are discussing is reported in figure III.8 The collimated IR beam is

directed to the beamsplitter whose function is to divide the beam into two parts having the same intensities. An ideal beamsplitter reflects half of the incident light towards the stationary mirror and half towards the movable mirror. The beamsplitter must not be an absorber medium in the operating range of the interferometer. Once the original beam is divided in two beams, they travel towards the stationary and the movable mirror respectively where they are reflected back to the beamsplitter. At the beamsplitter, interference occurs. The movement of the movable mirror is controlled by a helium – neon laser. The movable mirror is displaced in order to change the optical path length so that the condition for constructive and destructive interference are consecutively met. The recombined IR beam passes the sample and reaches the detector where the signal is recorded. The moving mirror produces an optical path difference between the two arms of the interferometer. Indicating by λ the wavelength and by n a integer number, for path differences of $(n + {}^{1}/_{2})\lambda$, the two beams interfere destructively in case of the transmitted beam, and constructively in case of reflected beam.

The collected signal is called an interferogram and is a record of intensity vs time, also called time domain: to convert the interferogram to a IR spectrum (intensity versus frequency, also called frequency domain) Fourier Transform has to be used.

It is important to maintain the optical alignment of the interferometer during mirror movement.

III.3.3.3 Detector

We can divide the types of detectors used in IR spectroscopy in two main classes: thermal detectors and photon-sensitive detectors. A thermal detector is the pyroelectric DTGS (deuterated triglycine sulfate) whose response is wavelength independent in the MIR range. This is based on the principle that when heated or cooled, it is capable of generating a voltage across the material. The change in temperature causes a modification in the position of atoms within the crystal: this fact is responsible for a polarization change which causes the voltage to change. MCT (mercury cadmium telluride) is an example of photon-sensitive detectors: it is much faster than the former and is based on a photo effect in which IR

radiation excites one bound electron of the detector material to a free state increasing the detector material conductivity.

III.3.4 Infrared methods

Infrared spectroscopy is a powerful tool also because it allows to perform measurements on different kinds of samples. Typically two measurement methods can be used, depending on the material to investigate: Transmission mode and Attenuated Total Reflectance (ATR) mode.

III.3.4.1 Transmission mode

This is the most conventional measurement method in IR spectroscopy. This technique is applicable only to thin film deposited on appropriate transparent substrate or to liquid solution. The interferogram outgoing beam hits the sample and is transmitted through it till the detector. This method provides maximum sensibility and high sample throughput at a relatively low cost.

III.3.4.2 Attenuated Total Reflectance

Attenuated Total Reflectance (ATR) is a powerful IR spectroscopy method that can acquire IR spectra of opaque samples, thick film, painted samples, coatings and so on. This characterization method provides information only on the surface of the samples down to a depth of a few microns. A typical ATR instrument is reported in figure III.9.

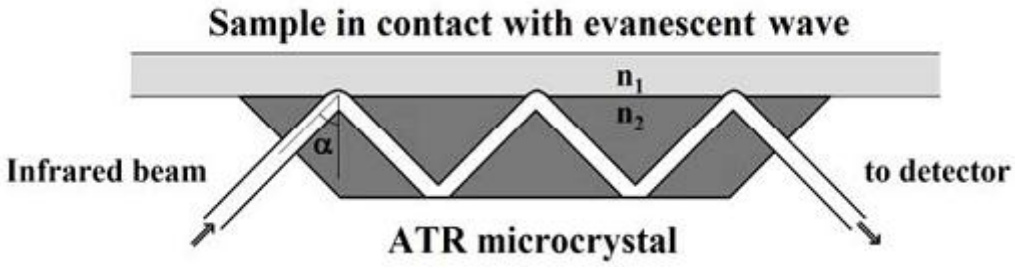

Figure III.9 Schematic Attenuated Total Reflectance (ATR) accessory. The IR beam is waveguided through the microcrystal and due to the tunneling effect it can penetrate the sample for a short distance (typically a few μm).

A high optical index of refraction crystal is the main component of the ATR device. When light travels through a high index of refraction medium and encounters a low index of refraction medium at the boundary, then light is reflected. If the incident angle is greater than the critical angle, then light is guided by TIR (total internal reflection) to the edge of the crystal through the low index of refraction medium. Even if light is reflected, the beam of light penetrates into the low index of refraction due to tunneling effect. This is called evanescent wave and has a certain penetration depth which is typically on the order of a few μm. Penetration of waves into the sample permits the interaction between sample molecules and IR beam, thus giving rise to absorption. This allows the collection of an IR absorption spectrum.

III.4 Differential Scanning Calorimetry

One of the main thermal analysis techniques used to characterize polymeric materials is Differential Scanning Calorimetry (DSC). Based on the correlation between enthalpy variation occurring to a sample during a thermal cycle and its specific heat, DSC measures the change of specific heat of a sample versus temperature. To be more specific, DSC measures heat flow variations between a reference and the sample of interest [4].

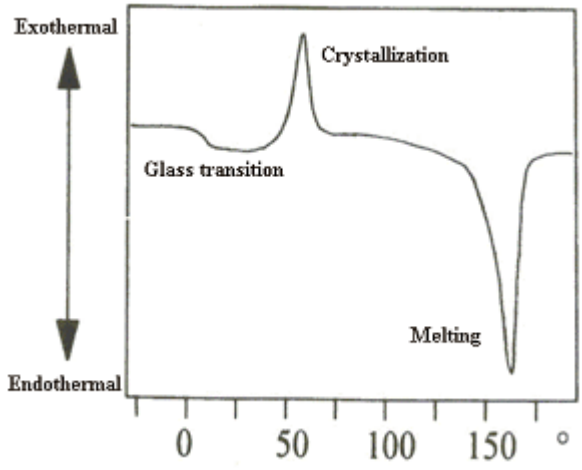

Figure III.10 Example of DSC curve. The figure depicts glass transition temperature, crystallization and melting.

Two crucibles in aluminum, one containing a few milligrams of materials to be investigated and the other which is empty and serves as reference, are put onto a heat-flux plate. A thermal cycle is set up. The temperature of the two crucibles will be different because one of them contains the sample. In this way we can measure the difference in temperature between the two crucibles and thus also the heat absorbed by the material during the thermal cycle. A typical DSC curve is represented in figure III.10.

DSC is a powerful tool in the analysis of polymeric materials because it permits to identify the presence of transition temperatures (in particular glass transition for polymers) but also crystallization and melting of polymers. Sometimes it can also be used to estimate reaction kinetics.

DSC's were carried out by means of a DSC/823e-Mettler Toledo. Three consecutive thermal scans were applied with a scan speed of 10 K/min

- -100° C → 200° C;
- 200 ° C → -100° C;
- -100° C → 200° C.

III.5 Photovoltaic tests

In this work photovoltaic tests were performed by means of Sun 2000 Solar Simulator produced by ABET technologies whose function is to shine the samples. This instrument is shown in figure III.11. Figure III.11 also depicts a Keithley 2612 system source digital multimeter.

Figure III.11 The Keithley 2612 Digital Multimeter is reported on the left while the Sun 2000 Solar Simulator on the right.

Let us focus now on the solar simulator and on the digital multimeter.

III.5.1 Solar Simulator

A solar simulator reproduces the full spectrum of light as natural light. The emission spectrum of sunlight at ground level is different depending on the location on Earth. Light emitted from the sun which strikes atmosphere is diffracted and absorbed by the different constituents of the atmosphere. Elevation contributes to the variation of the ground level spectrum as light will have to travel a shorter or a longer distance to reach the ground. To account for the effect due to atmosphere, several kinds of spectra were recognized. When the sun is directly overhead, the radiation travels for the shortest distance before reaching the surface of the Earth. This situation is referred to as “Air Mass 1 Direct” (AM1D). The

global radiation with the Sun overhead is referred to as “Air Mass 1 Global (AM1G). the difference in the AM1D and AM1G spectra is that the former accounts only for direct incident light while the latter considers also diffused light. Light collected out of the atmosphere in space will not travel through any mass. For this reason, the emission spectrum of the Sun before reaching the atmosphere is referred to as “Air Mass 0” (AM0). ASTM published three spectra, AM0, AM1.5D and AM1.5G for light incident on a 37 degree tilted surface. Figure III.12 depicts the AM0 and AM1.5G emission spectra of sun.

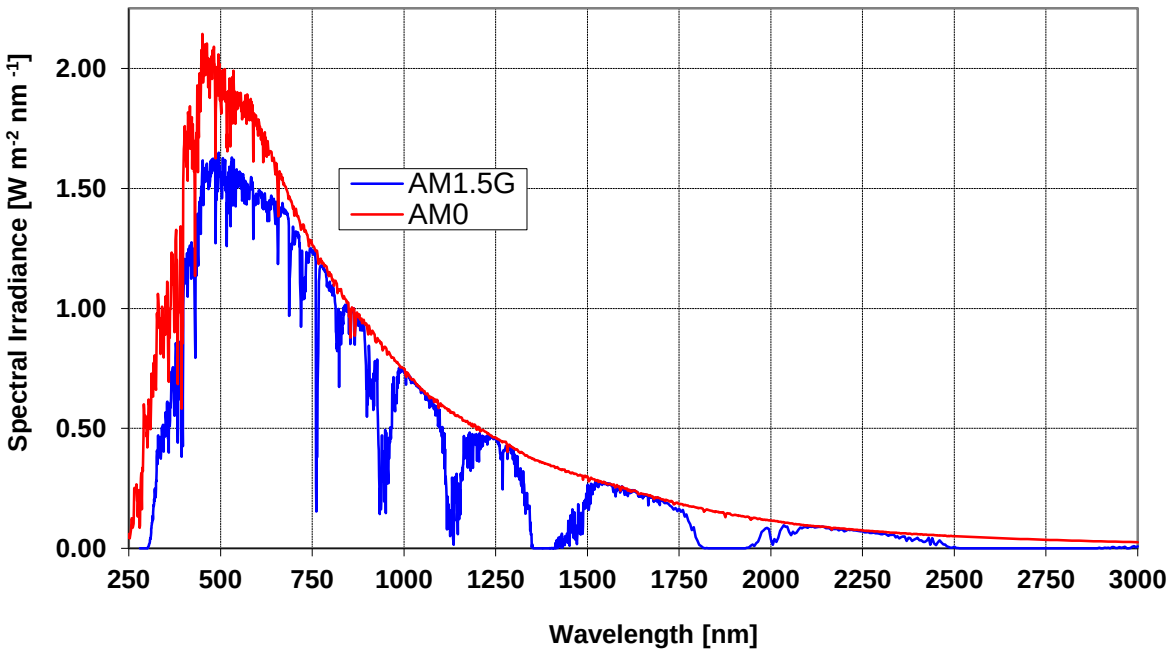

Figure III.12 AM0 and AM1.5G emission spectra of sun.

Let us now focus more in detail on the components of the solar simulator. A xenon lamp is the light source which is surrounded by an ellipsoidal reflector which does not permit to disperse an excessive amount of the radiation produced. Radiation is then focused onto an optical integrator that helps in producing a uniform diverging beam. The beam is successively diverted by a mirror onto a collimating lens. Filters are placed between the mirror and the collimating lens to match the radiation to different air masses. The output is a uniform beam that closely matches various air masses.

In this work photovoltaic tests were performed by shining the samples with an AM1.5G light emitted by the solar simulator.

III.5.2 Digital Multimeter

By means of a digital multimeter it was possible to carried out tests on the LSC fabricated. A digital multimeter is an electronic device which permits to measure different electrical parameters such as current, voltage and resistance of a device. During the PV tests, the digital multimeter sweeps the voltage applied at the electrodes of the LSC and it measures the current which varies as a consequence of the voltage variation. The range of voltage which we investigated was from -0.2 V to 0.6 V with 75 points taken in the whole interval. Each point is characterized by a value of voltage (which is imposed) and by a value of current (which is measured).

Therefore, the output of a PV test is the list of the 75 points each characterized by voltage and corresponding current. In our tests the digital multimeter also reported the short circuit current and the open circuit voltage.

III.6 Measurement of the specular reflectance of a surface

III.6.1 Gloss

To characterize the reflectivity of the back reflectors fabricated, we investigated their white surface with a glossmeter. In general, gloss is the perception by an observer of the shiny (or mirror like) appearance of a surface [5]. This perception changes whenever there is a change in the relative position or spectral distribution of the source, the sample or the observer: for this reason the appearance cannot be measured [6]. Gloss is generally associated with the specular reflection of light from the surface of the object [7-8]. The amount of light reflected in a specular manner depends on several parameters including the angle of incidence and the quality of the surface (roughness, imperfections). ASTM standard method D523 designates three angles (20°, 60° and 85°) for measurement of gloss unit, the latter being defined such that a value of 100 Gloss Units (GU) is given to a polished black glass material of

refractive index equal to 1.567, for any angle of incident light. Black pigments are added because incident light that is diffracted and enters the glass will be totally absorbed. In this way it is ensured that only specularly reflected light is measured [9]. In literature specific recommendations for measurement of the gloss of a surface are reported: preliminary measurements have to be performed at 60 degrees; this measure should be performed also in cases in which different samples have to be tested. After the first measurement and only if an absolute gloss value is searched, other tests should be performed. Three different cases should be distinguished: for a GU higher than 70, measurements should be performed at 20°, for GU lower than 10, 20° is the ideal choice in performing the measurement. For other surfaces with GU comprised in the range 10 – 70, samples should be tested at 85°.

III.6.2 Glossmeter

The glossmeter is the instrument used to determine the gloss unit of a surface. The instrument is very simple and the output is very fast. It consists of an illuminator and of a receiver (fig. III.13).

The illuminator is constituted by a light source and by a lens whose function is to focus light towards the surface. The receiver is constituted by a detector and by a lense whose function is to collect light and redirect it towards the detector. System output is digital and it consists of the Gloss unit which is analogous to the specular reflectivity of light. In a glossmeter, the detector signal will be proportional to the reflected light intensity.

Our measurements were performed on a MultiGloss 268 by Konica Minolta.

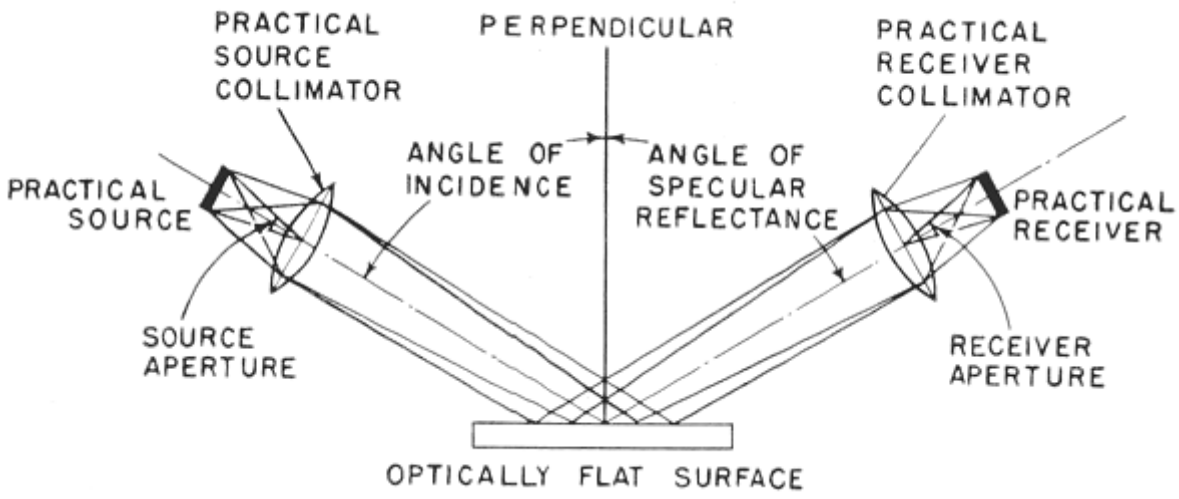

Figure III.13 Schematization of a glossmeter. The figure depicts the light source and a the collimator whose function is to focus light on the surface to be investigated. Once reflection has taken place, light is re-directed by a second collimator towards a receiver.

Numerous standards concerning glossmeter functioning and components part have been published but also numerous papers which suggest ideal choices in glossmeter components [10].

III.7 Profile and topography measurements

Profilometry is the technique used in the determination of several surface parameters, including surface roughness and thickness of a thin film. In addition, registration of the profile behavior is possible. In this section an overview will be presented on the techniques used to determine surface roughness and thickness of the thin films we fabricated. In the present work, we made use of an optical profilometer.

III.7.1 Profilometer

A profilometer is an instrument used to determine surface roughness of a sample on a two dimensional profile (along a line).

Surface roughness can be defined as the measure of the texture of a surface and it is quantified by the vertical deviations of a real surface from its ideal (flat) form. If these deviations are large, the surface is rough while if the vertical deviations are small, the surface is smooth. Two different definition of surface roughness are usually defined: arithmetic, R_a, and root mean squared, R_q.

The former is defined as eq. III.6

$$R_a = \frac{1}{l}\int_0^l y \qquad \text{Eq.III.6}$$

While the latter as eq.III.7

$$R_q = \sqrt{\frac{1}{l}\int_0^l |y|^2} \qquad \text{Eq.III.7}$$

Where y is the departure from a reference line placed on the surface of the sample and l the length over which the evaluation of the roughness is made. Usually profilometers can be divided in two main groups: contact and non-contact methods. The contact method is typically used in profilometers having a really small diamond stylus which moves over the surface. The stylus gets into contact with the surface and its vertical movement is registered while the stylus is moved laterally. The major advantage of contact profilometry is that the method is rapid and inexpensive while the diameter of the stylus limits its use to surface features larger than the stylus diameter. Another problem concerning contact profilometry is that surface distortion and damaging can occur during a measure. The resolution typically ranges from 10 nanometers to 1 millimeter.

Non-contact profilometry is based on optical methods such as the use of a laser which replaces the tip of the stylus. A light beam is focused on the surface of the sample and reflected by it; the output is converted into an electronic format. As in the case of contact

profilometry, the light spot represents a limiting factor. Typically this is a slower measurement technique than that based on stylus but has the big advantage of not damaging the surface investigated. The resolution limit is in the nanometric range. in this work, an optical profilometer was used (Microfocus by UBM).

III.8 Degradation studies

Degradation studies were carried out to determine the susceptibility to degradation of the OLSC devices we investigated. Different studies were carried out: weathering in solar box and UV aging.

III.8.1 UV aging

The ultraviolet spectrum can be sub-divide into three parts. UV-C, the most energetic, ranges from 100 to 280 nm. UV-B ranges from 280 to 315 nm while UV-A, which is the closest to visible, ranges from 315 to 400 nm. Two different types of UV aging were carried out: UV-C and UV-A. In performing a UV aging test, samples are put into a dedicated chamber equipped with a vent to control the temperature, so as to avoid excessive heating of the sample under study due to lamp emission.

III.8.1.1 UV-A aging

UV-A aging is performed by irradiating the samples with UV-A light emitted by a mercury lamp type S by Helios Italquartz Srl. The emission spectrum of this lamp is mainly characterized by two emission peaks. The first one is approximately centered at 365 nm in the UV-A while the second at approximately 450 nm in the visible. This kind of lamp has additional peaks in the visible range. The external transparent tube constituting the lamp is made of quartz. Quartz is transparent to UV radiation and if pure quartz is considered, all the light emitted from the lamp passes without being stopped. But if a certain amount of glass is added to quartz, then emitted light starts to be partially absorbed because glass is UV

absorbing. The intensity of the absorbed light is a function of the amount of glass. The lamp described above presents a certain amount of glass which stops all the emission below 350 nm and permits the transmission of the remaining radiation.

III.8.1.2 UV-C aging

UV-C aging is performed by irradiating the samples with a UV-C light emitted by a mercury lamp type P by Helios Italquartz Srl. The emission spectrum of the lamp presents a series of peaks from 254 nm on. Indeed a series of high energy peaks are present in the range 200 – 300 nm.

III.8.2 Accelerated weathering tests

Weathering tests were carried out by a weather-o-meter (solar box) produced by Cofomegra Srl. In our study this kind of test is aimed at the determination of long term behavior of LSC fabricated. This test is accelerated and the testing conditions are similar to outdoor conditions. The aim is to extrapolate long term stability/degradation behavior in shorter times.

The samples are placed into a testing chamber which has an aperture on top through which light passes to irradiate the samples. The lamp is a mercury lamp. The emission of the lamp ranges from the UV to the Infrared. For this reason a vent is placed into the chamber to control temperature which increases due to infrared radiation. The feedback system is a black standard (BS). It is a black plate whose characteristics resembles that of a black body. It is placed into the chamber and its function is to control the inside temperature. When the temperature of the BS reaches a pre-set value, then the vent starts operating to remove some heat.

A filter is placed between the samples and the light source. We use an outdoor filter which stops all the radiations below 280 nm, thus stopping a large portion of high energy UV light. This condition is similar to that used in the literature for weathering of plastics.

A digital display shows all the parameters characterizing the test: relative humidity (RH), temperature and time elapse counting.

In the ASTM D5272 standard for weathering tests of photodegradable plastics, the lamp irradiance is specified which should be 550 W/m^2 for this kind of tests. The irradiance level was set as indicated. In addition a powermeter was used to monitor the actual irradiance in the test chamber. The total irradiance measured is approximately 1000 W/m^2 and this value was found to be constant for the entire duration of the test. The difference in the power density (550 W/m^2 vs 1000 W/m^2) is due to the different wavelength range measured. Indeed the solar box is equipped with a photodiode that absorbs all the wavelengths in the range 300 – 800 nm while the powermeter we used to perform the measurements is of thermo-pile type and it can detect a wider wavelength range. This accounts for the difference in the irradiance which have been recorded.

With a UV photodiode we measured also the irradiance of UV spectrum which is 50 W/m^2 (295 – 400 nm wavelength range).

Additional parameters that can be monitored are RH whose value is approximately 20 % and inside temperature which is 38° C.

Tests were carried out in continuum exposure conditions and lasted about 1000 hours. Samples were periodically taken out of solar box to perform tests.

III.9 External Quantum Efficiency measurement

External Quantum Efficiency (EQE) measurements are essential to characterize a PV device because in this way it is possible to calculate the specific contribution to device efficiency given by each photon energy. EQE is a function of incident wavelength and represents the ratio of the number of photons incident on a device to the number of generated charge carriers. It considers all the incident photons on the surface of the PV device and is usually expressed as percentage. Thus the most efficient device will have the highest EQE.

The key in performing EQE measurements is to accurately measure the monochromatic light incident to the device under test and how much current is generated.

Test were performed on an Oriel QE-PV-SI instrument which consists of several components: light source, monochromator, filters and a photodiode as detector. A picture of the instrument used is reported in figure III.14.

Figure III.14 Set up of the instrument used to perform EQE tests.

Figure III.15 Silicon detector used in performing EQE test.

The light source is an incandescent Quartz Tungsten Halogen (QTH) lamp light with a higher luminous efficacy which emits light from the deep UV to the IR. This lamp is coupled with a monochromator whose function is to produce a very high resolution and excellent throughput. The monochromator removes all not desired wavelengths and is controlled by a Tracq Basic software. Optics are also present and their function is to focus light and control the output spot. An Oriel Cornerstone™ 260 1/4 m lock-in is present and consists in three main components: a pre-amplifier (to enhance the signal), a chopper and a Silicon detector (see figure III.15). the silicon detector operates in the range from 200 nm to 1100 nm and serves as photon counter. The lock-in amplifier is utilized when sensitive optical power and current measurements are needed, so that even weak signals can be registered.

III.10 References

[1] B. Valeur, “Molecular Fluorescence: principles and applications”, Ed. Wiley-VCH, 2002 pp 21 – 33;

[2] J.R. Lakowicz, “Principles of fluorescence spectroscopy”, Ed. Springer, third edition, 2006, pp 27 – 60;

[3] M. Hof, “Basics of Optical Spectroscopy” in “Handbook of Spectroscopy”, Ed. Wiley-VCH, 2003, pp 37 – 152;

[4] M.E. Brown, “Introduction to thermal analysis: technique and applications”, Ed. Chapman and Hall, 1988, pp 59 – 77;

[5] M.E. Nadal, E.A. Early, E.A. Thompson, “Specular Gloss”, National Institute of Standards and Technologies Special Publication SP250-70, 2006, pp 1 – 14;

[6] M.E. Nadal, E.A. Thompson, “New primary standard for specular gloss measurement”, Journal of Coatings Technology, 72, 2000, pp 61 – 66;

[7] F. Leloup, P. Hanselaer, J. Versluys, S. Forment, S.-L. KaHo, “BRDF and gloss measurements”, in Proceedings of the CIE expert symposium on visual appearance, 2007, pp 1 – 6;

[8] M. E. Becker, “Evaluation and characterization of display reflectance”, Displays, 19, 1998, pp 35 – 54;

[9] G. Antonioli, F. Fermi, C. Oleari and R. Reverberi, “Reflectoscopic analysis of cultural goods for knowledge and preservation”, Convegni Aracne 13, Aracne Editrice srl, 2005, pp 2 – 3;

[10] H. K. Hammond III and I. Nimeroff, “Measurement of sixty-degree specular gloss”, Journal of Research of the National Bureau of Standards, 44, 1950, pp 585 – 598.

IV
Results and discussion

LSC's are a promising alternative to large PV panels as they permit to reduce material costs, thus potentially favoring a larger diffusion of PV technology. Much work has still to be done before LSC's can actually hit the market. As regards this, the first step to their commercialization is definitely the optimization of the actual LSC design. In order to achieve this purpose, a number of parameters must be optimized, such as luminescent dye concentration, host matrix thickness, LSC's dimensions and use of back reflectors. PMMA is considered to be one of the best host matrices in terms of low cost and high performance but its main limiting factor is susceptibility to degradation which limits significantly its use for LSC's large scale production. We can divide this chapter into three parts: in the first one we will discuss about the optimization of LSC's on a model host matrix (PMMA) and a commercial luminescent dye (Lumogen F Red 305), in the second one we will propose the synthesis and optimization of alternative matrices which in theory should retain their properties on a long time scale, and in the final part we will present the results on accelerated weathering tests on the optimized devices, trying to highlight the potential advantages given by the use of the polymeric matrices prepared in this work compared to PMMA.

In the following a series of PV parameters will be recalled and thus it is important to briefly reintroduce them.

To calculate the efficiency of LSC devices, two different approaches were used. A first estimate was obtained by calculating the absolute power conversion efficiency of the LSC device, PCE^{LSC}, according to eq. IV.1

$$PCE_{abs}^{LSC} = FF^{LSC} \frac{(I_{SC}^{LSC}/A^{LSC})}{P_{IN}} V_{OC}^{LSC} \qquad \text{Eq IV.1}$$

Where FF^{LSC}, I_{SC}^{LSC}, V_{OC}^{LSC} and A^{LSC} are respectively the fill factor, the short-circuit current, the open-circuit voltage and the active area of the LSC. The absolute power conversion efficiency, PCE_{abs}^{LSC}, represents the actual efficiency of the LSC device and takes into account the contribution to photon absorption of the surface area of the LSC thin film, thus allowing comparisons between LSC devices with different dimensions and equal solar cell type.

A second approach, the efficiency gain, ΔPCE, is considered. It is useful in calculating the increase (%) in the PCE of the cell when it is coupled to a thin-film LSC. ΔPCE can be calculated by equation IV.2:

$$\Delta PCE = \frac{PCE_{rel}^{LSC} - PCE^{cell}}{PCE^{cell}} * 100 \qquad \text{Eq. IV.2}$$

where PCE^{cell} is the power conversion efficiency of the cell calculated as equation IV.3 depicts:

$$PCE^{cell} = FF^{cell} \frac{(I_{SC}^{cell}/A^{cell})}{P_{IN}} V_{OC}^{cell} \qquad \text{Eq. IV.3}$$

PCE_{rel}^{LSC} is the relative power conversion efficiency of the LSC device calculated as equation IV.4 depicts.

$$PCE_{rel}^{LSC} = FF^{LSC} \frac{(I_{SC}^{LSC}/A^{cell})}{P_{IN}} V_{OC}^{LSC} \qquad \text{Eq. IV.4}$$

being A^{cell} the cell active area. In the following we will refer to relative or absolute PCE of the LSC plate. If no particular mention is done, in this work PCE will be the relative one.

Once all the parameters have been briefly recalled, we can start with the discussion of the obtained results.

IV.1 Optimization of LSC with PMMA as host matrix

Before starting the discussion, it is convenient to define the nomenclature adopted to distinguish one LSC from another. In this section only nomenclature relative to PMMA will be shown.

We identify by the abbreviation PxLy a generic thin film LSC with PMMA as host matrix (P stands for PMMA) and Lumogen F Red 305 as doping dye (L stands for Lumogen). x identifies the weight ratio of the polymer with respect to the solvent used in solution preparation: in mathematical terms, $W_{PMMA}/W_{CHCl_3} * 100$. (W stands for the weight of the substance indicated in the subscript) y, on the other hand, identifies the weight ratio of the dye with respect to polymer matrix, i.e. $W_{Lumogen}/W_{PMMA} * 100$.

IV.1.1 Optimization of the dye concentration

The very first optimization process done was the determination of the optimal Lumogen F Red 305 (LFR305) concentration in a given PMMA (as host matrix) content. To reach this aim, PMMA solid concentration was fixed at 10%. Waveguide dimensions (glass substrates) were 50 x 25 mm^2. LFR305 was dissolved at different concentrations with respect to solid PMMA content. All the different LFR305 weight concentrations investigated are 1, 2, 3, 4, 5, 6, 7, 10 %. Our goal was to investigate the effects of dye concentration on the performance of LSC device and ultimately to determine the optimal dye concentration which gives the best performance of the LSC.

IV.1.1.1 PV parameters

Figure IV.1 shows ΔPCE variation as a function of LFR305 concentration. All the points are averaged on three LSC's. As it appears clearly from the plot, that the maximum PCE is obtained for a dye concentration of 5 %.

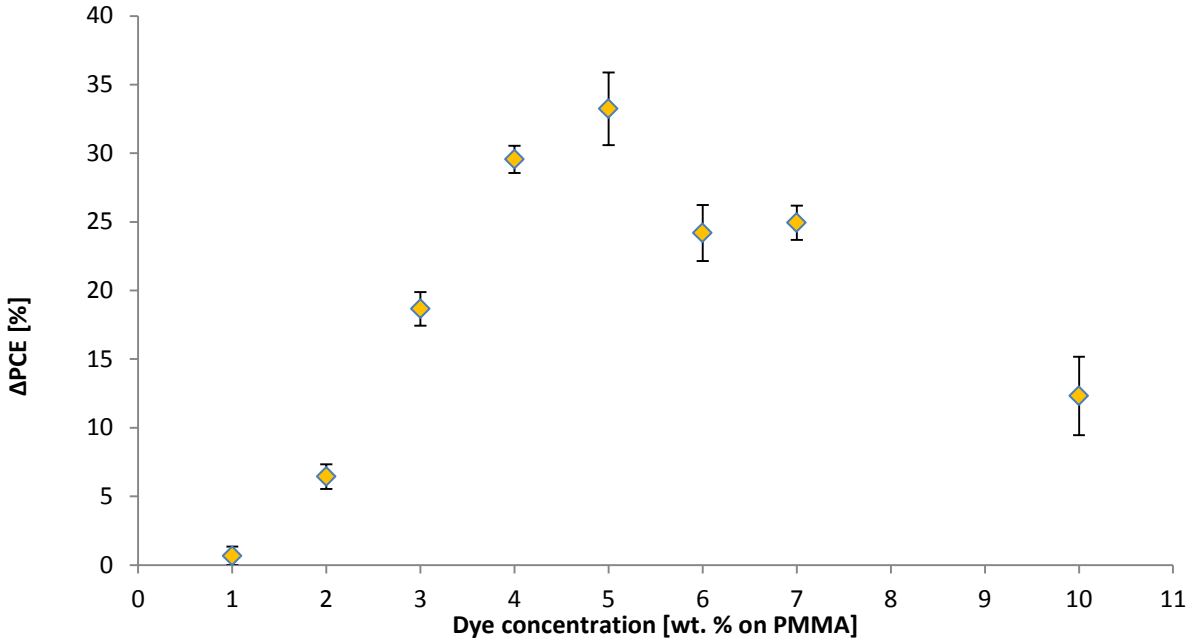

Figure IV.1 Power conversion efficiency variation versus LFR305 concentration for P10Lx. x represents the dye concentration.

Up to 5% of dye concentration the curve shows a monotonic behavior characterized by increasing ΔPCE. In PMMA LFR305 concentration of 5 % can thus give the highest efficiency gain with respect to the base cell. In these conditions, the maximum increment achievable is 35% with respect to the cell. It should be noted, however, that 4% and 5% dye concentration give nearly the same results. The trend observed in the first ascending part of the curve can be explained by considering that at increasing dye concentration, the LSC plate can absorb and re-emit a larger number of photons: as a result more photons can reach the cell and more electrons can flow in the external circuit. After the maximum, the curve shows a decrease of ΔPCE even if theoretically the number of molecules is higher at increasing dye concentration. This decrease may result from the fact that at concentrations after a threshold limit, the plate absorbs more photons but a lower number of them reaches the cell because in the waveguiding process any photon re-encounters a larger number of dye molecules making the re-absorption process more probable. The problem of the optimization of dye concentration was already faced in the literature [1, 2] and it emerges that attention should attend to avoid losses due to self-absorption. In this work, no dye concentrations lower than 1% and higher than 10 were tested on LSC's because of their poor

interest. Indeed a concentration lower than 1% would result in a ΔPCE lower than 0 because of the limited presence of dye molecules which can capture and re-emit only a few photons. Concentrations higher than 10%, on the other hand, would allow to absorb a large number of photons but the overall re-absorption events would be more likely and thus less photons would reach the PV cell.

Table IV.1 collects the main PV parameters for all the dye concentrations tested.

Dye content [%]	I_{SC} [mA]	V_{OC} [V]	FF [%]	PCE^{cell} [%]	ΔPCE [%]	PCE^{LSC} [%]
1	14.57 ± 0.28	0.53 ± 0.002	54.61 ± 0.87	9.3 ± 0.29	0.66 ± 0.68	0.34 ± 0.01
2	15.28 ± 0.49	0.54 ± 0.005	57.96 ± 2.51	10.48 ± 0.53	6.44 ± 0.90	0.38 ± 0.02
3	17.03 ± 0.16	0.54 ± 0.005	56.86 ± 2.30	11.55 ± 0.49	18.67 ± 1.23	0.42 ± 0.02
4	18.56 ± 0.27	0.55 ± 0.01	58.27 ± 2.81	13.23 ± 0.96	29.55 ± 0.99	0.48 ± 0.03
5	18.33 ± 0.40	0.53 ± 0.01	51.16 ± 5.64	11.02 ± 1.47	**33.24 ± 2.64**	**0.40 ± 0.05**
6	17.08 ± 0.41	0.53 ± 0.01	51.34 ± 3.51	10.31 ± 0.69	24.19 ± 2.04	0.37 ± 0.02
7	17.29 ± 0.61	0.54 ± 0.01	56.35 ± 2.36	11.75 ± 1.05	24.93 ± 1.24	0.42 ± 0.04
10	15.27 ± 1.52	0.53 ± 0.01	54.95 ± 3.37	9.89 ± 1.80	7.85 ± 8.85	0.36 ± 0.07

Table IV.1 Main photovoltaic parameters of P10Lx with x LFR305 concentration. ΔPCE, PCE^{LSC} of the best performing LSC are reported in bold.

IV.1.1.2 UV-Visible absorption spectroscopy

UV-Visible spectra taken on different dye concentrations in PMMA can support our hypothesis made in the previous section. Figure IV.2 displays UV-Vis absorption spectra of thin film LSC's at different dye concentration in the range 350 nm – 700 nm. UV-Vis spectra were collected for all dye concentrations presented in the previous section, but for sake of clarity only 0.1 % (P10L0.1), 1 % (P10L1), 5 % (P10L5) and 10 % (P10L10) dye concentrations have been included in the plot. We registered also 0.1 % and 0.01 % dye concentration in order to demonstrate that at low dye concentration, absorption of light is quite negligible.

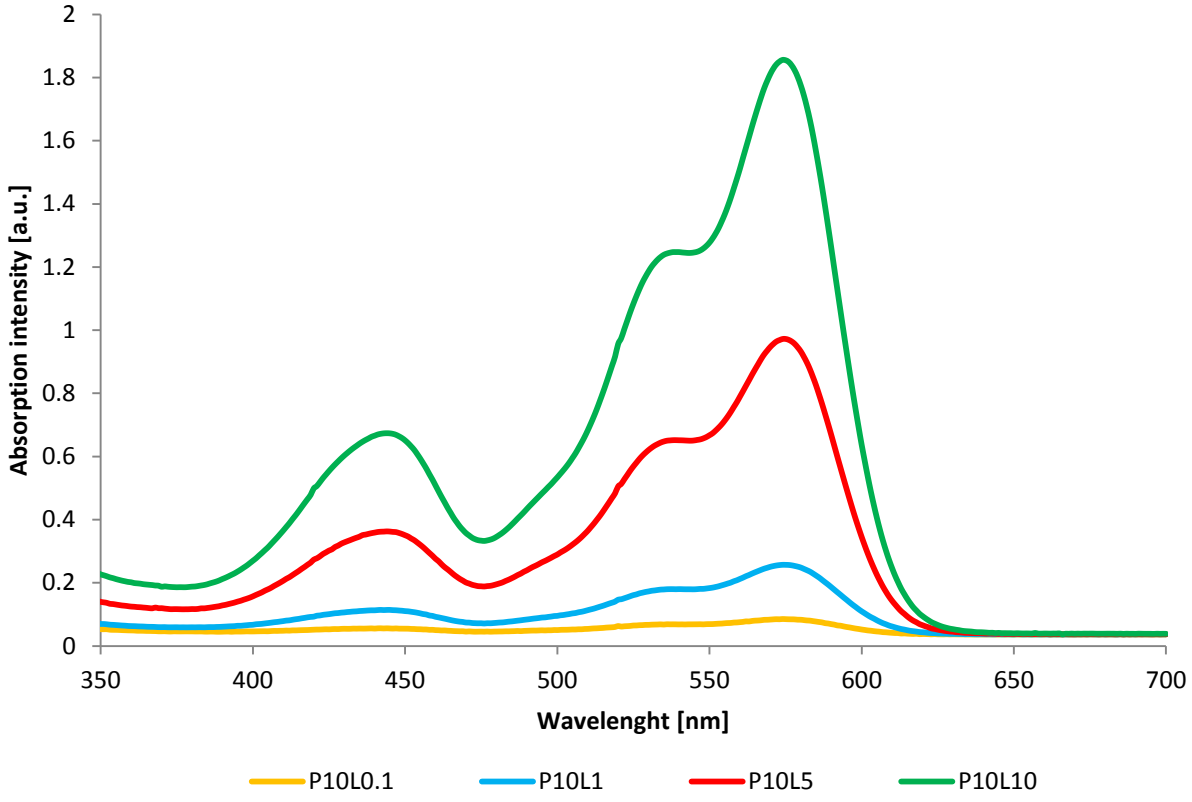

Figure IV.2 UV-Vis light absorption spectrum of P10L0.1, P10L1, P10L5 and P10L10.

The 0.1 % dye concentration results in a very low absorption intensity. Obviously, absorption intensity increases as the concentration of the dye is increased. By recalling the Lambert-Beer law, the only parameter which changes is dye concentration because the optical path length and also absorption coefficient are constant. Thus concentration of the absorbing species is at the basis of the different absorption intensities. Lambert-Beer law is followed for any concentration tested and this can be seen by the following figure (figure IV.3) which shows the main peak absorption intensity versus dye concentration.

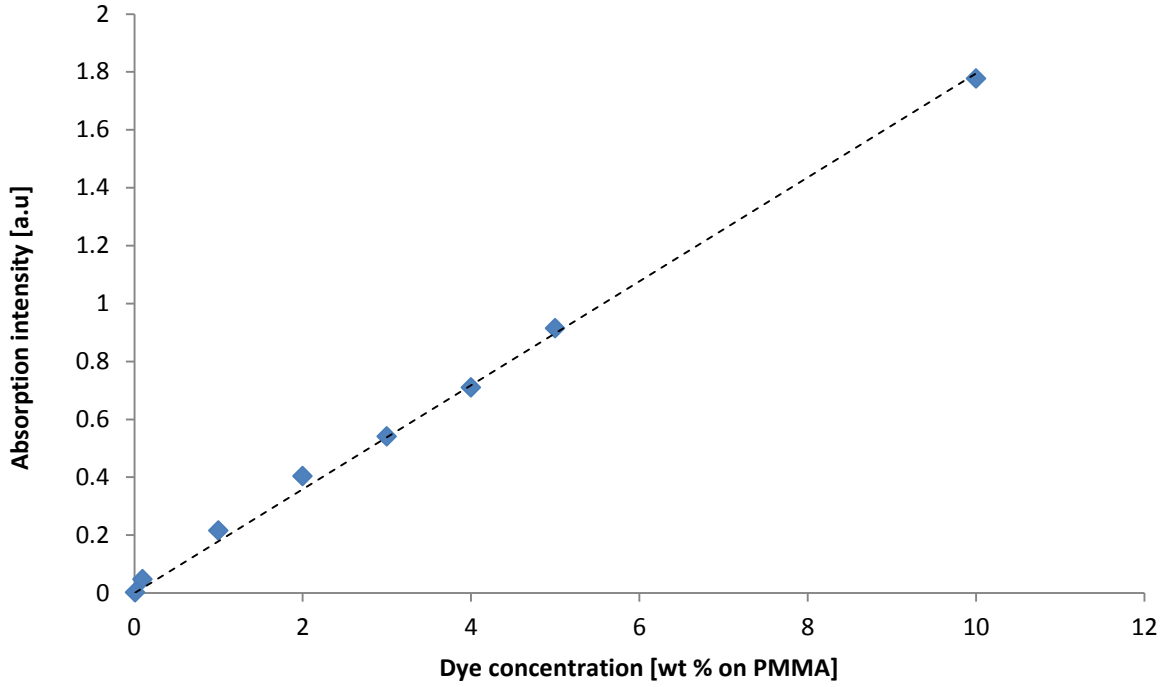

Figure IV.3 Absorption intensity versus dye concentration. The Lambert-Beer law is followed for all the dye concentrations tested, as can be seen from the interpolation by the black line whose equation is y = 0.180x (R^2 = 0.98).

In the literature through the UV-Vis absorption spectroscopy it was possible to observe the onset of formation of aggregates of dye molecules in the solid state, as the dye concentration is increased [3, 4]. In the literature [5] a dye concentration of 5 ppm is indicated as a limiting concentration to exclude formation of dye aggregates. These effects were observed on systems containing LFR305 and this observation arises from the increase in the absorption intensity of the higher energy peak of LFR305 while the lower energy peak shows a decrease in the absorption intensity. In our work no such modifications of the UV-Vis absorption spectrum for progressively increasing dye concentrations were observed. However this does not necessarily mean that aggregates are absent. In fact our concentrations, even in the less concentrated system, range from 100 ppm (for the 0.01 % dye concentration) to 100000 ppm (for the 10 % dye concentration). This may indicate that our systems are in a condition of aggregate supersaturation.

IV.1.1.3 Fluorescence spectroscopy

Fluorescence emission spectra were recorded for all the LSC's considered. In figure IV.4 fluorescence spectra of P10L0.1, P10L1, P10L5 and P10L10 are reported to compare them with the UV-Vis spectra presented in figure IV.2. Although LFR305 presents two absorption peaks (a lower intensity peak at 444 nm and a higher intensity peak at 571 nm) as shown in the its UV-Vis absorption spectrum (see figure IV.2), fluorescence emission spectra were recorded at an excitation wavelength λ = 445 nm, in order to avoid signal saturation.

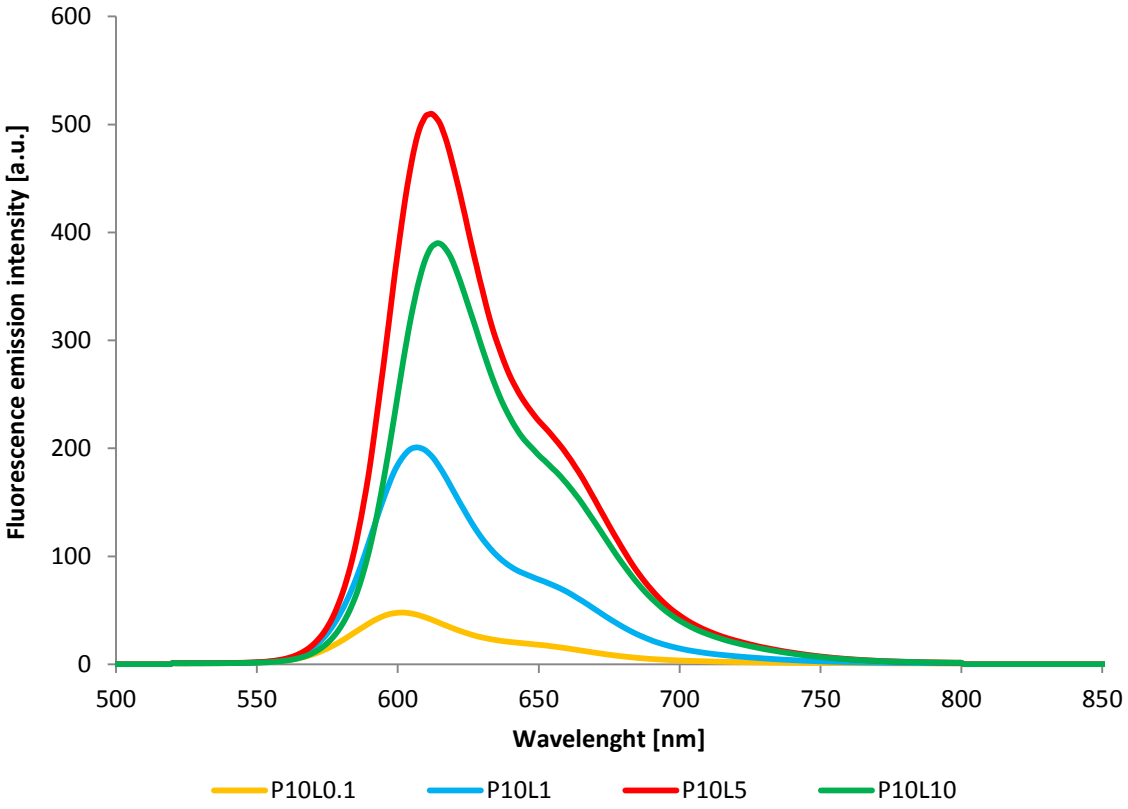

Figure IV.4 Fluorescence emission spectrum of P10L0.1, P10L1, P10L5, P10L10. The excitation wavelength was λ = 445 nm.

As shown in figure IV.4, emission intensity grows with dye concentration and reaches a maximum for 5 % dye concentration. Above this value the emission intensity decreases (see emission spectrum of P10L10). This trend observed for the emission intensity agrees well with the data obtained from the PV characteristic of LSC devices. The maximum in emission

intensity is registered for the 5 % dye concentration and may be related to the fact that this sample emits more photons than the other samples. Conversely, P10L0.1 emits a less number of photons compared to all the other samples, as can be expected by looking at the UV-Vis absorption spectra. The behavior of P10L10 is partially surprising. Despite the fact that this sample shows the highest absorption intensity as shown in figure IV.4, its emission intensity is not the highest. This behavior may be explained by considering figure IV.5, where emission intensity versus absorption intensity is plotted for samples at different dye concentrations.

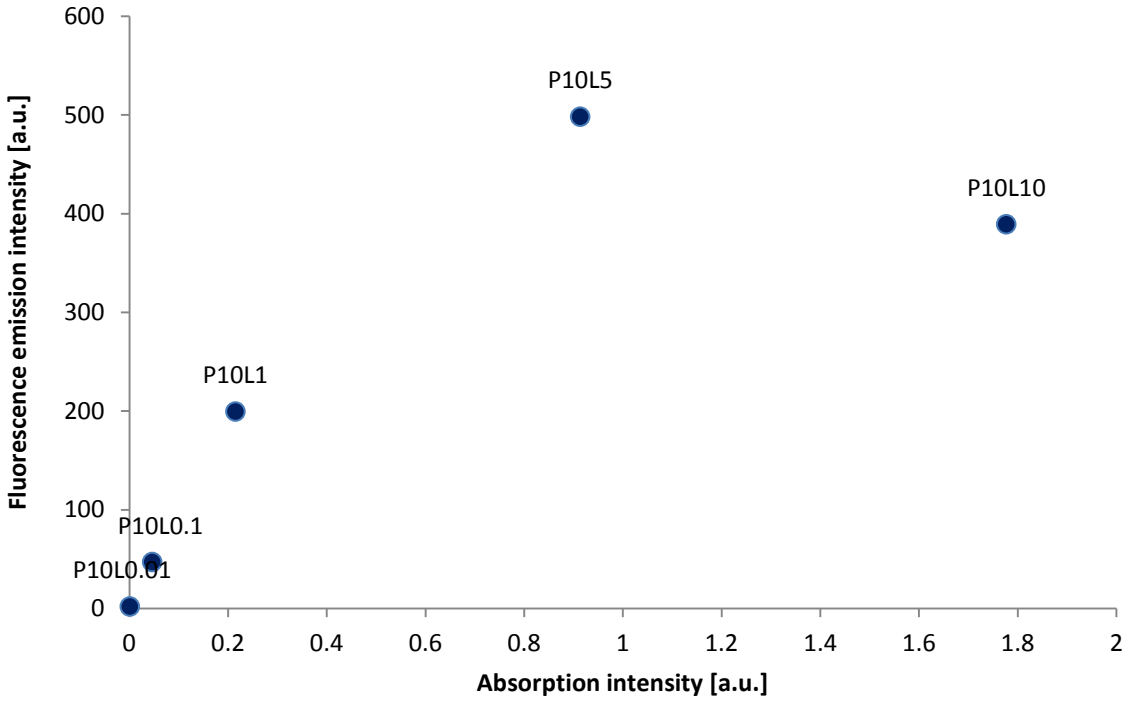

Figure IV.5 Emission intensity versus absorption intensity for P10L0.01, P10L0.1, P10L1, P10L5 and P10L10. P10L0.01 was reported to highlight that its absorption and emission intensities are low.

As shown in the plot, for dye concentrations up to 5 %, the emission intensity increases with absorption intensity. When the dye concentration is further increased, the emission intensity undergoes a decrease in spite of the significant increase in absorption intensity. This behavior may be justified by the fact that for P10L10 a large portion of the absorbed photons are lost. This dissipative process may be due to aggregates formation which may

cause a reduction in luminescence quantum yield thus leading to fluorescence quenching [6]. Indeed, in a 10 % dye concentrated system aggregation is more pronounced than for all the other concentrations. Haines et al. [4] showed this effect on perylene diimide (PDI), a very similar system to that under investigation. In particular, they showed that the decrease in fluorescence quantum yield caused by aggregates formation reduces the conversion efficiency of absorbed light into luminescence. In addition, Yoo et al. [9] showed that at increasing PDI concentrations, a larger amount of non radiative decay pathways may be present, leading to a decrease in photoluminescence quantum yield. Such aggregates can lead to the formation of low-energy electronic states, such as excimers[2], that act as trapping sites for emitted photons [5]. A further explanation of this trend can be found by considering the effect of reabsorption losses in the LSC. In fact, for increasing dye concentrations, the optical density[3] of the LSC film increases, and this may yield a higher probability of reabsorption of an emitted photon by another dye molecule. In our work this effect appears relevant for dye concentrations higher than 5 %.

Finally, it is worth mentioning that a redshift in fluorescence intensity can also be noticed by visual investigation. In fact, the color appearance of the thin film LSC changes from a brilliant red for the 5 % sample to a red-bordeaux intense color for the 10 % sample. This effect can be seen in figure IV.6.

[2] An excimer (originally "excited dimer") is a short-lived dimeric or heterodimeric molecule formed from two species, at least one of which is in an electronic excited state. Excimers are often diatomic and are composed of two atoms or molecules that would not bond if both were in the ground state.

[3] Optical density: for a given wavelength, the optical density is an expression of the transmittance of an optical element. The optical density is expressed by $\log_{10}(1/T)$ where T is the transmittance. It results that the higher the optical density, the lower the transmittance.

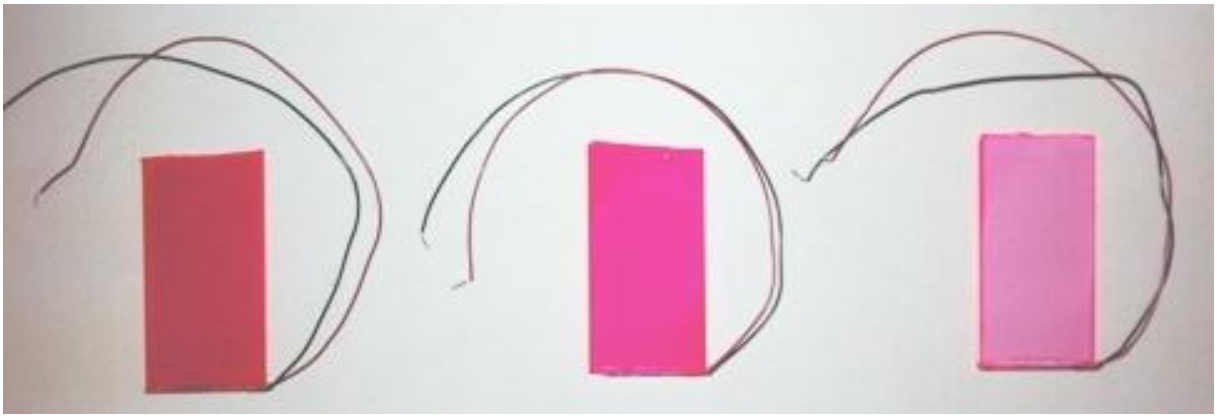

Figure IV.6 LSC's with different dye concentrations. In particular, P10L10 is on the left, P10L5 in the middle and P10L1 on the right.

Another interesting outcome of the analysis of fluorescence spectra is the appearance of a progressive shift of the emission peak towards longer wavelengths as the dye concentration is increased (see figure IV.7).

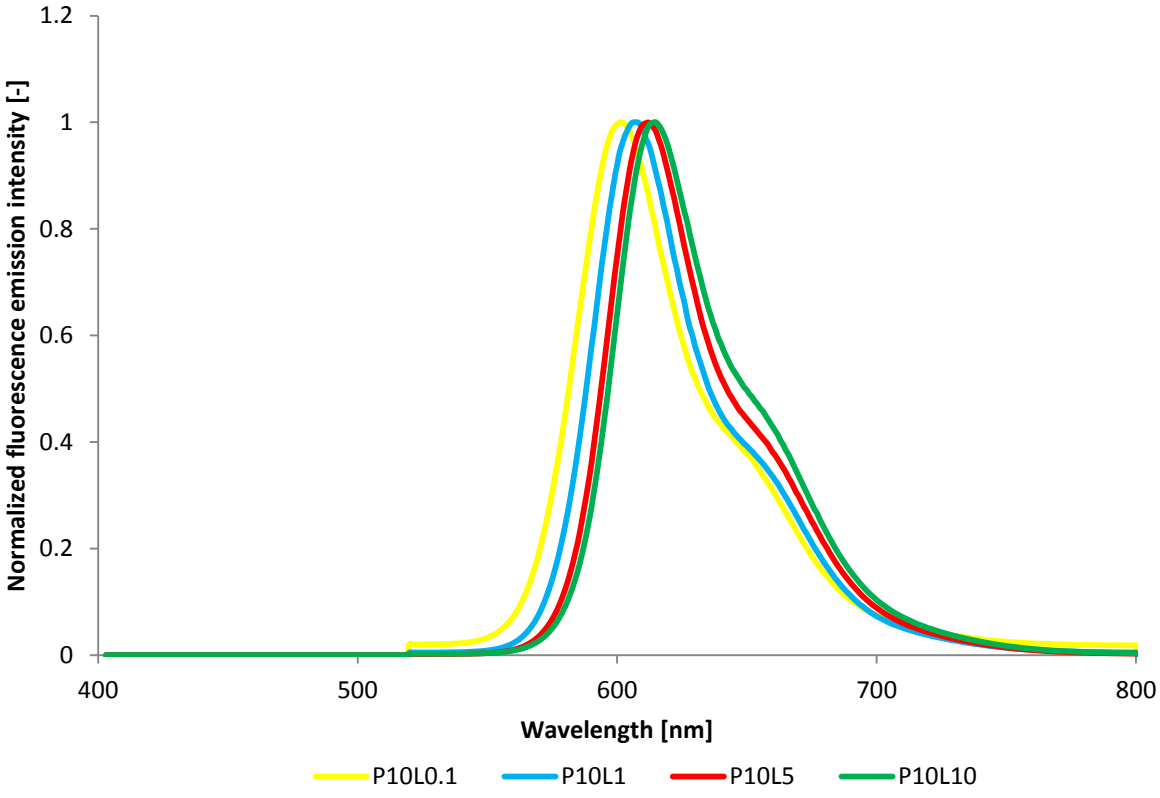

Figure IV.7 Fluorescence emission spectrum of P10L0.1, P10L1, P10L5 and P10L10.

In particular, a 17 nm redshift of the emission spectrum is observed when dye concentration is increased from 0.01 % to 10 %. Since no spectral shifts were observed in the UV-Vis spectra at varying dye concentrations (see figure IV.2), the redshift observed in fluorescence spectra results in an increase of the Stokes shift. In fact, a 23 nm Stokes shift is observed for 0.01 % dye concentration, which increases up to 40 nm for 10 % dye concentration thin film. This effects is better exemplified in figure IV.8 where the Stokes shift is presented as a function of dye concentration.

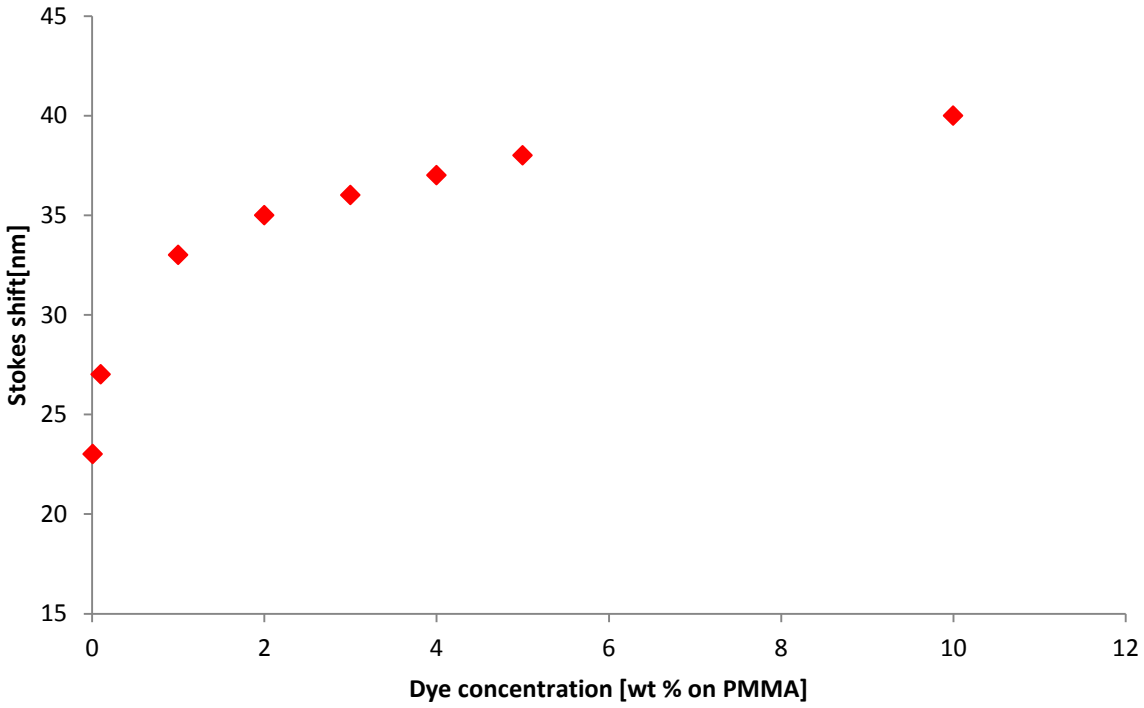

Figure IV.8 Stokes shift versus dye concentration.

This effect has already been observed in literature [4, 6-9] and is attributed to re-absorption processes mainly due to the formation of dye aggregated molecules. An emitted photon (a so called first generation photon) has a certain probability to be reabsorbed by another dye molecule depending on dye concentration. This probability increases as the dye concentration is increased. If an emitted photon is absorbed a second time and if it is re-emitted, than the emission wavelength will be higher. Indeed during a fluorescence process the energy of the emitted photon is always lower than that of absorbed photons. In the

determination of the probability that an emitted photon is reabsorbed, concentration of the dye plays a crucial role. In fact, a high dye concentration results in a high number of photons re-absorbed and thus in a more pronounced energy dissipation. This gives rise to a bathochromic shift of the emission spectrum as the concentration is gradually increased. On the other hand, at low dye concentration, the LSC film is less sensitive to re-absorption events because photons have a lower probability to be absorbed for a second time as less dye molecules are present.

IV.1.1.4 EQE measurements

EQE is defined as the percentage of incident photons that produce charge carriers and is a function of photons wavelengths. In mathematical terms, it is defined as

$$EQE = \frac{number\ of\ electrons\ produced\ by\ the\ PV\ device}{number\ of\ incident\ photons\ on\ the\ active\ surface} \qquad \text{Eq. IV.5}$$

EQE accounts for all the dissipative processes in a photovoltaic device, including reflection, transmission, losses from the escape cone, re-absorption of emitted photons, but also non-unity photo-luminescent quantum efficiency of the dye molecules. EQE measurements were carried out by irradiating the samples with light at increasing wavelength at a fixed distance (5 mm) from the edge of the plate opposite to the PV cell

In figure IV.9 EQE spectra are reported for three LSC samples with different dye concentrations. In particular we recorded these spectra for 1 % (P10L1), 5 % (P10L5) and 10 % (P10L10) dye concentration, respectively.

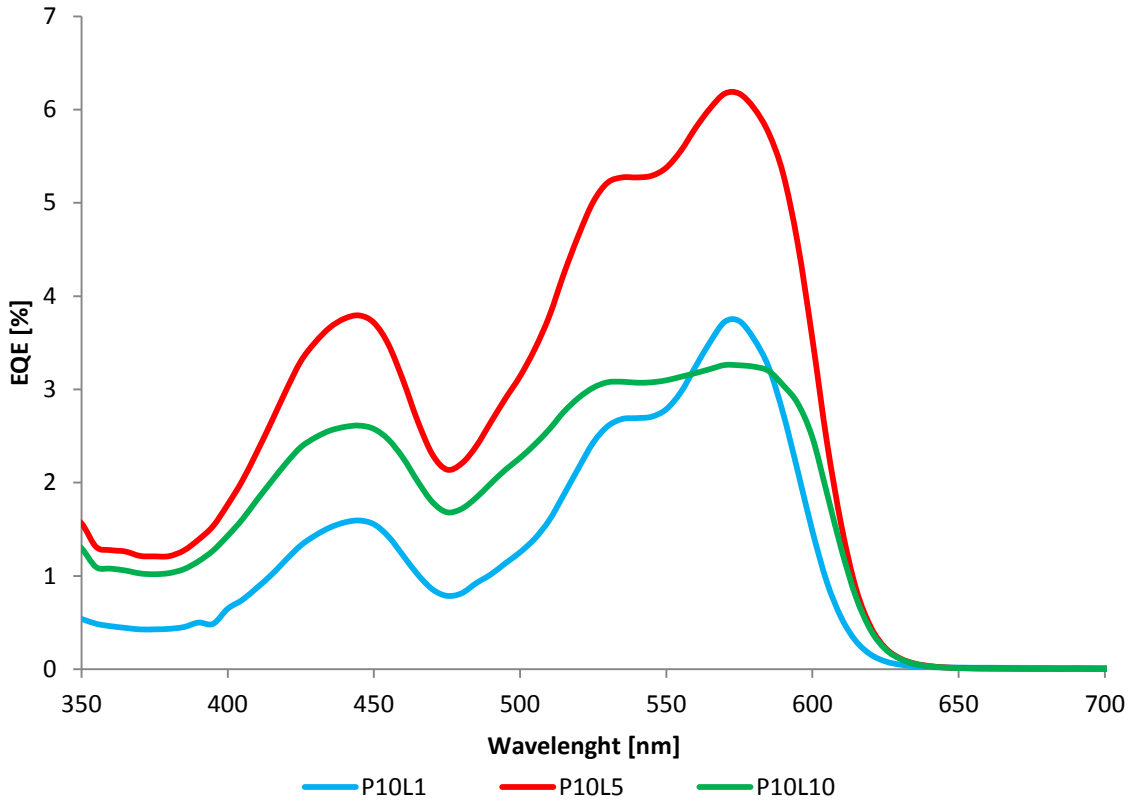

Figure IV.9 EQE spectrum of P10L1, P10L5 and P10L10. The sample which shows the maximum in the EQE is P10L5, in agreement with photovoltaic results.

As a first consideration, the shape of the EQE spectra resembles that of the UV-Vis absorption spectrum of the dye. This is not surprising because only photons that are absorbed by the LSC plate can produce charges in the external circuit.

The second effect that can be seen is that the most efficient system is P10L5 as it shows the highest EQE value and this result is in accordance with our PV results. Indeed, P10L5 generates the highest ΔPCE and also has the highest EQE. It means that a higher percentage of the incident photons compared with the other devices reaches the PV cell and is converted into useful electrical charges. It is not surprising that P10L5 presents a higher EQE than P10L1 for any wavelength because the former system absorbs a higher percentage of photons with respect to the latter, as also confirmed by the intensity of their respective UV-Vis absorption spectra. A 6 % EQE is found for P10L5 device for the peak centered at 575 nm, while only 3.7 % is reported for P10L1 for the same peak. However, other effects may also

be considered. As a matter of fact, by increasing the concentration of the dye molecule in the polymer matrix, dissipative processes may become progressively more important. In particular, reabsorption losses due to higher optical density of the LSC thin film (higher concentration of dye) and the increase in the probability of dye aggregation due to the lower dye-to-dye distance give a progressively higher contribution to the reduction of the number of photons that can reach the PV cell. In fact, despite the highest UV-Vis absorption intensity, P10L10 generates a lower number of electrical charges compared to P10L5, as shown by the lower EQE spectra observed for P10L10 compared to P10L5. This indicates that in this system, a larger number of dissipative processes take place compared to P10L5 that negatively affect the photon-to-current conversion efficiency.

By comparing the EQE spectra of P10L1 and P10L10, it is worth noticing that EQE spectrum for P10L10 lies above that of P10L1 in most part of the wavelength range 350 – 650 nm, except in the range 550 – 600 nm. In order to explain that, it is useful to monitor the higher intensity peak of every sample (575 nm) with respect to the lower intensity peak (445 nm) as a function of concentration. It is evident that the former peak becomes smaller with respect to the latter with a higher rate when dye concentration is progressively increased. It means that by increasing dye concentration, lower wavelength photons become more effective than longer wavelength photons in the production of electrical charges. This behavior may be related to the fact that for increasing dye concentration, “red” (longer wavelength) photons are more susceptible to dissipative processes compared to “blue” (shorter wavelength) photons. This effect may be correlated with the redshift of the fluorescence emission spectrum with respect to the absorption spectrum, that results in a progressively higher Stokes shift at increasing dye concentration. Such increasingly higher Stokes shift yields a progressively lower overlapping of absorption and emission spectra as dye concentration is increased.

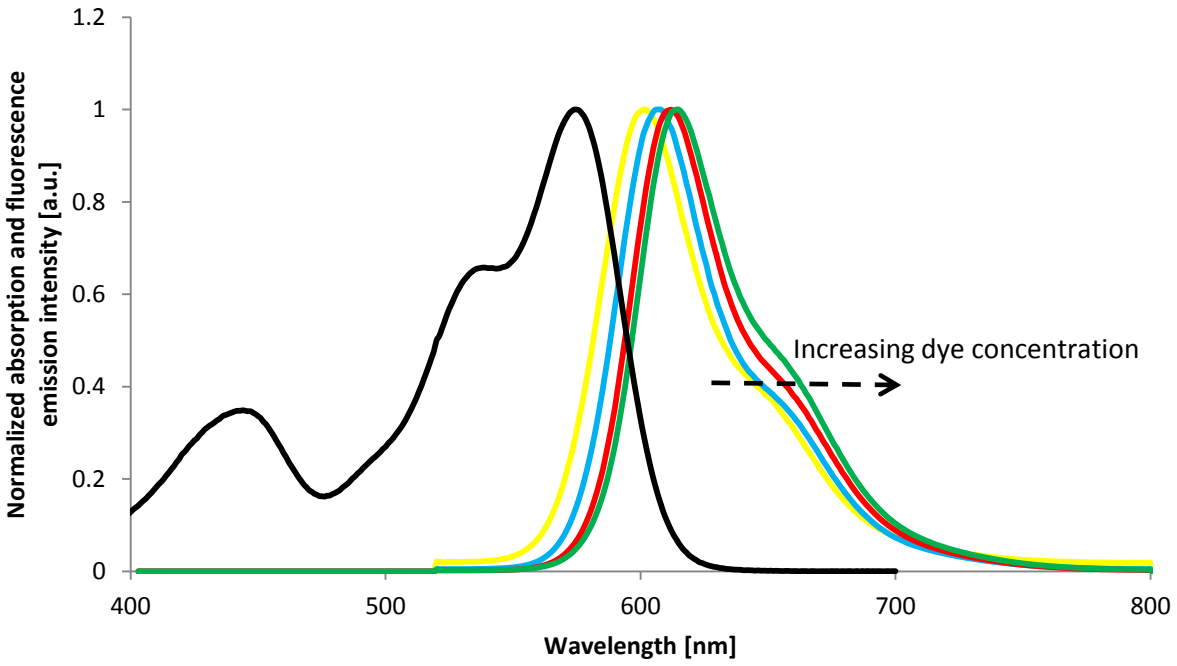

Figure IV.10 Schematization of the overlapping of the absorption and emission spectra for increasing dye concentration. As the emission spectrum progressively redshifts, the overlapping with the UV-Vis absorption spectrum decreases, leading to a progressively reduced area comprised within the two spectra.

This behavior is represented in figure IV.10. Although partial overlapping of absorption and emission spectra is always present (therefore reabsorption events are always present), the redshift of the emission spectra causes the overlapping portion to progressively decrease at higher dye concentrations. This decrease results in a progressively higher portion of photon wavelengths to be excluded from reabsorption phenomena. In particular, an increasingly larger amount of lower wavelengths photons are expected not be reabsorbed by other adjacent dye molecules. This behavior may give an explanation to the modifications to the EQE spectra observed in figure IV.8 at increasing dye concentration.

In conclusion, 5 % appears to be the optimal concentration for LFR305 in a PMMA matrix at a concentration of 10 % wt with respect to solvent. For this concentration, the highest ΔPCE is obtained in LSC devices and this trend is confirmed by different supporting techniques such as UV-Vis absorption spectroscopy, fluorescence emission spectroscopy and EQE measurements.

IV.1.2 Optimization of the thickness of the PMMA-based LSC device.

After optimizing dye concentration, the second step is the optimization of the thickness of the thin film matrix. This can be achieved by maintaining a constant dye concentration (5 %) and by varying the concentration of the polymer in solution. In particular, the following host matrix concentrations were tested: 5% (P5L5), 10 % (P10L5), 15 % (P15L5), 20 % (P20L5) and 30 % (P30L5). The purpose of this section is to highlight the effect of LSC thin film thickness on device parameters and ultimately to determine the optimal matrix concentration.

As stated above, variation of PMMA concentration leads to modification of LSC thin film thickness. Table IV.2 shows the thicknesses of PMMA matrix thin-films doped with 5 % in weight of LFR305 as a function of PMMA matrix concentration. The reported values are averaged on two measures on each sample.

Matrix content [%]	Average thickness [µm]	Standard deviation [µm]
5	1.65	0.07
10	4.25	0.07
15	9.05	0.63
20	12.70	0.42
30	35.50	0.70

Table IV.2 Average thickness of different matrix concentrations LSC thin film.

The table clearly shows that increasing the PMMA concentration results in an increase of LSC thin film thickness. In fact, thin films deposited by spin-coating can result in different thicknesses depending on several variables. One of them is polymer solution concentration. Usually, thickness increases as the polymer solution concentration increases [10].

IV.1.2.1 PV parameters

Figure IV.11 shows the power conversion efficiency gain as a function of matrix (PMMA) thickness for different samples. The reported values are averaged on three LSC's.

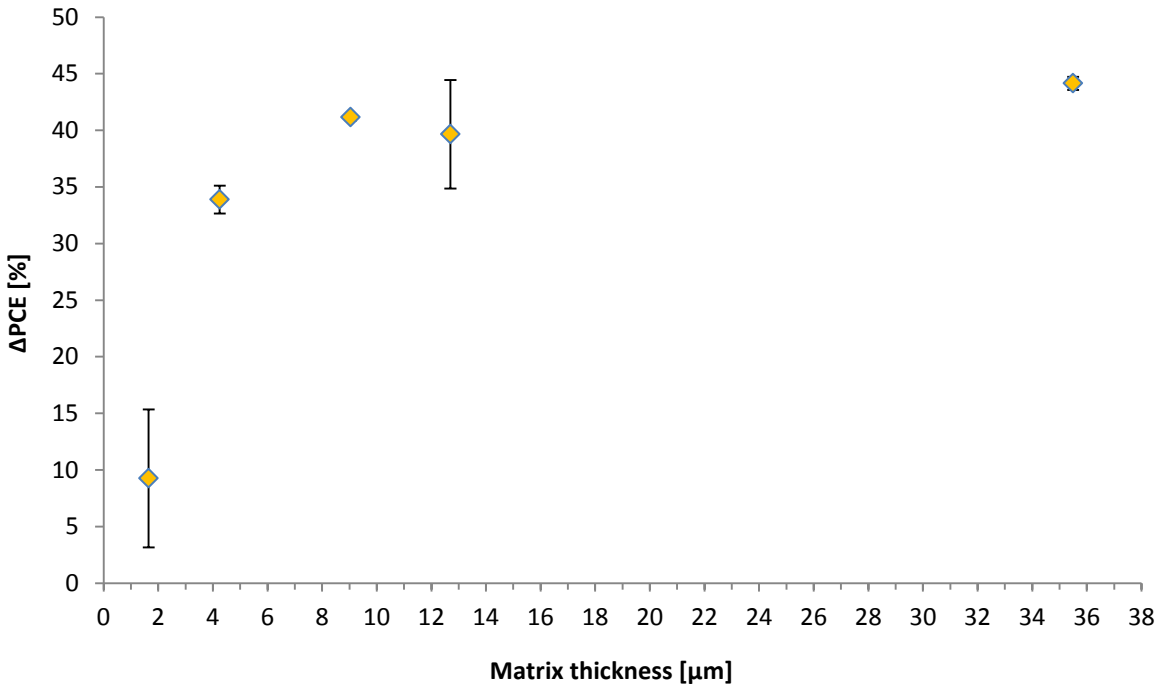

Figure IV.11 Power conversion efficiency gain versus matrix thickness. Data shown are averaged on three LSC devices.

From the graph it is apparent that increasing the matrix thickness results in an increase of ΔPCE up to a plateau value. In fact, the 9.05 µm thick matrix, the 12.07 µm thick matrix and the 35.50 µm thick matrix show the same ΔPCE (~ 42 %), thus indicating that these systems are equivalent under a PV point of view. The main PV parameters for the different PMMA thicknesses are reported in table IV.3.

Matrix thickness [μm]	I_{SC} [mA]	V_{OC} [V]	FF [%]	PCE^{cell} [%]	ΔPCE [%]	PCE^{LSC} [%]
1.65	15.41 ± 0.17	0.53 ± 0.003	54.39 ± 0.34	9.79 ± 0.22	9.26 ± 6.10	0.35 ± 0.01
4.25	19.4 ± 0.20	0.56 ± 0.001	59.03 ± 1.03	14.22 ± 0.09	33.89 ± 1.83	0.51 ± 0.00
9.05	20.31 ± 0.18	0.55 ± 0.01	56.20 ± 3.75	13.88 ± 0.36	**41.15 ± 0.27**	**0.50 ± 0.05**
12.7	20.65 ± 0.35	0.54 ± 0.01	54.83 ± 0.83	13.23 ± 0.05	39.65 ± 4.80	0.49 ± 0.00
35.5	21.17 ± 0.40	0.56 ± 0.01	59.29 ± 0.58	15.46 ± 0.65	44.15 ± 0.17	0.56 ± 0.02

Table IV.3 Photovoltaic parameters of different matrix thickness LSC. In bold the ΔPCE and PCE^{LSC} of the best performing LSC.

As cab be seen from table IV.3, the increasing ΔPCE is mainly due to the increasing current for increasing matrix thickness. This happens up to 9 μm thickness matrix, after which a plateau is observed. Indeed, the current intensities for the 9 μm, the 12 μm and the 35 μm thick matrices are analogous.

IV.1.2.2 UV-Vis absorption spectroscopy

UV-Vis absorption spectra were recorded for the different samples having different matrix thickness.

On the basis of the thicknesses reported in table IV.2, the expectation is that the more the matrix is concentrated, the more light is absorbed. Indeed this effect is shown in figure IV.12. where the UV-Vis absorption spectra for the PMMA-based films with different thickness are reported. The 35 μm-thick film was not included in figure IV.12 because its UV-Vis absorption spectrum could not be recorded by the instrument due to signal supersaturation.

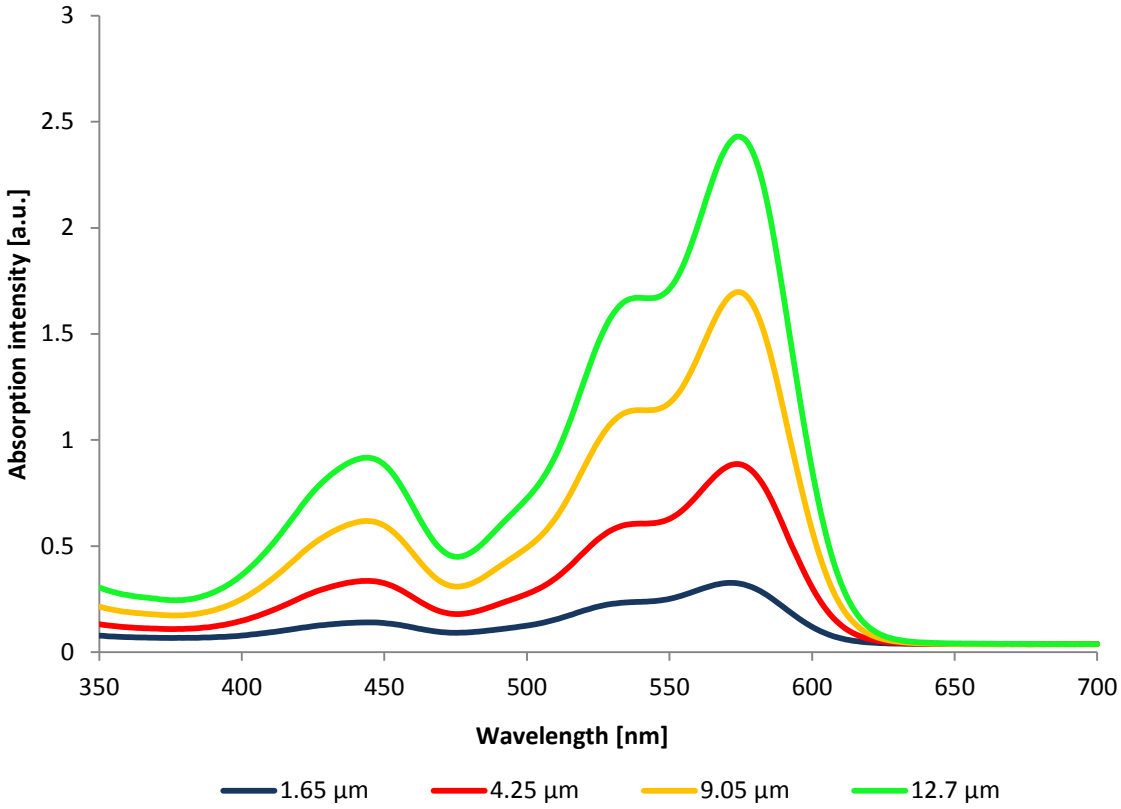

Figure IV.12 UV-Vis absorption spectra of PMMA matrices with different thickness. The absorption spectrum of the 35 µm-thick matrix could not be recorded due to signal supersaturation.

According to the results obtained from UV-Vis absorption spectroscopy, the 35 µm-thick matrix absorbs more photons than any other LSC sample. On the other hand, the thinner LSC sample is characterized by a low absorption intensity. On the basis of these results, UV-Vis spectroscopy only is not able to justify the PV behavior of LSC with different polymer matrix thicknesses.

To investigate more deeply the optimization of the thickness of the matrix, additional tests were performed. In the next section the fluorescence emission spectra will be considered.

IV.1.2.3 Fluorescence spectroscopy

In this section the fluorescence emission spectra for LSC samples with different matrix thickness are discussed.

In figure IV.13 the emission spectra are reported. Emission spectra were recorded with an excitation wavelength of 445 nm.

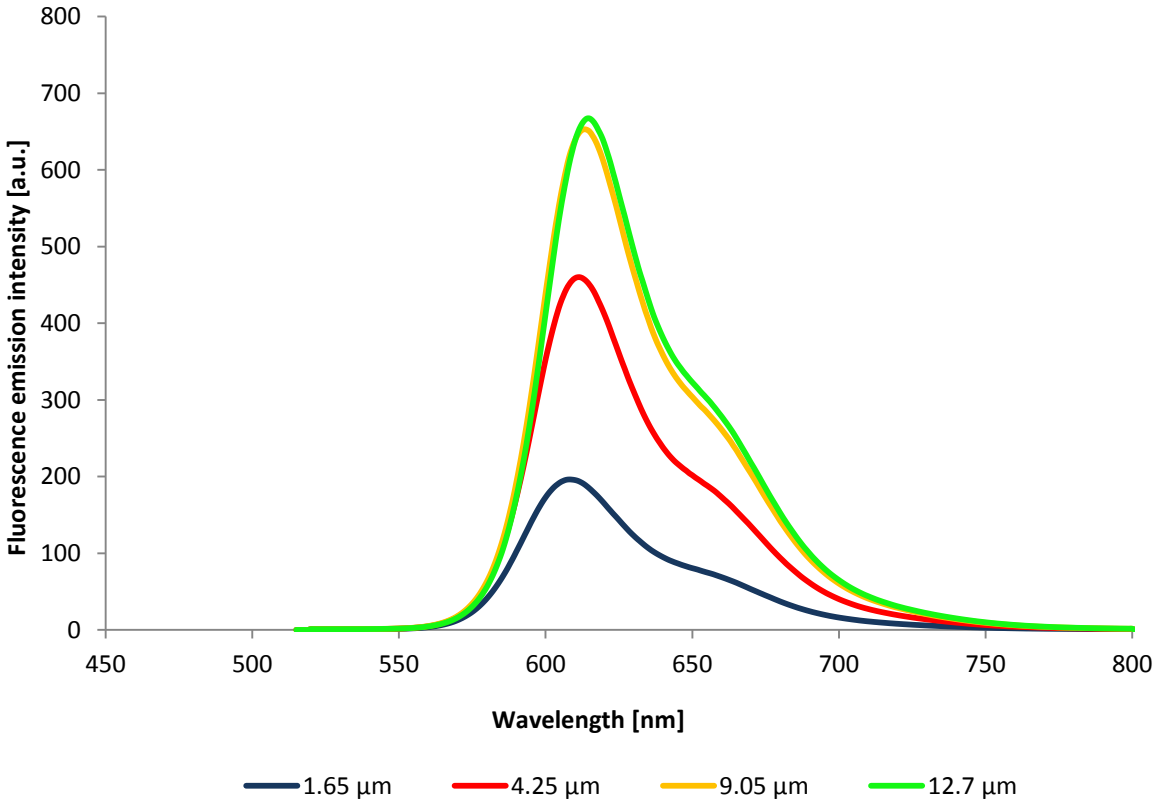

Figure IV.13 Fluorescence emission spectra of PMMA-based matrices with different thickness.

From the spectra two major effects can be observed: the variation of the emission intensity with matrix thickness and a progressive redshift as the thickness of the matrix is increased. Let us focus on the first effect.

Fluorescence emission intensity increases as the thickness of the matrix is increased. Considering the absorption spectra this is a reasonable effect, as it can clearly be correlated with the amount of photons absorbed that can be emitted by a dye molecule. Indeed if dissipative processes are considered to be constant, the more light is absorbed by a sample,

the more light is emitted. It was shown in the previous section that dye aggregation may be present in the systems under study. However, the formation of dye aggregates is mainly dependent on the concentration of dye molecules in the LSC thin film. In this paragraph, LSC samples with constant dye concentration are considered. Therefore the negative contribution to the LSC efficiency given by aggregate formation should be equal for all the systems. As a result, the variation of emission intensity with film thickness may be related to the number of photons absorbed by each LSC sample, thus to their UV-Vis absorption spectrum.

At increasing film thickness, a higher absorption intensity is observed. This should proportionally correspond to a higher emission intensity at increasing film thickness, in the case no dissipative phenomena are present.

In order to clarify this aspect, chart IV.14 shows the fluorescence emission intensity versus the UV-Vis absorption intensity for samples at increasing film thickness. The thickest sample (35 µm thick matrix) was not included in the figure because its UV-Vis spectrum could not be collected due to instrument limitations (see previous discussion).

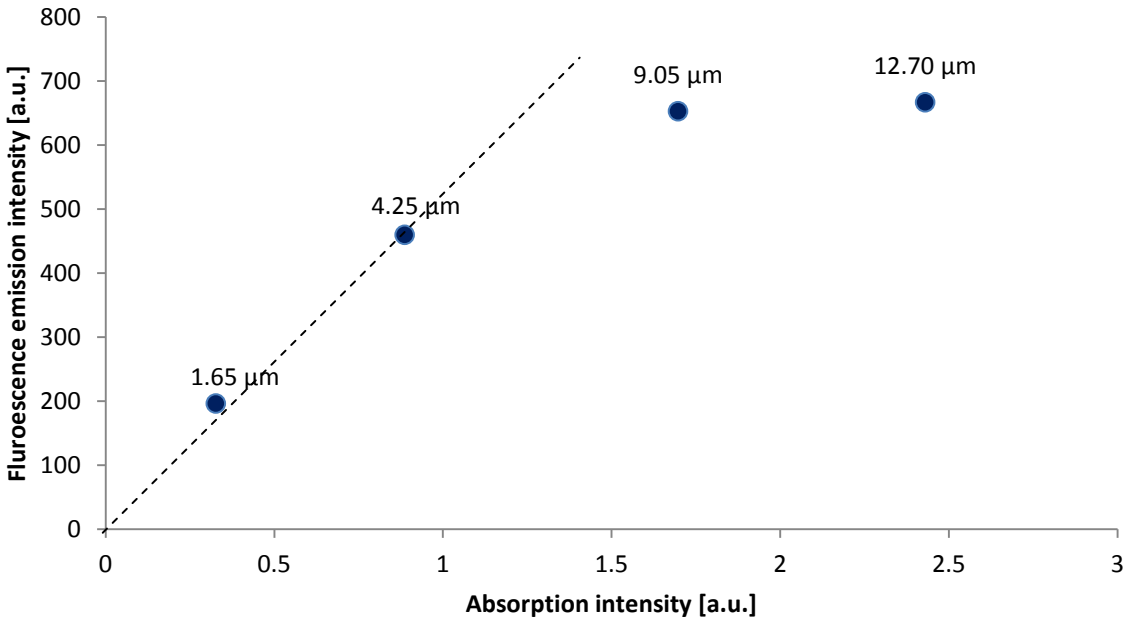

Figure IV.14 Fluorescence emission intensity versus UV-Vis absorption intensity for PMMA-based matrices with different thickness. The linearity of the plot is respected only for the 1.65 µm thick and 4.25 µm thick matrix as can be observed from the interpolating dashed line. The equation of the line is: y = 528.4x (with a R^2 = 0.98).

As shown in the plot, for matrix thickness up to 4.25 µm the emission intensity increases linearly with the absorption intensity, indicating that dissipation phenomena, if present, can be considered negligible. However, when the thickness is further increased (9.05 µm and 12.7 µm) deviation from this linearity is observed. In particular, the increase of absorption intensity is higher than the corresponding increase in emission intensity, thus indicating that dissipative mechanisms take place. This effect could be due to the occurrence of reabsorption events that may cause a decrease of the number of re-emitted photons resulting in a progressively higher loss of fluorescence (increasing dissipation) as the film thickness increases. As the LSC film thickness increases (from 9.05 µm to 12.7 µm), a higher amount of photons is absorbed whose positive effect is however counterbalanced by the increased dissipation processes. This results in a constant emission intensity normalized on the absorption intensity. This trend well correlates with the results obtained from PV characterization of LSC devices. A further confirmation of this trend will be given in the next section where EQE spectra will be analyzed.

Let us now focus on the redshift of the emission spectra as the thickness of the matrix increases.

Figure IV.15 depicts the normalized emission spectra for LSC's with different PMMA thickness.

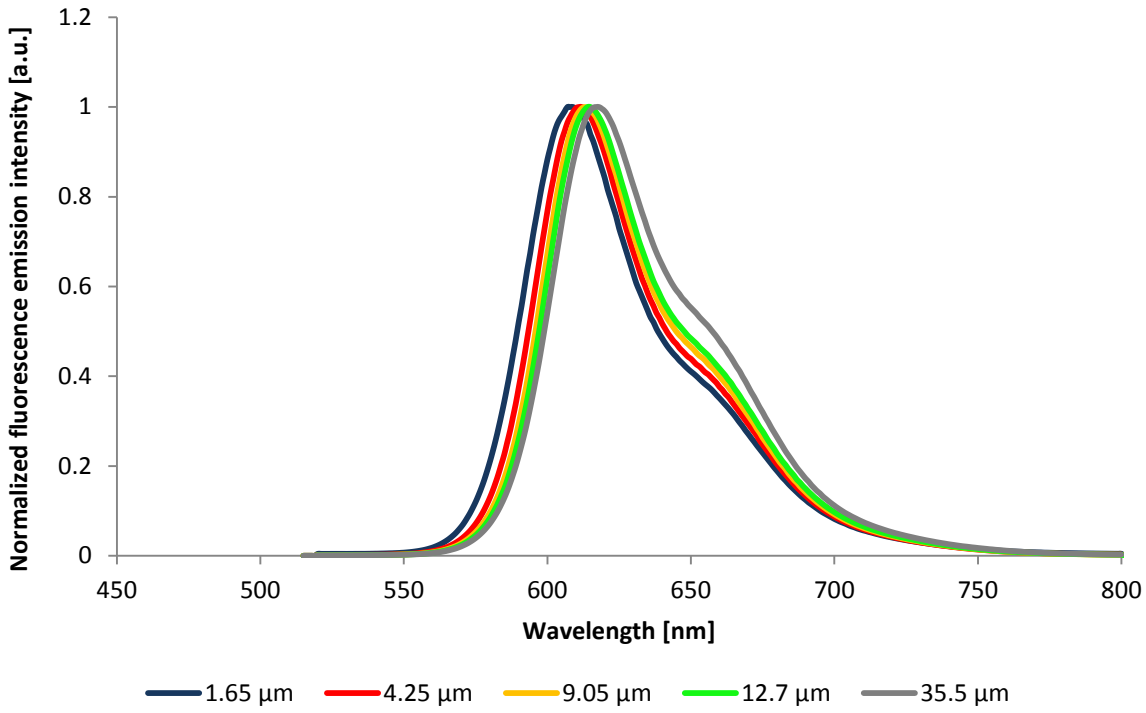

Figure IV.15 Normalized fluorescence emission intensity for 1.65 µm thick, 4.25 µm thick, 9.05 µm thick, 12.7 µm thick and 35.5 µm thick matrices. Also the normalized fluorescence emission spectrum of the 35.5 µm thick matrixis reported in order to clarify the increasing redshift as the matrix thickness increases.

As can be seen from the chart, there is a progressive redshift of the emission spectrum as the PMMA thickness is increased (increased PMMA concentration in solution). Being the absorption spectrum not subjected to shifts, the increasing redshift of the fluorescence emission spectrum results in a progressively increasing Stokes shift. A quantification of this Stokes shift is presented in figure IV.16 where the values of Stokes shift are reported as a function of matrix thickness. Note that it was not possible to report the redshift of the thickest sample (that with a matrix thickness of 35 µm) because its absorption spectrum cannot be recorded.

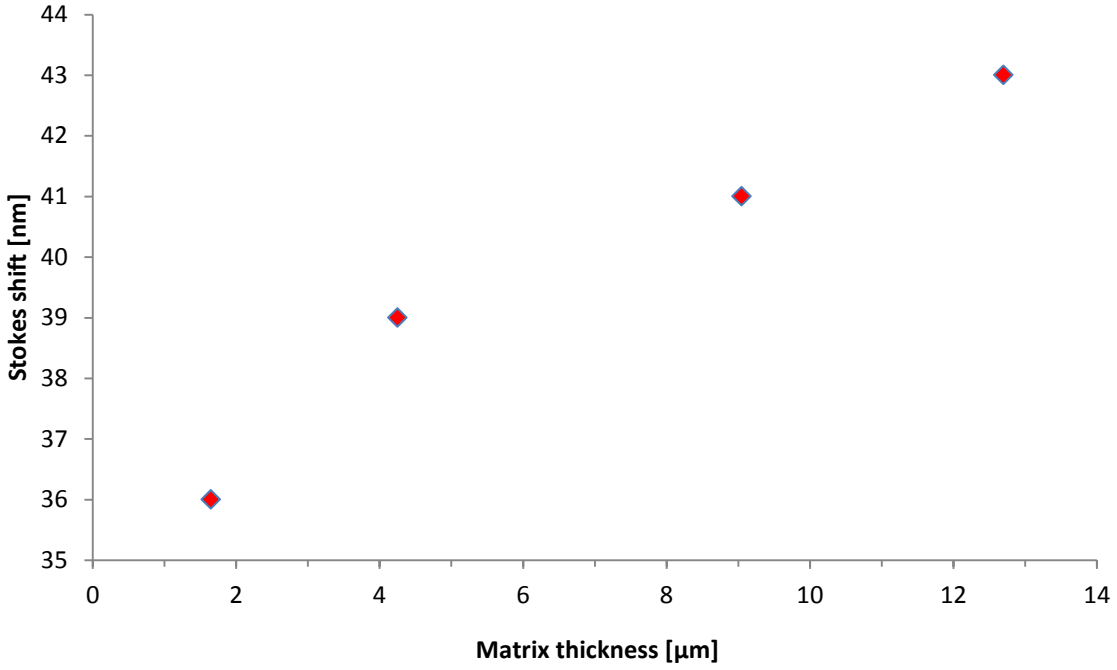

Figure IV.16 Stokes shift versus matrix thickness. As the matrix become thicker, the Stokes shift increases.

The 12.7 µm thick matrix showed a 43 nm Stokes shift while the 1.65 µm thick matrix only 36 nm. The same trend is expected for the 35.5 µm thick matrix. This increasing Stokes shift can be explained by the higher path length that an emitted photon must travel. The fluorescence spectrum of a sample is recorded by irradiating the surface of the sample with a light spot. The illuminated surface is always the same but the overall number of dye molecules interested by the light beam increases as the thickness increases. In fact, despite the dye concentration is constant, the higher film thickness results in a higher number of dye molecules. Let us consider for example an incident photon. If this photon is absorbed and re-emitted, than it must travel a longer distance to exit the LSC film and reach the collector. This is due to the higher thickness of the luminescent film. Because the distance is longer, it experiences a higher probability to be reabsorbed by another dye molecule due to the higher number of molecules he encounters during its travel towards the collector. The higher number of dye molecules that an emitted photon sees is due to the higher thickness of the LSC film which increases the path length the emitted photon must travel into the film. If a photon is re-absorbed and emitted once again, than its energy will be lower than the

original photon emitted. This energy decrease may explain the redshift of the emission spectrum as the film thickness is increased.

Maggioni et al. [3] studied a parylene matrix in which Lumogen F Red 305 was dispersed as a possible luminescent solar concentrator. They performed spectroscopy analysis for different matrix thickness of the thin film. They showed that if the absorption peak does not shift but the emission one does, than the effect can be ascribable to the thickness of the film which increases the optical density.

In order to investigate more deeply the effect of reabsorption and to clarify which photons are prone to this effect, EQE measurements were performed, that are discussed in the next section.

IV.1.2.4 EQE measurements

EQE measurements were performed by irradiating the LSC at a distance of 5 mm from the edge opposite to the attached PV cell. EQE spectra are reported in chart IV.17.

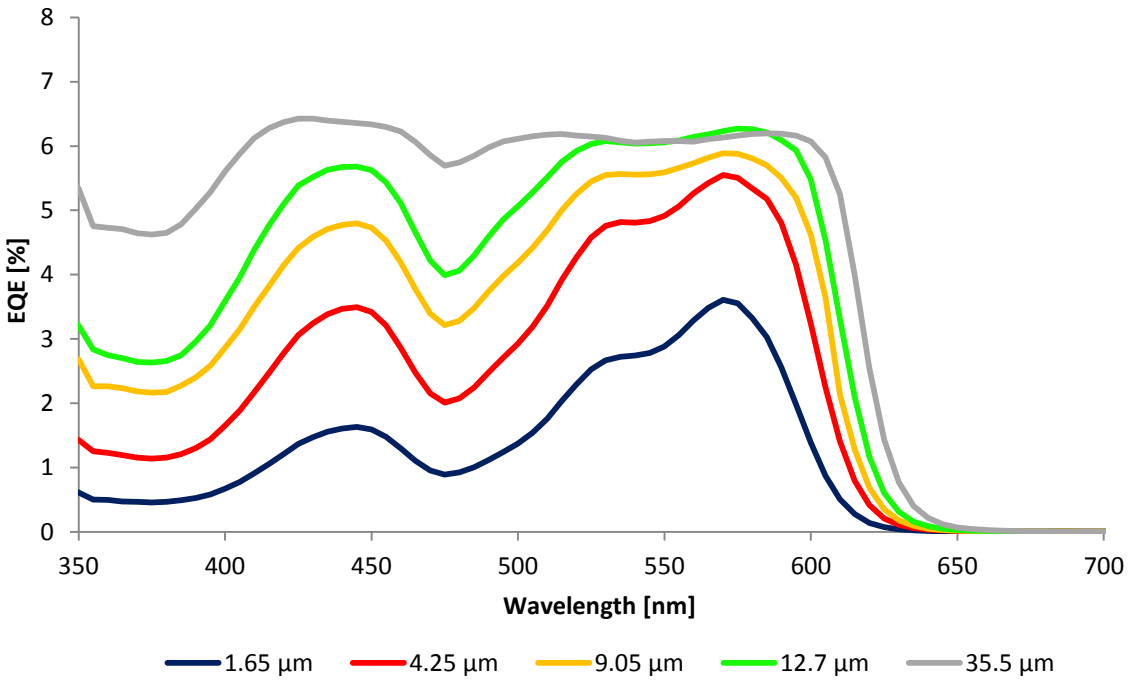

Figure IV.17 EQE spectra for different matrix thickness PMMA-based LSC devices.

To understand the EQE presented a premise is mandatory. These measurements were carried out on the LSC that, for a fixed film thickness, gave the highest ΔPCE. In practice, the PV data reported (see section IV.1.2.1) are average on three LSC's. EQE measurements, on the other hand, were done on one sample, the one giving the highest ΔPCE. Thus it is not surprising that despite the similar average ΔPCE of the 9.05 μm thick and the 12.7 μm thick matrix, their EQE are different. In fact, the EQE of the latter lies slightly above that of the former because the 12.7 μm film LSC tested was characterized by a ΔPCE of 43 % while the 9.05 μm film LSC device tested showed a ΔPCE of 41 %.

Two effects can be seen from the chart. The first one concerns the intensity of the curves while the second refers to the smoothening of the long wavelength part of the curve as the matrix concentration is increased.

The first effect can be interpreted in the following way. As the film thickness is increased, ΔPCE increases until it reaches an approximately constant value which is registered from 9.05 μm film thick on (see figure IV.10). In addition, for the 9.05 μm-thick film, 12.7 μm-thick film and the 35.5 μm-thick film, small differences in the EQE spectra are registered among each other, even though their ΔPCE value is approximately constant. In particular referring to ΔPCE for the LSC tested in the EQE test, the values are: $\sim$ 41 %, $\sim$ 43 %, $\sim$ 44 % for the 9.05 μm film, the 12.70 μm film and the 35.50 μm film respectively. This slight difference in the ΔPCE can be the reason that explains why the different EQE curves are not exactly superimposed. In general, the systems which give the lower ΔPCE should be those which give the lower EQE. This is confirmed in our case by looking at the EQE of the 1.65 μm film, 4.25 μm film and e.g. 12.7 μm film, one of the film thickness whose ΔPCE lies within the plateau. A higher EQE means that a higher percentage of photons is able to reach the cell and produce electrical charges.

The second observable effect is the progressive smoothening of the EQE curve on the red edge as the film thickness is increased. It is evident that the peak centered at 575 nm in the EQE spectra becomes smaller with respect to that at 445 nm with a higher rate, when thickness of the matrix is progressively increased. It means that by increasing matrix thickness, lower wavelength photons become more effective than longer wavelength photons in the production of electric charges. This behavior may be related to the fact that

for increasing matrix thickness, “red” (longer wavelength) photons are more susceptible to dissipative processes compared to “blue” (shorter wavelength) photons. This effect may be attributed to the redshift of the fluorescence emission spectrum with respect to the absorption spectrum, that results in a progressively higher Stokes shift at increasing film thickness. Such increasingly higher Stokes shift yields a progressively lower overlapping of absorption and emission spectra as film thickness is increased. This behavior is schematically represented in figure IV.18.

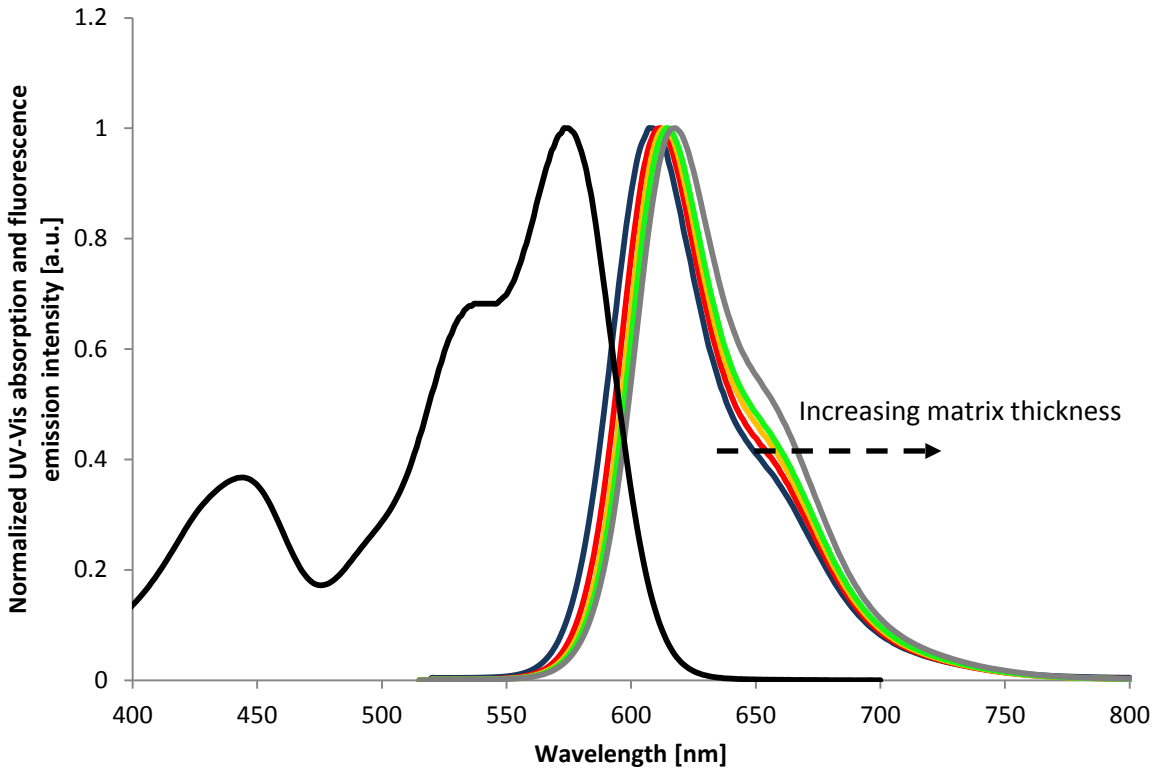

Figure IV.18 Overlapping between the absorption and fluorescence emission spectra as the matrix thickness is increased. As the emission spectrum progressively redshifts, the overlapping with the UV-Vis absorption spectrum decreases, leading to a progressively reduced area comprised within the two spectra.

Although partial overlapping of absorption and emission spectra is always present, the redshift of the emission spectra causes the overlapping portion to progressively decrease at higher film thickness. This decrease results in a progressively higher portion of photon wavelength to be excluded from reabsorption phenomena. In particular, an increasingly amount of lower wavelengths photons will not be reabsorbed by other adjacent dye

molecules. This behavior may explain the modifications to the EQE spectra observed in figure IV.17 at increasing film thickness.

In the following parts of this work, the optimal film thickness will be fixed at 9 µm that corresponds to fixing the polymer solution concentration at 15 % on weight. This system gave the highees ΔPCE, that is approximately 40 %. Although other matrix thickness (12.7 µm and 35.5 µm) gave the same results, we decide to choose the PMMA matrix thickness that gave the highest performance with the lowest amount of material.

IV.1.3 Optimization of the waveguide aspect ratio

A further optimization step considered in this work is the optimization of the waveguide aspect ratio. In the literature there already exist studies [11, 12] aimed at the determination of the optimal aspect ratio (L/W), in which L is the length of the plate and W is its width onto which a PV cell is placed. This study was performed by fixing the thin-film composition, i.e. using a 15 % PMMA matrix concentration and a 5 % LFR305 dye concentration (P15L5). To investigate different L/W ratios, we fixed the width of the plate (25 mm) and varied its length. In figure IV.19 a sketch of the different LSC's L/W ratio tested is reported.

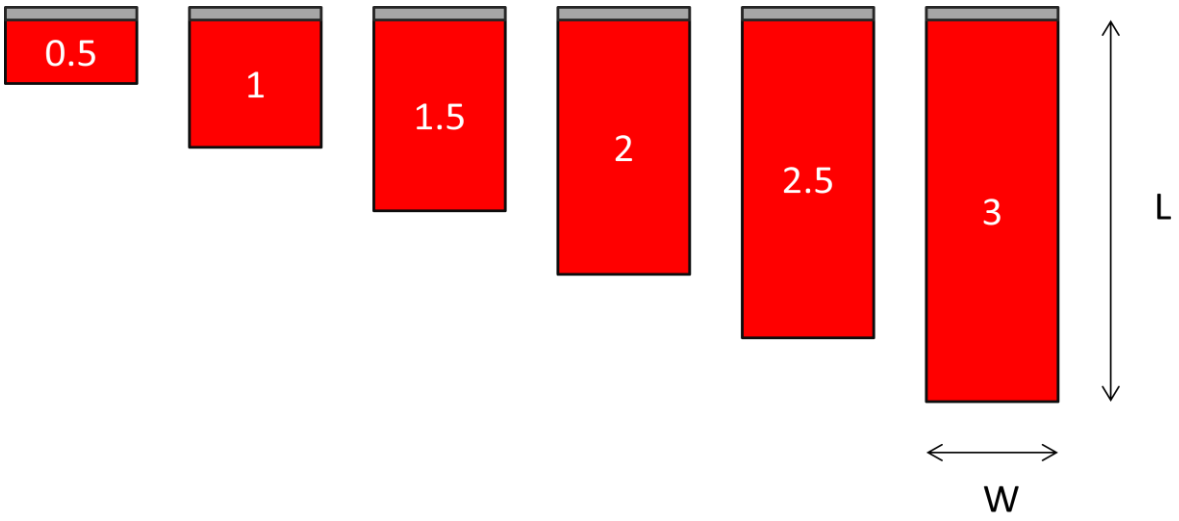

Figure IV.19 Luminescent solar concentrators with different L/W ratio. The number reported on the surface of the LSC is the value of the L/W ratio. The luminescent plate is attached to the PV cell which is indicated by the grey rectangle.

IV.1.3.1 Testing configurations

Different configurations were tested. First of all we built different concentrators with different dimensions and we performed tests on these samples. In this way, different thin films and different PV cells were compared with each other. This approach led to the appearance of some difficulties in appreciating V_{OC} variations resulting from modifications of LSC dimensions. This was due to the slightly variable performance characteristics of each PV cell tested. To eliminate all the differences we decided to perform tests onto a unique plate (25 x 75 mm^2) and by properly reducing the light exposed LSC area. We reduced LSC area by covering the LSC plate with a black adhesive tape. The black color was used to avoid that the ideally un-exposed area could receive photons. All the incident photons on the black surface are thus absorbed and do not enter the waveguide. In another configurations we used a black cardboard instead of the black adhesive tape that was slided over the LSC area, so that an increasing portion of it could be covered. The two configurations are equivalent from a practical point of view because both show the same results as can be seen from chart IV.20, which displays ΔPCE versus L/W ratio. In addition, similar trends are observed when different concentrators are employed. Thus it is absolutely the same to consider results obtained from any of the configuration studied (Different LSC's, Black adhesive tape or Black cardboard). For practical reasons, results obtained from the configuration employing black adhesive tape to cover the LSC are will be presented in the following.

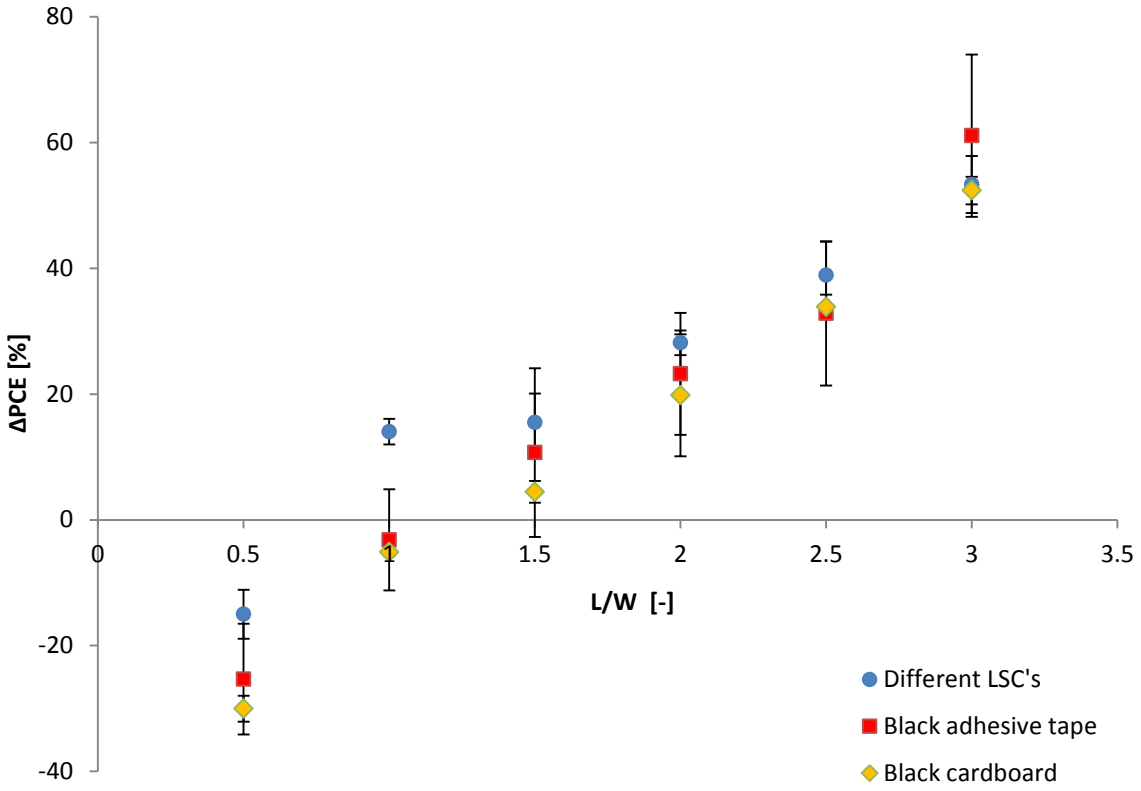

Figure IV.20 Power conversion efficiency gain versus L/W ratio. Different configurations are taken into account. Each of the point is averaged on three LSC's.

IV.1.3.2 PV parameters

As we can see from chart IV.20, using a longer waveguide results in a larger ΔPCE. Thus the longer the waveguide, the higher the efficiency increment ΔPCE. On the other hand the absolute PCE of the LSC device based on the illuminated area of the LSC, PCE^{LSC}, reduces when length is increased. This effect can be clearly seen in chart IV.21 where the normalized trends for ΔPCE and PCE^{LSC} are reported as a function on L/W ratio. From here on, all the data shown come from the LSC device that gave the best performance for L/W equal to 3 and whose exposed area was progressively reduced by means of black adhesive tape.

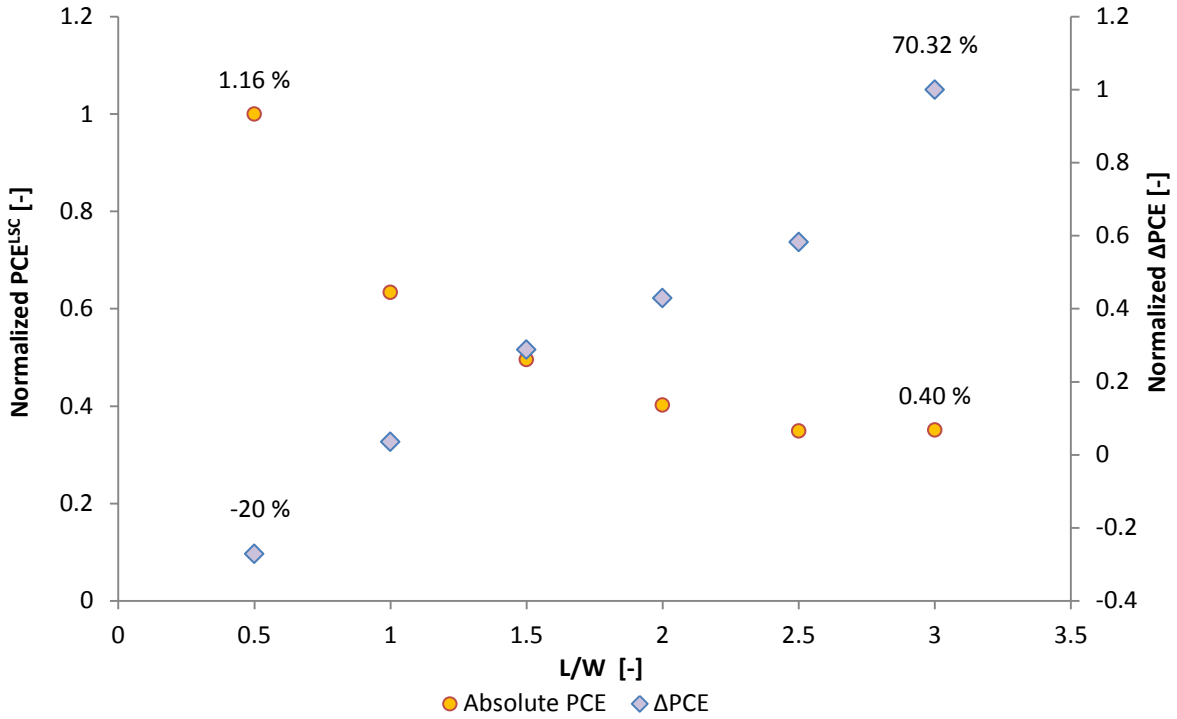

Figure IV.21 Normalized PCE^{LSC} and ΔPCE versus L/W ratio. Actual values for L/W = 0.5 and L/W = 3 are also specified.

First of all a rapid comment should be done on the absolute PCE. In absolute terms, the LSC efficiencies are rather low and this is a clear signal that indicates that this promising technology should be further optimized before practical exploitation. The efficiency gain ΔPCE, on the other hand, is four-times larger as the L/W passes from 0.5 to 3. By considering the absolute PCE, as the length of the plate is increased, absolute efficiency decreases. The reason for this behavior can be explained as follows: a longer waveguide, due to the higher illuminated area, has a higher number of luminescent molecules which can absorb and re-emit photons. The number of photons absorbed and re-emitted is much higher than in the case of a shorter waveguide: supposing that the quantum efficiency of the luminescent species does not vary with plate length, in case of a longer waveguide more photons reach the PV cell in absolute terms and so more photons are able to produce photo-current. However a longer waveguide implies that re-emitted photons have to travel on average a longer distance to reach the PV cell. If a photon has to be waveguided for a longer path length then it has a higher probability to be reabsorbed by other dye molecules or scattered,

and thereby to be lost. In a shorter waveguide, on the other hand, photons have to travel for on average a shorter path before reaching the photovoltaic cell. Being the photon path reduced, also the probability for the photons to be lost is reduced. In this way we mean that a shorter waveguide is more efficient because a higher percentage of the re-emitted photons can reach the PV cell. The increased path length in long waveguides compared to short waveguides, is responsible for the reduction of absolute PCE versus L/W ratio. This trend can be further analyzed by considering the behavior of normalized photo-current densities calculated on the basis of the active area of the LSC plate and on the basis of the active area of the PV cell (see figure IV.22).

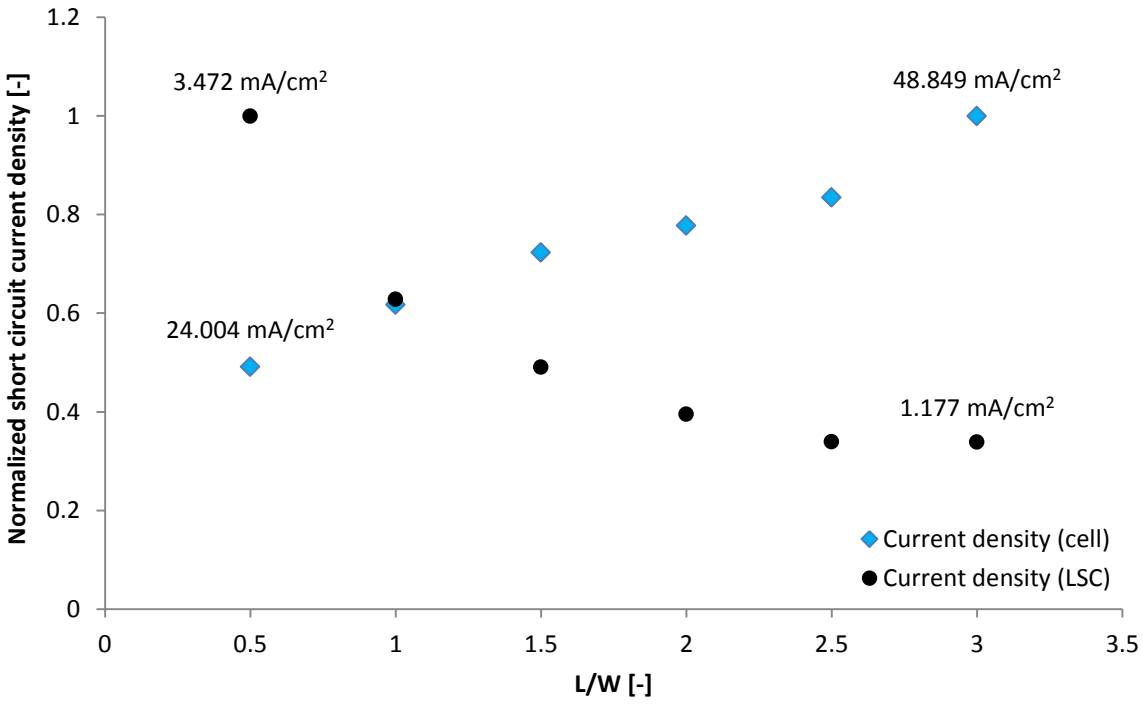

Figure IV.22 Normalized current densities calculated on cell area and on LSC area. Actual values for L/W = 0.5 and L/W = 3 are also specified.

Current density calculated with respect to cell area, goes from more or less 24 mA/cm^2 to 48 mA/cm^2. On the other hand, current density calculated with respect to the entire area of the LSC plate decreases from 3 mA/cm^2 to 1 mA/cm^2 by increasing L/W ratio. The results shown

are in accordance with those found in the literature [11, 12]. A higher current density with respect the LSC entire area results in a more efficient LSC. Following this reasoning, a short waveguide produces more current than a longer waveguide with respect to the exposed LSC area. Despite a longer luminescent plate produces a higher absolute value of current, current produced per area exposed is lower. Current density calculated on the cell area shows the same behavior as that given by the current, because the PV cell area is the same for each dimension of the LSC plate considered (is independent of L/W ratio), and thus current density is calculated with respect to the same area for each LSC. This is not the case for current density with respect to LSC area because each LSC plate has a different active area.

When considering the behavior of V_{OC}, it can be seen that also this parameter undergoes slight changes depending on L/W ratio, as shown in figure IV.23. In particular V_{OC} is shown to increase as the aspect ratio of the waveguide is increased (length is increased). Since the quantum yield of the dye is not expected to vary with aspect ratio an explanation can be given by considering that more light reaches the collector as the LSC length is increased and so the total current increases, determining a V_{OC} growth.

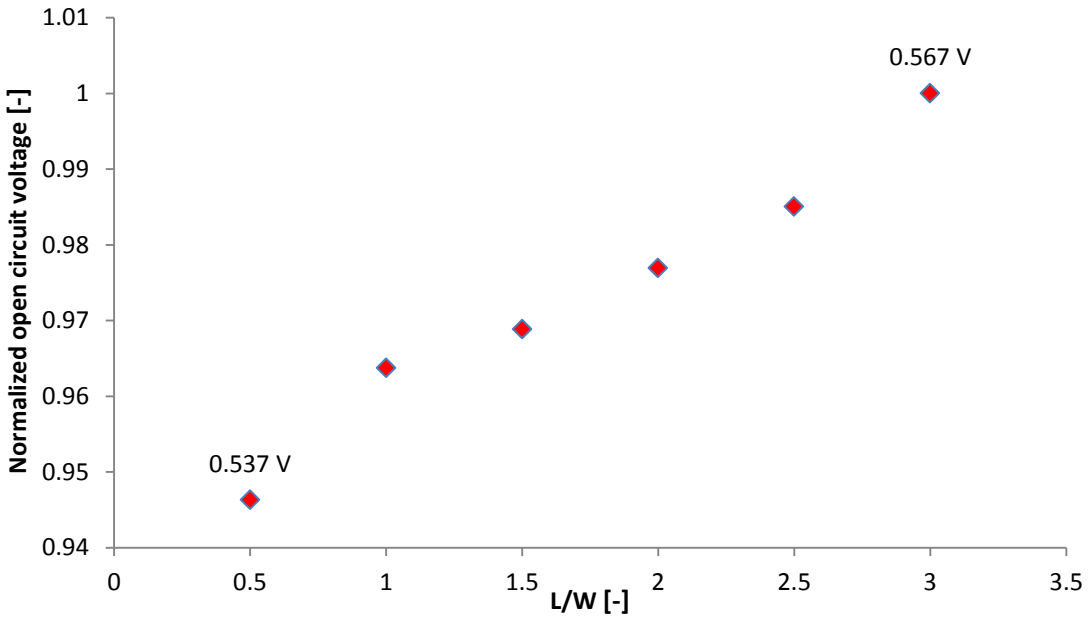

Figure IV.23 Normalized open circuit voltage versus aspect ratio (L/W). As the L/W passes from 0.5 to 3, the open circuit voltage varies of 30 mV. On the lower and bigger L/W points are reported also the correspondent open circuit voltages

In the figure, in addition to the normalized trend, the actual V_{OC} values are reported for the lowest and the highest L/W LSC plates. V_{OC} variations result in an increase of 30 mV.

We have seen that the longest luminescent plate is the less efficient in absolute terms (PCE^{LSC} is the lowest) but promotes the largest ΔPCE with respect to the attached PV cell. The shortest plate, on the other hand, is the most efficient but it promotes the smallest ΔPCE.

IV.1.3.3 EQE measurements

One way to investigate more in depth the effect of L/W aspect ratio on LSC performance is to carry out EQE measurements.

EQE measurements were performed by illuminating the film at a fixed distance (5 mm) from the edge of the luminescent plate opposite to the PV cell. In this way an attempt is made to highlight effect on LSC performance of path length of photons, which travel in waveguides of different length.

The EQE spectra for different aspect ratios (L/W) are presented in figure IV.24. We restrict wavelengths of interest to the absorption range of Lumogen F Red 305, thus from 350 nm to 650 nm. Outside this range, no appreciable EQE is detected.

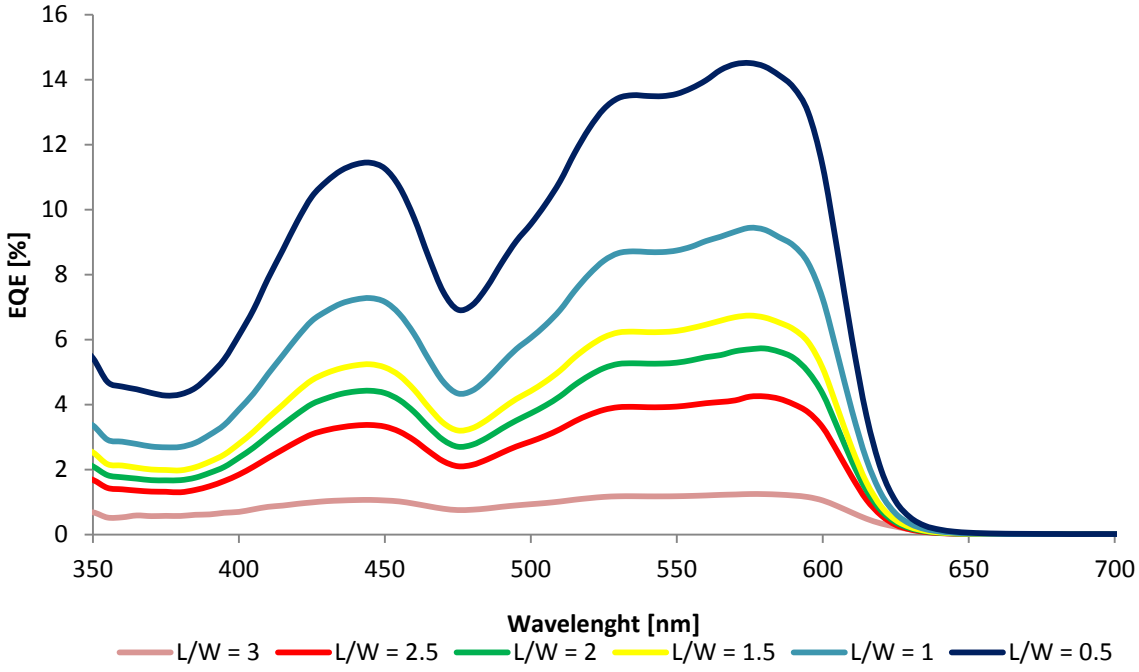

Figure IV.24 EQE (%) curves versus wavelength for samples characterized by different L/W ratio.

From the chart it emerges clearly that the shortest LSC is the most efficient because for any wavelength, a higher percentage of incident photons can provide electrons in the external circuit (the EQE spectrum increases as L/W decreases). As the L/W is increased, that is as its length is increased, the plate become less efficient and this is in accordance with EQE spectra. As the length is increased, EQE spectra is shifted downward. This means that any photon emitted in a longer waveguide has a larger probability to experience a dissipative process such as re-absorption, scattering and escaping from the waveguide via escape cone. This results are in agreement with literature reports [11] where a theoretical study was carried out on analogous systems.

IV.1.4 Use of back reflectors

A back reflector (BR) is a powerful tool to increase the performance of a LSC because it redirects photons transmitted or escaped from the waveguide back towards the waveguide. In this way the overall number of photons travelling in the waveguide by TIR is higher than the case in which back reflector is not used.

Before proceeding with the discussion, it may be useful to summarize the nomenclature in the case of tests on back reflectors testing. A general abbreviation for back reflector identification is the following one: PxTy, where P stands for PMMA (which is the binder in which the white pigment was dispersed) while T for TiO_2 (which is the pigment we used to promote light scattering). x identifies the weight ratio of polymer with respect the solvent used in preparing the solution. In mathematical terms, $W_{PMMA}/W_{CHCl_3} * 100$. y, on the other hand, identifies $W_{Titanium\ dioxide}/W_{PMMA} * 100$.

Testing was done on P15L5 luminescent solar concentrators while the length of the luminescent plate was fixed at 50 mm and the width was set equal to that of the PV cells, i.e. 25 mm.

Varying the polymer solution concentration results in thickness variation. In particular, as the matrix concentration increases, the thickness of the deposited film increases too. This

effect can be observed in table IV.4 where the thickness corresponding to a given matrix concentration is reported.

Matrix concentration [%]	Average thickness [µm]	Standard deviation [µm]
5	1.98	0.18
10	6.91	0.86
15	13.52	0.94

Table IV.4 Average thickness of different binder (PMMA) concentrations.

It is worth noticing that thickness was found not to vary with TiO_2 content for a fixed binder concentration.

IV.1.4.1 Testing configurations

With our instrumentation we were not able to deposit reflecting films directly on the bottom of the luminescent plate so we deposited reflecting films on top of another glass slide of the same dimension as the LSC plate. Before testing the LSC, we placed the back reflectors on the bottom of the luminescent plate. We tested different back reflectors, each having a different thickness and a different white TiO_2 pigment content. PMMA was used as binder. We tested two different configurations: a first configuration in which a small air gap (3 mm) is allowed between the LSC plate and the BR; a second configuration in which the luminescent plate is placed on the back reflector, with no air gap in between them. Studies on similar configurations were reported in the literature [11, 12] on different systems. Figure IV.25 presents a sketch of the two configurations tested.

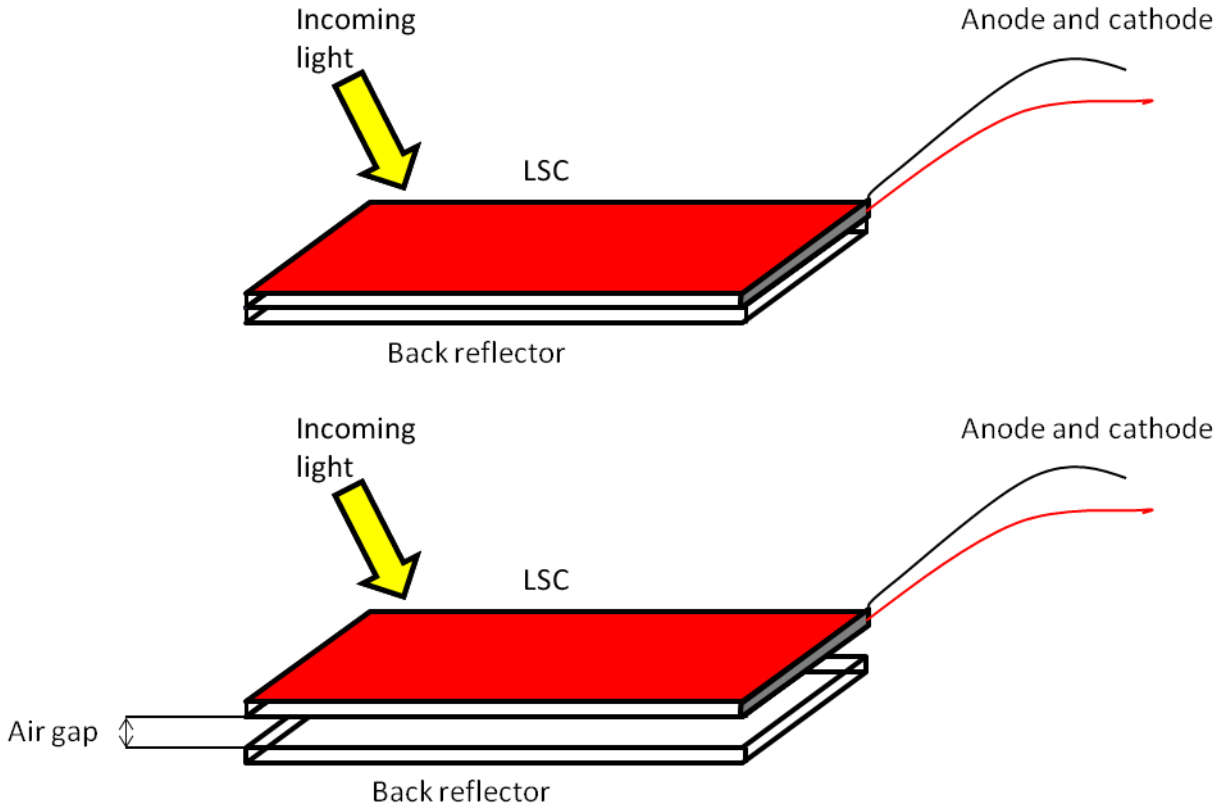

Figure IV.25 Configurations tested in the case of back reflectors optimization. In the upper part of the figure, the configuration with no air gap is depicted while in the lower part of the figure the configuration with the air gap is considered.

As shown in chart IV.26 where ΔPCE for a fixed coating thickness (14 µm) as a function of TiO_2 content is presented, the two configurations tested give substantially the same results and can therefore be considered identical. ΔPCE in case of back reflectors is calculated by considering as a reference the same LSC placed on a black cardboard. In this way we are able to study the effect of the white BR on LSC performance and compare it with a black BR.

$$\Delta PCE = \frac{PCE_{cell}^{BR} - PCE_{cell}^{BLACK}}{PCE_{cell}^{BLACK}} * 100 \qquad \text{Eq. IV.5}$$

BR stands for back reflector, BLACK stands for black cardboard.

The two configurations are identical from the point of view of ΔPCE increase trend. In figure IV.26 normalized ΔPCE associated to a 2 µm white coating with different TiO_2 content (1 %, 5

%, 10 %, 20%) is reported for the two cases studied. Each of the point is the result of an averaging on three back reflectors.

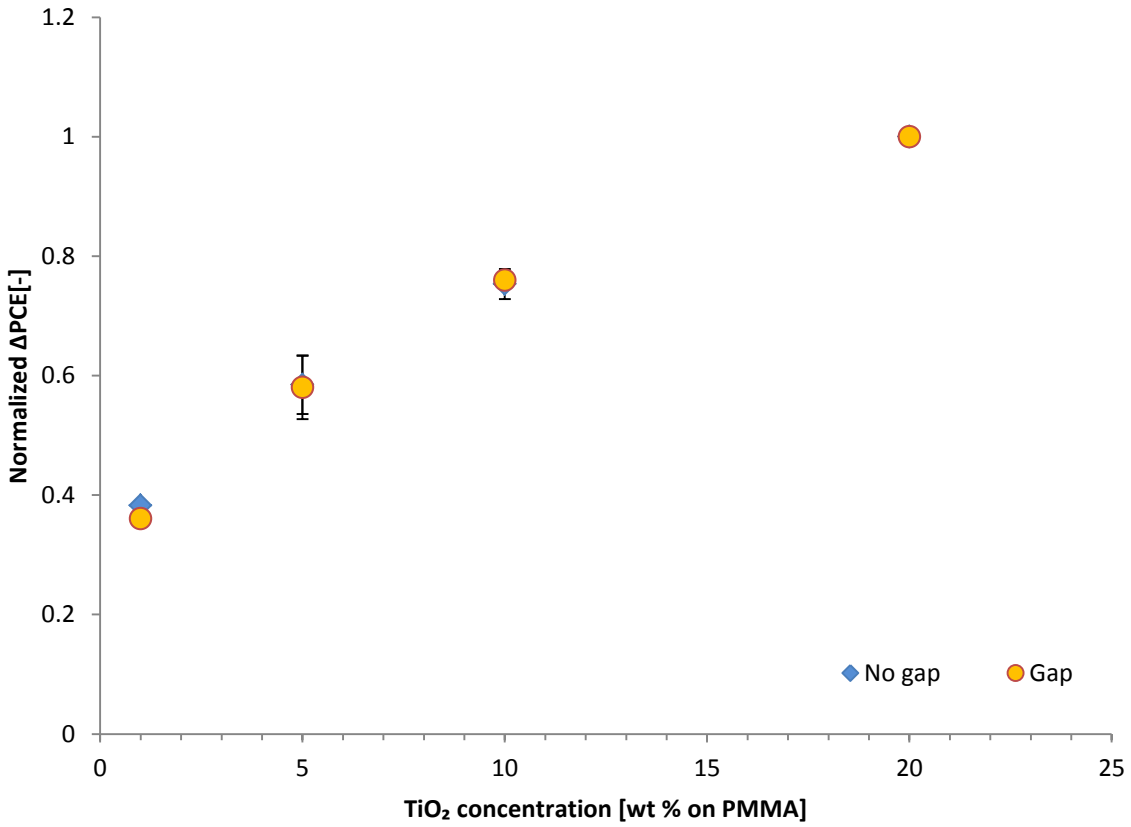

Figure IV.26 Normalized ΔPCE associated to 2 µm coating with different TiO_2 content is reported for the two cases studied. Each of the point is the result of an averaging on three back reflectors.

Since the two configurations give the same results, from here on only results obtained from studies on "gap" configuration will be presented.

IV.1.4.2 PV parameters

As apparent from IV.26 increasing TiO_2 concentration results in a progressive higher ΔPCE variation with respect to a black back reflector. This is due to the fact that white TiO_2 molecules are increasingly more concentrated and thus the hiding power is more intense

and the scattering process more efficient. Figure IV.27 shows ΔPCE variations for different film thickness at increasing TiO_2 concentration. All of these values are average on three BR's.

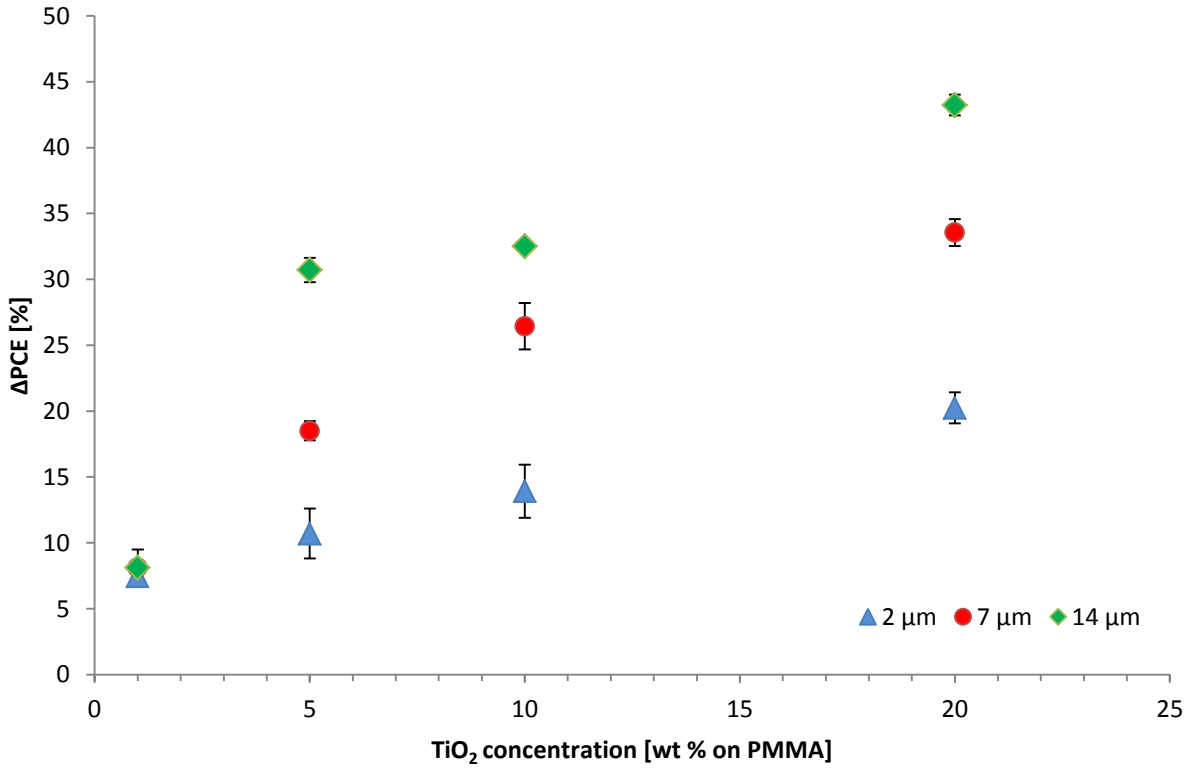

Figure IV.27 ΔPCE versus TiO_2 concentration for back reflectors with different film thickness: 2 µm, 7 µm, 14 µm.

As shown in this chart, an increase in PMMA concentration (increase of thickness of BR) results in a higher ΔPCE. In addition, the general trends reported at increasing TiO_2 content for the different binder concentrations considered seem to be similar. This behavior can also be observed on graph IV.28 which presents short circuit current values versus TiO_2 content, for different binder concentrations.

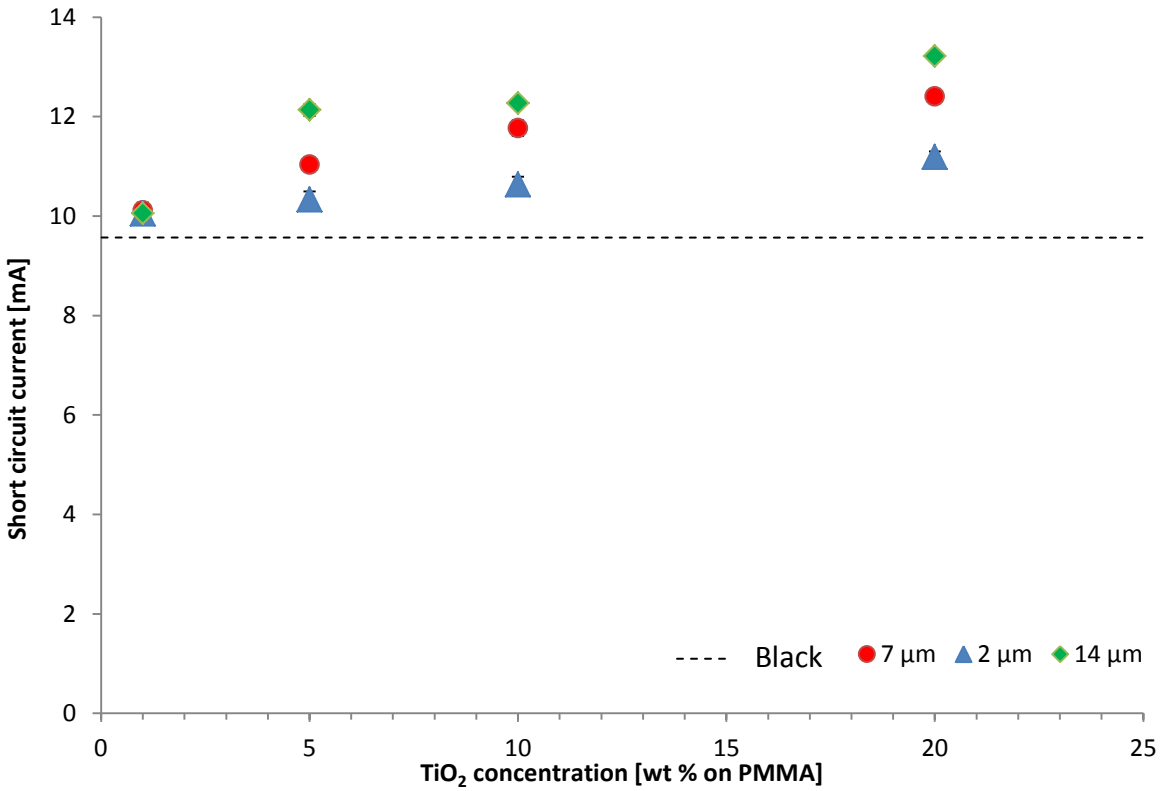

Figure IV.28 Short circuit current versus TiO_2 concentration for different binder (PMMA) concentrations. The dashed line represents the short circuit current of the LSC placed on a black back reflector (black BR). It was not possible to report the normalized short circuit current trends because the trends for different binder concentration are substantially similar and do not permit to appreciate PV parameter variations.

This means that by using a white back reflector one can increase the overall current produced by the PV cell. Supposing that the luminescence quantum efficiency of the organic dye is constant, initially transmitted photons are reflected by the back reflector and re-enter the waveguide. In this way an increase of current is registered because a larger amount of photons can be absorbed by the dye and in turn can be re-emitted and be made available for the waveguiding process.

Due to the current variation, also V_{OC} experiences a slight increase. As an example chart IV.29 presents the V_{OC} variation as a function of the different amount of TiO_2 included in PMMA binder.

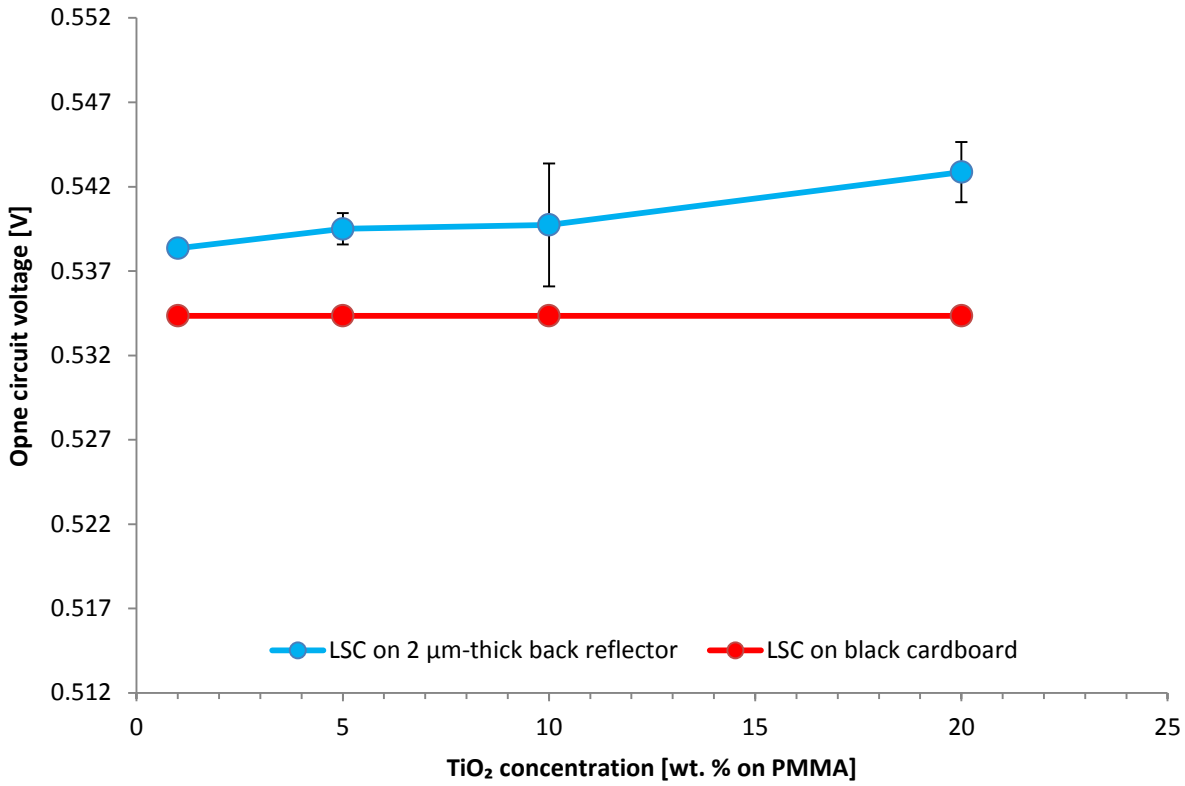

Figure IV.29 Open circuit voltage versus TiO_2 concentration. The reported values refer to P5 back reflectors.

V_{OC} increases slightly because more charges are produced by the PV devices. This means that more photons reach the PV cell.

In order to characterize more deeply the BR's fabricated, additional tests were performed: in the next sections topographic measurements and gloss measurements are presented for the different BR fabricated.

IV.1.4.3 Roughness measurements

In turn, a higher thickness will promote a higher ΔPCE variation for a fixed TiO_2 content as shown in figure IV.27. This is substantially true for all the titanium dioxide percentage except 1%. Probably this is due to the high transparency of all back reflectors with this titanium dioxide content which does not allow to appreciate significant differences between BR with

different PMMA concentrations. For all other TiO_2 contents, thickness variation is responsible for the different PV performances for a fixed TiO_2 content.

To get a complete characterization of the BR functioning, additional tests were carried out. We performed roughness measurements and the results are reported in table IV.5.

Sample	Average R_q [µm]	Standard deviation [µm]
P5T1	0.055	0.005
P5T5	0.080	0.013
P5T10	0.090	0.004
P5T20	0.113	0.009
P10T1	0.127	0.071
P10T5	0.182	0.040
P10T10	0.208	0.061
P10T20	0.215	0.072
P15T1	0.226	0.041
P15T5	0.286	0.053
P15T10	0.292	0.072
P15T20	0.309	0.089

Table IV.5 Average root mean square surface roughness and standard deviation of different samples with different film thickness and TiO_2 concentrations.

From the table two effects can be seen. First of all, by increasing TiO_2 content for a fixed film thickness, an increase of roughness can be observed. This is due to the increased amount of TiO_2 particles which are on the surface of the BR films and contribute to the increase of roughness. The other observable effect is an increase of surface roughness as film thickness increases. This second effect can be ascribed to difficulties in obtaining a homogeneous thin film by spin coating due to the increasingly higher solid content. In the following section, we will try to correlate roughness to surface gloss unit (G.U.) and thus to BR ability of reflecting light.

IV.1.4.4 Gloss measurments

One way to further characterize BR's is to perform gloss measurements. As already noted in the previous chapter, Gloss Unit (G.U.) is representative of the specular reflectivity of a surface; that is, the higher the G.U., the higher the specular reflectivity. The latter is defined as the capacity to reflect light preferentially in one direction (specularly).

As mentioned in chapter III, we are not interested in absolute values of gloss. Rather, we are trying to qualitatively describe the trends obtained from gloss measurements on BR with a fixed BR thickness and varying TiO_2 content.

In chart IV.30 the gloss unit for the 2 µm thick BR is reported together with power conversion efficiency variation at different TiO_2 content. Chart IV.31 and IV.32 show the same behavior for two other BR thicknesses, namely 7 µm and 14 µm.

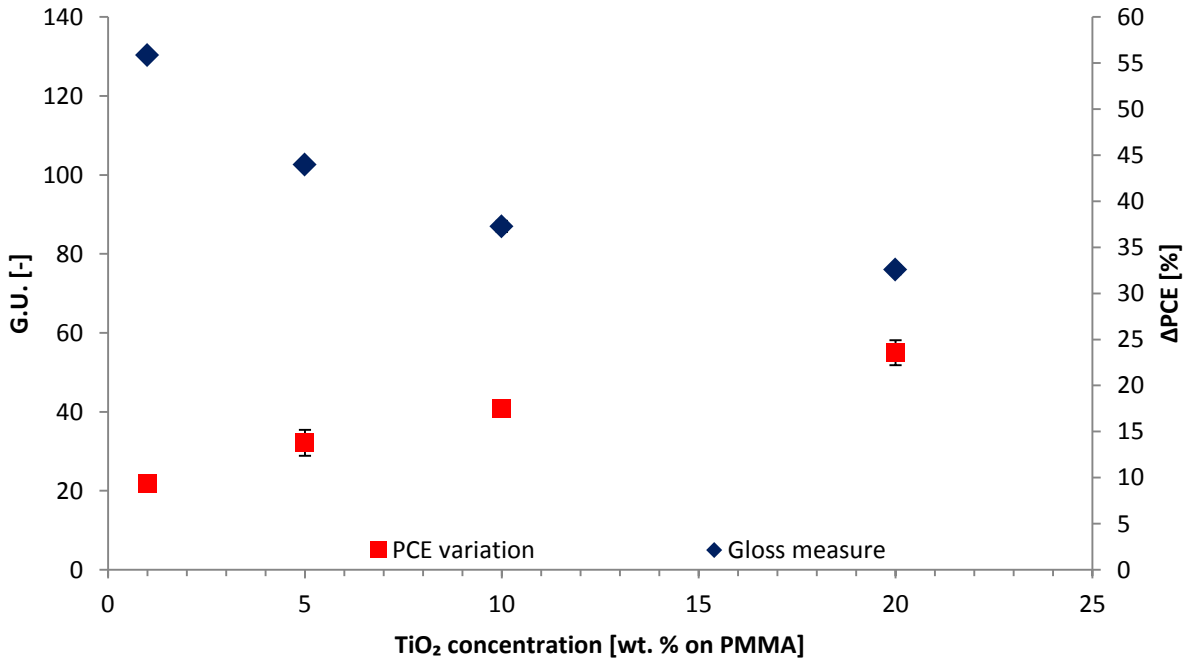

Figure IV.30 ΔPCE and G.U. versus TiO_2 concentration for a fixed BR thickness (2µm).

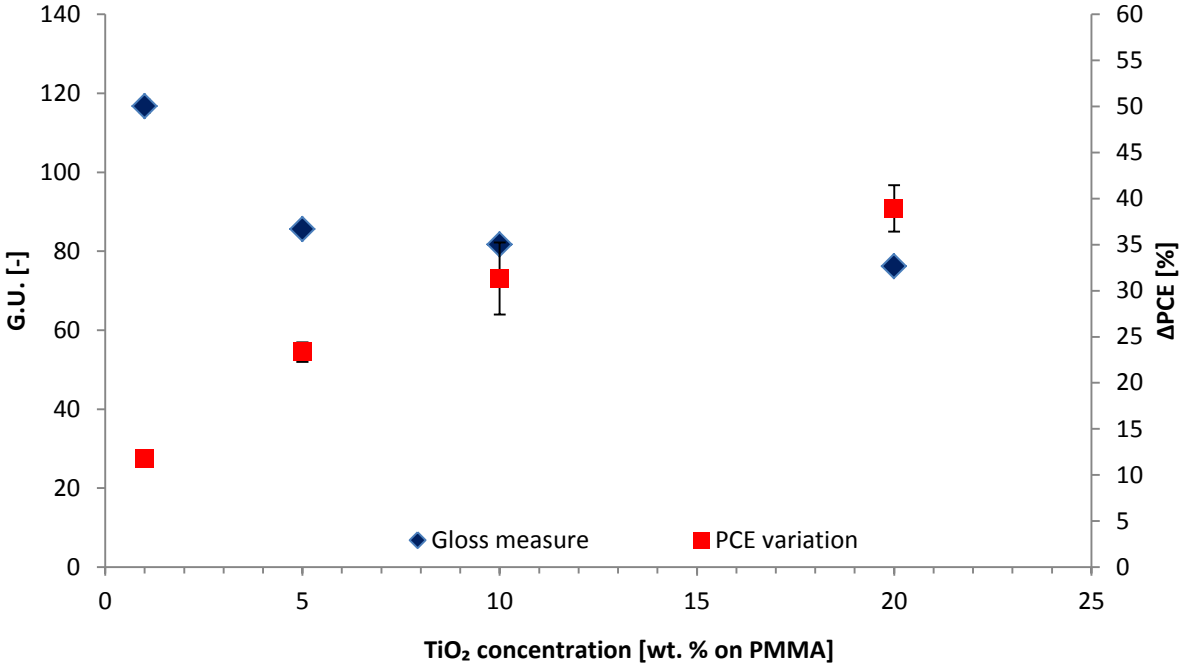

Figure IV.31 ΔPCE and G.U. versus TiO_2 concentration for a fixed BR thickness (7 µm).

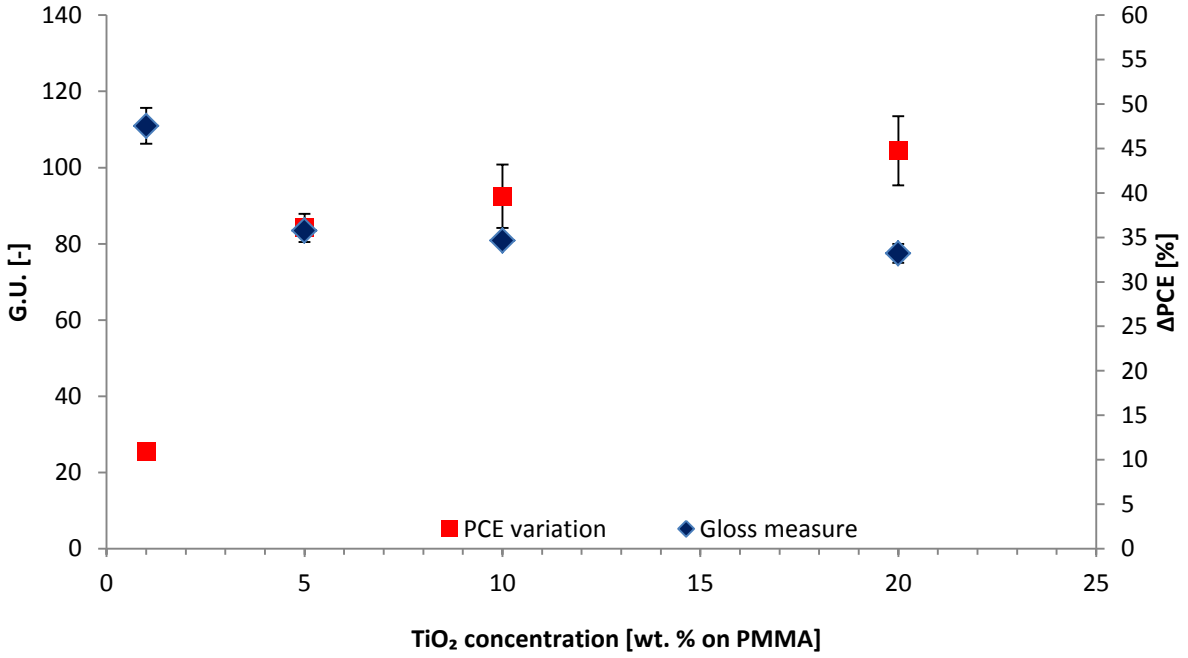

Figure IV.32 ΔPCE and G.U. versus TiO_2 concentration for a fixed film thickness (14 µm).

It appears clearly that by increasing the TiO_2 content, that is by increasing mean square roughness, R_q, the Gloss Unit decreases. This means that the specular reflectivity decreases

as titanium dioxide increases. A higher specular reflectivity is reached when the surface is extremely polished and has thus a very low roughness. This happens with the lowest TiO_2 content back reflector. A back reflector with a high G.U. is not very efficient because it reflects light predominantly in one direction (specular) and thus the probability to reflect light into the waveguide is lower. More light is lost due to the specular reflection. This fact explains the reduced PCE increment with the lower TiO_2 back reflector content with respect to the higher titanium dioxide concentration with equal PMMA concentration.

The higher titanium dioxide back reflectors are characterized by low gloss unit: this means that those BR's reflect light in the all directions and not towards a preferred direction. This results in more light being scattered and reflected towards the waveguide. Consequently ΔPCE increases. These results are in accordance with roughness measurements. A larger TiO_2 amount will promote a higher BR surface roughness and a more randomly distributed reflected light (lower G.U.) that will be re-directed with higher efficiency towards the waveguide.

This behavior appears to be independent of BR thickness as shown in charts IV.30, IV.31 and IV.32.

IV.1.4.5 Effect of silica on back reflectors

In the previous chapter we concluded that two parameters are important in the characterization of BR's: thickness and roughness. The former can be varied via modification of the binder (PMMA) concentration, while the latter can be modified by varying the amount of white pigment (TiO_2). Roughness can be also varied by including Silica particles, SiO_2, to the back reflectors. The increase of roughness may be beneficial to the performance of BR (see previous sections)

To prove this hypothesis, a low amount (1 % on weight) of SiO_2 was added to the PMMA, $CHCl_3$ and TiO_2 solution. The purpose was to increase the surface roughness of the back reflector leading to an increased diffusion of light, thereby decreasing the Gloss Unit. The decrease in G.U. of the BR surface could result in an increase of the amount of light redirected towards the LSC plate. In order to verify these hypothesis, the 14 μm film-thick

BR back reflector (corresponding to a 15 % of PMMA was chosen as benchmark. We prepared another solution in which we dispersed 1 % of SiO_2. Figure IV.33 depicts ΔPCE as a function of TiO_2 concentration for a fixed film thickness (14 µm).

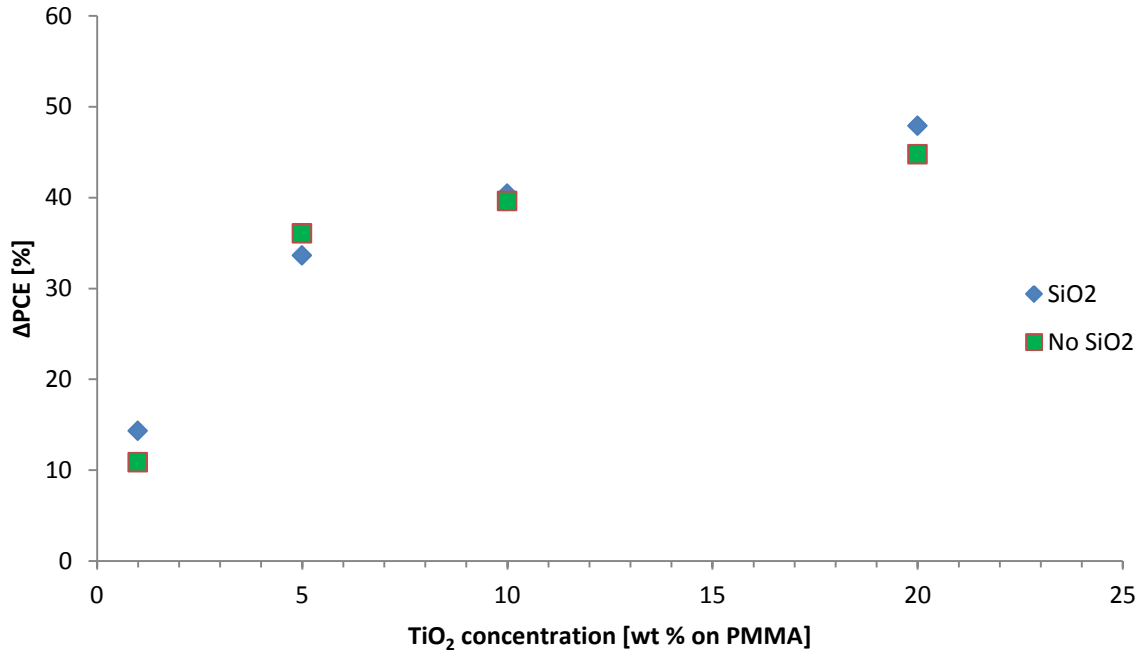

Figure IV.33 ΔPCE versus TiO_2 concentrations in case of use of a 14 µm thick BR.

The figure clearly shows that the use of 1 % of SiO_2 does not give beneficial effects on power conversion efficiency gain. In fact, the trend of ΔPCE in the two cases is absolutely the same. The reason for these results may be found in the very low amount of SiO_2 used in the tests. It is likely that a higher amount of SiO_2 is needed to increase surface roughness of back reflectors and lead to improvement in photovoltaic properties of LSC's. Further tests will be carried out to verify this aspect.

IV.2 Alternative host matrices for LSC devices

PMMA currently represents the state-of-the-art matrix for LSC devices design, and the use of this material in working LSC's was extensively discussed in the previous section. However, PMMA-based devices suffer from degradation due to the limited outdoor stability of the polymer. This is a significant limit in the current LSC technology and alternative systems to PMMA that can ensure significantly improved stability of LSC devices are needed. Along these lines, in this work new polymer matrices are presented and their use as host matrices in LSC devices is discussed, in the attempt to enhance the lifetime of LSC devices under operation. As a common design strategy for all host matrices considered in this work, a fluoro-polymer binder was used in all systems studied. In fact, due to the high strength of the carbon-fluorine bond compared to the carbon-hydrogen bond, fluoro-polymers may offer a high intrinsic resistance to photodegradation, thus allowing for prolonged LSC device lifetime. As a matter of fact, fluoro-polymers are used as coatings in a variety of technological applications in which durability is a critical issue. In addition, another common approach to all systems presented here is the matrix crosslinking by means of specific crosslinking agents, as a tool to further improve environmental stability of the polymer matrix. Indeed, a crosslinked polymer structure can guarantee a significantly lower permeability towards external agents such as oxygen and moisture compared to a non-crosslinked structure, due to the lower free-volume present. This may result in a significantly reduced rate of degradation and thus in a long-term stability of LSC devices. According to what introduced so far, the materials selected and employed in this work are presented in the following table (table IV.6). For each material, the main characteristics are also shown.

Reactant	Function	Basic molecular unit	Reacting groups	Product of crosslinking chemistry
Lumiflon LF-910LM	Binder	Fluoro ethylene vinyl ether (FEVE)	-OH	---
Tolonate HDT-LV2	Crosslinker	Hexamethylene diisocyanate cyclic trimer (HDI)	-N=C=O	Urethane
Vestanat T1890/100	Crosslinker	Isophorone diisocyanate cyclic trimer (IPDI)	-N=C=O	Urethane
Cymel 303	Crosslinker	Hexamethoxymethylmelamine (HMMM)	-O-CH_3	Ether

Table IV.6 Nature of the reactants, functionalities involved in the reaction and type of bonding.

Lumiflon LF-910 was chosen as fluoro-polymer binder in the preparation of fluoro-based crosslinked matrices for LSC devices. In figure IV.34 the molecular formula of Lumiflon LF-910LM is reported. Some of the R-groups are hydrogens, leading to the presence of reactive hydroxy groups (100 mg KOH/g polymer). Due to the presence of both carbon-fluorine and carbon-chlorine bonds in its repeating unit, Lumiflon LF-910LM presents a sufficiently high polarity and solubility in most organic solvents that would allow easy incorporation and dissolution of the luminescent organic dye used in this work (Lumogen F Red 305).

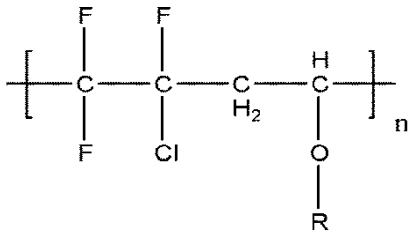

Figure IV.34 Lumiflon LF-910LM repeating unit.

To crosslink Lumiflon LF-910LM, different crosslinkers were tested, leading to different types of polymer networks. A first class of crosslinked matrices was obtained by combining Lumiflon LF-910LM and Tolonate HDT-LV2 and Vestanat T1890/100, and is based on the urethane crosslinking bond. The polymer network is obtained by the reaction of a hydroxy group present in Lumiflon LF-910LM and a isocyanate group (-N=C=O), present in the cyclic trimer. A second class of crosslinked matrices was obtained by reaction of Lumiflon LF-910LM with Cymel 303. In this system the crosslinking reaction occurs between the -OH groups of Lumiflon LF-910LM and the methoxy (-O-CH_3) groups of Cymel 303 to form a polyether network. In the following, not only the preparation of these host matrices will be

presented, but also the optimization of LSC devices based on these new systems. In particular, the thickness of the LSC thin film and the concentration of the organic dye in the LSC devices will be presented. Let us now briefly focus on the nomenclature which will be adopted in the following.

- Lumiflon LF-910 – Tolonate HDT-LV2 systems: the acronym LTxLy will be used, with the first L standing for Lumiflon LF-910, T standing for Tolonate HDT-LV2, the second L standing for Lumogen F Red 305, x indicating the overall solid content expressed as percentage weight with respect to the solvent used and y the organic dye weight percent with respect to the total solid content.
- Lumiflon LF-910 – Vestanat T1890/100 systems: the acronym LVxLy will be used. V stands for Vestanat T1890/100 and the remaining letters of the acronym are equal as in the previous case.
- Lumiflon LF-910 – Cymel 303 systems: C stands for Cymel 303. The other letters of the acronym are the same as in the previous cases.

IV.2.1 Characterization of the matrices

IV.2.1.1 Lumiflon – Tolonate system

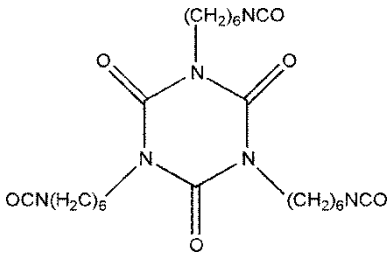

Figure IV.35 Molecular formula of hexamethylene diisocyanate (HDI).

This paragraph will be dedicated to the characterization of the polymer obtained by crosslinking Lumiflon LF-910 and Tolonate HDT-LV2. The molecular formula of the hexamethylene diisocyanate (HDI), the basic molecular unit of Tolonate HDT-LV2, is shown in figure IV.35. The reacting functionalities are -OH for Lumiflon LF-910LM and -NCO for Tolonate HDT-LV2, to form urethane bonds via polyaddition reaction, whose general schematization is reported in figure IV.36.

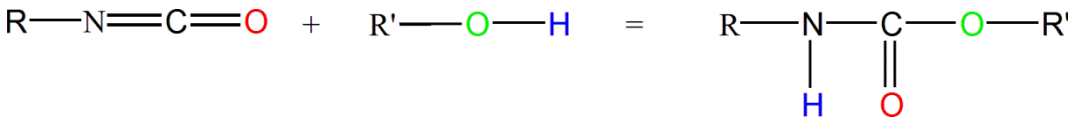

Figure IV.36 Reaction between a hydroxyl group and a isocyanate group to form urethane bond. Only the reacting functionalities are reported, identifying with R and R´ the remaining part of the molecules.

Since the average functionality of the two resins is higher than 3, the final result is a crosslinked polyurethane. An important structural parameter in polyurethane reactions is the stoichiometric ratio between the -NCO and -OH functionalities (NCO/OH). Preliminary photovoltaic tests were carried out on films prepared at different NCO/OH ratios to identify the optimal NCO/OH ratio under a device point of view. Entering in more detail, we tested NCO/OH ratios of 0.97, 1.1, 2 and 3. A stoichiometric excess of –NCO normally leads to formation of urea linkages. As a result from PV tests an NCO/OH ratio of 0.97 (slight excess of –OH) was chosen because it gave the highest ΔPCE for a given Lumogen F Red 305 concentration. In the following, unless otherwise stated, an NCO/OH ratio of 0.97 for the LT system will be considered.

The physical characterization of the fluorinated matrices prepared requires, first of all, the optimization of the heating cycle to allow crosslinking. The second step involves the measurement of the glass transition temperature (T_g) of the matrix.

Let us now consider the optimization of the crosslinking conditions. In order to allow for crosslinking to take place, heating at 150 °C was performed on the LTx LSC thin films at increasing heating times. The NCO groups have a FTIR absorption peak which is centered approximately at 2260 cm^{-1} [13, 14]. This peak is associated to stretching vibrations of the NCO group. During the crosslinking process, NCO groups progressively decrease and then disappear because the polymerization reaction occurs leading to a reduction of the concentration of the NCO groups. It is possible to state that crosslinking is complete when the NCO peak in the FTIR spectrum of LTx thin film disappears completely. Figure IV.37 depicts the portion of interest of the FTIR spectra taken at different heating times for the system LT20 under thermal annealing at 150 °C.

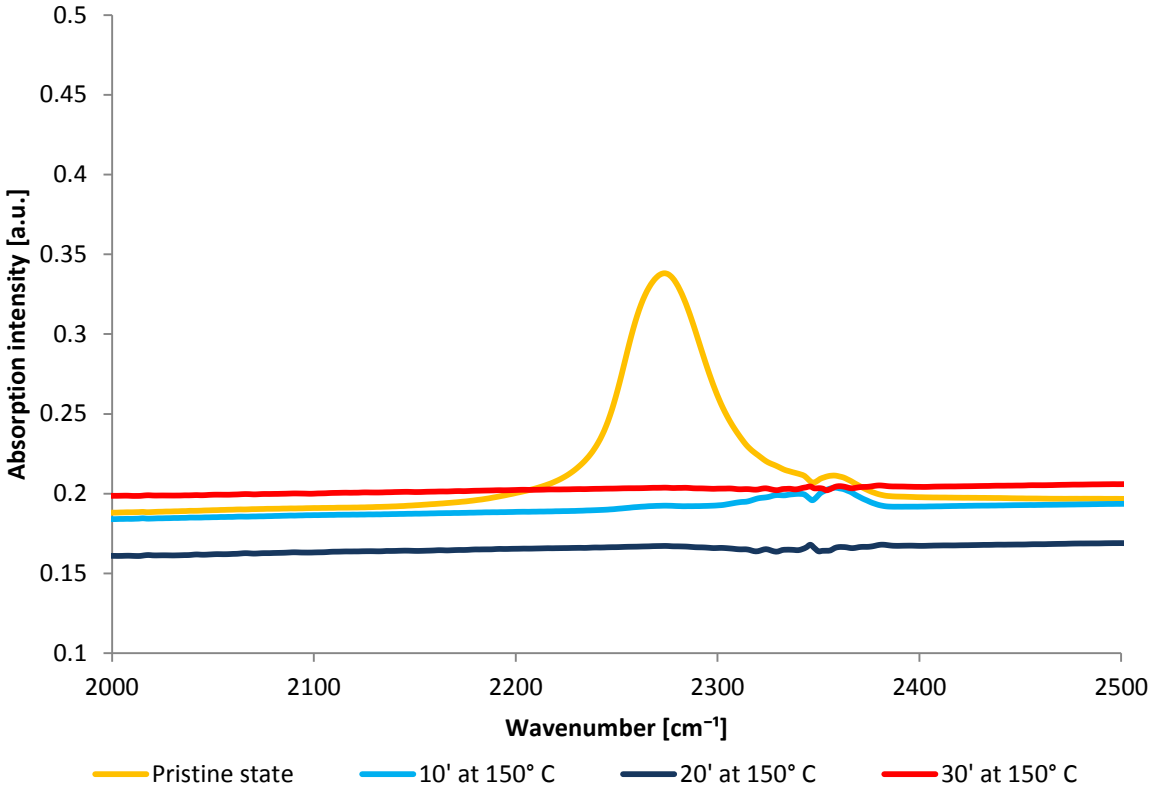

Figure IV.37 FTIR spectrum of LT20 for different times of thermal annealing at 150 °C.

As can be seen, the NCO peak decreases with annealing time at 150 °C. In order to guarantee complete crosslinking, i.e. complete disappearance in the FTIR spectrum of the signal centered at 2260 cm^{-1} (N=C=O stretching), an optimal annealing time of 30 minutes was identified.

Differential scanning calorimetry was used to investigate the glass transition temperatures of the crosslinked matrices. For LSC purposes, the glass transition temperature of the matrix should be, in principle, higher than room temperature (approximately 25 °C). In fact, during prolonged outdoor exposure high temperatures can be reached, especially during summer and the stability of the polymer matrix must be ensured even in these conditions.

The DSC curves of the neat resins are shown in figure IV.38 and IV.39.

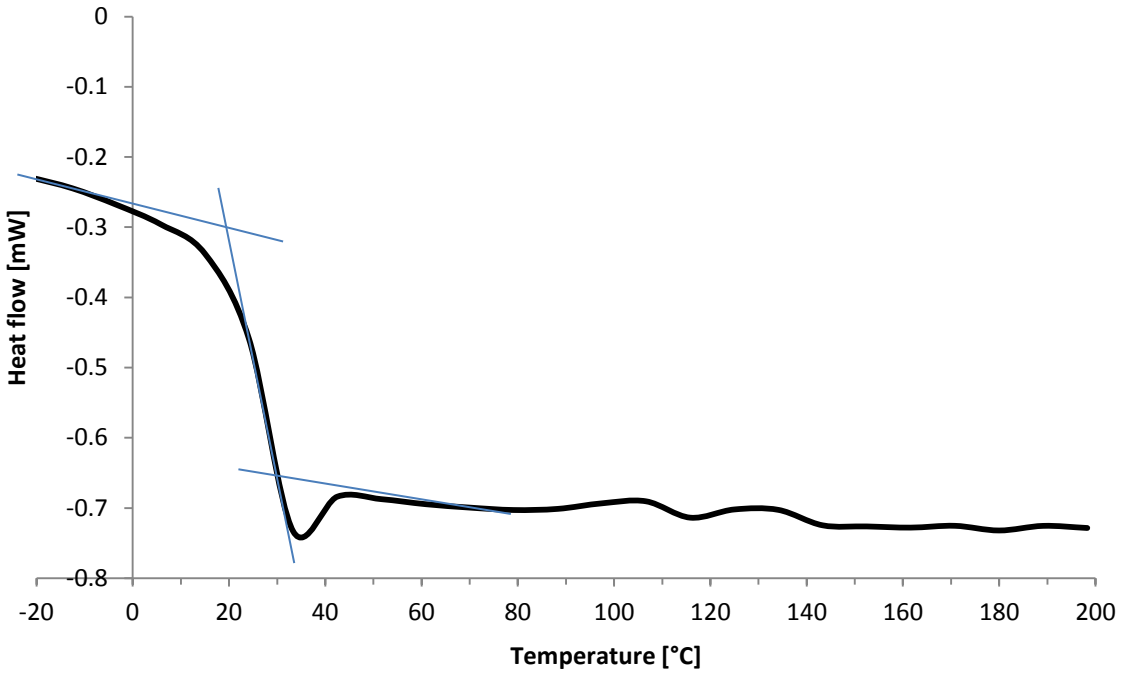

Figure IV.38 DSC curve of Lumiflon LF910-LM. The glass transition temperature of Lumiflon LF-910LM is 25 °C.

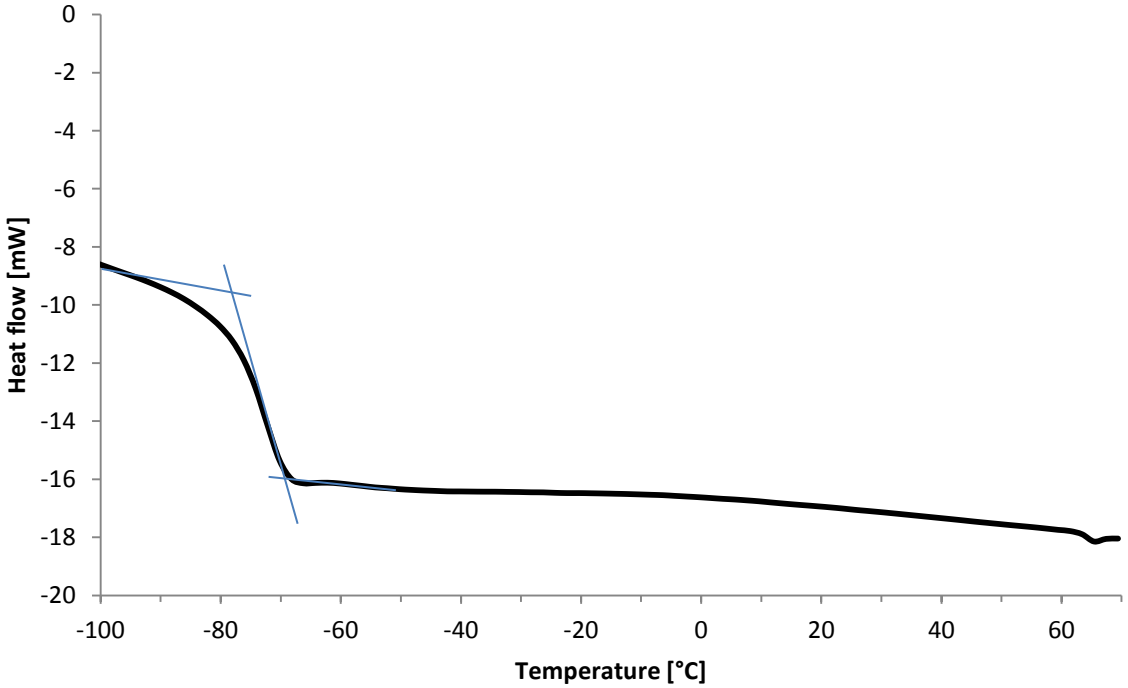

Figure IV.39 DSC curve of Tolonate HDT-LV2. The glass transition temperature of Tolonate HDT-LV2 is -75 °C.

Pristine Lumiflon and Tolonate show a glass transition temperature of about 25 °C and -75 °C. Once the two reactants undergo crosslinking, the T_g rises as a consequence of the crosslinking process. The structure becomes stiffer due to the reduction of free volume nodes. Figure IV.40 shows the DSC curve of the crosslinked matrix LT20.

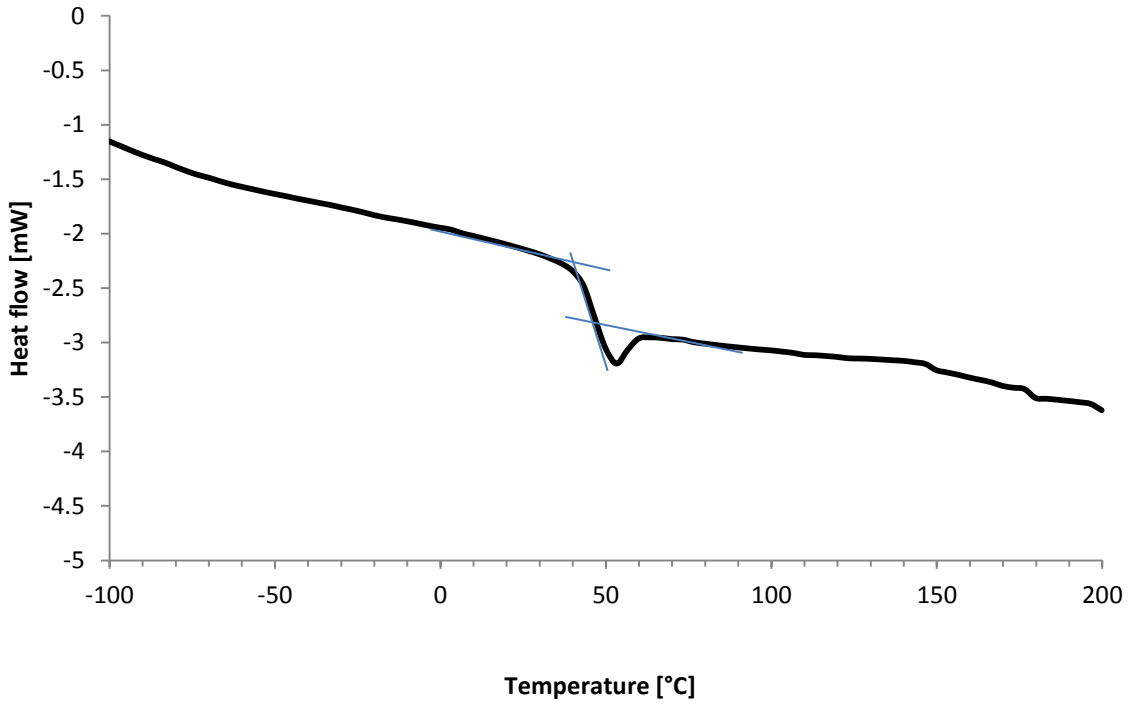

Figure IV.40 DSC curve of the crosslinked matrix LT20. The glass transition temperature of the crosslinked LT system is 45 °C

As shown in the DSC scan, a T_g of about 45 °C is registered. In order to characterize the thermal transitions in the actual LSC thin film, the addition of the organic dye must also be taken into account. In particular, as LFR305 shows a T_g value of approximately 145 °C (see figure IV.41), it is expected that the dye doped crosslinked matrix (i.e. the actual LSC thin film, LT20Lx) manifests a higher T_g (as predicted by the Flory-Fox equation[4]) compared to the undoped crosslinked matrix. In particular, according to the Flory-Fox equation, a T_g value of approximately 4 °C is expected.

[4] The Flory-Fox equation serves the purpose of providing a model for how glass transition temperature changes over a given molecular weight range. In mathematical terms it is expressed as: $1/T_g = w_1/T_{g,1} + w_2/T_{g,2}$ where w_1 and w_2 are the weight fractions of component 1 and 2 while $T_{g,1}$ and $T_{g,2}$ are their glass transition temperatures respectively.

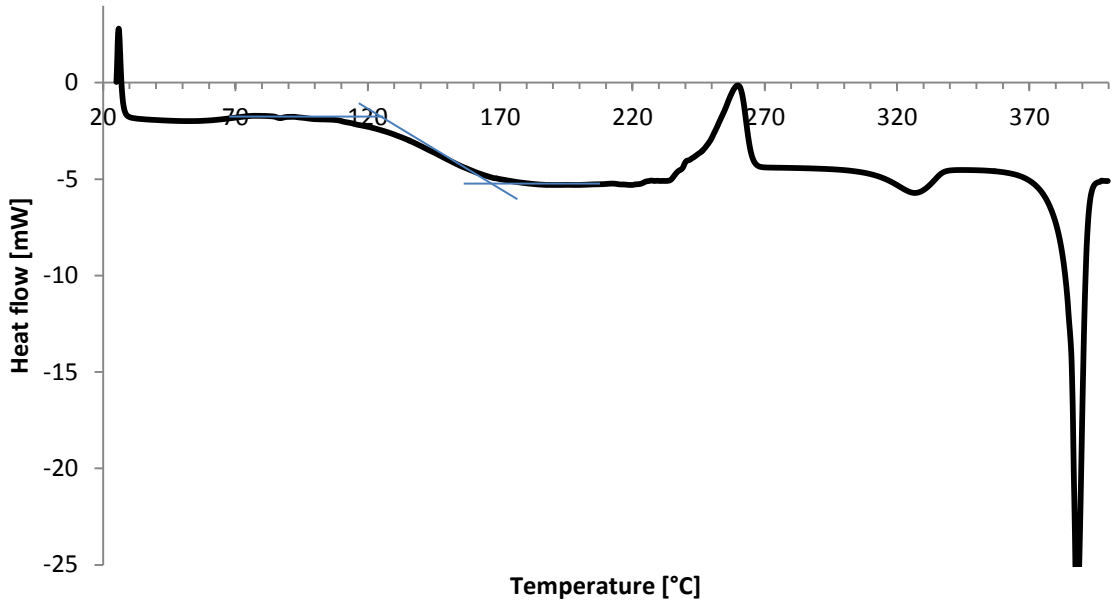

Figure IV.41 DSC curve of Lumogen F Red 305. The glass transition temperature of Lumogen F Red 305 is 144 °C.

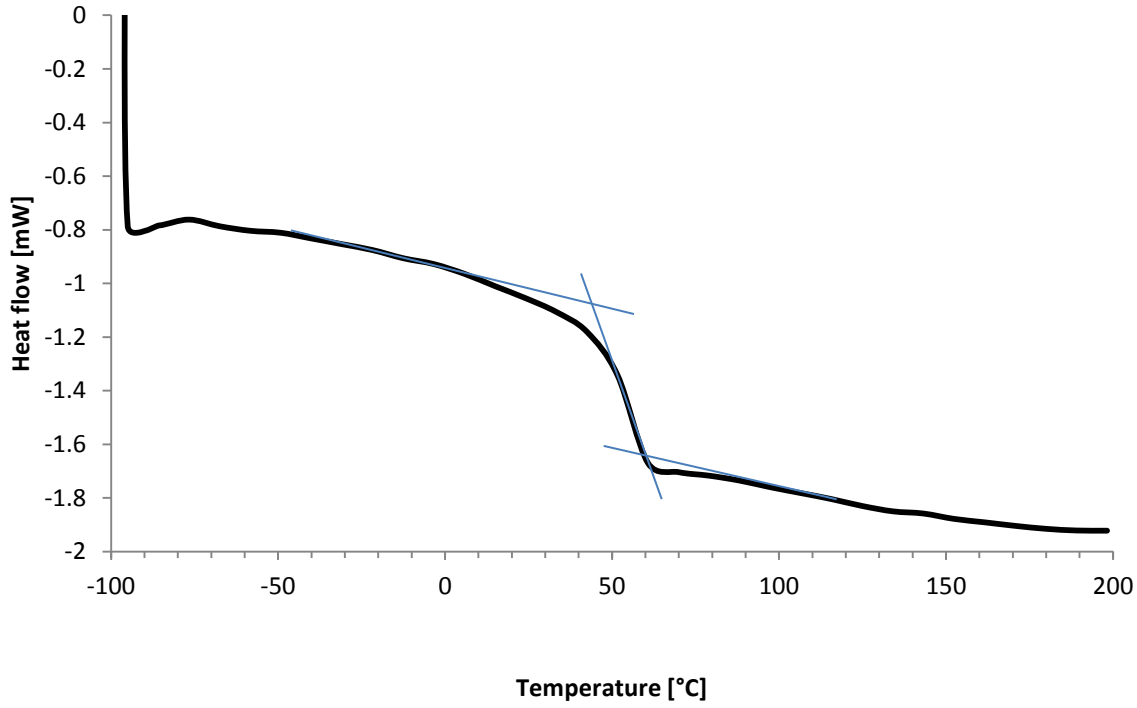

Figure IV.42 DSC curve of LT20L5. The glass transition temperature of the crosslinked LT20L5 is 50 °C.

As shown in figure IV.42, where the DSC curve of LT20L5 is reported, a T_g of 50 °C is found for this system. This value is not in accordance with respect to the Flory-Fox equation, probably because the Flory-Fox model does not consider the effect of crosslinking which

causes an increase in the glass transition temperature of a polymeric system. Considering what introduced at the beginning of this section, it is worth pointing out that this system fully satisfies the minimum requirements for long term outdoor exposure (T_g higher than T ambient).

IV.2.1.2 Lumiflon – Vestanat system

A possible alternative to Tolonate HDT-LV2 as crosslinking agent is Vestanat T1890/100, a isocyanurate trimer based on isophorone diisocianate (figure IV.43).

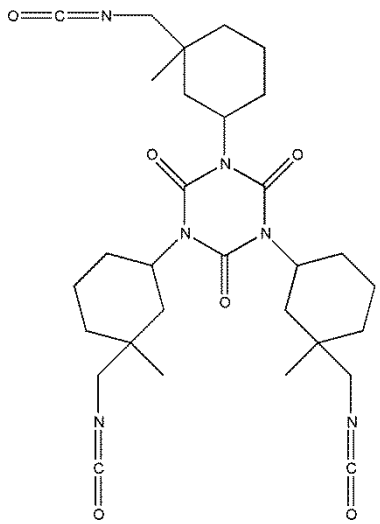

Figure IV.43 Isophorone diisocyante cyclic trimer (IPDI).

The same NCO/OH ratio as that employed in the previous section (0.97) was used for this system.

The extent and optimization of crosslinking of the Lumiflon LF-910LM – Vestanat T1890/100 system was studied by FTIR spectroscopy, similarly to what already discussed in the previous section. In this case, an optimal crosslinkig time of 30 minutes at 150 °C was employed for LSC preparation.

In order to determine the usability of this crosslinked system as host matrix in LSC operating devices, its thermal transitions were monitored.

Figure IV.44 shows the DSC curve for neat Vestanat T1890/100 resin. As shown by the curve, Vestanat T1890/100 has a much higher T_g (~ 73 °C) with respect to Tolonate (T_g ~ - 75°C), the former being a glassy solid at room temperature.

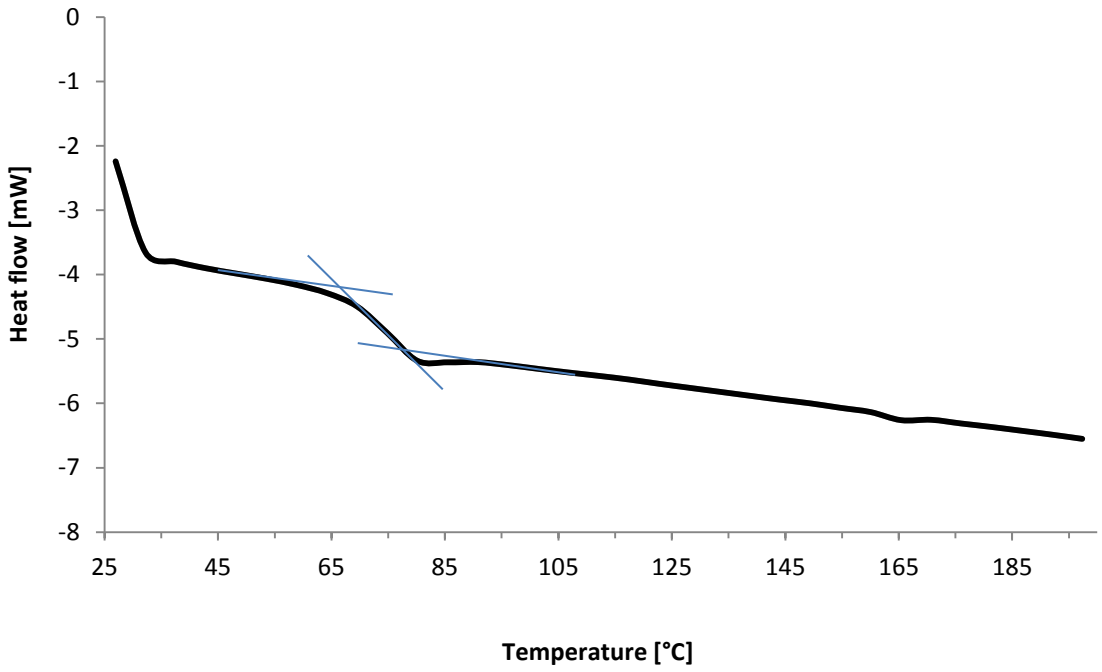

Figure IV.44 DSC curve of Vestanat T1890/100. The glass transition temperature is approximately 83 °C.

Figure IV.45 shows the DSC curve of the crosslinked matrix LV20. The glass transition temperature is around 83° C, significantly higher than that of the Lumiflon – Tolonate system, as expected (see figure IV.40).

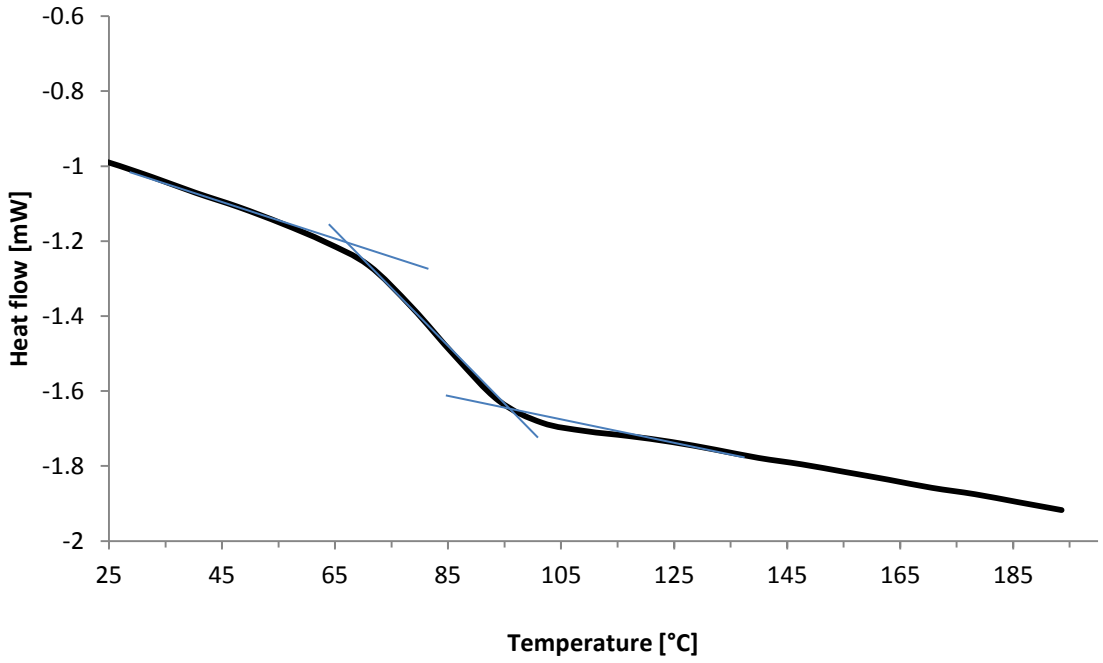

Figure IV.45 DSC curve of the crosslinked LV20 matrix. Its glass transition temperature is 63 °C.

In order to evaluate the effect of the organic dye on the glass transition temperature of the matrix, a DSC experiments was carried out also on LV20L5 sample. Figure IV.46 shows the DSC curve for LV20L5.

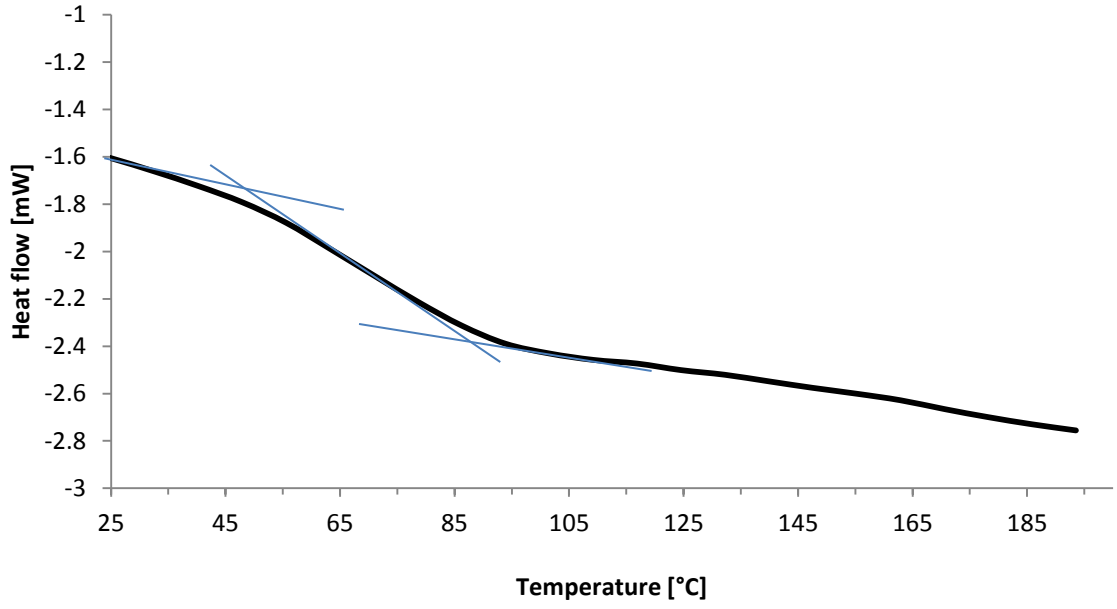

Figure IV.46 DSC curve of LV20L5. The glass transition temperature of the crosslinked LV20L5 system is 67 °C.

The incorporation of the organic dye into the crosslinked polymer matrix yields a slight decrease of T_g. The organic dye therefore seems to work as a plasticizer of the crosslinked matrix, with a slight decrease of the concentrator T_g.

IV.2.1.3 Lumiflon – Cymel

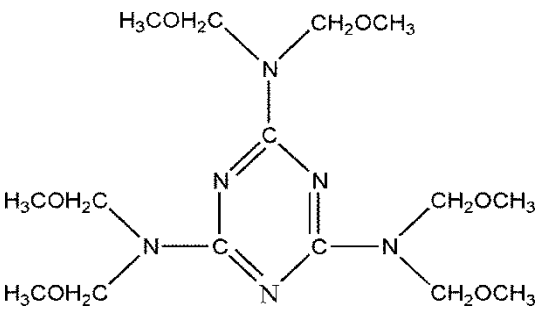

Figure IV.47 HMMM molecular unit.

The last LSC polymer matrix that was prepared and tested in this work is based on the use of Lumiflon LF-910 and Cymel 303 as crosslinker. Cymel 303 is based on the Hexamethoxymethylenemelamine unit (HMMM, figure IV.47). The reactive species in this system are the –OH functionalities in Lumiflon and the -O–CH_3 functionality in Cymel 303. The result of the crosslinking reaction is an ether bond by transetherification reaction. The reaction between the functionalities is schematically represented in figure IV.48.

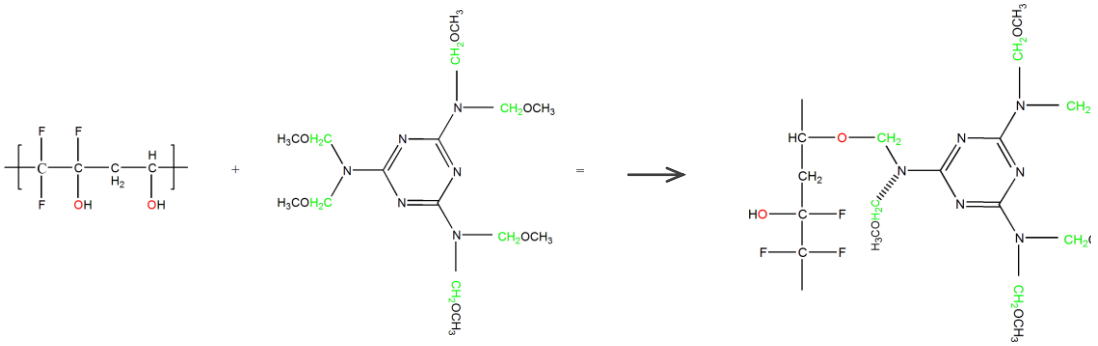

Figure IV.48 Reaction between Lumiflon LF-910LM and HMMM

A true stoichiometric reaction can hardly be obtained by using melamines since normally several self-condensation reactions occur. Formulations were made by using a 20 % on weight of the overall solid in the LC solution with respect to solvent. In order to monitor the extent of crosslinking reaction, DSC measurements were performed, together with tests on solubility of the crosslinked films. The latter, in particular, were performed by making use of the solvent test, i.e. by dipping the prepared samples in chloroform for about 5 minutes. In order to promote crosslinking, after the coating process, the LSC thin film samples were placed into an oven at 150° C for 30 minutes. The optimal heating time was identified after successive rubbing tests on the crosslinked matrix, which only led to minimal swelling of the film.

The physical characterization of the matrix primarily concerns DSC tests which give information about the transition temperatures.

First of all DSC curve for Cymel is reported in figure IV.49, where a glass transition temperature of -45 °C can be clearly distinguished.

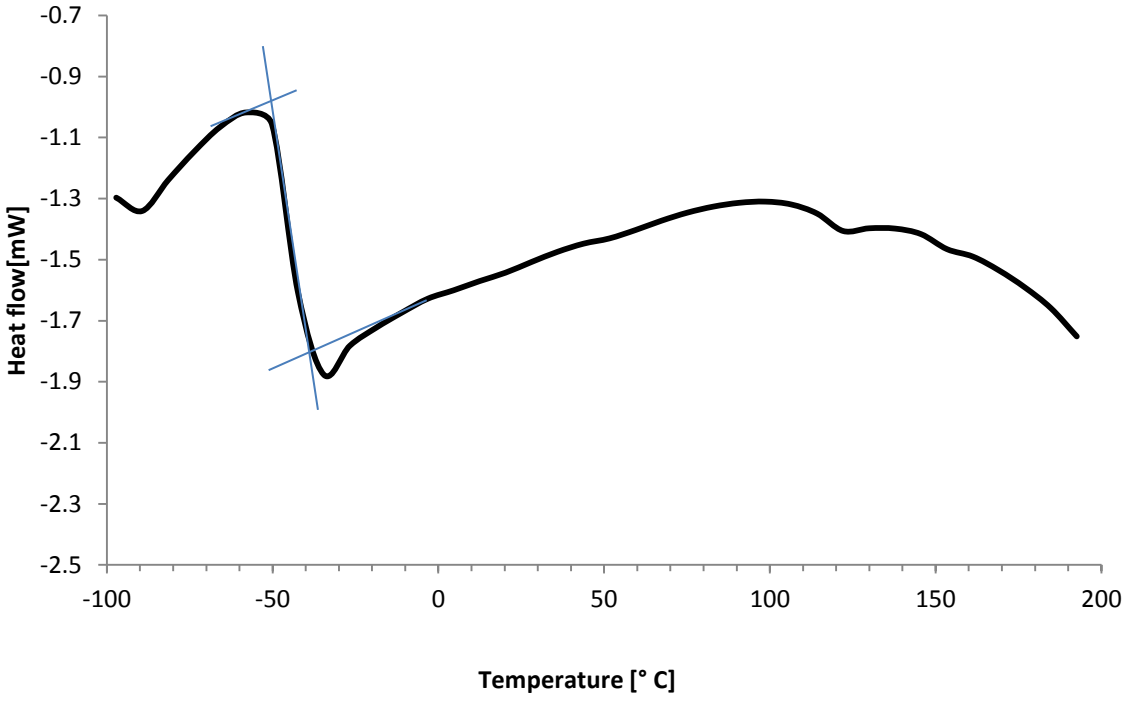

Figure IV.49 DSC curve for Cymel 303. The glass transition temperature of Cymel 303 is -45 °C.

The DSC curve for the undoped crosslinked LC matrix is reported in figure IV. 50.

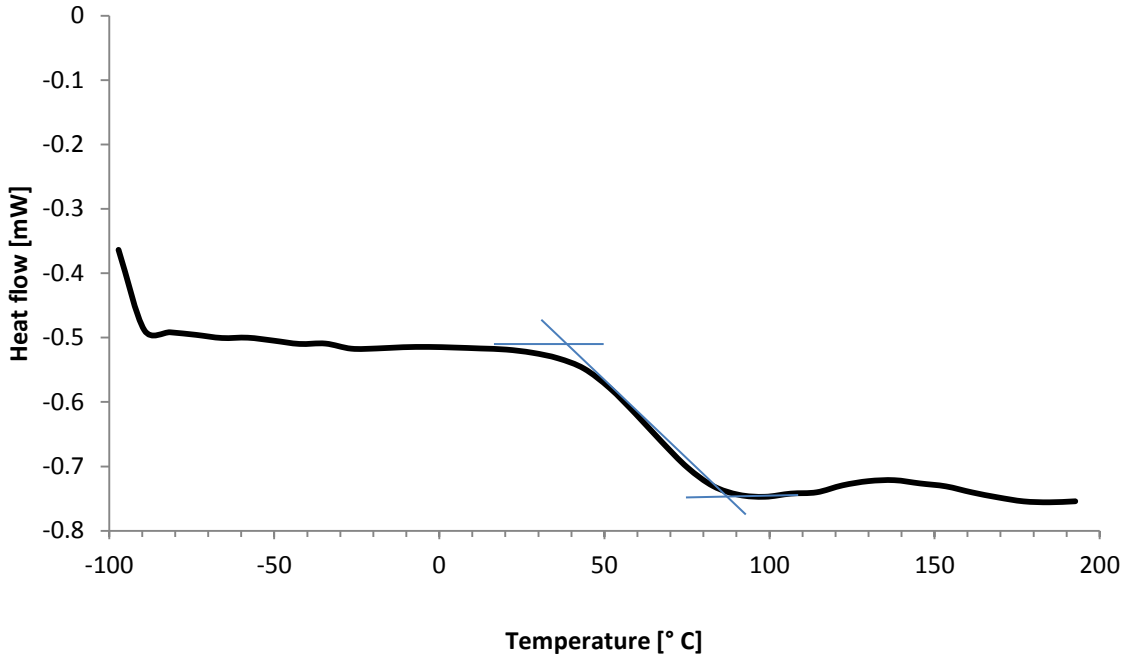

Figure IV.50 DSC curve for the crosslinked matrix LC20. The glass transition temperature of the crosslinked LC20 matrix is 62 °C.

LC20 shows a glass transition temperature higher than room temperature, namely 62° C. A further increase in T_g is expected once the organic dye is incorporated in the crosslinked polymer matrix. As shown in figure IV.51, on an LSC system doped with LFR305 at a concentration of 4 % (LC20L4), the T_g of this system is approximately 79° C.

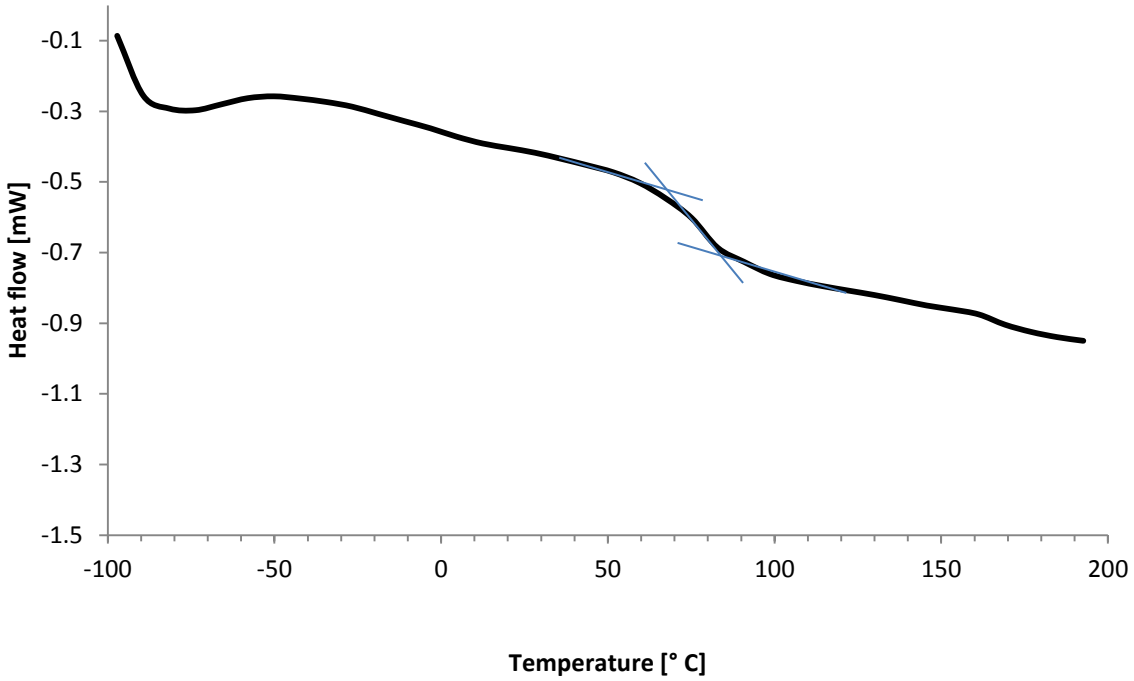

Figure IV.51 DSC curve for the doped crosslinked matrix, LSC20L5. The glass transition temperature is 79 °C.

After the physical-chemical characterization of the new matrices presented in the previous sections, optimization of the main LSC device parameters was carried out on working LSC's employing those materials as host matrices. In particular dye concentration and LSC thin film thickness were varied and the results are presented in the following.

IV.2.2 Optimization of the dye concentration

Different Lumogen F Red 305 concentrations were tested for the fluoropolymer-based LSC systems. Concentrations were namely 1 %, 2 %, 3 %, 4 %, 5 %, 6 %, 7 %, 10 % dye on total solid weight.

IV.2.2.1 Photovoltaic parameters

In this section the PV parameters of LT20Lx, LV20Lx and LC20Lx together with the optimization of dye concentration are presented.

Figure IV.52 shows the ΔPCE variation as a function of dye concentration for all systems considered in this work.

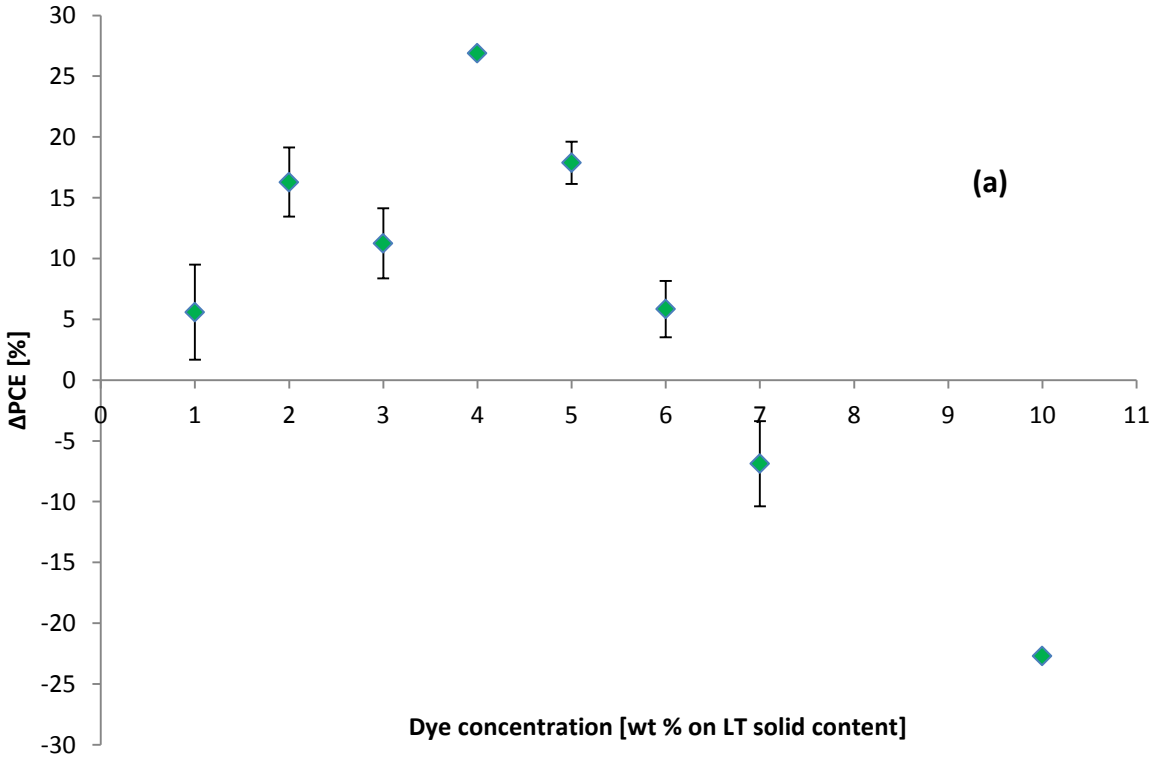

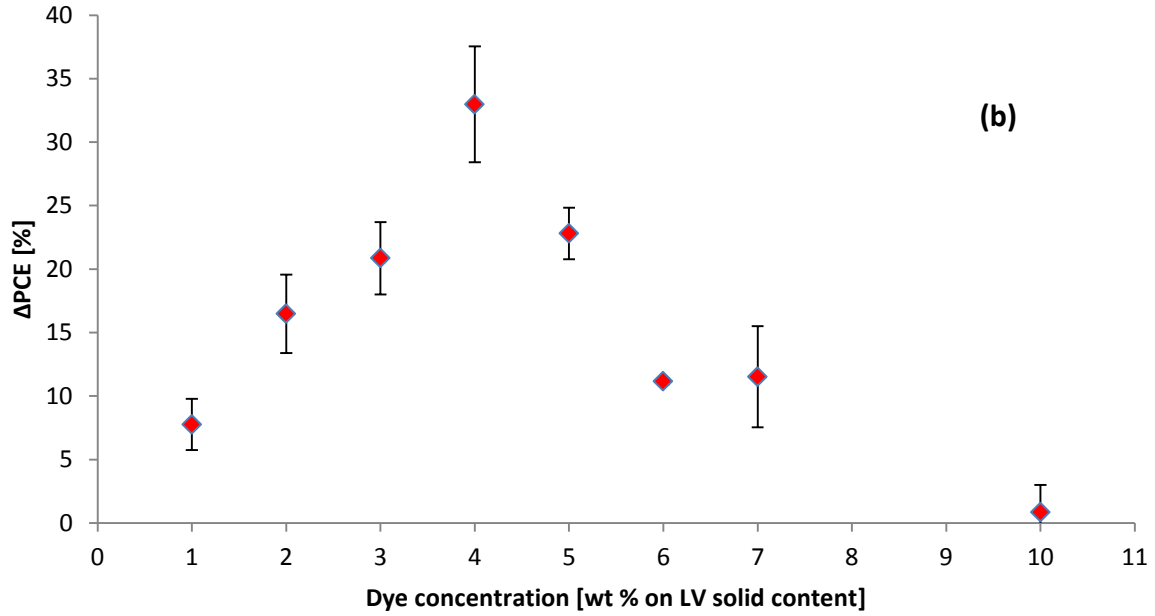

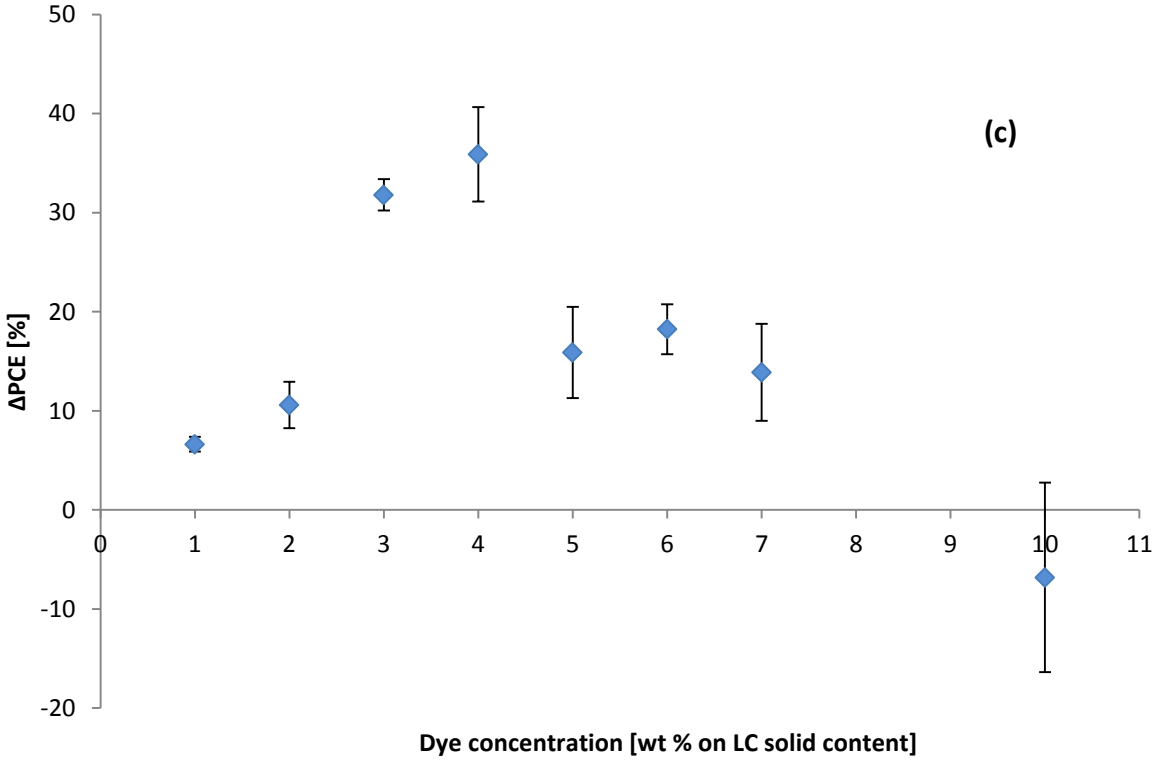

Figure IV.52 ΔPCE versus dye concentration for LT20Lx system (a), LV20Lx system (b) and LC20Lx system (c). x is the dye concentration (%). Each point is averaged on three LSC devices

In all systems, for increasing dye concentration, the ΔPCE values increases up to a maximum found for a dye concentration of 4 %. Above this concentration, a decrease in LSC performance is observed down to negative ΔPCE values, indicating that the performance of the systems comprising the luminescent plate attached to the PV cell is worse than the PV cell alone. This is verified for all systems except for LV20Lx which shows a nearly zero ΔPCE as minimum value.

A summary of all LSC device parameters at increasing dye concentration is presented in table IV.7, where a clear maximum ΔPCE is observed for 4 % dye concentrations.

Dye content [%]	I_{SC} [mA]	V_{OC} [V]	FF [%]	PCE^{cell} [%]	ΔPCE [%]	PCE^{LSC} [%]
Lumiflon – Tolonate (LT) system						
1	14.93 ± 0.63	0.55 ± 0.01	60.64 ± 0.60	10.97 ± 0.71	5.58 ± 3.91	0.40 ± 0.03
2	17.09 ± 0.73	0.55 ± 0.00	59.71 ± 0.27	12.40 ± 0.58	16.29 ± 2.85	0.45 ± 0.02
3	16.19 ± 0.59	0.53 ± 0.02	56.63 ± 4.30	10.82 ± 1.59	11.24 ± 2.89	0.39 ± 0.06
4	18.55 ± 0.23	0.55 ± 0.001	60.08 ± 0.29	13.57 ± 0.13	**26.90 ± 0.15**	**0.49 ± 0.00**
5	17.07 ± 0.38	0.55 ± 0.001	60.02 ± 0.91	12.42 ± 0.06	17.88 ± 1.73	0.45 ± 0.00
6	15.10 ± 0.22	0.55 ± 0.004	59.91 ± 0.96	11.00 ± 0.28	5.84 ± 2.31	0.40 ± 0.01
7	13.24 ± 0.37	0.51 ± 0.02	53.52 ± 1.91	8.02 ± 0.59	-6.88 ± 3.51	0.29 ± 0.02
10	10.38 ± 1.88	0.49 ± 0.02	53.07 ± 2.58	6.00 ± 1.56	-30.04 ± 10	0.22 ± 0.06
Lumiflon – Vestanat (LV) system						
1	15.40 ± 0.13	0.54 ± 0.01	57.23 ± 1.61	10.53 ± 0.51	7.77 ± 2.01	0.38 ± 0.02
2	16.88 ± 0.62	0.54 ± 0.03	56.56 ± 5.56	11.54 ± 2.08	16.48 ± 3.08	0.42 ± 0.08
3	17.39 ± 0.05	0.54 ± 0.02	56.78 ± 2.83	11.73 ± 1.05	20.86 ± 2.86	0.42 ± 0.04
4	18.78 ± 0.39	0.55 ± 0.02	53.58 ± 10.24	12.31 ± 2.38	**32.98 ± 4.56**	**0.45 ± 0.10**
5	18.65 ± 0.06	0.56 ± 0.00	58.38 ± 0.55	13.37 ± 0.14	22.80 ± 2.03	0.48 ± 0.01
6	16.51 ± 0.35	0.55 ± 0.01	58.67 ± 3.31	11.74 ± 1.11	11.15 ± 0.23	0.42 ± 0.04
7	16.40 ± 0.58	0.55 ± 0.01	59.71 ± 1.17	11.88 ± 0.75	11.52 ± 3.99	0.43 ± 0.03
10	14.42 ± 0.30	0.52 ± 0.01	55.76 ± 1.01	9.24 ± 0.33	0.85 ± 2.16	0.33 ± 0.01
Lumiflon – Cymel (LC) system						
1	15.05 ± 0.01	0.54 ± 0.01	60.00 ± 1.56	10.86 ± 0.37	7.03 ± 0.56	0.39 ± 0.01
2	15.81 ± 0.86	0.52 ± 0.01	56.05 ± 3.27	10.30 ± 0.89	10.58 ± 2.34	0.37 ± 0.03
3	18.95 ± 0.63	0.56 ± 0.00	60.09 ± 0.21	14.06 ± 0.55	31.79 ± 1.60	0.51 ± 0.02
4	19.25 ± 0.60	0.56 ± 0.00	59.82 ± 0.66	14.22 ± 0.58	**35.19 ± 4.76**	**0.51 ± 0.02**
5	16.22 ± 0.71	0.55 ± 0.01	59.59 ± 1.71	11.67 ± 0.43	15.88 ± 4.60	0.42 ± 0.02
6	16.44 ± 0.24	0.53 ± 0.02	57.14 ± 2.78	11.16 ± 1.26	18.23 ± 2.51	0.40 ± 0.04
7	15.78 ± 0.75	0.54 ± 0.01	57.44 ± 2.47	10.73 ± 0.35	15.75 ± 4.91	0.38 ± 0.01
10	13.31 ± 1.16	0.54 ± 0.01	59.20 ± 1.75	9.39 ± 1.29	-6.82 ± 9.58	0.34 ± 0.04

Table IV.7 Main PV parameters for LT20Lx, LV20Lx and LC20Lx systems

The same trend is observed on the absolute PCE^{LSC} except for the LV system in which a maximum PCE^{LSC} is found for 5 % dye concentration (0.48 %) although ΔPCE is maximum at a dye concentration of 4 % (33 %). This discrepancy is ascribed to the higher efficiency of the PV cell employed for 5 % dye concentration LV devices (PCE = 13.37 %), compared to that used for 4 % LV devices (PCE = 12.31 %) which determines an increased absolute system efficiency. This observation further supports the need of considering the efficiency gain ΔPCE rather than the absolute efficiency PCE^{LSC} as the figure of merit for evaluating LSC devices performances, as the former is independent from PV cell efficiency.

The maximum values found for all devices are comparable to those found for PMMA-based devices presented in chapter IV.1.1 (ΔPCE = 27 %, 33 %, 35 % for LT, LV, LC compared to ΔPCE = 33 % for PMMA). These results indicate that the new systems presented here perform as well as the standard material in terms of PV performance. The decrease of ΔPCE after the 4 % dye concentration may be ascribed to the presence of dissipative effects such as fluorescence quenching which becomes prominent for higher dye concentrations. To better clarify the origin of the trends observed in the PV behavior of LT-based, LV-based and LC-based LSC devices at increasing dye concentration, additional tests were carried out. In particular, UV-Vis spectroscopy and fluorescence spectroscopy tests were carried out and are presented in the next sections.

IV.2.2.2 UV-Vis absorption spectroscopy

Figure IV.53 presents the UV-Vis absorption spectra of LT20Lx, LV20Lx and LC20Lx systems. For the sake of clarity, only the absorption spectra of dye concentrations of 1 %, 4 % and 10 % are shown.

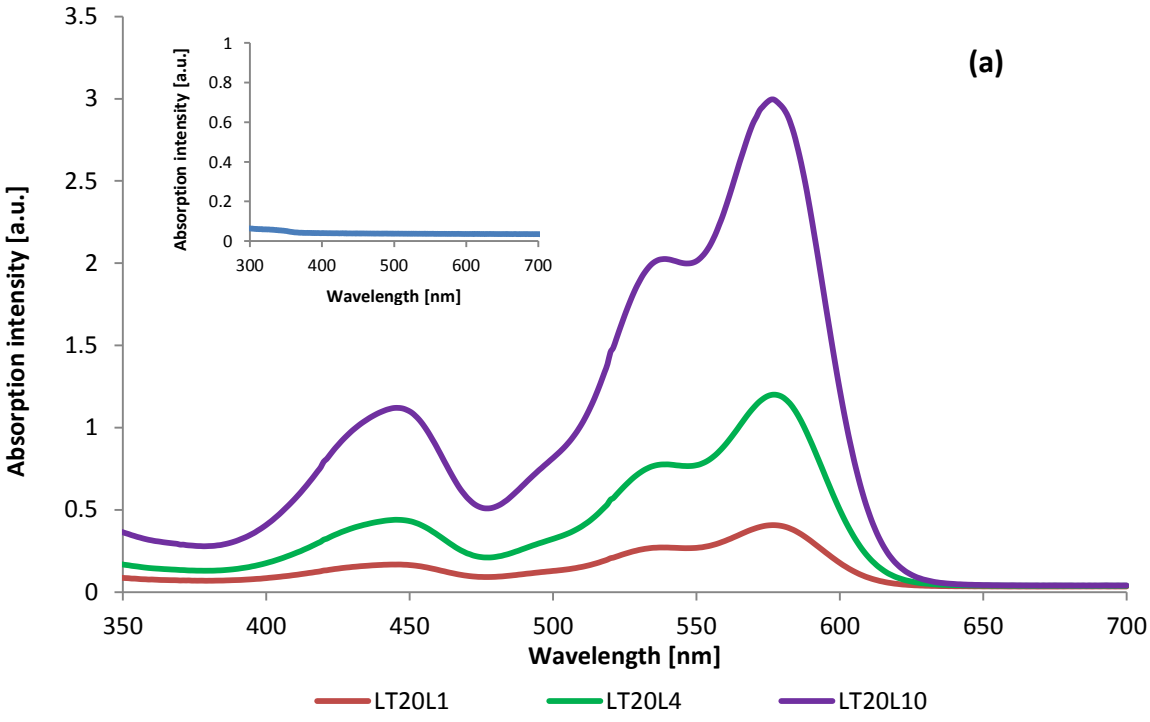
(a)
Absorption intensity [a.u.]
Wavelength [nm]
LT20L1
LT20L4
LT20L10

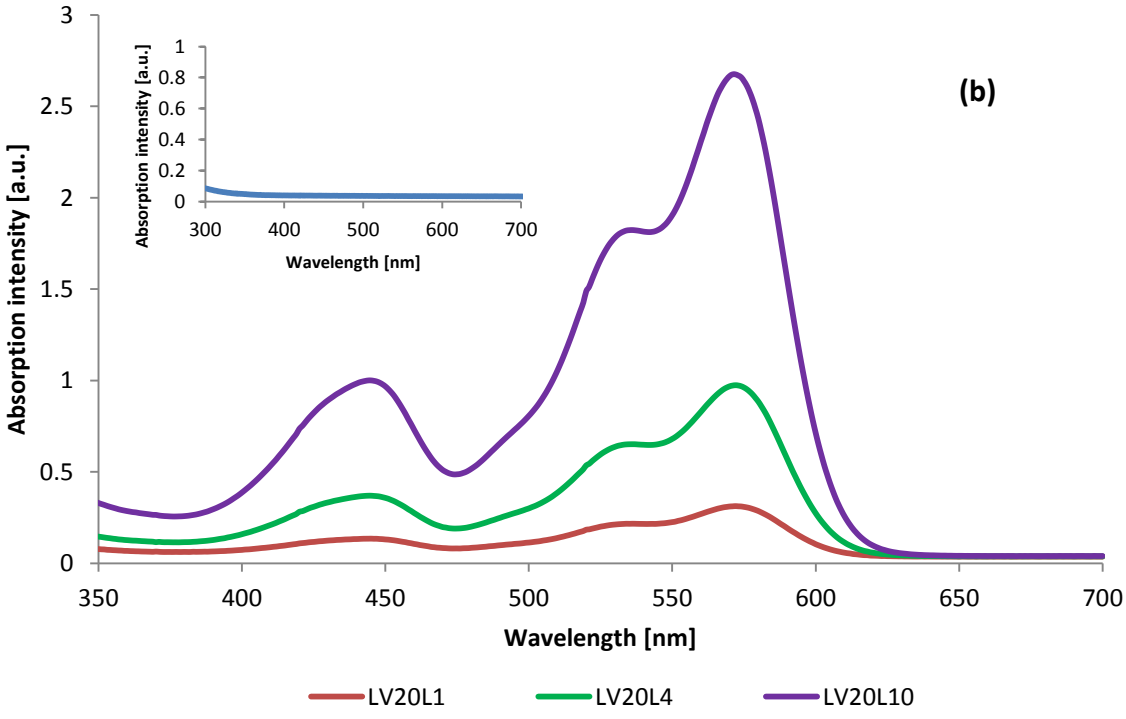
(b)
Absorption intensity [a.u.]
Wavelength [nm]
LV20L1
LV20L4
LV20L10

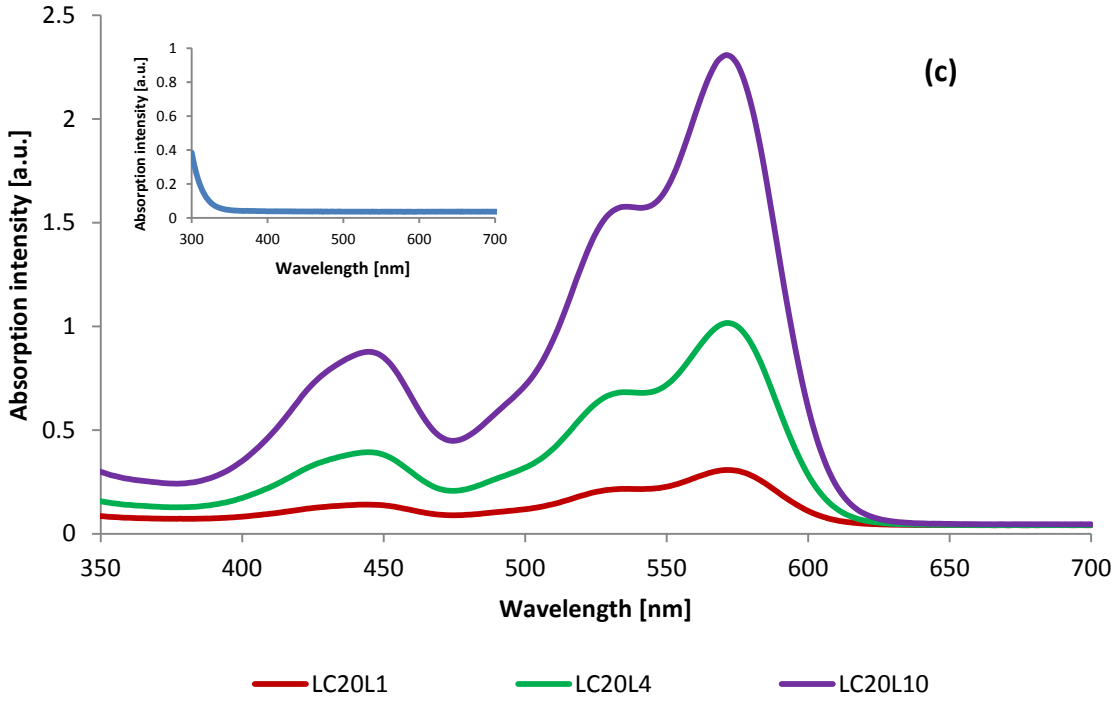

Figure IV.53 UV-Vis absorption spectra of LSC devices with different dye concentration for (a) LT , (b) LV and (c) LC system. In the inset of the spectrum of each system the UV-Vis absorption spectrum of the undoped matrix is reported

As expected, the higher the dye concentration, the higher the absorption intensity. Because the optical path length and the extinction coefficient of the absorbing species are constant, the registered effect can be assigned only to variations of dye concentrations.

Figure IV.54 represents the absorption intensity of the main UV-Vis absorption peak (576 nm) for different dye concentrations. All dye concentrations investigated are reported in the following figure.

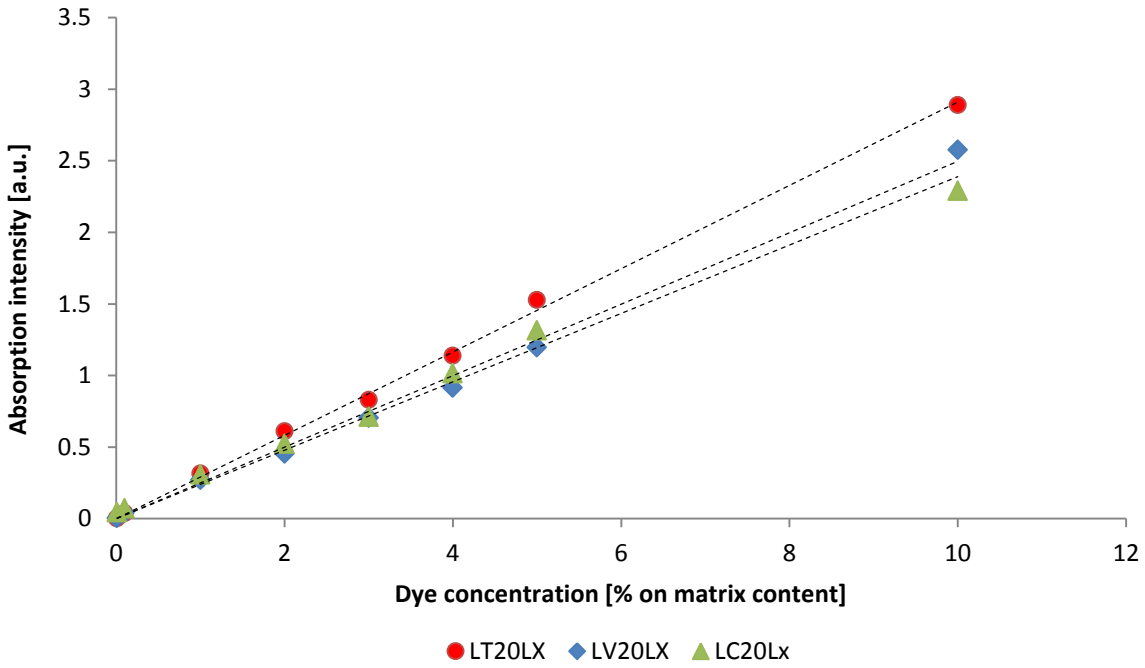

Figure IV.54 UV-Vis absorption intensity of the main absorption peak (576 nm) versus dye concentration for LT20Lx, LV20Lx and LC20Lx. For LT20Lx, the equation of the line is y = 0.291x (R^2 = 0.99). For LV20Lx the equation of the line is y = 0.250x (R^2 = 0.99) while for LC20Lx the equation of the interpolating line is y = 0.239x (R^2 = 0.99).

As shown from the plot in all the fluoropoymer-based matrices, the Lambert-Beer law applies, as already shown in the previous chapter for PMMA-based systems,.

Considering both figures IV.52 and IV.53, it seems that for each LSC matrix considered, the device doped with 10 % of LFR305 is interested by the highest number of dissipative processes because despite the highest UV-Vis absorption, the 10 % LFR305 doped samples always show the lowest ΔPCE. It means that probably a very high number of photons are dissipated in these systems.

In order to further investigate the origin of these dissipative processes and their dependence on dye concentration, fluorescence spectroscopy was performed and it is the topic of the next section.

IV.2.2.3 Fluorescence spectroscopy

Figure IV.55 shows the emission spectra of the samples considered in the previous section. It can be seen that in all systems, a maximum in emission intensity is recorded for a dye concentration of 4 %, which is also the system which yields the highest ΔPCE (see figure IV.52).

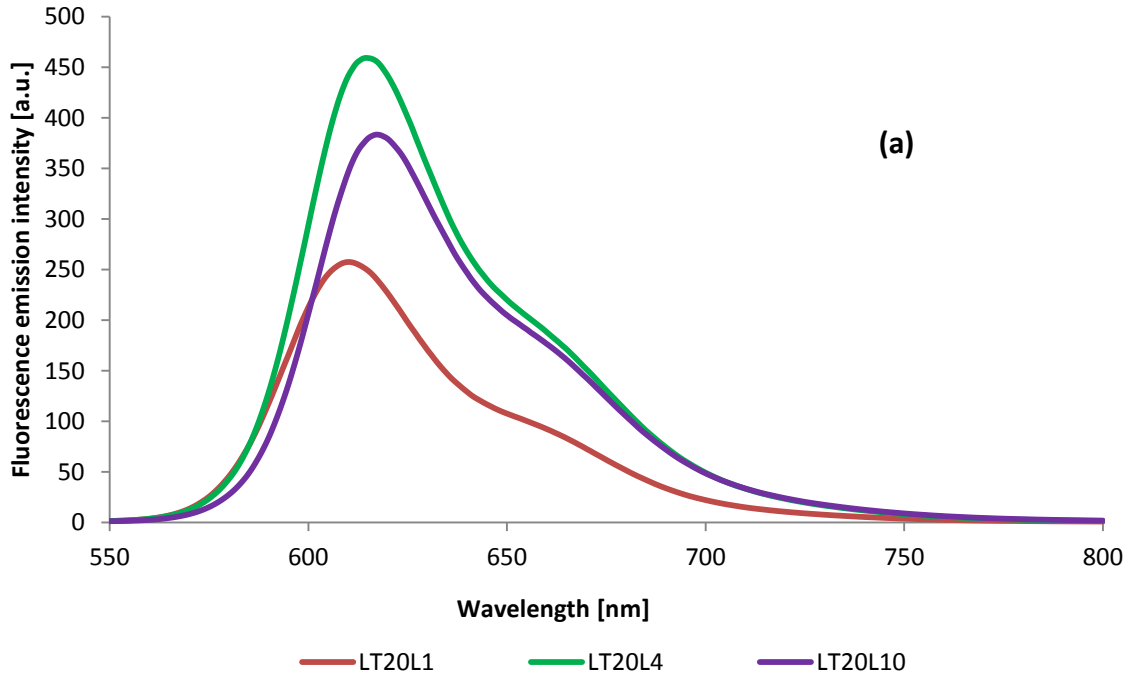

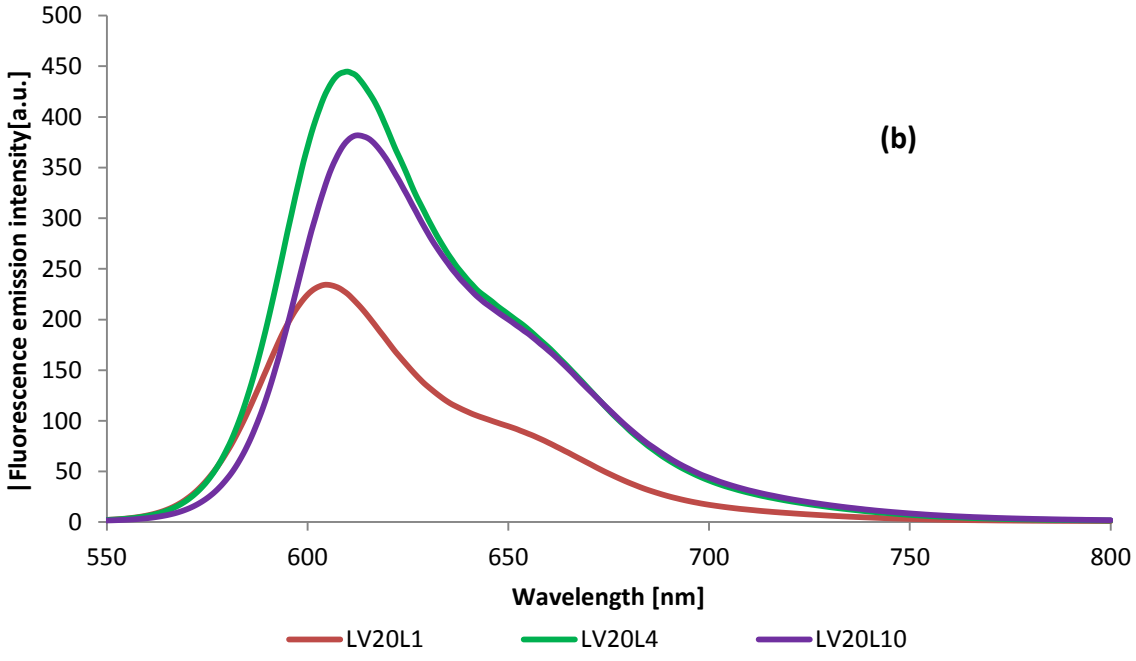

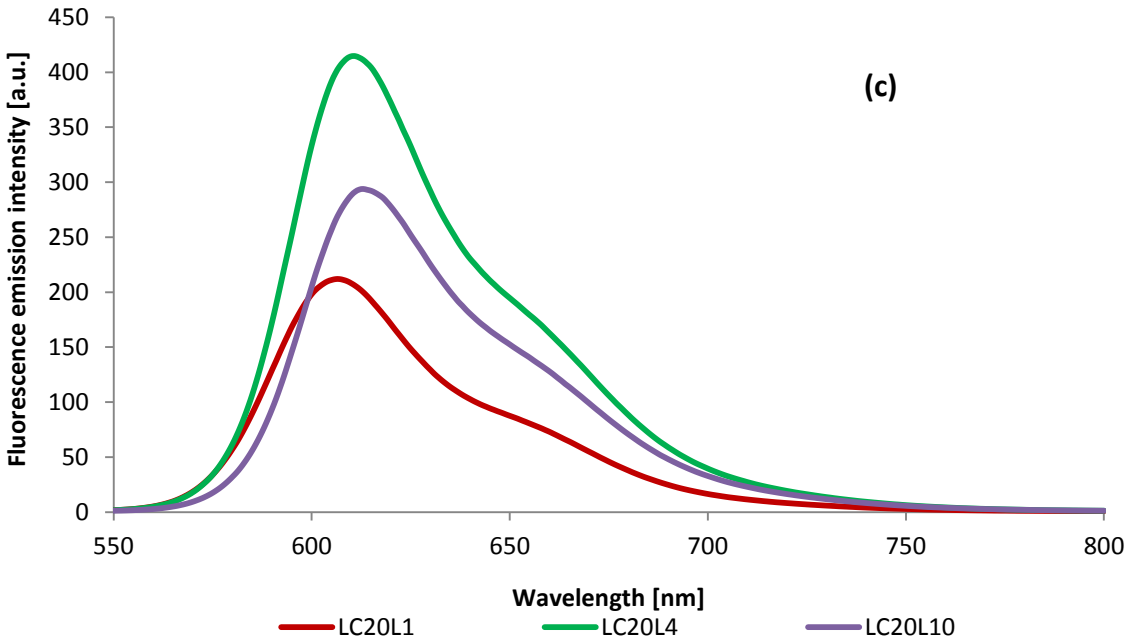

Figure IV.55 Fluorescence emission spectra of LT20Lx (a), LV20Lx (b) and LC20Lx (c). x is the dye concentration and is equal to = 1, 4, 10 %.

Morevover, samples with 10 % of LFR305 do not show the highest emission intensity despite their highest UV-Vis absorption intensity. This effect can be attributed to quenching of fluorescence due to the presence of dye aggregates, which becomes more pronounced at high dye concentrations where the optical density of the LSC thin film is maximum. Being a dissipative process, quenching of fluorescence can be the cause which explains the lowest ΔPCE for samples with 10 % of LFR305 [4 – 6, 9].

Figure IV.56 depicts the emission intensity versus the absorption intensity for different LSC samples. The reported trends show that for increasing dye concentration, the fluorescence emission increases accompanied by an increase in the UV-Vis absorption intensity. This behavior is observed up to a maximum found for a dye concentration of 4 %. Above this value (10 %), a lower emission intensity than the 4 % sample is observed, despite the higher absorption intensity. This means that the 10 % dye concentration LSC thin films present the lowest fluorescence efficiency which well correlates with decreased PV performance

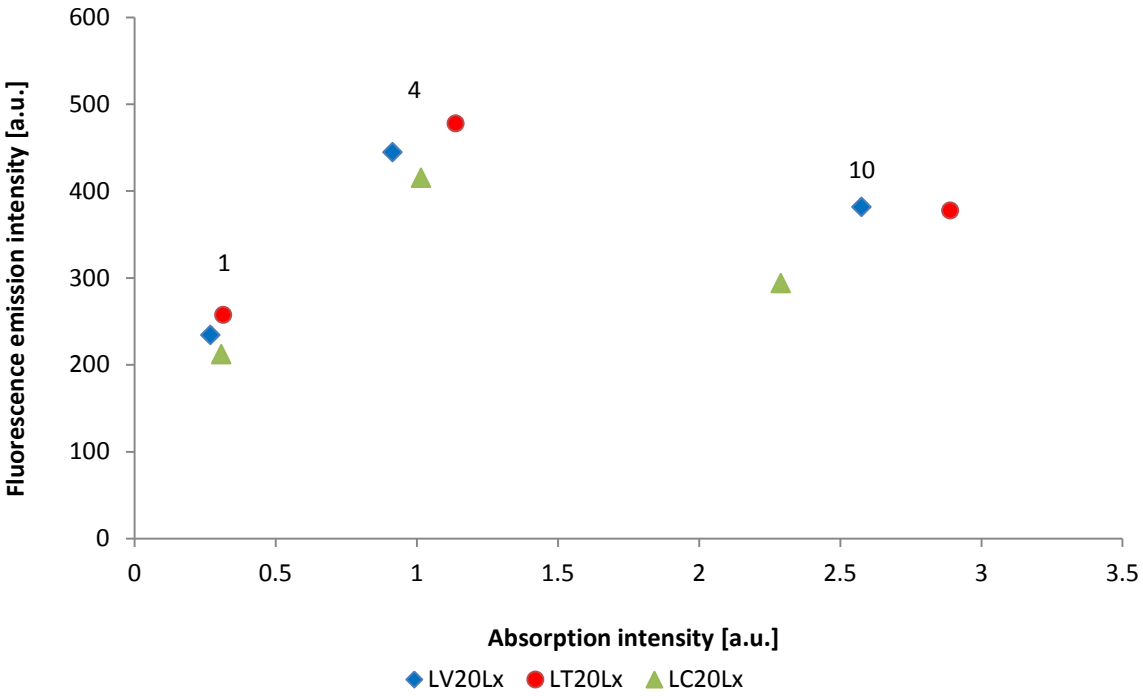

Figure IV.56 Emission intensity versus absorption intensity for LT20Lx, LV20Lx and LC20Lx. x represents the LFR305 concentration and is equal to 1, 4, 10 %.

Another noteworthy result of fluorescence spectroscopy tests is the observation that, the higher the concentration of the dye, the longer the Stokes shift. This effect is analogous to that observed in PMMA based LSC's (see chapter IV.1.1.3). The longer Stokes shift is the result of the progressive redshift of the emission spectrum as the dye concentration increases, accompanied by no shifts in the UV-Vis absorption spectrum. For a detailed explanation of the origin of this effect, the reader is referred to IV.1.1.3. Briefly, this effect can be related to reabsorption processes which become more pronounced at increasing dye concentrations (increased optical density).

This progressive redhisft of the emission spectrum at increasing dye concentration results in a progressive increase in the Stokes shift which tends to level off at highest dye concentrations. This effect can be observed in figure IV.57.

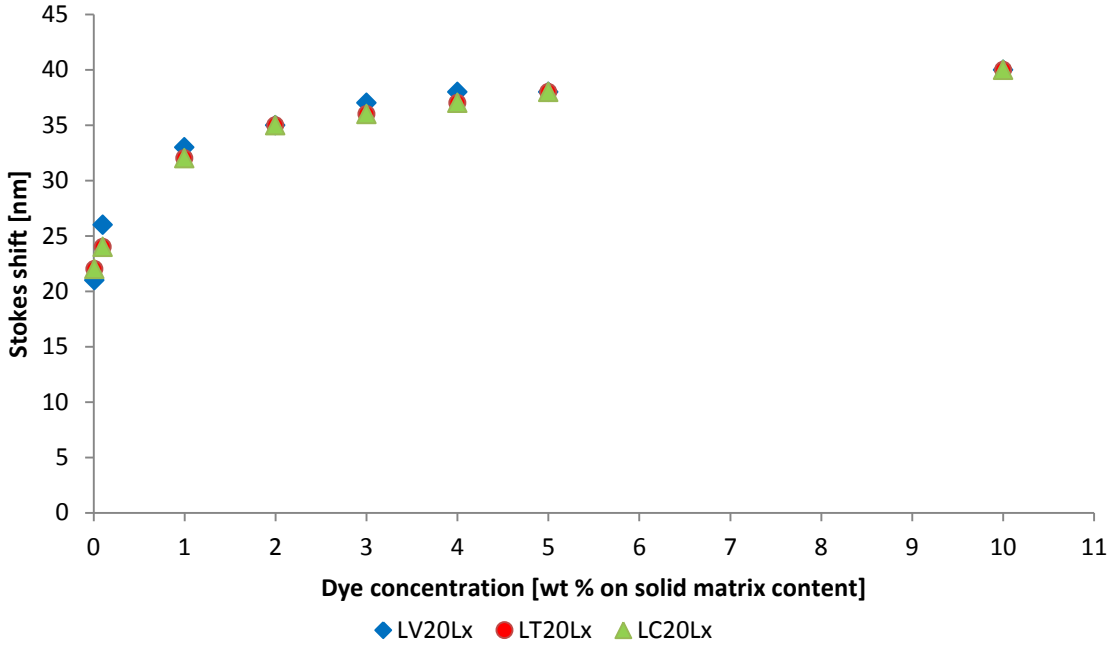

Figure IV.57 Stokes shift as a function of dye concentration for LT20Lx, LV20Lx and LC20Lx.

The trends presented here are similar for all systems studied and, for a dye concentration of 10 %, a maximum Stokes shift of 40 nm is observed for all the systems under investigation. These values are comparable with those presented in paragraph IV.1.1.3 on PMMA-based devices.

As a result from this study, an optimal dye concentration of 4 % was found. In the following, to further optimize LSC's with fluoropolymer-based matrix, the concentration of dye will be maintained constant (4 %) and the thickness of the matrix will be varied to explore its effect on LSC performance. This will be the topic of the next paragraph.

IV.2.3 Optimization of the thickness of the fluoropolymer-based LSC devices

In order to vary the thickness of the fluoropolymer-based matrices, different polymer solution concentrations were tested (10 % , 15 %, 20 % and 30 %) for the spin coating deposition of the LSC film, at constant dye concentration (4%). No matrix concentrations

higher than 30 % were tested due to the difficulty found in the fabrication of reproducible LSC devices at such high solid content. In fact, increasing the matrix concentration results in very rough and non-homogeneous thin-films. Table IV.8 shows the average thickness of the different matrices considered in this study and the corresponding starting solution concentrations.

Matrix concentration [%]	Lumiflon - Tolonate		Lumiflon - Vestanat		Lumiflon - Cymel	
	Average thickness [µm]	Standard deviation [µm]	Average thickness [µm]	Standard deviation [µm]	Average thickness [µm]	Standard deviation [µm]
10	1.85	0.07	2.35	0.21	1.73	0.14
15	3.70	0.14	3.95	0.07	3.24	0.14
20	5.65	0.07	6.00	0.28	5.38	0.21
30	13.2	0.28	18.50	0.14	6.26	1.13

Table IV.8 Average matrix thickness as a function of polymer solution concentration for the different systems considered.

As shown in the table, in each system studied a maximum thickness was found for a matrix concentration of 30 %.

IV.2.3.1 Photovoltaic parameters

Photovoltaic tests were carried out on LSC devices to find the optimal thickness of the matrix in terms of PV performance. Figure IV.58 shows the ΔPCE versus film thickness for a fixed LFR305 content for each matrix considered. Each data is an average of the performance of three LSC's.

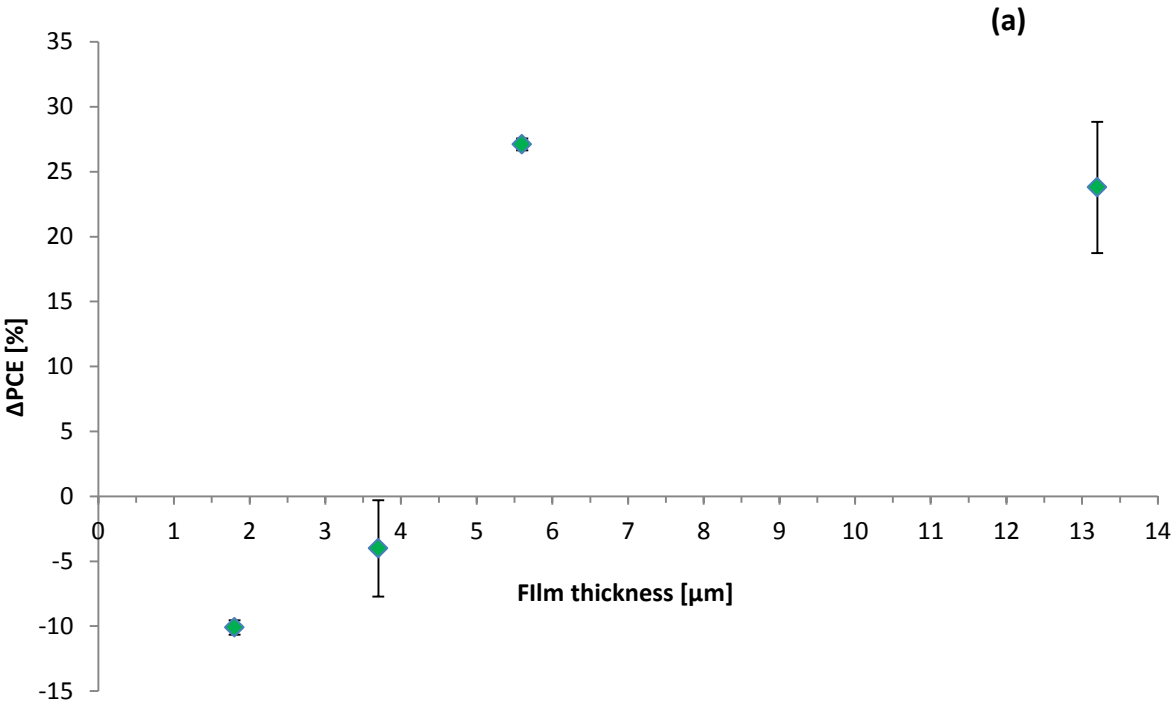
(a)
ΔPCE [%]
35
30
25
20
15
10
5
0
-5
-10
-15
0 1 2 3 4 5 6 7 8 9 10 11 12 13 14
FIlm thickness [µm]

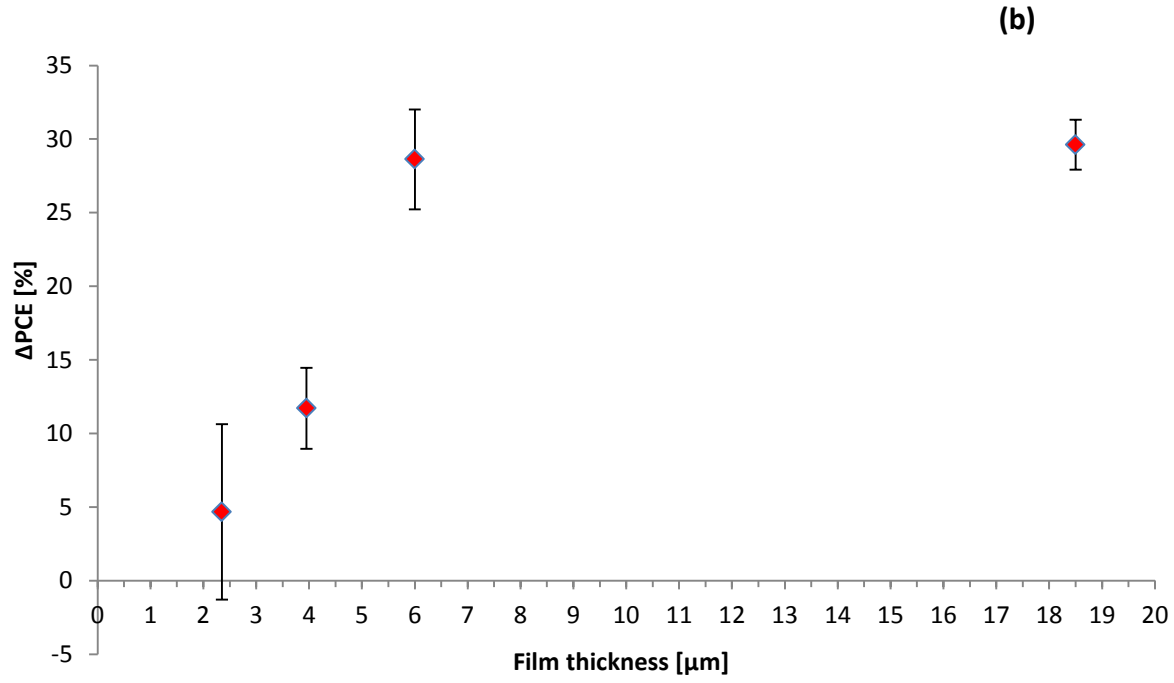
(b)
ΔPCE [%]
35
30
25
20
15
10
5
0
-5
0 1 2 3 4 5 6 7 8 9 10 11 12 13 14 15 16 17 18 19 20
Film thickness [µm]

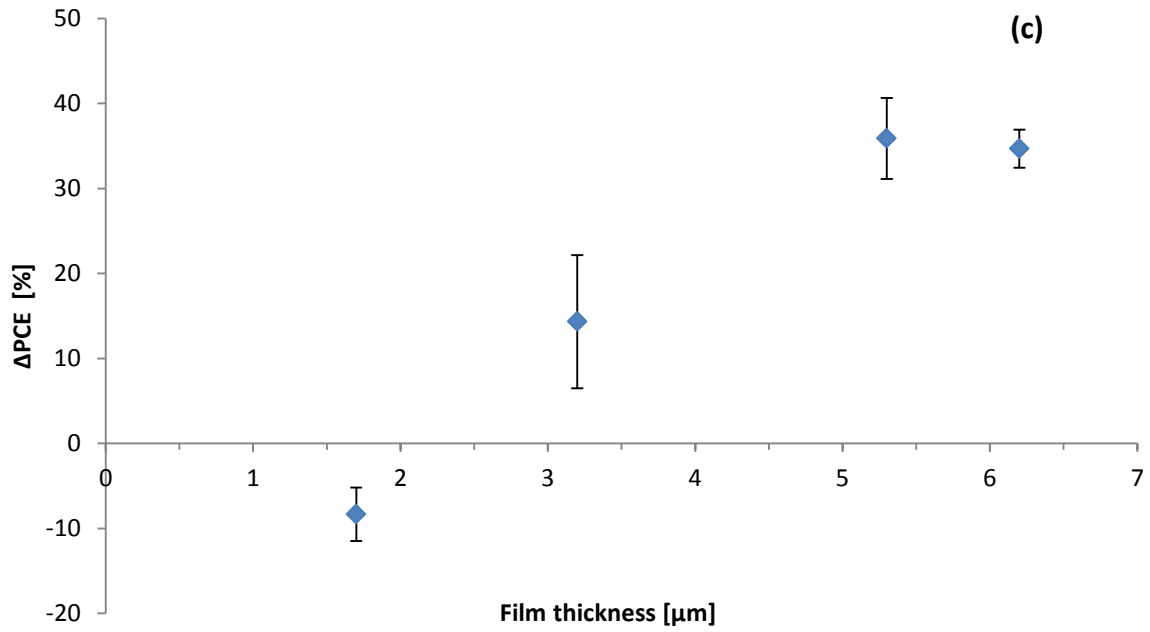

Figure IV.58 ΔPCE versus film thickness for (a) LTxL4, (b) LVxL4 and (c) LCxL4. Each point is averaged on three LSC devices.

A maximum in PV performance was found for all the systems for a film thickness of about 5 µm. For LT and LC thicknesses lower than this value yield negative or slightly positive PV performances. For film thicknesses higher than 5 µm, it seems that the LSC photovoltaic performance appears to maintain a roughly constant value even if the film thickness is further increased. This is observed for all systems considered. Table IV.9 shows the main PV parameters for different matrix thicknesses. It appears clearly that above the 20 % matrix concentration, no further increases in PV performance are attained.

Film thickness [μm]	I_{SC} [mA]	V_{OC} [V]	FF [%]	PCE^{cell} [%]	ΔPCE [%]	PCE^{LSC} [%]
Lumiflon – Tolonate (LT) system						
1.85	13.37 ± 0.41	0.54 ± 0.01	60.17 ± 2.16	9.58 ± 0.21	-10.09 ± 0.56	0.35 ± 0.01
3.70	13.53 ± 0.62	0.54 ± 0.02	58.76 ± 5.05	9.49 ± 0.66	-4.02 ± 3.71	0.34 ± 0.02
5.65	18.55 ± 0.23	0.55 ± 0.00	60.08 ± 0.29	13.57 ± 0.13	**26.90 ± 0.15**	**0.49 ± 0.00**
13.2	17.71 ± 0.11	0.55 ± 0.01	59.03 ± 1.34	12.73 ± 0.53	23.79 ± 5.05	0.43 ± 0.02
Lumiflon – Vestanat (LV) system						
2.35	15.4 ± 1.09	0.55 ± 0.02	58.60 ± 2.88	10.94 ± 1.58	4.67 ± 5.96	0.40 ± 0.05
3.95	15.22 ± 0.96	0.54 ± 0.01	55.49 ± 4.67	10.25 ± 1.60	11.72 ± 2.75	0.37 ± 0.06
6.00	18.72 ± 0.46	0.56 ± 0.00	58.94 ± 1.68	13.62 ± 0.84	**28.62 ± 3.39**	**0.49 ± 0.03**
18.50	18.68 ± 0.37	0.56 ± 0.00	60.23 ± 0.93	13.91 ± 0.24	29.61 ± 1.70	0.50 ± 0.01
Lumiflon – Cymel (LC) system						
1.75	13.60 ± 0.05	0.54 ± 0.01	58.22 ± 2.03	9.45 ± 0.48	-8.34 ± 3.14	0.34 ± 0.02
3.26	15.97 ± 1.09	0.55 ± 0.01	59.41 ± 2.27	11.64 ± 0.45	14.32 ± 7.32	0.42 ± 0.05
5.32	19.25 ± 0.60	0.56 ± 0.00	59.82 ± 0.66	9.49 ± 0.01	**35.19 ± 4.76**	**0.34 ± 0.00**
6.25	19.15 ± 0.15	0.55 ± 0.02	57.33 ± 3.42	13.32 ± 1.32	34.68 ± 2.24	0.48 ± 0.040

Table IV.9 Main PV parameters for different film thickness for all systems considered.

In order to further investigate the effect of LSC thickness on device performance, UV-Vis spectra were recorded for the different film-thickness LSC devices considered so far, as shown in the following section.

IV.2.3.2 UV-Vis absorption spectroscopy

In figure IV.59 UV-Vis absorption spectra for the LSC with different film thicknesses are reported for all kinds of matrices studied.

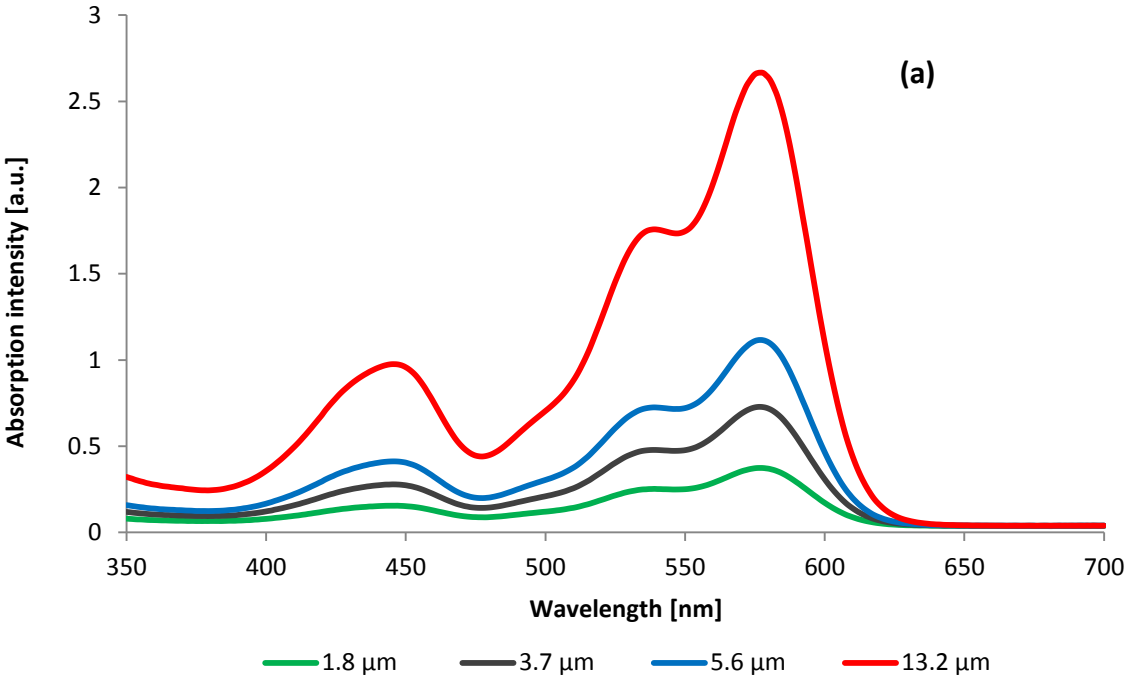
(a)
Absorption intensity [a.u.]
Wavelength [nm]
1.8 µm
3.7 µm
5.6 µm
13.2 µm

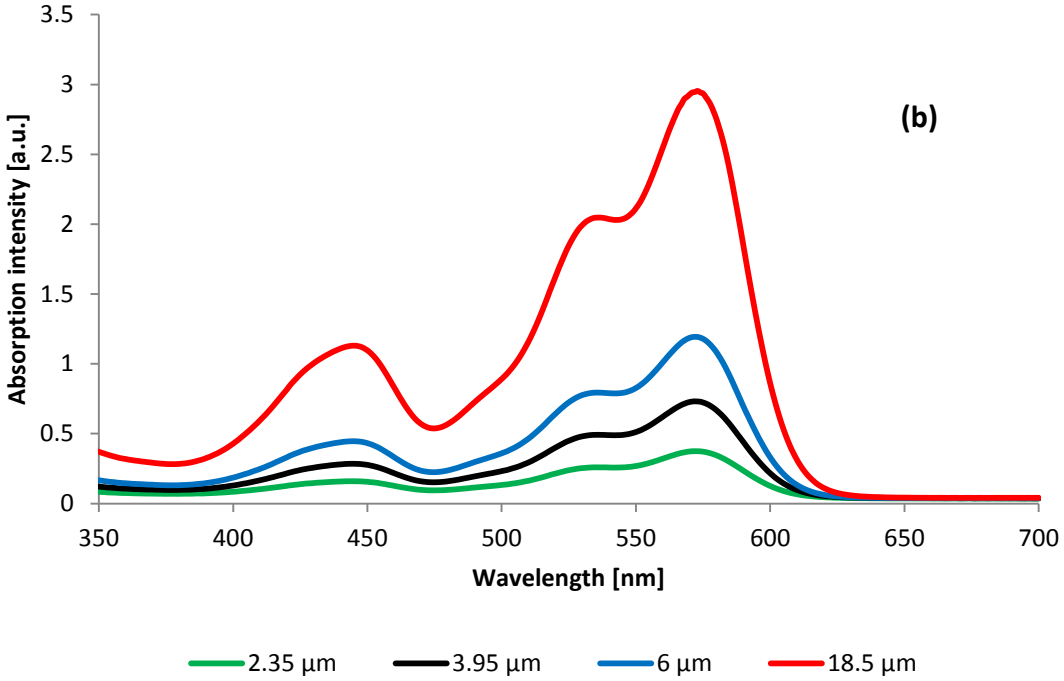
(b)
Absorption intensity [a.u.]
Wavelength [nm]
2.35 µm
3.95 µm
6 µm
18.5 µm

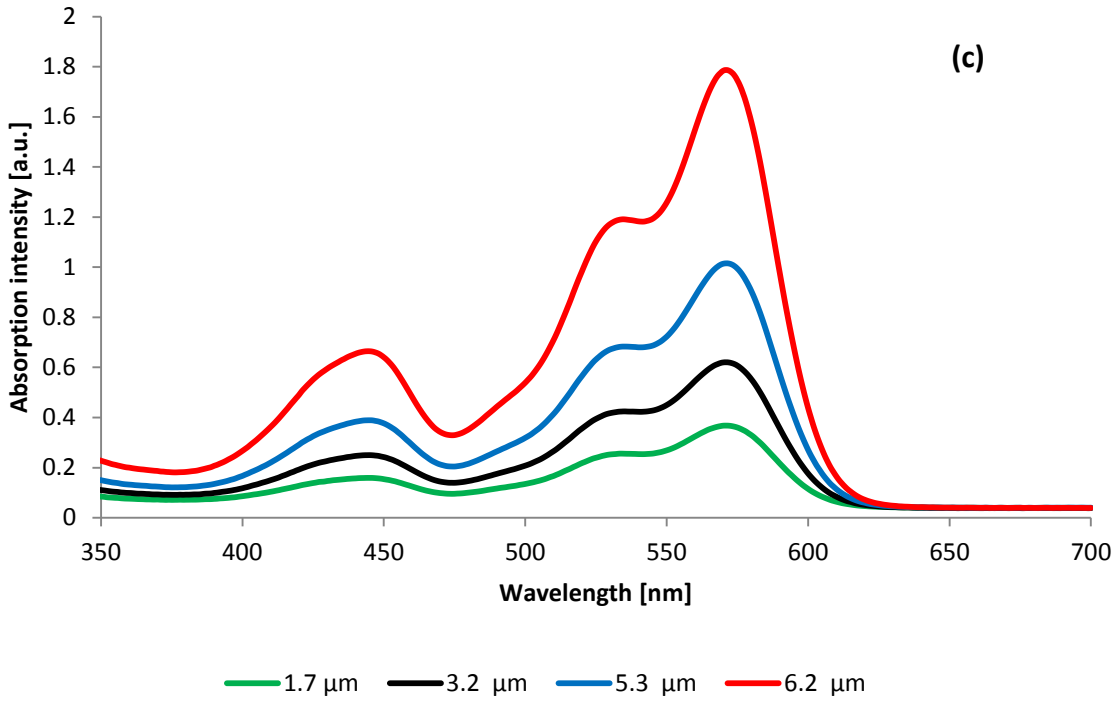

Figure IV.59 UV-Vis absorption spectra for different matrix thickness for the LT (a), LV (b) and LC (c) systems.

The recorded spectra highlights that the higher the film thickness, the higher the UV-Vis absorbance of the doped matrix. In particular, the highest film thickness results in the highest UV-Vis absorption intensity. In addition, no shifts of the absorption spectra were observed as the thickness of the matrix is increased.

Although in each system the thickest sample absorbs more light than the other film thickness LSC devices, it does not generally show the highest PV performance. Indeed, in all the matrices studied, the two thickest samples give the same PV results despite their corresponding absorption intensity is different. As a consequence, the thickest LSC sample in each host matrix system is expected to be more prone to dissipative processes occurring in the LSC device. Those dissipative processes are probably not due to aggregate formation because aggregate concentration is approximately constant for all samples (as it is primarily dependent on dye concentration which is held constant in these tests). A different dissipative process may be responsible for the similar PV performance observed in the two thickest samples, despite their different absorption intensity.

Fluorescence spectroscopy can help in further clarifying the origin of this dissipative process.

IV.2.3.3 Fluorescence spectroscopy

Fluorescence spectroscopy was performed on the samples which were investigated also by UV-Vis absorption spectroscopy. Figure IV.60 depicts the effects on the fluorescence spectra given by the variation of film thickness for the different systems considered.

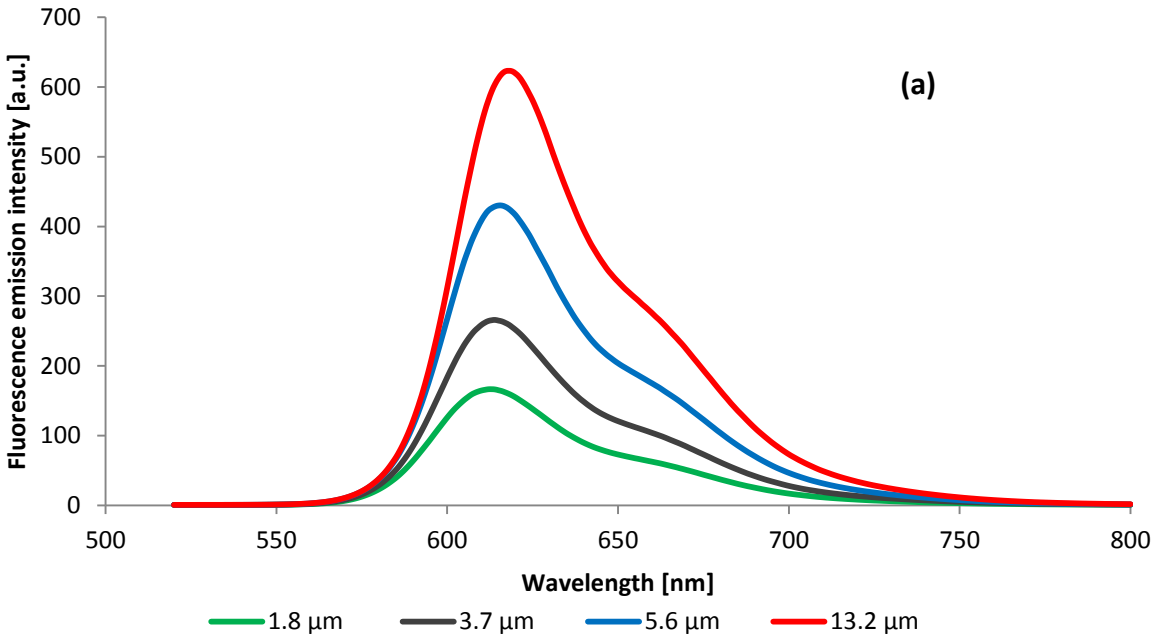

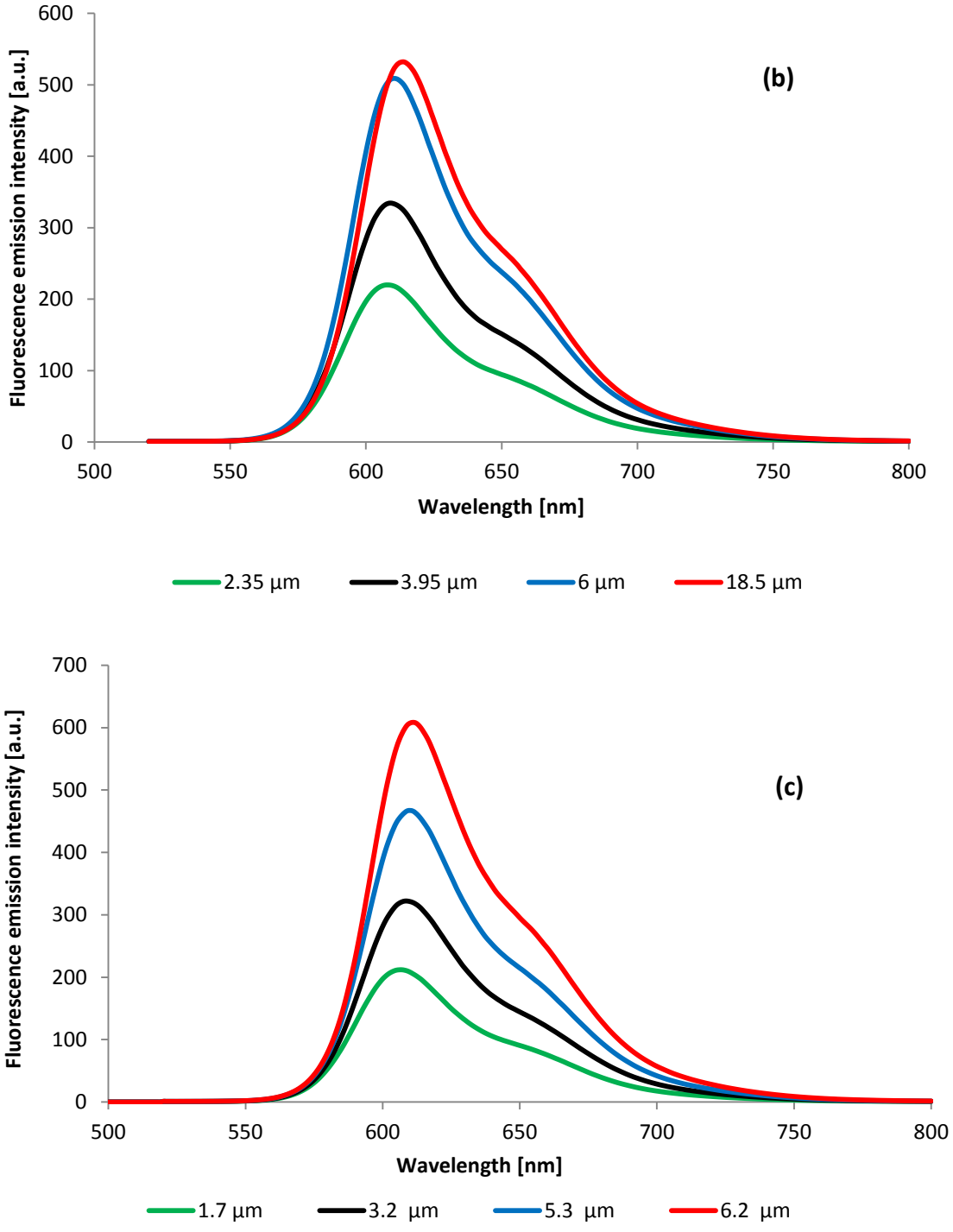

Figure IV.60 Fluorescence emission spectra of (a) LTxL4, (b) LVxL4 and (c) LCxL4 for different matrix thickness.

Two effects can be seen from the observation of the figure. The first one is that increasing film thickness results in an increase of the emission intensity. This is a reasonable effect because no fluorescence quenching is expected since dye concentration is kept constant.

The second observable effect is a progressive redshift of the emission spectra as the film thickness is progressively increased. For a detailed explanation of the possible reasons of this effect, the reader is referred to paragraph IV.1.2.4. In that discussion, re-absorption events were recognized to be responsible for the progressive redshift of the emission spectrum. In fact a similar role is played by reabsorption events in the case of PMMA-based LSC matrix. A similar conclusion was drawn by Maggioni et al. [3] on a different LSC system.

As the thickness of the matrix increases, the increasing redshift of the emission spectrum leads to a Stokes shift increase which can be observed in figure IV.61, where the Stokes shift as a function of film thickness is reported for all the matrices prepared.

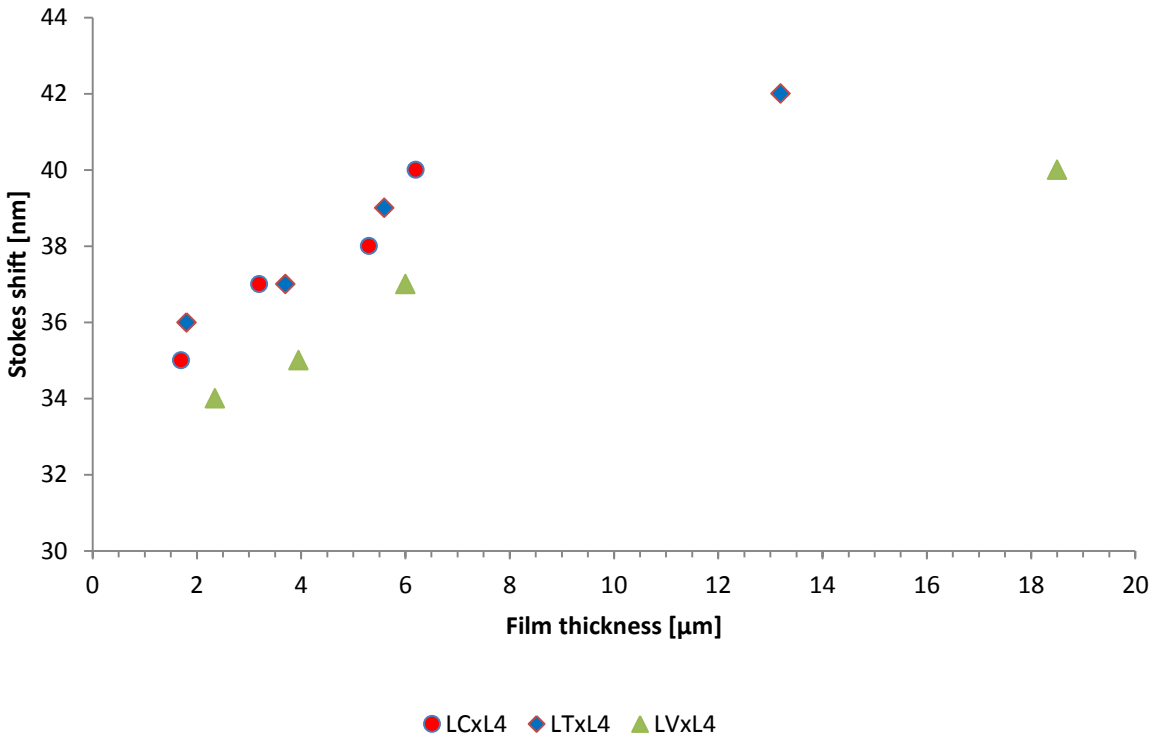

Figure IV.61 Stokes shift versus film thickness for different matrix systems fluoropolymer-based.

In the next section, EQE measurements will be shown to further clarify the role of reabsorption events in LSC performance.

IV.2.3.4 EQE measurements

EQE measurements were performed on all LSC devices tested previously. EQE spectra are reported as a function of thickness for the fluoropolymer-based LSC devices in figure IV.62.

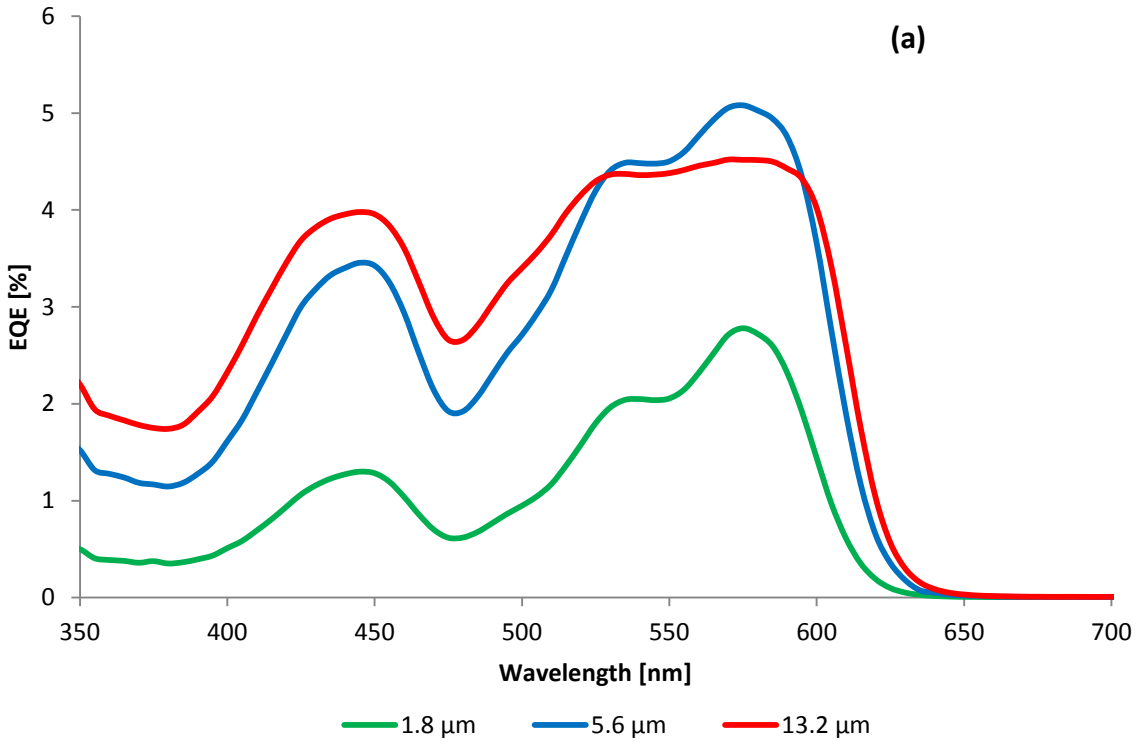

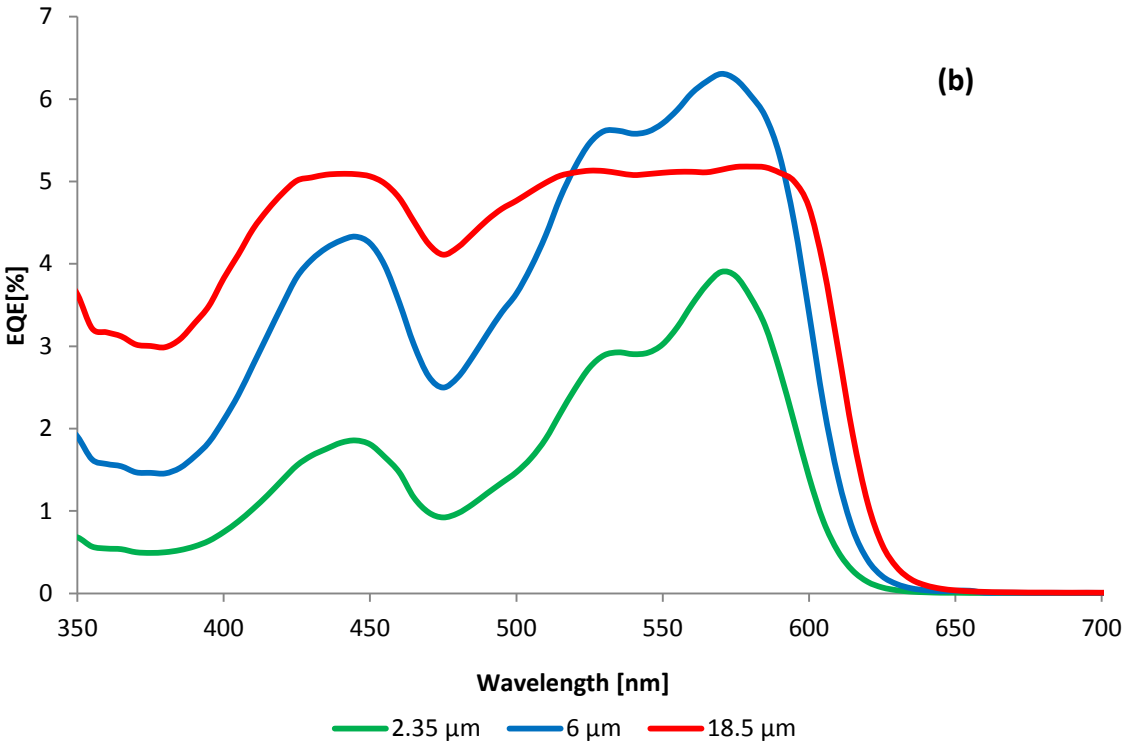

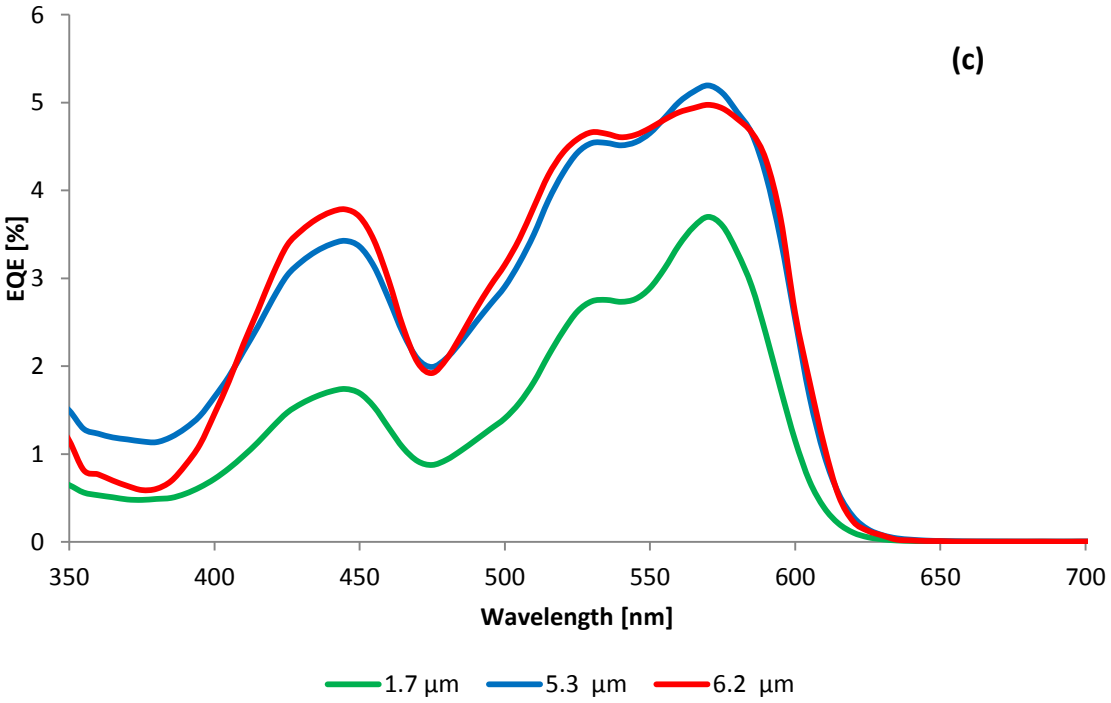

Figure IV.62 EQE spectra for LSC devices with different film thickness. (a) LTxL4, (b) LVxL4 and (c) LCxL4.

The shape of the EQE curves is in all cases similar to that of UV-Vis absorption spectra and this is a confirmation that only absorbed photons can effectively be converted into electrical charges.

For each system, the EQE spectra of the two thickest samples show a similar behavior and are characterized by nearly the same values. This can explain the fact that the two thickest LSC's perform comparably in terms of photovoltaic performance. Although the number of incident photons on the surface of the LSC thin film is equal for the two thickest samples, their absorption intensity varies, as observed in the UV-Vis absorption spectra. In particular, in each system the thickest LSC sample shows a much higher absorption intensity compared to the other samples. The fact that two different film thickness LSCs show similar EQE spectra despite their significantly different absorption intensity is a further clear indication that the thickest systems are more subjected to reabsorption phenomena which limit their device performance.

In all cases under investigation, the thinner LSC, which is the less efficient system, shows an EQE curve which is always below the EQE curve of the other LSC samples. This effect can be attributed to the less intense UV-Vis absorption intensity of the thinner LSC. This observation is in agreement with the results obtained in PV tests, where the thinnest LSC's yielded the lowest device performance.

The second observation that can be made after analyzing figure IV.62 is a progressive smoothing of the EQE curve in the range 550-600 nm as the LSC film become thicker. On the other hand, in the other part of the curve (in the 400-500 nm range) this effect is not observed as the film thickness is increased. A similar trend was found on PMMA-based LSC's at varying thickness. As already discussed, this effect may mean that by increasing film thickness, lower wavelength photons may become more effective than longer wavelength photons in the production of electric charges. This behavior may be related to the fact that for increasing film thickness, "red" (longer wavelength) photons may be more susceptible to dissipative processes compared to "blue" (shorter wavelength) photons. This effect may be attributed to the redshift of the fluorescence emission spectrum with respect to the absorption spectrum, that results in a progressively higher Stokes shift at increasing film thickness (see figure IV.61). Such increasingly higher Stokes shift yields a progressively lower

overlapping of absorption and emission spectra as film thickness is increased. This behavior is represented in figure IV.63 where the normalized absorption and emission spectra are reported for each system considered.

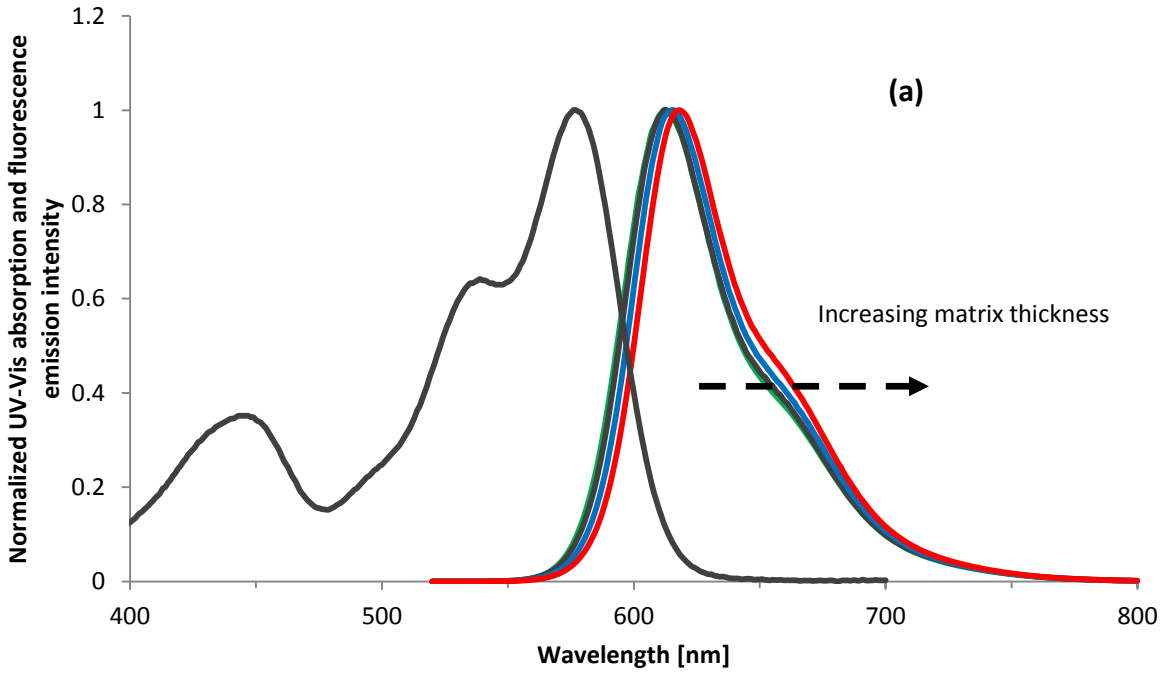

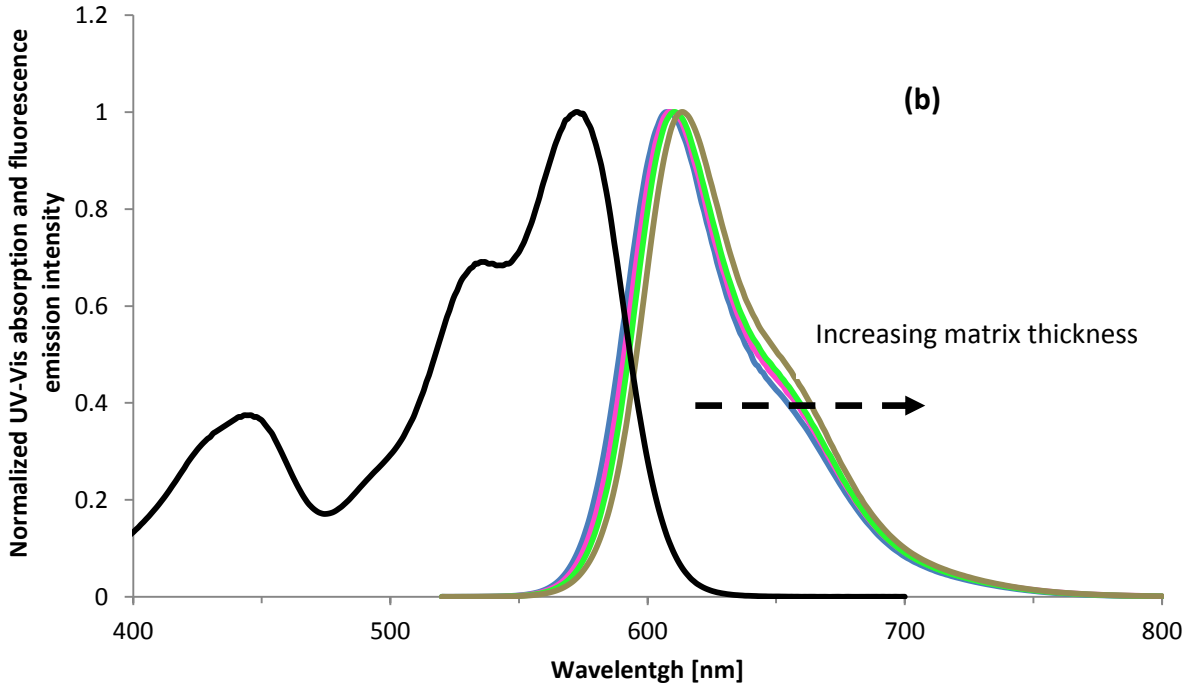

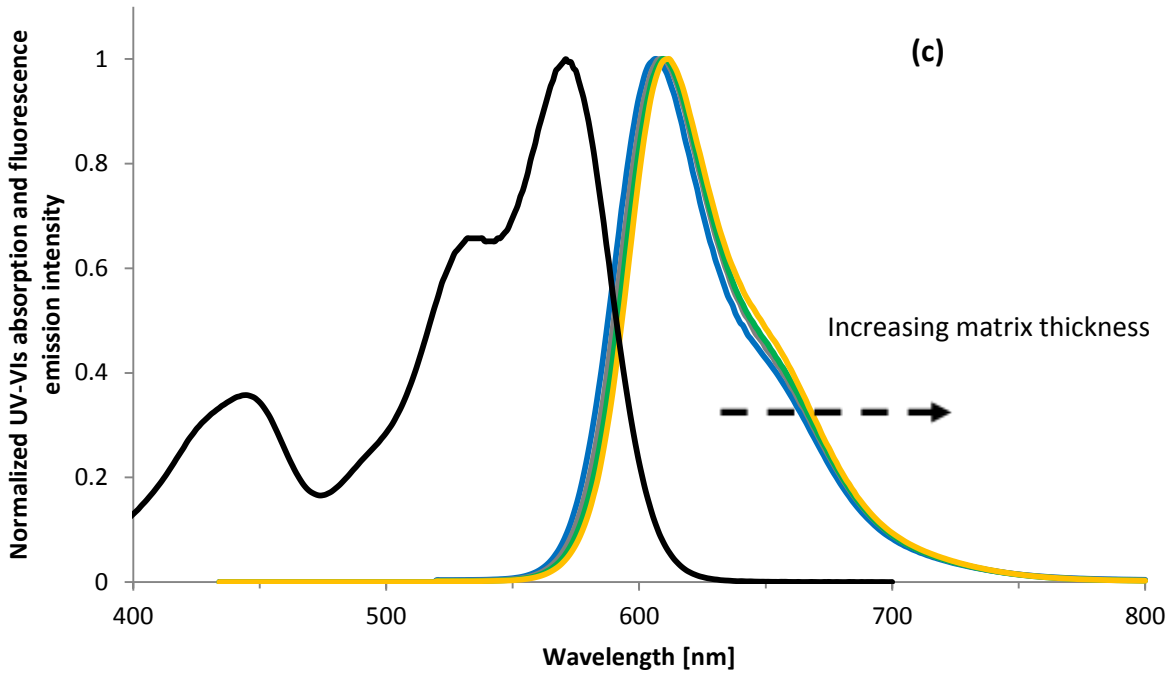

Figure IV.63 Normalized UV-Vis absorption and fluorescence emission spectra for different matrix thickness. (a) LTxL4, (b) LVxL4 and (c) LCxL4.

Although partial overlapping of absorption and emission spectra is always present, the redshift of the emission spectra causes the overlapping portion to progressively decrease at higher film thickness. As can be seen from the figures, reabsorption events are always present. This decrease results in a progressively higher portion of photon wavelengths to be excluded from reabsorption phenomena. In particular, an increasingly higher amount of lower wavelengths photons will not be reabsorbed by other adjacent dye molecules. This behavior may be related to the modifications to the EQE spectra observed in figure IV.63 at increasing film thickness.

In conclusion, the different Fluoropolymer-based LSC devices presented similar trends in the PV optimization of the LSC devices from the photovoltaic point of view. In particular, for all host matrix systems, the optimal heating time to allow crosslinking was found to be 30 minutes at 150 °C, the optimal dye concentration was identified at 4 % on weight with respect to the total solid content, the optimal matrix thickness was found to be around 5 µm. These parameters will be kept constant in the following part of the work.

IV.3 Accelerated weathering studies on optimized LSC devices

This section will be dedicated to accelerated weathering tests. The performed tests were aimed at the characterization of the long-term behavior of the systems presented in the previous sections. As stated before, the outdoor degradation is one of the main disadvantages of organic-based Luminescent Solar Concentrators due to the susceptibility to photo-oxidation of the organic materials employed for the host matrix and dyes. A degraded matrix could, in fact, affect detrimentally the waveguiding process during LSC operation.

The accelerated weathering tests were performed on the optimized LSC devices as resulting from the study presented in the previous chapters. In particular, different accelerated weathering tests were performed. The first concerns the exposure of an optimized PMMA-based LSC (P15L5) to a UV-C light source in order to characterize the stability of LSC devices in short times and very strong radical-generating conditions. Then exposure to UV-A light of all the optimized devices was considered. Finally the last test was conducted on all optimized LSC devices in a weather-o-meter chamber where the samples were subjected to continuous light exposure for several hundreds of hours at constant T ($\sim$ 38 °C) and RH ($\sim$ 20 %). The results on LSC weathering behavior that will be presented in the following sections will mainly deal with the PV characterization of the LSC devices studied and will aim at the characterization of device performance and operational lifetime. However, further tests are needed to better clarify the molecular degradation mechanisms underlying the trends that will be observed. In order to do so, FTIR, UV-Vis and fluorescence emission spectroscopy investigations are currently underway, so as to gain a thorough optical and molecular characterization of the modifications occurring to these new host matrix systems and to give possible explanations about the degradation mechanisms occurring on a long-term timescale. This characterization was not carried out on the LSC devices subjected to weathering tests in the weather-o-meter chamber, due to the limited space within the chamber and especially due to the risk of mechanically damaging the LSC thin film surface

while performing those tests which would result in unwanted mechanically-induced worsening of their PV performance.

IV.3.1 UV stability of PMMA-based LSC devices

UV-C and UV-A weathering tests were performed on P15L5 LSC devices. In a first test, P15L5 LSC devices were exposed to UV-C light source and the PV data were collected periodically every 30 minutes of exposure. In a second test, new P15L5 LSC devices were exposed to UV-A light source by periodically collecting the PV data.

IV.3.1.1 Exposure to UV-C light

Figure IV.64 presents the evolution of LSC ΔPCE during UV-C exposure time while figure IV.65 shows the PCE^{LSC} versus UV-C exposure time. All the data refers to the best performing LSC based on PMMA.

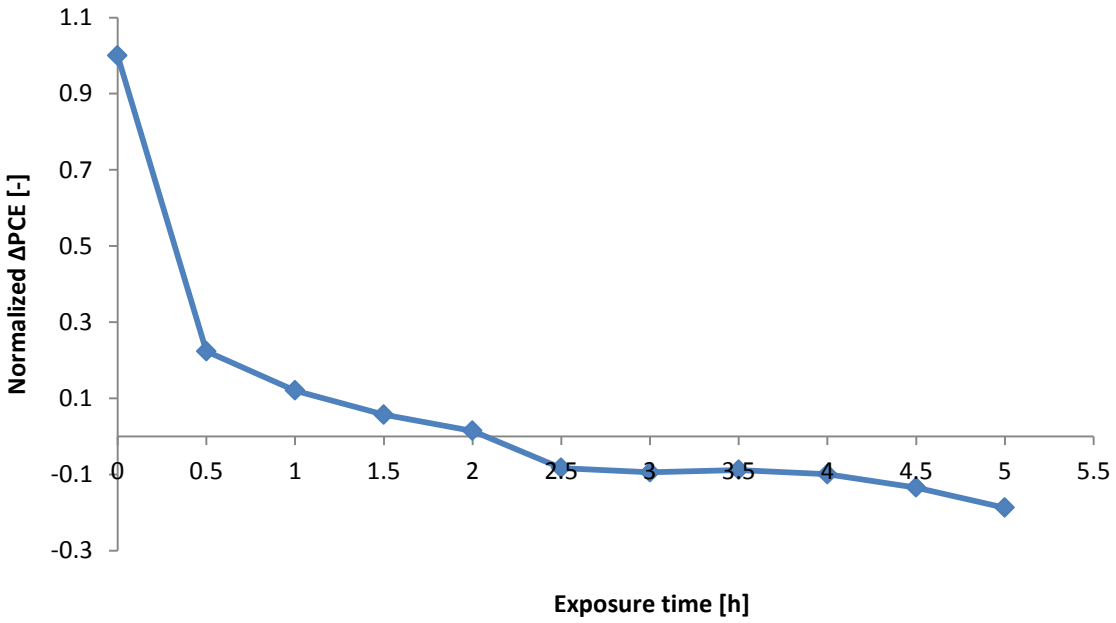

Figure IV.64 Normalized ΔPCE versus UV-C exposure time for P15L5 LSC device.

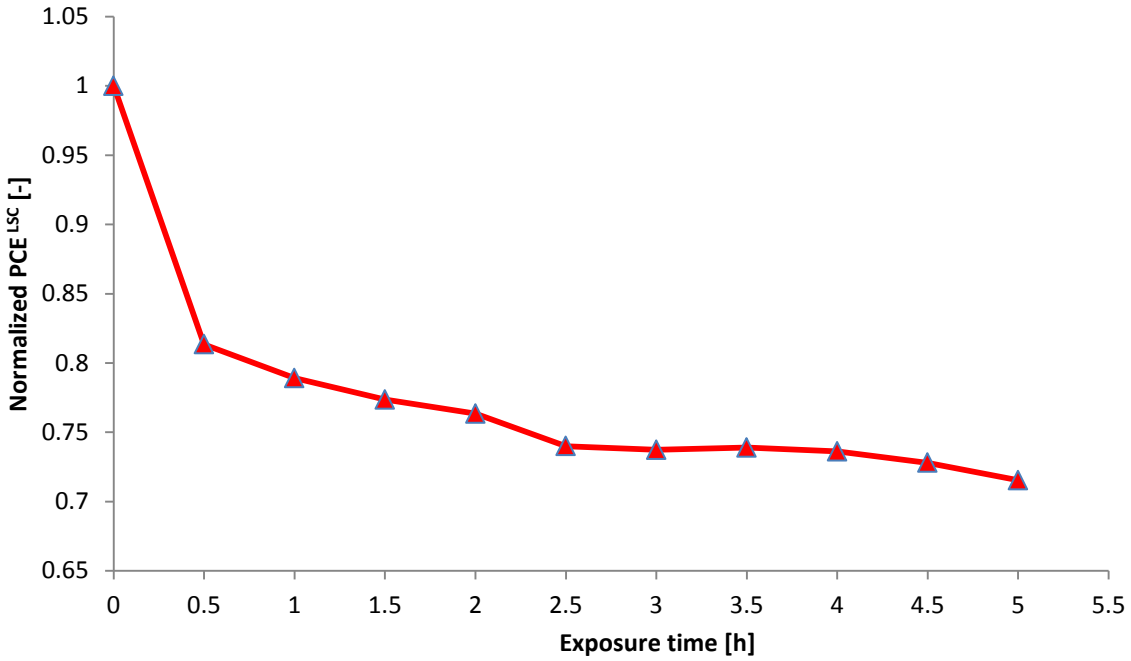

Figure IV.65 Normalized PCE^{LSC} versus UV-C exposure time for P15L5 LSC device.

A sharp decay in both the parameters is observed after 0.5 h of UV-C light exposure with a decrease of over 20% of PCE^{LSC} reflected in a nearly zero efficiency gain ΔPCE. Such an abrupt decay mainly results from a decrease in I_{SC}, while only a slight decrease in V_{OC} (figure IV.66) is observed during UV-exposure (0.4%), suggesting that a significantly lower amount of incident photons could be absorbed and redirected towards the edges of the LSC and made available to the PV cell.

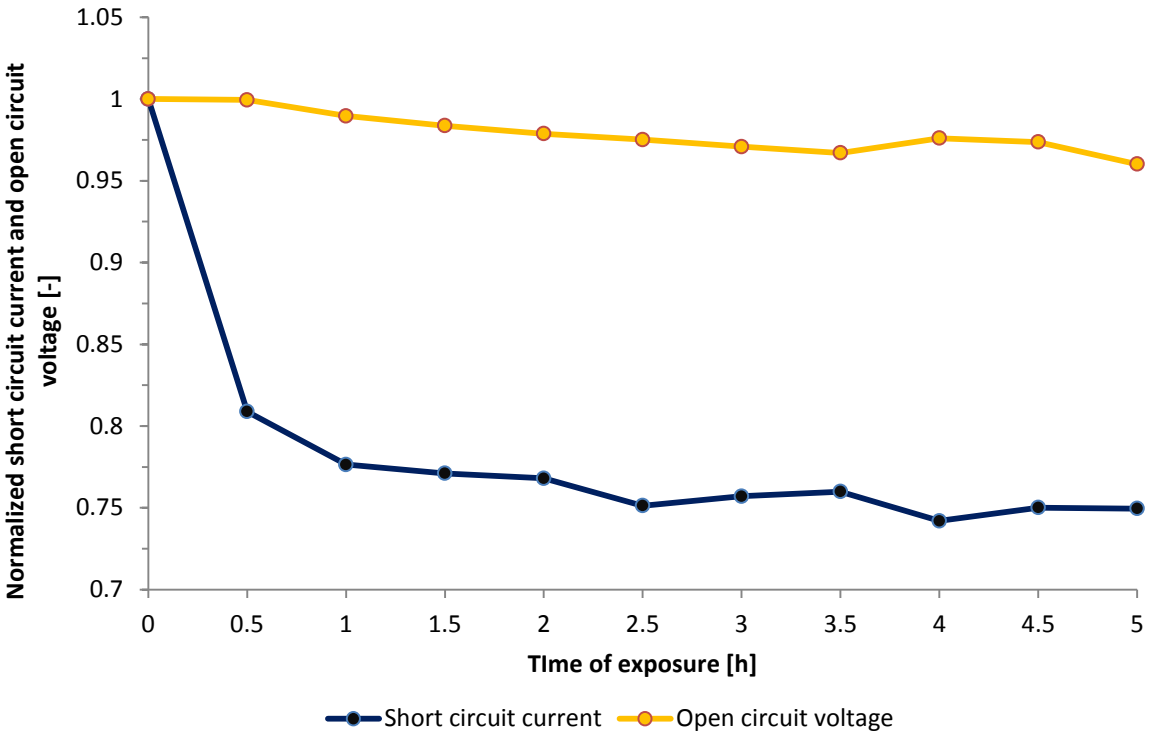

Figure IV.66 Normalized short circuit current and open circuit voltage versus UV-C exposure time for P15L5 LSC device

This effect can be due to a reduction in the light absorbed by the organic dye following its degradation but also to the degradation of the polymer matrix which may have occurred and may contribute to a decrease of light trapping and photon transport efficiency within the LSC thin film. For longer UV-C-exposure times, the rate of efficiency decay stabilizes and after 5 h of UV-exposure a 30% decrease of PCE^{LSC} is observed corresponding to a -20% efficiency gain ΔPCE. This negative ΔPCE value clearly indicates that at this exposure time the addition of an LSC thin film is detrimental to the operation of the solar cell alone. In particular, a higher power output would be obtained by simply shining sunlight on the photoactive area of the bare PV cell.

The test with UV-C light is very efficient for its short-time responses, but it is obviously very far from natural weathering-conditions.

IV.3.1.2 Exposure to UV-A light

P15L5 LSC devices were also exposed to UV-A light to evaluate the effects of milder conditions on the behavior of PMMA-based LSC devices. Figure IV.67 presents the normalized ΔPCE while figure IV.68 depicts the normalized absolute efficiency of the LSC, PCE^{LSC}.

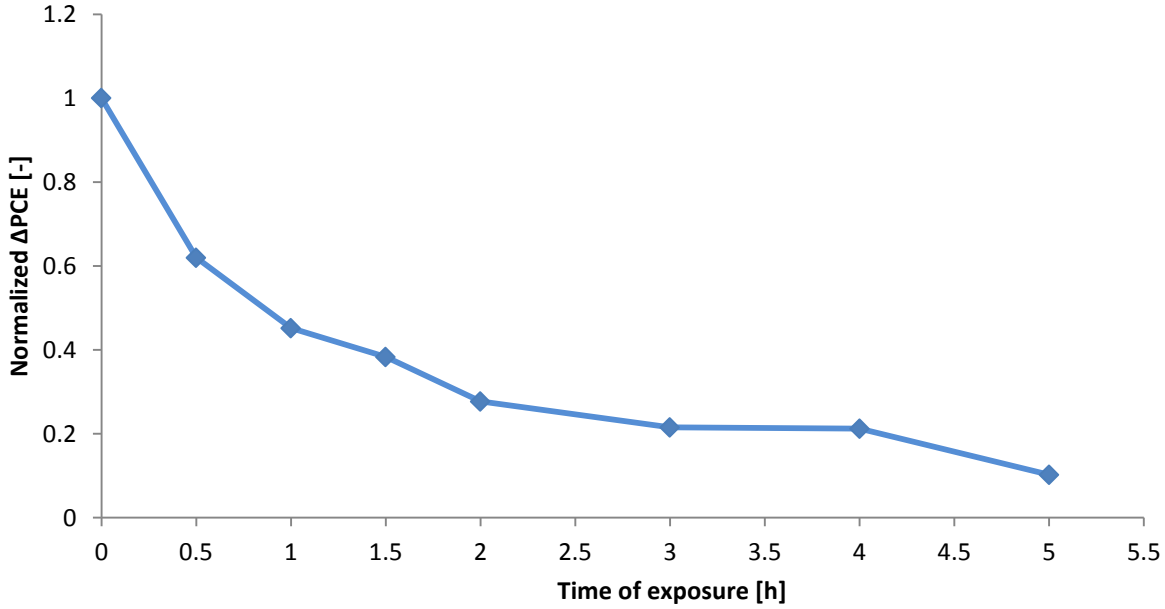

Figure IV.67 Normalized ΔPCE versus UV-A exposure time for P15L5 LSC device.

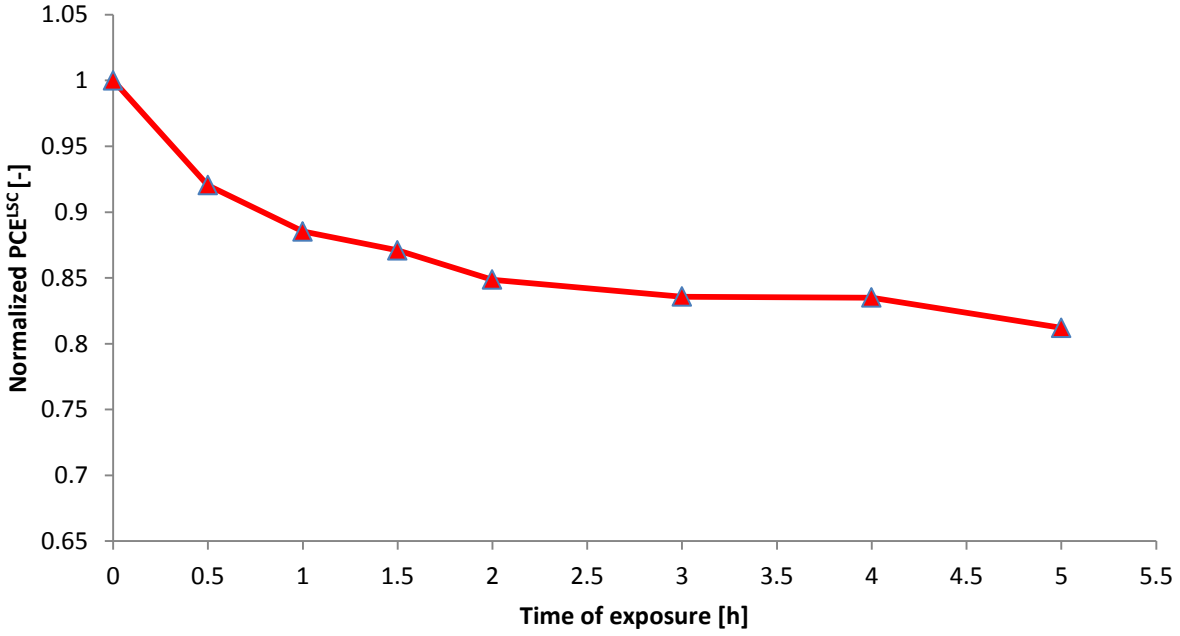

Figure IV.68 Normalized PCE^{LSC} versus UV-A exposure time for P15L5 LSC device.

As shown in the figures, degradation is effective in the first hour of exposure because it results in a decrease of 40 % in ΔPCE with respect to its initial value. After one hour of exposure, PCE^{LSC} shows a decrease of 10 %. A similar trend was observed in the UV-C exposure tests. As the time of exposure proceeds, both ΔPCE and PCE^{LSC} decrease, reaching respectively 10 % and 80 % of their initial value after 5 hours of exposure. However the rate of decay of the PV parameters is less sharp than in the case of UV-C exposure. For example, ΔPCE in the case of LSC exposed to UV-C radiation is negative after 5 hours of exposure, meaning that the PCE of the PV cell is higher than the PCE of the complete LSC system. On the other hand, ΔPCE for LSC exposed to UV-A radiation is positive after 5 hours of exposure, and this means that the LSC used still gives an efficiency gain with respect to the bare PV cell. The decrease in the PCE of the LSC derives from a decrease in the short circuit current due to the exposure to UV-A radiation. In particular, this effect can be better seen in figure IV.69 where the normalized short circuit current and the normalized open circuit voltage versus UV-A light exposure time are reported.

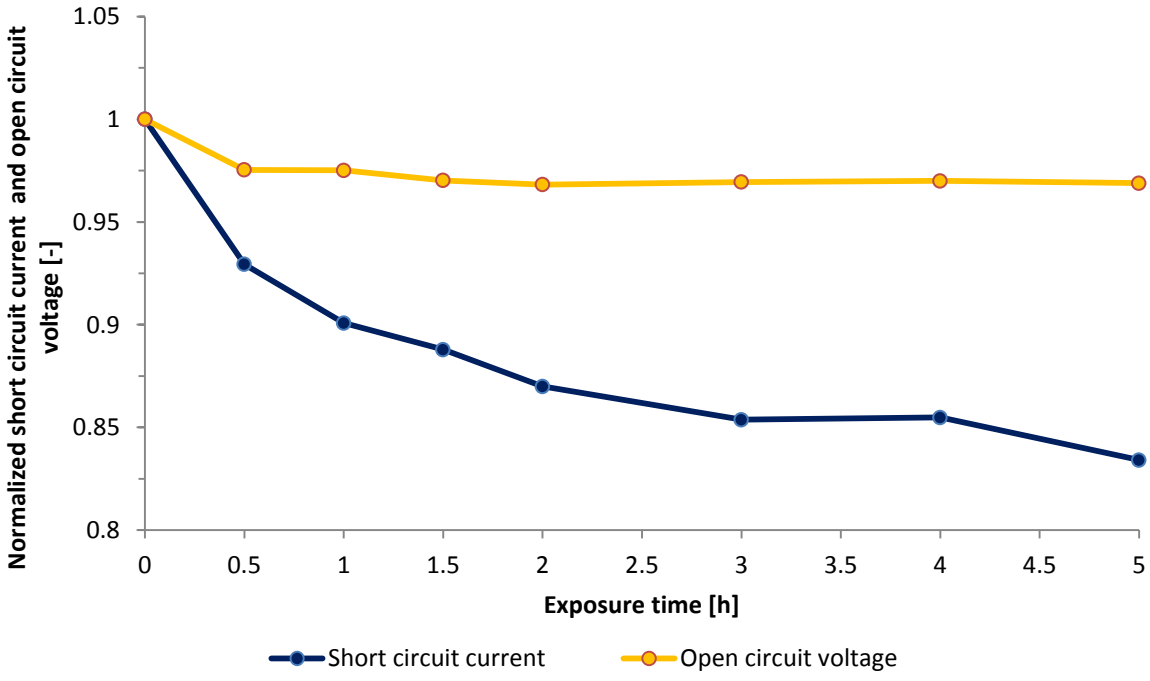

Figure IV.69 Normalized short circuit current and open circuit voltage versus UV-A exposure time for P15L5 LSC device.

During the first hour of exposure, the current experiences a decrease of 10 % with respect to its initial value, while the open circuit voltage decreases of about 3 %. The decrease in the short circuit current is the main cause of the decrease in the ΔPCE and PCE^{LSC}. This effect can be due to two main reasons: the first may be related to the reduced absorbance of the dye molecules and this effect may be related to dye degradation, while the second may be due to matrix degradation and may lead to a reduction in the optical efficiency of the LSC system. This latter efficiency includes all the contributions related to the optical transport, such as the light trapping efficiency and the photon transport efficiency.

IV.3.2 UV stability of fluoro-polymer-based LSC devices

IV.3.2.1 PV parameters

In order to carry out a comparison with PMMA-based LSC devices, in this paragraph the stability of fluoro-polymer-based LSC devices to UV-A light exposure is presented. In figure IV.70 the normalized ΔPCE versus UV-A light exposure time is reported for each system.

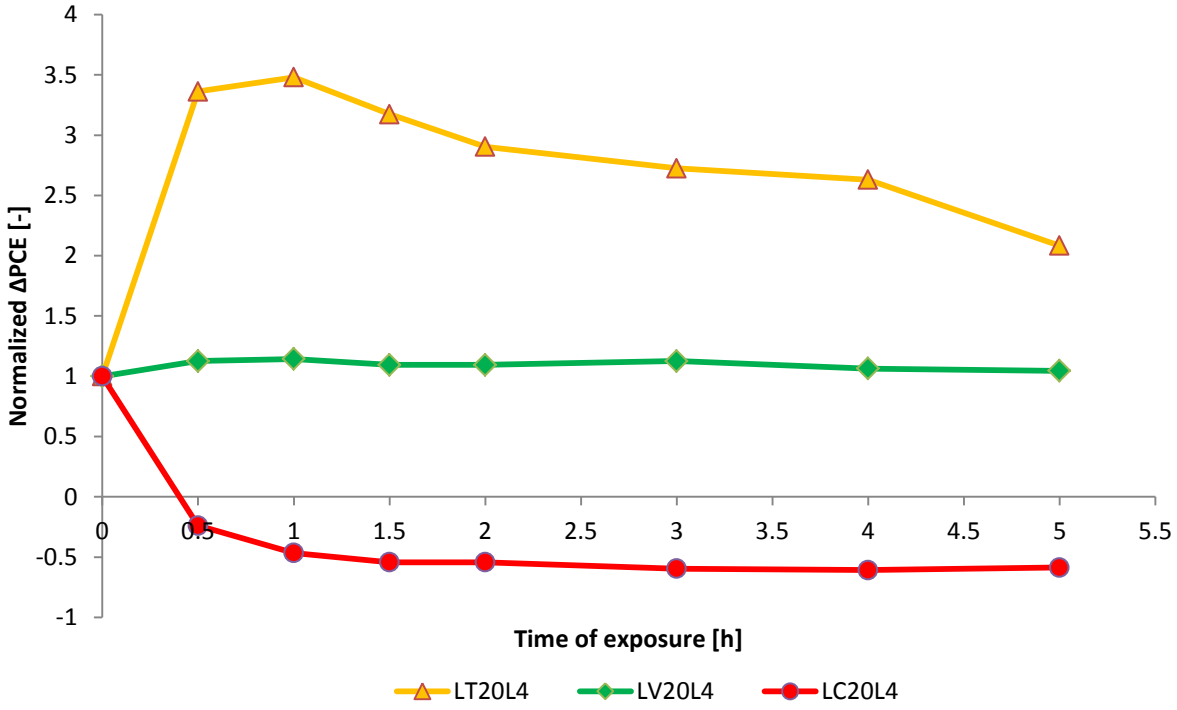

Figure IV.70 Normalized ΔPCE versus UV-A exposure time for LT20L4, LV20L4 and LC20L4.

As shown in the plot, significantly different behaviors are found for the three different matrix systems, clearly highlighting the fundamental role of the carrier polymer in the stability of the LSC device.

Let us start the discussion of the results obtained on the LC20L4 LSC device. After 30 minutes of light exposure, ΔPCE of LC20L4 device drops down to a negative value, showing a decrease in ΔPCE of 123 % from its initial value. Then, after 1 hour of exposure, the ΔPCE of LC20L4 LSC device stabilizes on a plateau value which is maintained until the end of the test (5 hours). The sudden decrease in ΔPCE experienced in the first hour of exposure may be due to the rapid degradation of the polymer matrix and of the organic dye. Thus, the LC matrix seems poorly resistant to degradation induced by UV-A radiation. This may be due to the instability to UV-A light of the melamine phase characteristic of this type of polymer matrix which may induce degradation of the polymer, worsening in the optical efficiency in the LSC system and abrupt decrease of the PV performance.

When considering the LT20L4 and LV20L4 systems, considerably different trends are observed. In particular as opposed to LC20L4, LV20L4 shows a 12 % increase of ΔPCE after 30 minutes of UV-A exposure. After this increase, the ΔPCE of the LV20L4 LSC device remains approximately constant over the entire duration of the test as can be seen from figure IV.70. After 5 hours of exposure, ΔPCE for this system is still higher than the initial ΔPCE by 4 %. A similar trend is observed on LT20L4 devices that also show a positive ΔPCE increase after 30 minutes of UV-A exposure. However a much sharper ΔPCE is observed in LT20L4 compared to LV20L4. In fact, ΔPCE is increased by a factor of 3.3 as a consequence of UV-A light exposure. Such a high initial increase in performance yields a final ΔPCE value (5 h exposure) higher than what observed before UV-A exposure. It is interesting to observe that such performance increase following UV-A exposure, although to different extents, is found in both urethane-based matrices (LT and LV), which also appear to be more resistant to light exposure than the ether-based (LC) matrix. No previous works dealing with this peculiar effect can be found in the literature and thus the reasons which may explain this behavior are currently under investigation; some hypotheses are made in the next paragraph, where additional tests such as UV-Vis absorption spectroscopy and fluorescence emission spectroscopy on LT, LV and LC systems are reported. FTIR studies are under evaluation too.

IV.3.2.2 UV-Vis absorption spectroscopy

Figure IV.71 presents the UV-Vis absorption spectrum of the unexposed LT20L4 LSC device and of LT20L4 LSC device after 30 minutes of UV-A exposure.

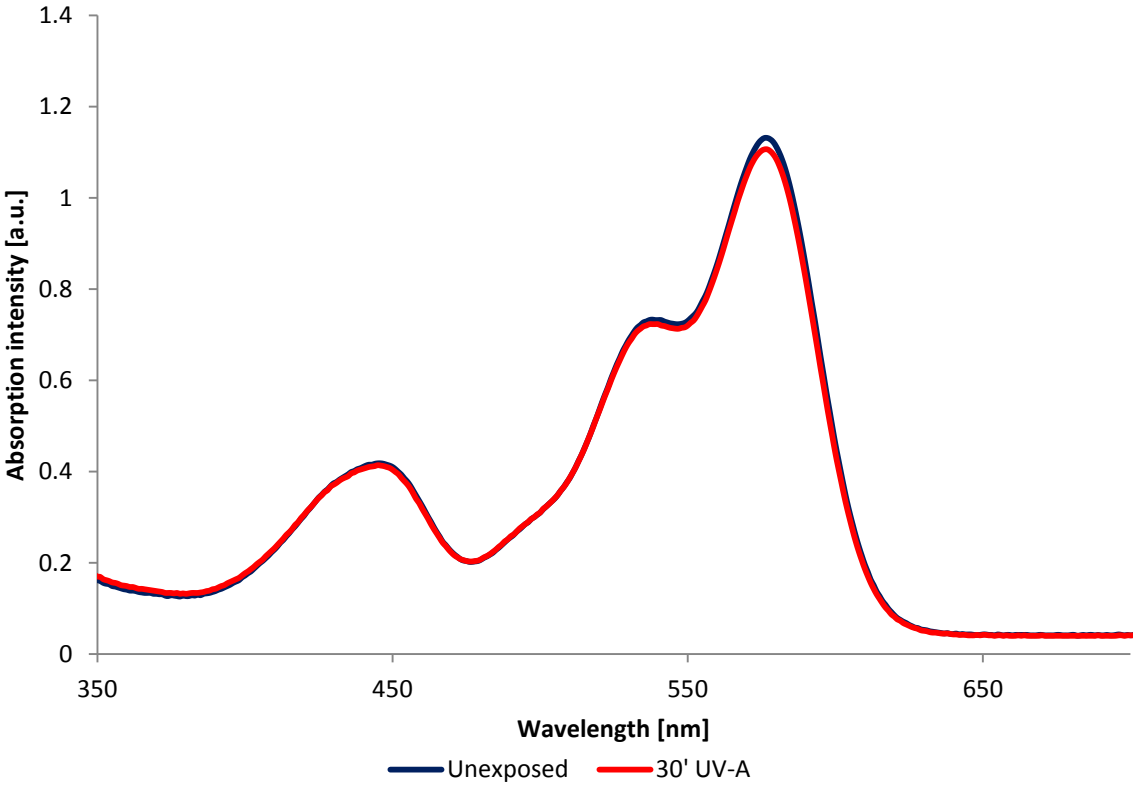

Figure IV.71 UV-Vis light absorption spectra of the unexposed LT20L4 and of LT20L4 after 30 minutes of exposure to UV-A radiation.

As shown in the figure, no significant changes can be detected between the two UV-Vis absorption spectra, indicating that the amount of light absorbed by the LSC device does not vary after 30 minutes of exposure to UV-A radiation. Similar trends were observed on the other LSC devices, namely LV20L4 and LC20L4 (figure IV.72 and figure IV.73 respectively).

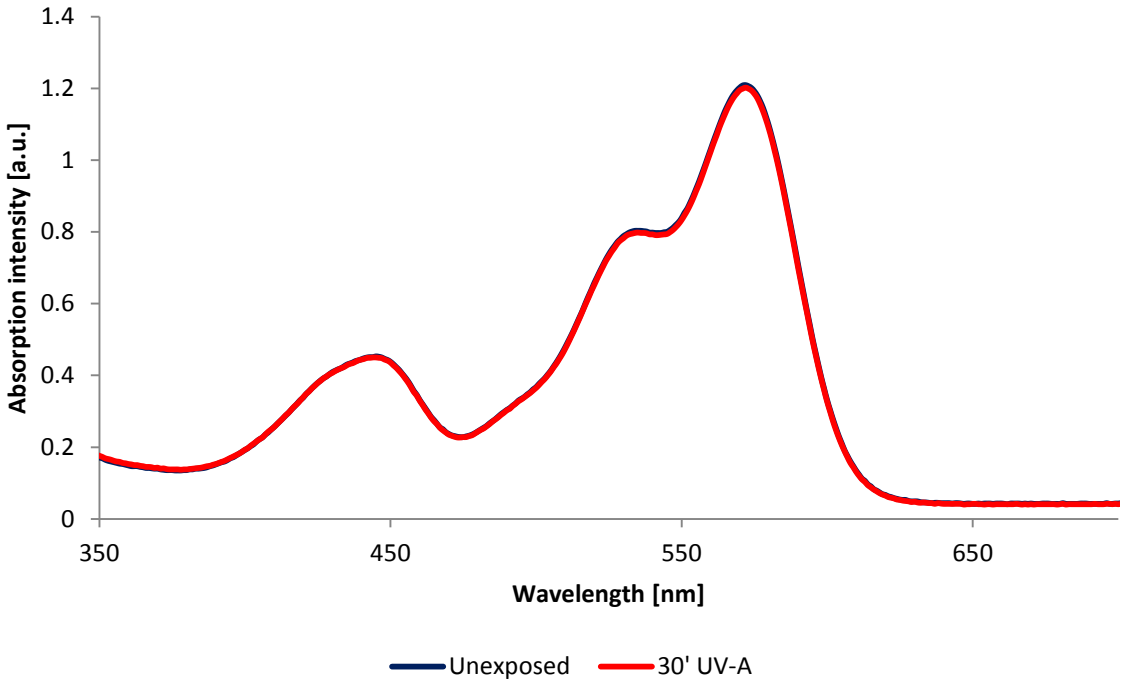

Figure IV.72 UV-Vis light absorption spectra of the unexposed LV20L4 and of LV20L4 after 30 minutes of exposure to UV-A radiation.

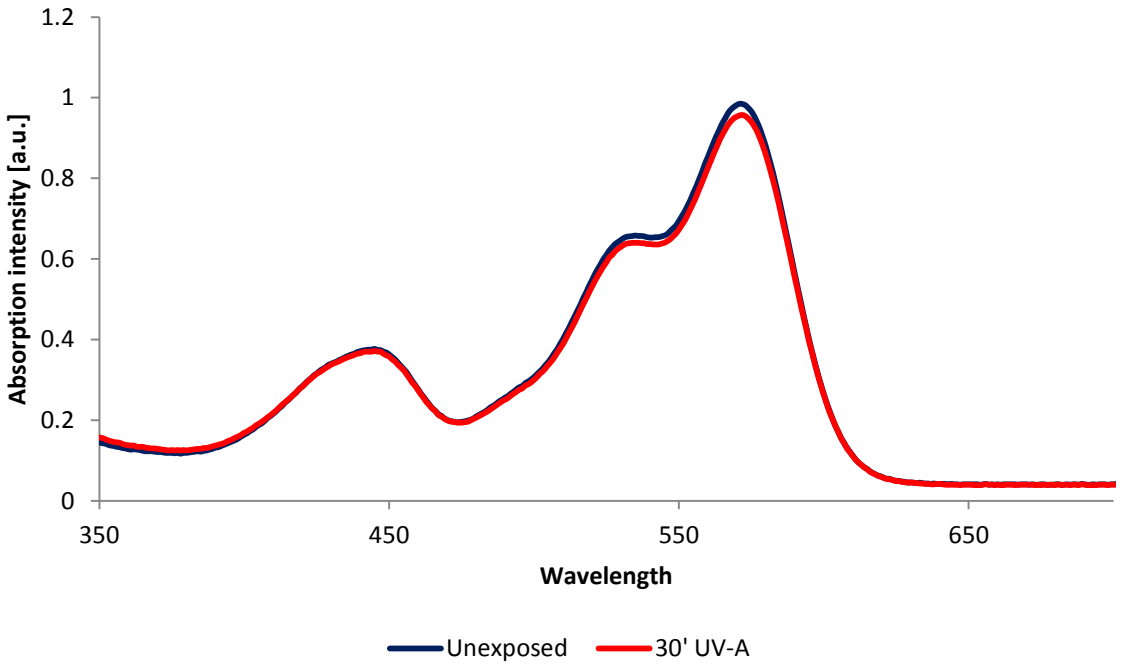

Figure IV.73 UV-Vis light absorption spectra of the unexposed LC20L4 and of LC20L4 after 30 minutes of exposure to UV-A radiation.

In the attempt to better clarify the increase of PV performance of LT and LV devices after 30 minutes of exposure to UV-A light, emission fluorescence spectroscopy was performed on the samples under investigation, and the results are presented in the next paragraph.

IV.3.2.3 Fluorescence spectroscopy

Figure IV.74 depicts the fluorescence emission spectrum of LC20L4 LSC thin film before and after 30 minutes of UV-A light exposure.

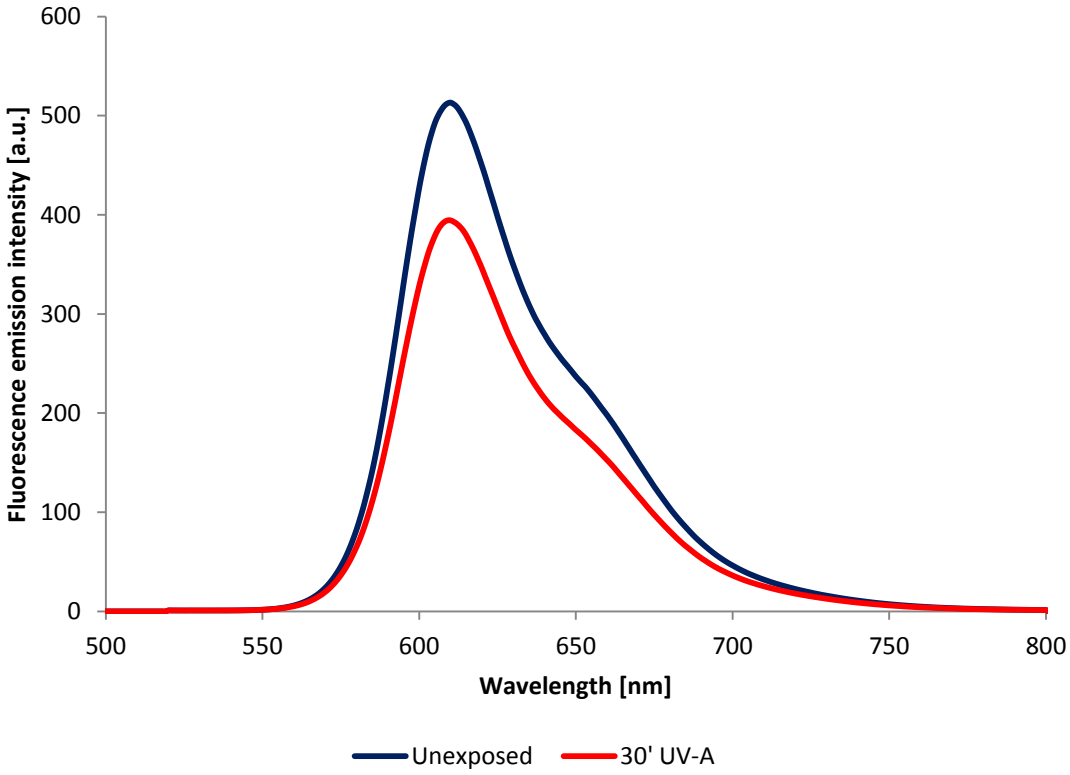

Figure IV.74 Fluorescence emission spectra of the unexposed LC20L4 and of LC20L4 after 30 minutes of exposure to UV-A radiation.

The LC20L4 LSC device shows a decrease in the emission intensity with UV-A light exposure which may be correlated with the decrease in PV performance observed after 30 minutes of exposure to UV-A light (see figure IV.70). Indeed, a reduced fluorescence emission intensity may be related to a lower amount of photons to be waveguided towards the PV cell.

Assuming a constant EQE of the PV cell, this reduction in the number of emitted photons yields a reduction in the produced photo-current. This effect may explain the decrease of ΔPCE of LC20L4 after 30 minutes of exposure to UV-A radiation.

On the other hand, a different effect is observed on LV20L4 and LT20L4. By considering the fluorescence emission spectra of LV20L4 before and after UV-A light exposure, a slight increase in fluorescence emission is clearly observed after 30 minutes of UV-A light irradiation (see figure IV.75).

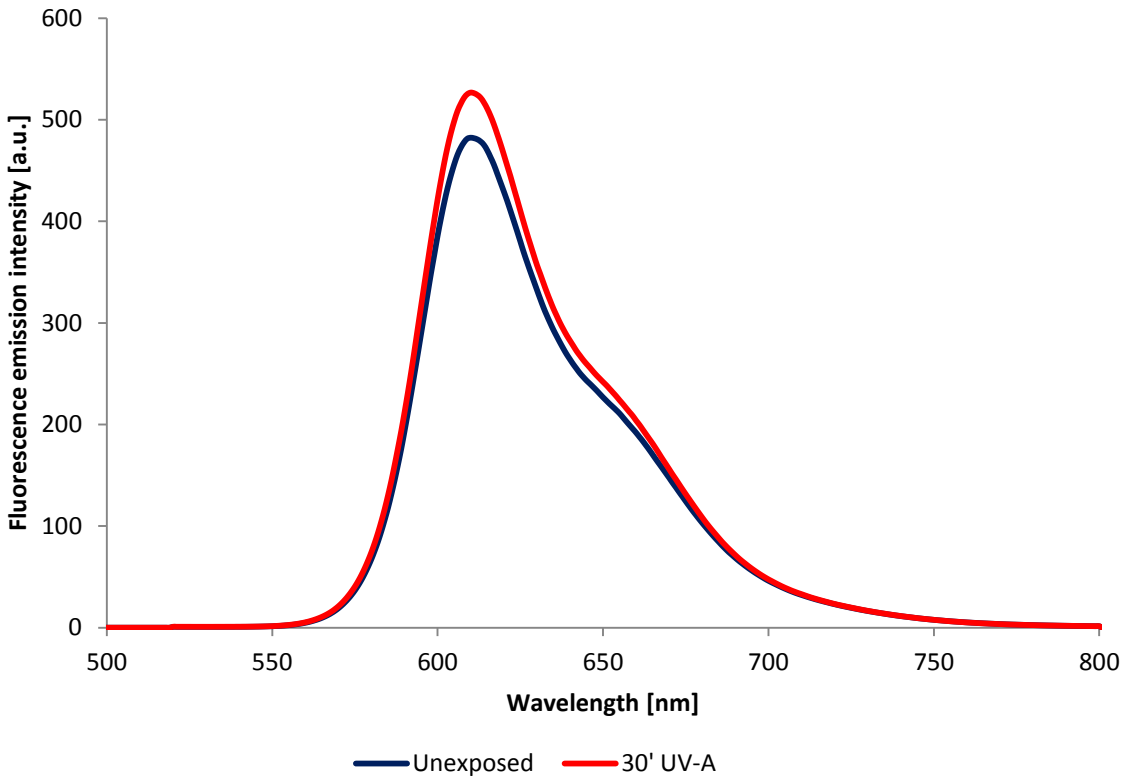

Figure IV.75 Fluorescence emission spectra of the unexposed LV20L4 LSC device and of LV20L4 after 30 minutes of exposure to UV-A radiation.

Such an increase may justify the increase in the ΔPCE after 30 minutes of exposure to UV-A light as observed from the PV data. Indeed, an increased emission of photons, even if slight, leads to an increased number of photons that can reach the PV cell and that can produce electrical charges. This in turn results in an increase in short circuit current and LSC device efficiency.

A similar effect was also observed on LT20L4. In this case, however, the emission intensity was shown to increase more significantly compared to the case of LV20L4 after 30 minutes of exposure to UV-A light. This effect can be seen in figure IV.76 where the emission spectrum of LT20L4 before and after 30 minutes of UV-A exposure is reported.

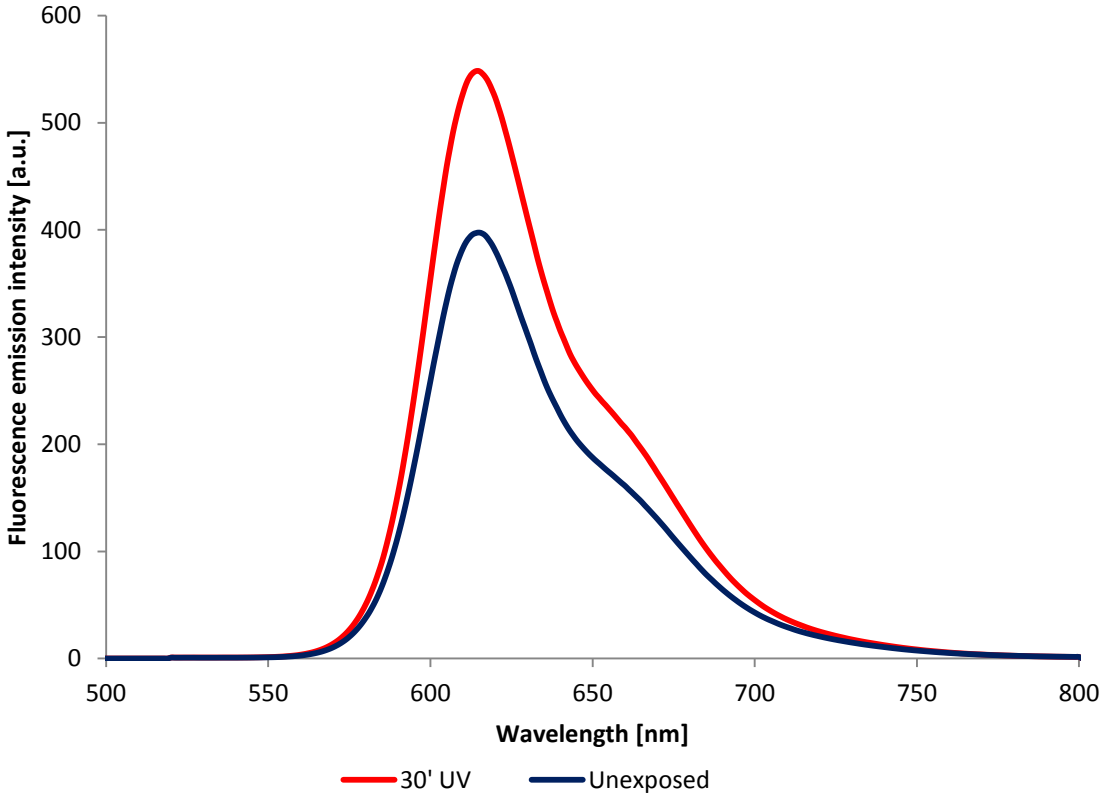

Figure IV.76 Fluorescence emission spectra of the unexposed LV20L4 LSC device and of LV20L4 after 30 minutes of exposure to UV-A radiation.

The increase in the fluorescence emission intensity of LT20L4 is significantly higher than for LV20L4, and this may explain the different extent of increase in ΔPCE which is observed on the two systems after UV-A light exposure. Being only the emission spectrum affected by UV-A light exposure, the reason for the PV performance increase in the LT and LV systems appears to be correlated to processes associated to the fluorescence mechanism. A possible reason may be related to the photoluminescent quantum yield of the dye molecule, which would however be in this case dependent on the polymer matrix in which the fluorescent dye is dissolved. The effects of the interaction between matrix and organic dye molecules on fluorescence quantum yield, if any, are however currently unknown. Therefore further tests

will need to be done to better clarify the hypothesis made, such as for instance photoluminescent quantum yield measurements and infra-red spectroscopy.

IV.3.3 Long-term behavior of the LSC device

In this section a discussion on long term durability of the LSC devices will be shown. The results were obtained by exposing the LSC's in a weather-o-meter to continuous illumination (for further information, see section III.8.2). Optimized LSC devices with and without stabilizing agents (NOR HALS) were tested for each system investigated.

The nomenclature of the samples will be the same as that shown in the previous paragraphs IV.1 and IV.2) and samples containing NOR HALS will be identified with the suffix NH.

In order to better identify the differences in long-term stability between the LSC's fabricated, also the behavior of the bare waveguide without any fluorescent film deposited was investigated and will be discussed in the next section.

IV.3.3.1 Transparent waveguide degradation

To be sure that PV performance of LSC devices was not affected by the degradation of the LSC waveguide, a transparent LSC (with no fluorescent film present) was tested against long-term stability in the weather-o-meter, and the PV data were collected periodically. Figure IV.77 shows the normalized ΔPCE of the transparent waveguide versus time of light exposure. With the nomenclature "transparent waveguide" we mean a glass substrate to which a PV cell is attached on the edge. In this case the polymer matrix is not deposited.

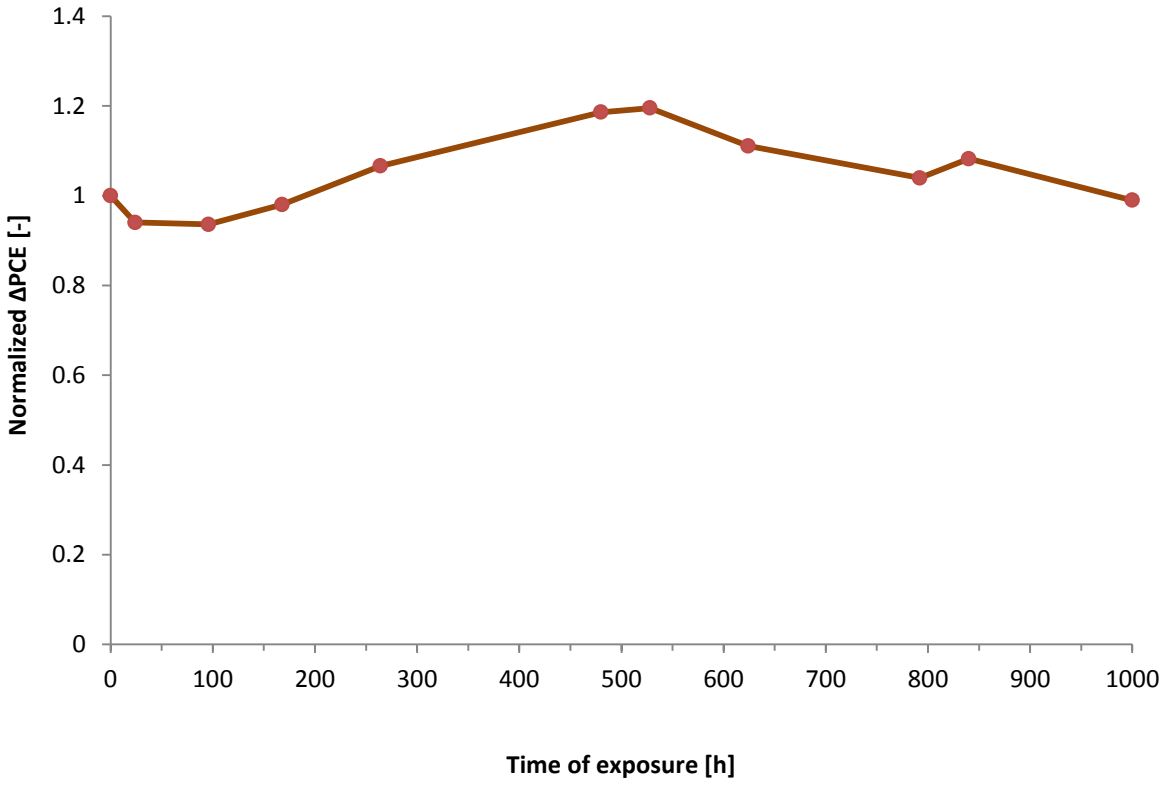

Figure IV.77 Normalized ΔPCE versus time of light exposure for the bare waveguide.

As shown in the plot, the normalized ΔPCE of the transparent waveguide is practically constant over the entire duration of the test. This means that the PV cell and the bonding agent do not undergo significant degradation phenomena over the entire exposure time. Therefore, the degradation behavior of the different LSC's that will be presented in the following excludes any effect due to PV cell or adhesive degradation and may thus clearly be assigned only to degradation phenomena occurring to the polymer matrix and the dye.

IV.3.3.2 Comparison between matrices

In this paragraph a comparison between the different LSC devices will be proposed in terms of long term PV stability. All polymer matrices presented in the previous chapters will be considered.

Figure IV.78 shows the normalized ΔPCE for the different matrices employed in this work.

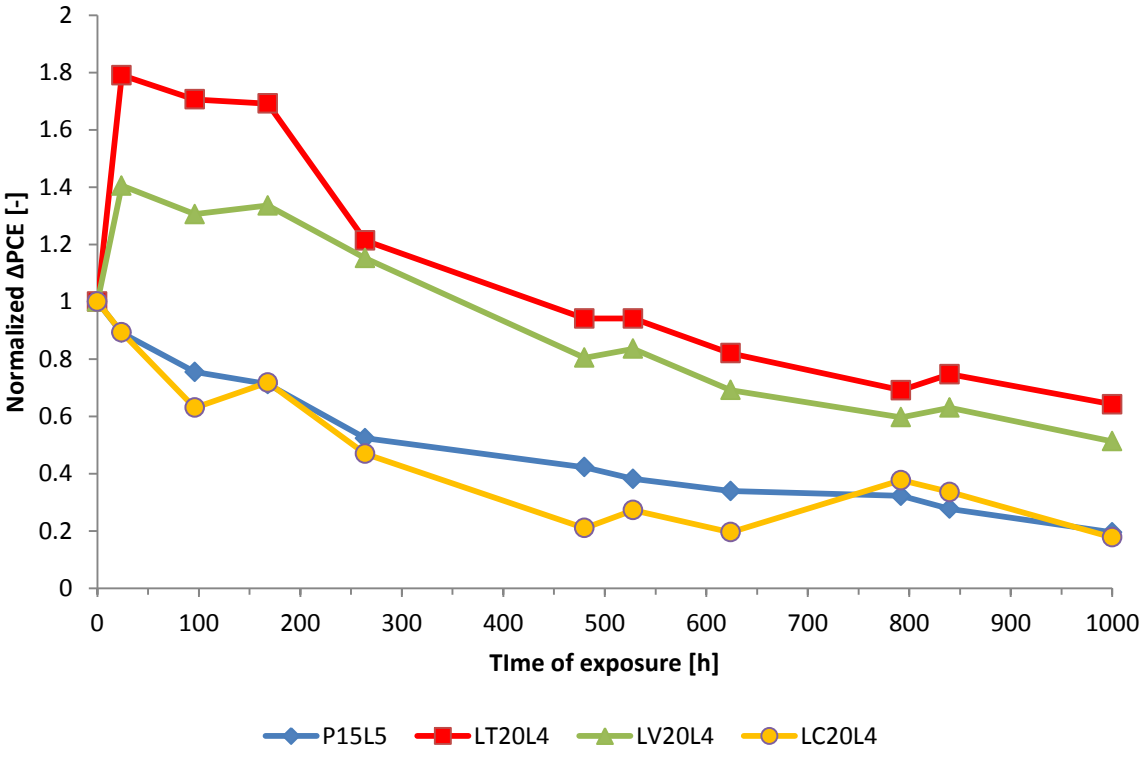

Figure IV.78 Normalized ΔPCE versus time of weathering for LT20L4, LV20L4, LC20L4 and P15L5.

As a first consideration, it is worth noticing that, after 1000 hours of continuous irradiation, all the LSC devices fabricated still show a positive ΔPCE. This means that all the LSC devices tested retain their primary function which is to increase the performance of the PV cell, even after 1000 hours of exposure. Although a general decrease in ΔPCE is observed for all systems, each LSC device shows a specific rate of decrease in ΔPCE. In fact, after 1000 hours of exposure, LT20L4, LV20L4, LC20L4, P15L5 lose about 40 %, 50 %, 80 % and 80 % of their initial efficiency respectively. By considering the specific trends observed for LT20L4 and LV20L4, an initial increase of ΔPCE in the first 24 hours of exposure is found for both systems. However, their initial ΔPCE increase is different, resulting in an increase of 80 % for LT20L4 and of 40 % for LV20L4 after 24 hours of exposure. On the other hand, the crosslinked LC matrix and PMMA-based devices, do not show any initial ΔPCE increase after light exposure. Rather, their behavior is characterized by an abrupt initial decrease in their PV performance. These behaviors confirm the results of weathering tests under UV-A light.

The behavior of LC-based LSC devices is very similar to that of standard PMMA matrix. In particular, this different behavior of LC matrix compared to LT and LV in the long term exposure regime may be explained by considering the different crosslinking bonds present in these crosslinked polymer matrices. While for LT and LV matrices, a urethane-bond network is formed upon crosslinking, LC undergoes crosslinking through the formation of an ether bond, which seems to be less stable than the urethane bond. LC20L4 and P15L5 show a similar rate of ΔPCE decrease resulting in a similar final efficiency loss (80 % after 1000 hours).

As a result, P15L5 and LC20L4 LSC devices appear to be more prone to weathering, resulting in a higher loss in PV performance when subjected to long-term light exposure. LV20L4 and LT20L4, on the other hand, seem to be the best choice for LSC devices in terms of long-term stability of PV performance, as they significantly outperform the PMMA-based LSC, which currently represents the state of the art in LSC technology.

IV.3.3.3 Effect of NOR HALS additives

In most technological applications, polymeric materials for high outdoor durability are typically doped with some additives in order to increase their stability towards solar light. NOR HALS are an example of this class of additives as they are normally employed to slow down the rate of the photooxidative degradation of polymeric materials. Also in this work, NOR HALS were employed in all LSC systems fabricated in order to potentially increase further the lifetime of LSC devices. The results on each system are presented in the next sections.

IV.3.3.3.1 PMMA-based LSC devices

Figure IV.79 shows the normalized ΔPCE's of P15L5 and P15L5NH versus light exposure time.

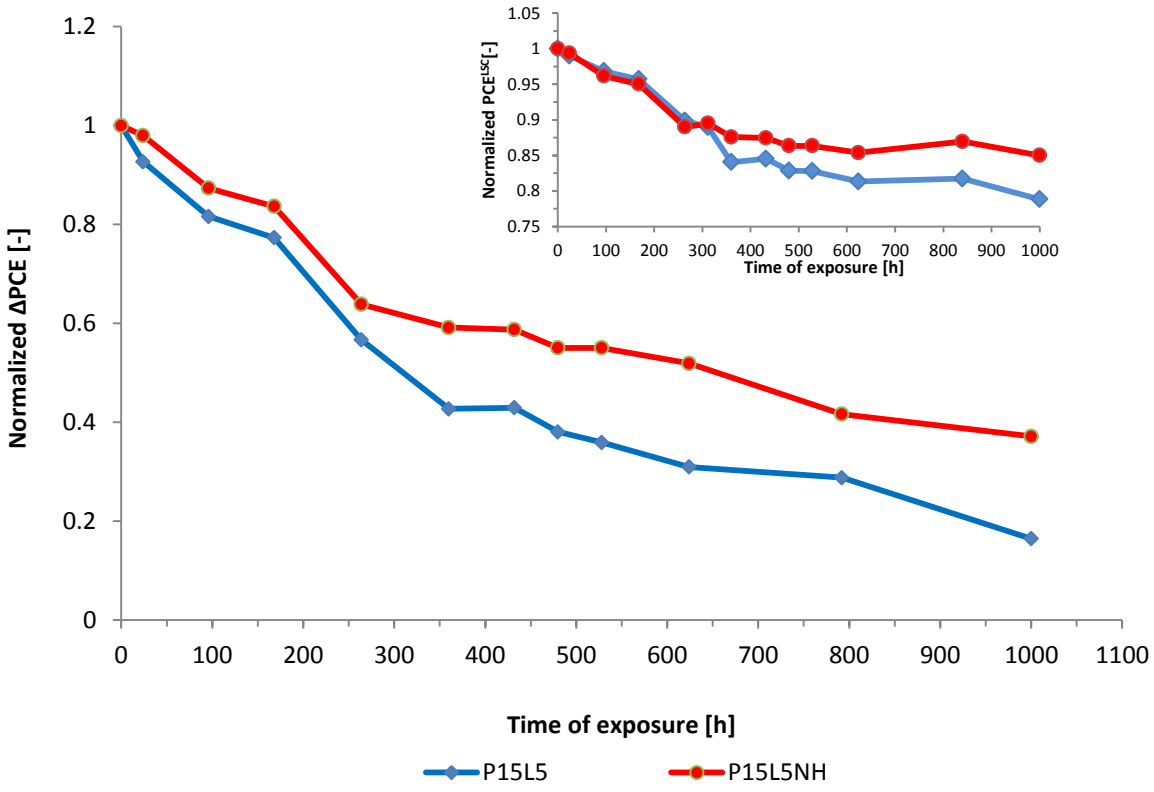

Figure IV.79 Normalized ΔPCE versus time of exposure for P15L5 and P15L5Nh. In the inset of the figure the normalized PCE^{LSC} as a function of time is reported fort both the samples.

As shown in the plot, the rate of ΔPCE decrease is different in the two systems. Although the rate of ΔPCE decay in the initial phase of the weathering test (up to 250 hours) is comparable for the two systems, for longer exposure times the system containing NOR HALS shows a slower ΔPCE decrease. In particular, after 500 hours of light exposure, the ΔPCE for P15L5NH is ~ 60 % of its initial value, while P15L shows a ΔPCE which is less than 40 % of its initial value. Therefore, NOR HALS seems to have an effect on PMMA-based thin film LSC devices on a long term basis; this difference is made even clearer after 1000 hours of accelerated weathering, when the ΔPCE of P15L5 thin film LSC is about 20 % of its initial value compared to the 40 % ΔPCE found for P15L5NH. The decrease in the normalized ΔPCE is reflected in the variation of PCE^{LSC}, as shown in the inset in figure IV.80. The decrease in ΔPCE and PCE^{LSC}

was found to be mainly associated to a decrease of the short circuit current (figure IV.80). In particular, the short circuit current of P15L5 decreases by 25 % while that of P15L5NH decreases by 20 % after 1000 hours of exposure.

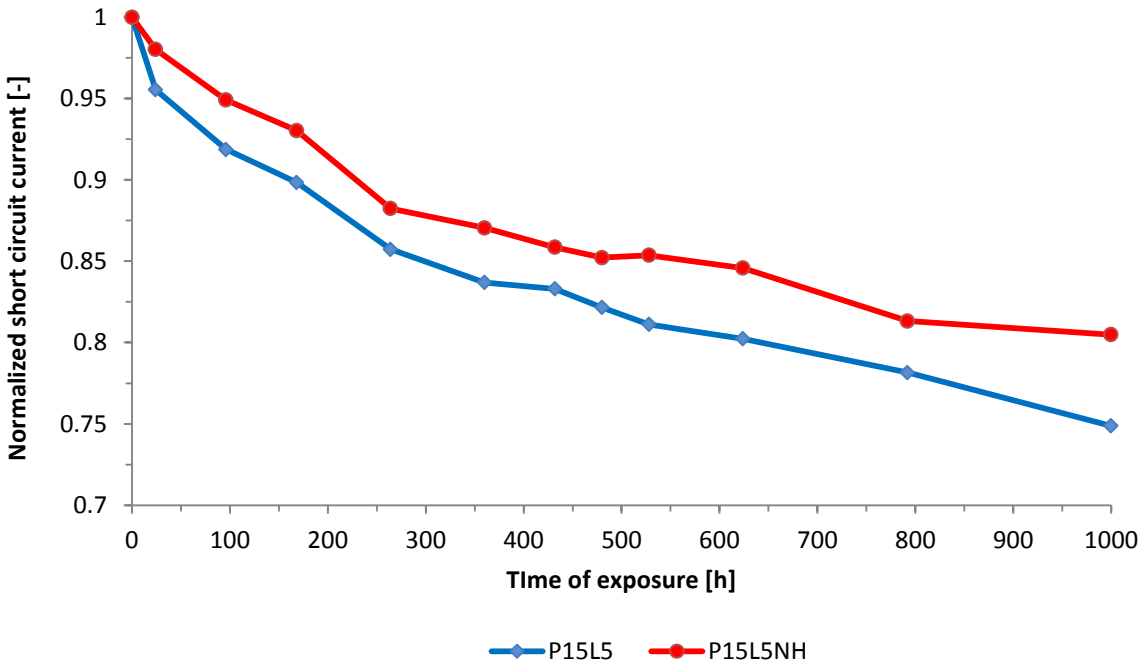

Figure IV.80 Normalized short circuit current as a function of time of light exposure.

The V_{OC} and the FF values were practically not influenced by light exposure (results not shown), substantially maintaining their initial value. Accordingly, in the following paragraphs, only modifications occurring to ΔPCE, PCE^{LSC} and short circuit current will be discussed as the other PV parameters (V_{OC} and FF) were shown in all cases to maintain a constant value during the weathering tests.

IV.3.3.3.2 LT-based LSC devices

Figure IV.81 shows the normalized ΔPCE versus light exposure time for LT20L4 and LT20L4NH.

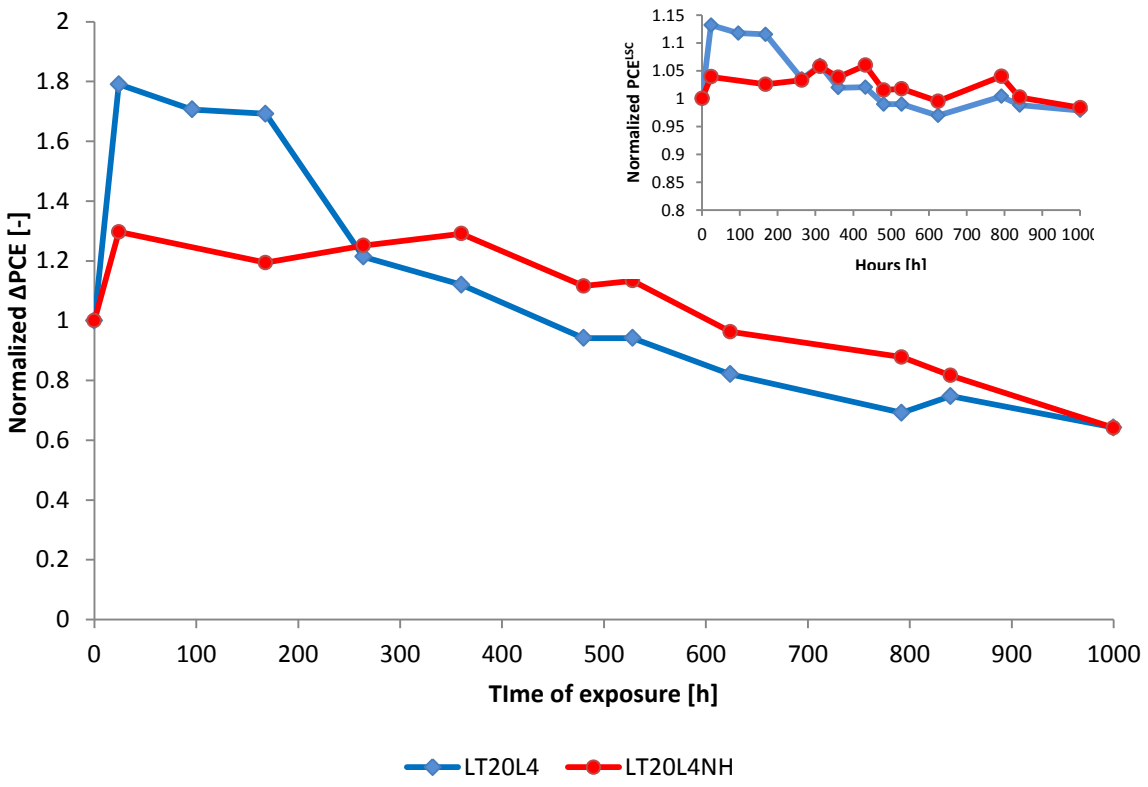

Figure IV.81 Normalized ΔPCE versus time of exposure for LT20L4 and LT20L4NH. In the inset of the figure the normalized PCE^{LSC} is reported for the two LSC devices.

As shown in the plot, both systems show an increase in ΔPCE in the initial phase of the light exposure test although to different extents. In particular, an 80 % increase in ΔPCE is observed for the LT20L4 system during the first 24 hours of light exposure, while LT20L4NH shows a ΔPCE increase of ~ 30 %. Thus the addition of stabilizers has a certain effect on the initial increase of ΔPCE. In spite of these initial differences between stabilized and unstabilized systems, the long-term durability seems very similar and the normalized ΔPCE after 1000 hours is the same.

In the inset of figure IV.81 the normalized absolute power conversion efficiency, PCE^{LSC} as a function of light exposure is reported for LT20L4 and LT20L4NH systems. Both samples are characterized by a PCE^{LSC} which maintains nearly the same value after 1000 hours of exposure. Indeed, after 1000 hours of exposure LT20L4 and LT20L4NH show PCE^{LSC} decreased by only 2 %. The slight reduction in PCE^{LSC} is mainly due to the reduction of the short circuit current, as can be seen in figure IV.82, where the short circuit current as a function of light exposure time is reported for both samples (LT20L4 and LT20L4NH).

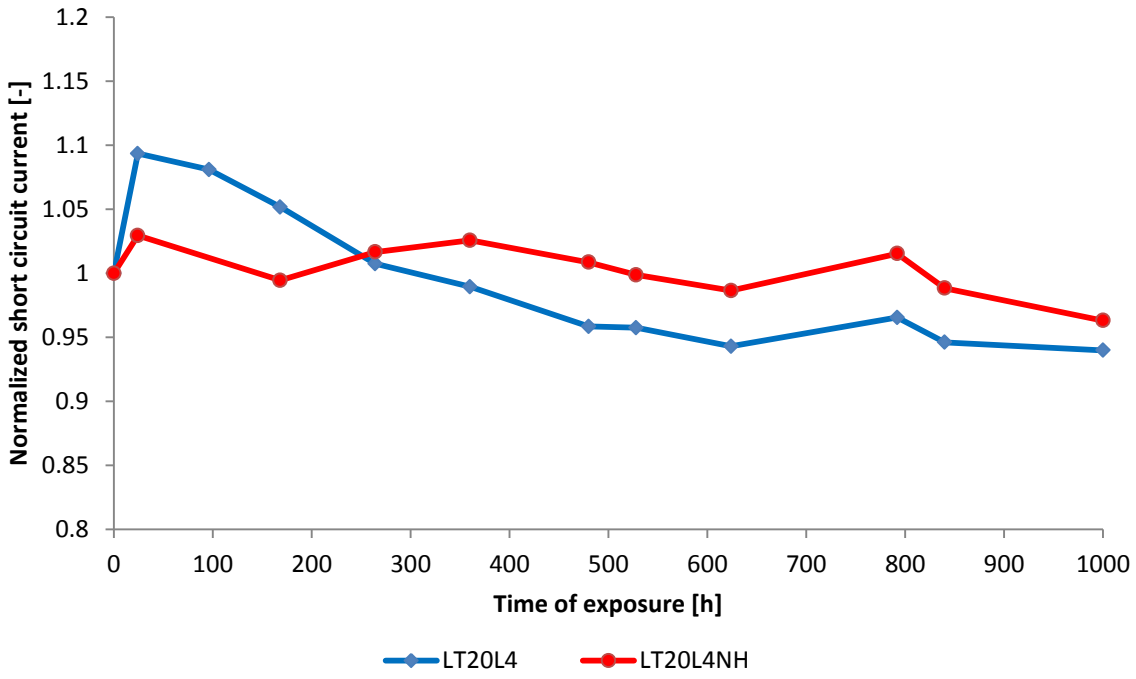

Figure IV.82 Normalized short circuit current versus time of light exposure for the stabilized and unstabilized LT systems.

Thus, in conclusion, the presence of NOR HALS partially hinders the UV-induced increase of ΔPCE at short irradiation times, but at the same time allows for a slightly better retention of properties after long irradiating times.

IV.3.3.3.3 LV-based LSC devices

Figure IV.83 shows ΔPCE versus light of exposure time for LV20L4 and LV20L4NH.

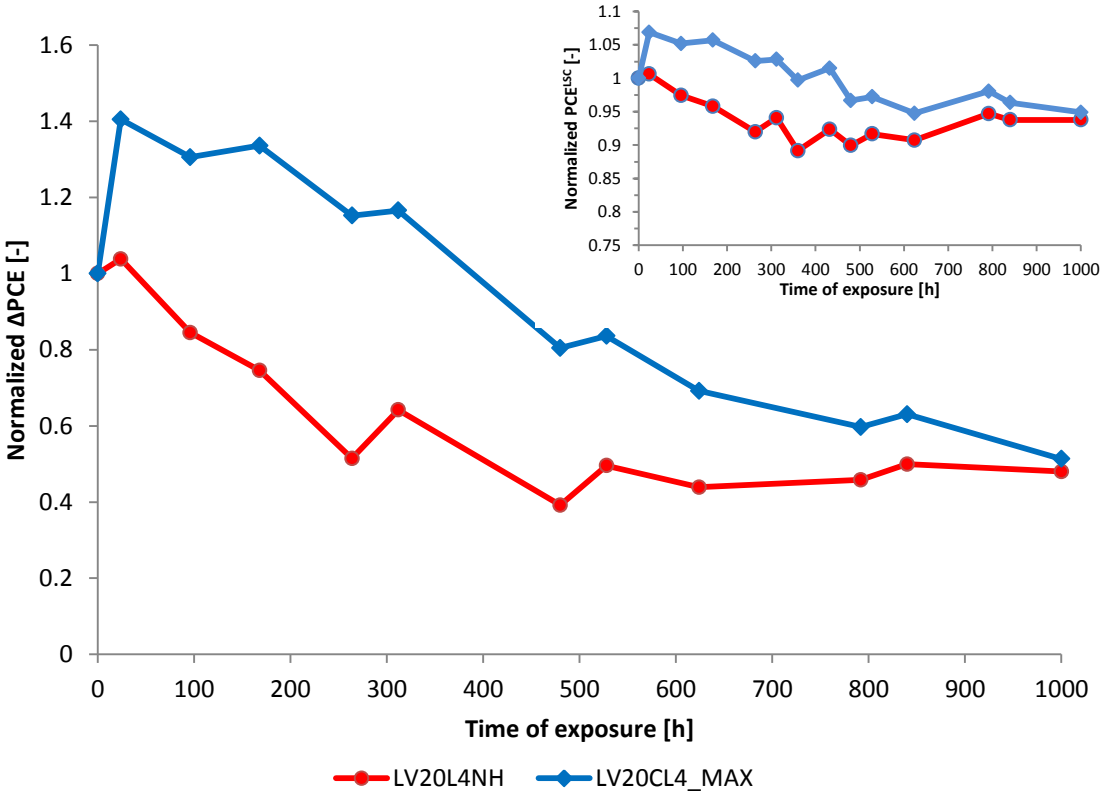

Figure IV.83 Normalized ΔPCE versus time of light exposure for LV20L4 and LV20L4Nh systems. In the inset the normalized PCE^{LSC} as a function of time of exposure is reported.

Also for this system the presence of stabilizers eliminates almost completely the UV-induced ΔPCE increase at short irradiating times. After 1000 hours of exposure, the ΔPCE of the two LSC devices is similar, resulting in a decrease of 53 % with respect to the initial value. For both LSC device samples, the decrease of the ΔPCE can be associated to the decrease in the absolute power conversion efficiency, PCE^{LSC} (inset of figure IV.83). After 1000 hours of weathering, the PCE^{LSC} of LV20L4 decreases by 5 % while that of LV20L4 decreases by 6 % with respect to the initial value. As in the case of ΔPCE, there is an initial difference between the values of PCE^{LSC} of LV20L4 and LV20L4NH which reduces as time of exposure proceeds. The decrease in the absolute PCE, PCE^{LSC} is mainly due to a short circuit current decrease as can be seen in figure IV.84 which displays the normalized short circuit current versus light exposure time for both systems. The other PV parameters concurring in the determination of PCE^{LSC} remain constant over the entire duration of the test and will thus be omitted.

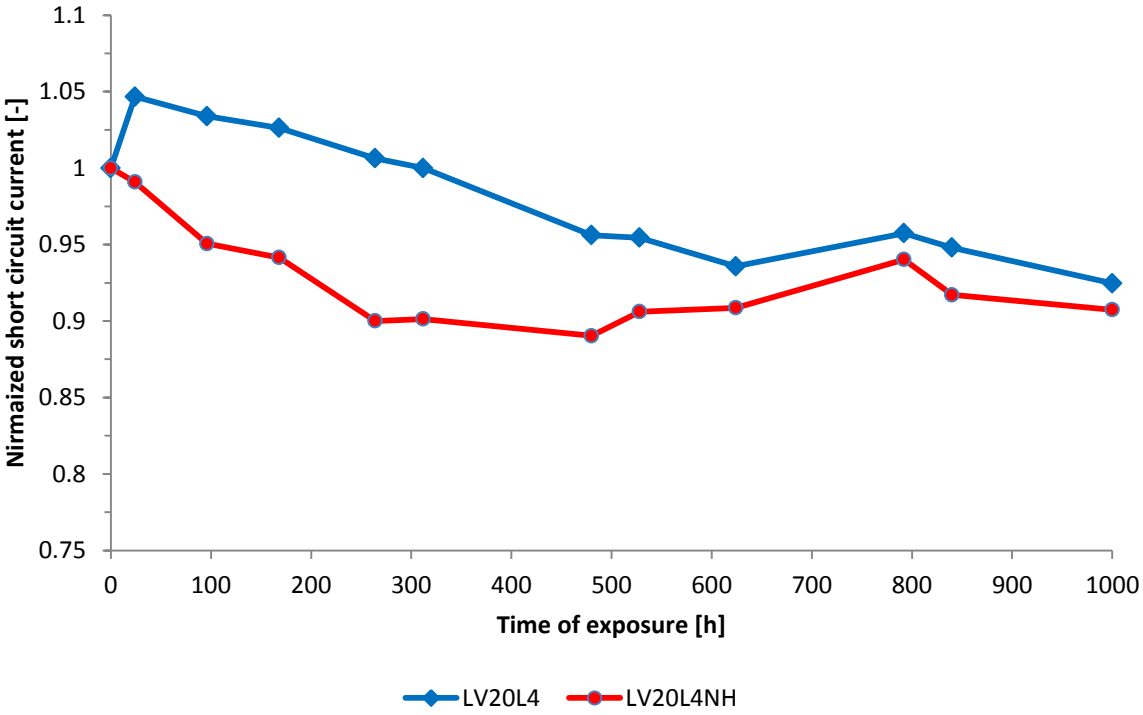

Figure IV.84 Normalized short circuit current versus time of exposure for LV20L4 and LV20L4NH systems.

Both the short circuit currents of LV20L4 and LV20L4NH decrease by 8 % with respect to their initial value after 1000 hours of continuous exposure, even though I_{SC} of LV20L4 shows an initial increase of 5 %. This is a further confirmation of the beneficial effects of the addition of NOR HALS.

IV.3.3.3.4 LC-based LSC devices

Figure IV.85 presents the normalized ΔPCE versus light exposure time for LC20L4 and LC20L4NH.

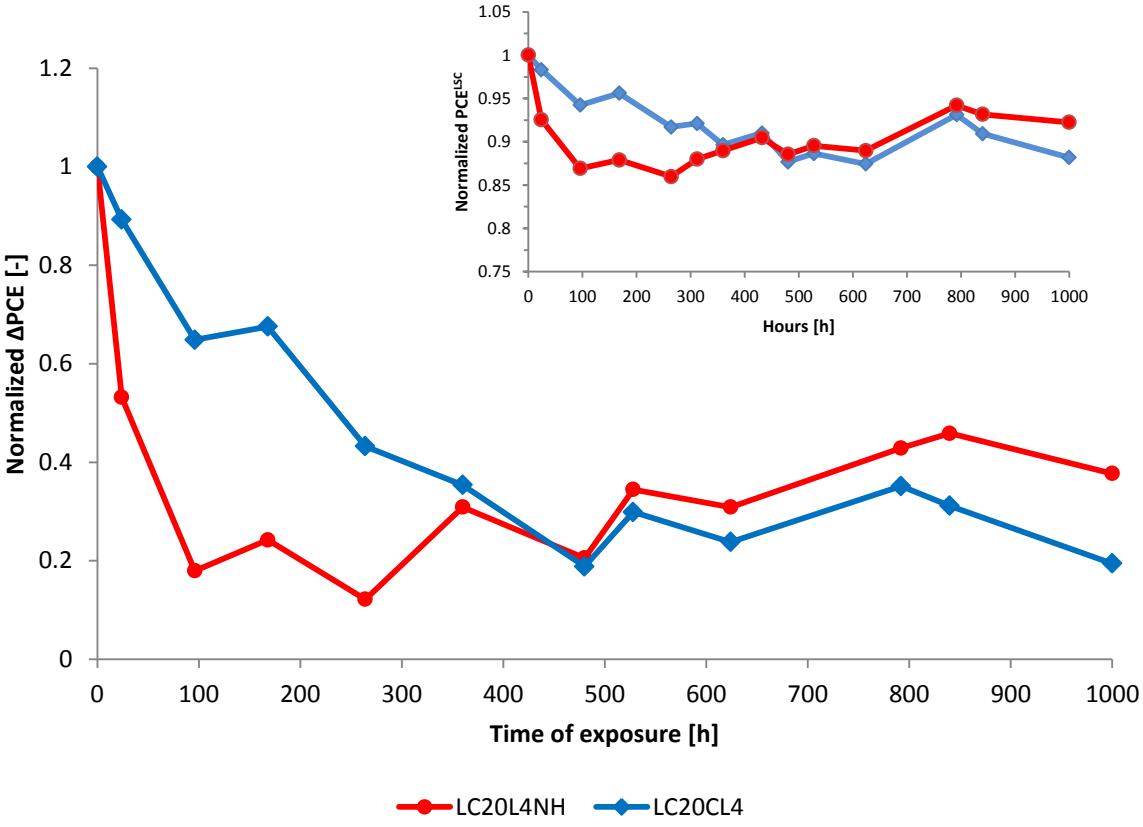

Figure IV.85 Normalized ΔPCE versus time of exposure for LC20L4 and LC20L4NH. In the inset of the figure the normalized PCE^{LSC} is reported as a function of time.

As shown in the figure, after the first 24 hours of light exposure, both samples show a strongly decreasing ΔPCE. While LC20L4 shows a slight decrease of ΔPCE of about 11 % with respect to the initial value, LC20L4NH undergoes a much sharper ΔPCE decrease (47 %). After 100 hours of light exposure, the ΔPCE for both systems further decreases abruptly, resulting in a ΔPCE decrease of 37 % for LC20L4 and of 83 % for LC20L4NH. Moreover, despite this large ΔPCE difference in the initial phase of the weathering tests, for longer light exposure times the performance of the two systems approach to each other after 1000 hours of continuous exposure. In particular, despite the high initial decrease registered in the first 300 hours, LC20L4NH performance stabilizes. In fact, from 300 hours on, the ΔPCE of LC20L4NH does not vary significantly as time proceeds. On the other hand, the performance of LC20L4 decreases progressively as time goes on. After 350 hours the ΔPCE's of LC20L4 and LC20L4NH show the same decrease (31 % with respect to their initial values).

From 480 hours on, the performance of LC20L4NH is even better than that of LC20L4, thus showing a beneficial effect on this system, slowing down its rate of degradation. Therefore, as for the other polymer systems already observed, additives seem to have some limited beneficial effect on the performance of the LSC. This effect can also be seen in the chart reported in the inset of figure IV.85, which depicts the absolute power conversion efficiency PCE^{LSC} versus light exposure time. The absolute power conversion efficiency, PCE^{LSC}, of LC20L4 decreases by 12 % with respect to the initial value after 1000 hour of continuous while that of LC20L4NH decreases by 8 %. This is a further confirmation that NOR HALS additives have beneficial effects on this system. The decrease in PCE^{LSC} arises from the decrease in the short circuit current as presented in figure IV.86 which shows the short circuit current versus time of weathering for both LC20L4 and LC20L4NH systems.

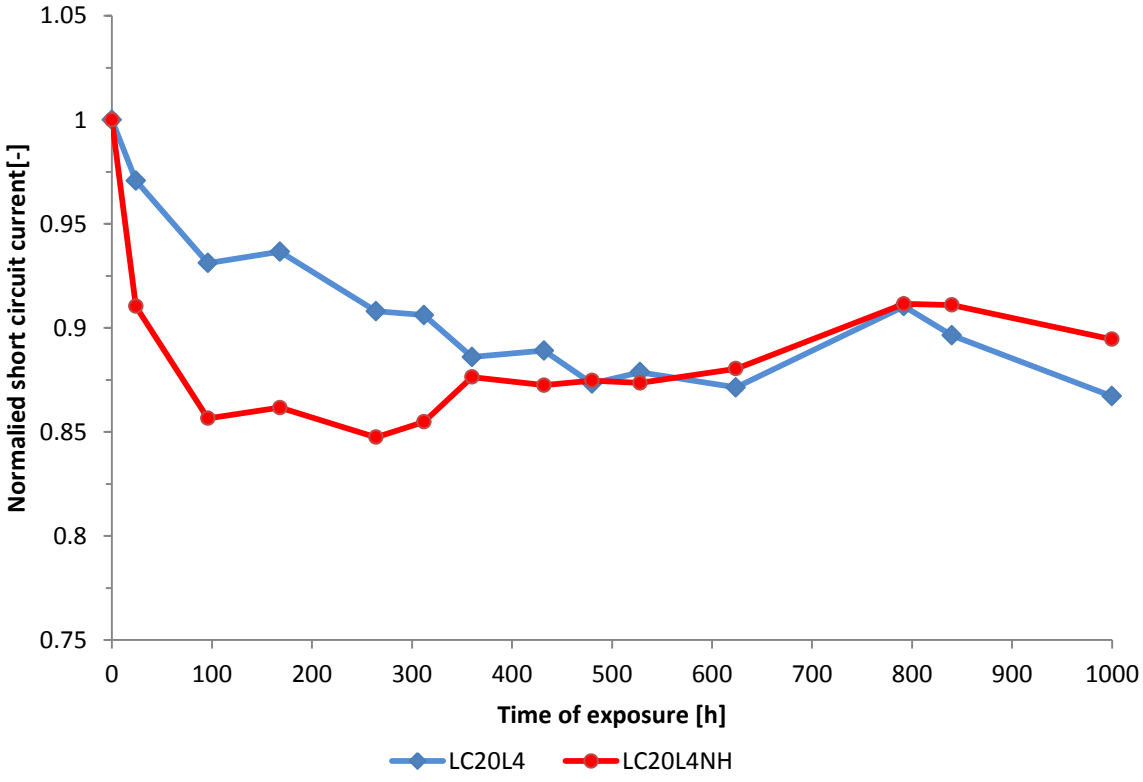

Figure IV.86 Normalized short circuit current versus weathering time for LC20L4 and LC20L4NH.

After 1000 hours of continuous exposure, the short circuit current of LC20L4 is 86 % of its initial value while after the same time, the short circuit current ofLC20L4NH is 89 % with respect to its initial value.

In conclusion, the eventual stabilizing effect of NOR HALS can be seen at long exposure times (1000 hours) as expected, for both polyurethanes and melamine-cured fluoropolymers.
The effect at short irradiating times is more controversial, and it should be reconsidered after a better clarification of the UV-induced increase of ΔPCE.

IV.4 References

[1] A. A. Earp, G. B. Smith, P. D. Swift and J. Franklin, “Maximizing the light output of a luminescent solar concentrator”, Solar Energy, 76, 2004, pp 655 – 667;
[2] Y. S. Lim, C. K. Lo and G. B. The, “Unsaturated polyester resin blended with MMA as potential host matrix for luminescent solar concentrator”, Renewable Energy, 45, 2012, pp 156 – 162;
[3] G. Maggioni, A. Campagnaro, S. Carturan and A. Quaranta, “Dye-doped parylene-based thin film materials: Application to luminescent solar concentrators”, Solar Energy Materials & Solar Cells, 108, 2013, pp 27 – 37;
[4] C. Haines, M. Chen and K. P. Ghiggino, “The effect of perylene diimide aggregation on the light collection efficiency of luminescent concentrators”, Solar Energy Materials & Solar Cells, 105, 2012, pp 287 – 292;
[5] L. R. Wilson, B. C. Rowan, N. Robertson, O. Moudam, A. C. Jones and B. S. Richards, “Characterization and reduction of reabsorption losses in luminescent solar concentrators”, Applied Optics, 49, 2010, pp 1651 – 1661;
[6] M. Buffa, S. Carturan, M. G. Debije, A. Quaranta and G. Maggioni, “Dye-doped polysiloxane rubbers for luminescent solar concentrator system”, Solar Energy Materials & Solar Cells, 103, 2012, pp 114 – 118;
[7] K. A. Colby, J. J. Burdett, R. F. Frisbee, L. Zhu, R. J. Dillon and C. J. Bardeen, “Electronic energy migration on different time scales: concentration dependence of the time-resolved anisotropy and fluorescence quenching of Lumogen Red in poly(methyl methacrylate)”, Journal of Physical Chemistry A, 114, 2010, pp 3471 – 3482;

[8] R. O. Al-Kaysi, T. S. Ahn, A. M. Müller and C. J. Bardeen, “The photophysical properties of chromophores at high (100 mM and above) concentrations in polymers and as neat solids, Physical Chemistry Chemical Physics, 8, 2006, pp 3453 – 3459;

[9] H. Yoo, J. Yang, A. Yousef, M. R. Wasielewski and D. Kim, “Excimer formation dynamics of intramolecular π-stacked perylenediimides probed by single-molecule fluorescence spectroscopy”, Journal Of American Society, 132, 2010, pp 3939 – 3944;

[10] F. C. Krebs, “Fabrication and processing of polymer solar cells: a review of printing and coating technique”, Solar Energy Materials & Solar Cells, 93, 2009, pp 394 – 412;

[11] L. H. Slooff, A. R. Burgers and E. Bende, “The luminescent solar concentrator: a parameter study towards maximum efficiency, in Proc. Of SPIE, Photonics for solar energy systems II, 2008;

[12] J. C. Goldschmidt, M. Peters, A. Bösch, H. Helmers, F. Dimroth, S. W. Glunz and G. Willeke, “Increasing the efficiency of fluorescent concentrator systems”, Solar Energy Materials & Solar Cells, 93, 2009, pp 176 – 182;

[13] G. Socrates, “Infrared and Raman characteristic group frequencies, Third edition, John Wiley and Sons, 2001;

[14] E. Pretsch, P. Bühlmann and C. Affolter, “Structure determination of organic compounds, Third Edition, Springer, 2000;

[15] R. Kindermann, L. H. Sloof, A. R. Burgers, N. J. Bakker, A. Bütchemann, R. Danz and J. A. M. van Roosmalen, “I-V performance and stability study of dyes for luminescent plate concentrators”, Journal of Solar Energy Engineering”, 129, 2007, pp 277 – 282;

V

Conclusions and future developments

V.1 Conclusions

This thesis work had three main purposes: the optimization of PMMA-based LSC devices through the study of several device parameters including dye concentration, thickness of the luminescent thin film, waveguide aspect ratio (L/W) and use of back reflectors; the preparation of new host matrices based on fluoro-polymers and their chemical, physical and device characterization; the investigation of the environmental stability of optimized fluoro-based LSC devices and PMMA-based LSC devices.

V.1.1 Optimization of PMMA-based LSC devices

In PMMA-based devices, the optimal LFR305 dye concentration was found to be 5 % due to the highest PV performance which can be correlated to the highest fluorescence emission intensity and the highest EQE with respect to the other dye concentrations. For dye concentrations higher that 5 %, the lower PV performance with respect to the LSC with 5 % of LFR305 was attributed to the increased probability of aggregation of dye molecules and to the increased probability of reabsorption of emitted photons by other dye molecules.

In terms of PV efficiencies, the optimal thickness of PMMA-based LSC devices was found to be around 9 µm. LSC devices with film thicknesses of 12 µm and 35 µm were found to give comparable performance to 9 µm thick LSC devices. This similar PV performance of LSC's with different film thickness was attributed to the occurrence of reabsorption of the emitted photons, which increase as the film becomes thicker due to increased optical density.

Fluorescence emission spectroscopy and External Quantum Efficiency (EQE) tests confirm that the optimal fluorescent film thickness is around 9 µm.

The optimal aspect ratio (L/W, L = length and W = width of the waveguide) was found to be 0.5 because it shows the highest PCE^{LSC}. EQE measurements confirm this effect; in fact, in the shortest plate (corresponding to an aspect ratio of 0.5), waveguided photons have to travel for a shortest distance to reach the PV cell and they experience a lower probability to be reabsorbed by other dye molecules with respect to a longer waveguide.

Titania (TiO_2) filled white back reflectors (BR) were found to increase the PV performance of the LSC. As the film thickness increases, the performance of the LSC increases due to the lower probability of photons to be transmitted and escaped from the waveguide. In this sense, an optimal BR film thickness was found to be around 13 µm. Increasing the TiO_2 concentration in a given BR leads to an increased PV performance of the LSC device due to the higher surface roughness of the BR which helps in diffusing transmitted light towards the waveguide.

V.1.2 Optimization of new host matrices for LSC devices

As alternative to conventional PMMA-based devices, new fluoro-based matrices were tested on LSC devices. The first kind of matrix was a crosslinked polyurethane formed by functional chlorotrifluoro ethylene-vinylether copolymers and cycloaliphatic isocyanurates, Lumiflon LF-910 and Tolonate HDT-LV2, also named LT-based devices. Also on this system, optimization of dye concentration (4 %) and device thickness (5 µm) was carried out to lead a maximum ΔPCE of 27 %.

A similar optimization study was carried out on a second crosslinked fluorinated polyurethane matrix, formed by Lumiflon LF-910 and Vestanat T1890/100 which is a cycloaliphatic isocyanurates (LV-based devices). In this system a maximum in PV performance (ΔPCE = 33 %) was found for LSCs doped with 4 % of LFR305 dye molecules and LSC film thickness of 6 µm.

Finally, a melamine crosslinked fluoropolymer matrix formed by Lumiflon LF-910 and Cymel 303 (LC-based devices) was also considered. The best PV performance (ΔPCE = 35 %) for this

system was found to be for a 4 % dye concentration and for a LSC device thickness of ~ 4 µm.

All matrices were also characterized by means of fluorescence spectroscopy, UV-Vis spectroscopy and EQE measurements.

V.1.3 Aging and accelerated weathering tests

Accelerated weathering tests were performed on all optimized LSC devices.

UV-C aging was performed on the optimized PMMA-based device and a decrease in the efficiency gain ΔPCE in the very first hour of exposure was observed, mainly due to the high energetic radiation negatively affecting the stability of both the polymer matrix and the organic dye molecules.

PMMA-based devices and fluoro-based devices were subjected to aging under UV-A radiation. The result was a decrease in PV performance of PMMA-based and LC-based LSC devices, with comparable rates of decrease. On the other hand, LT and LV-based LSC devices showed an initial increase in PV performance followed by a substantial stability over irradiation time. This effect, only observed on polyurethane-based devices, was correlated with an increase in the emission intensity upon UV-A exposure.

Finally, continuous exposure (1000 hours) of all optimized LSC devices was also carried out in a weather-o-meter chamber equipped with xenon-arc lamp. LC and PMMA showed a decrease in ΔPCE by 80 % with respect to their initial value while LT and LV based devices showed a ΔPCE decreased by 36 % and 51 % respectively. Thus, it was concluded that fluorinated polyurethane-based devices are less susceptible to degradation phenomena.

The effect of long term stabilizers (NOR HALS) was also shown on the optimized devices. On PMMA-based devices, additives played some effects leading to a reduced rate of degradation. On LC-based devices no effect of NOR HALS was observed. On LT and LV systems, some effects was also observed concerning the long-term exposure behavior.

V.2 Future developments

The current study showed that alternative host matrices like fluorinated polyurethanes can be proposed in LSC technology improving the long-term stability of the device. While fluoropolymers show intrinsically high stability towards photo-oxidation, even better durability could be obtained preventing oxygen diffusion in the polymer layer. Encapsulation with getter materials or coating with barrier layers can be proposed to this aim. A particular point concerns the UV-activated increase of photo-conversion efficiency observed with excellent repeatability for fluorinated polyurethane LSC's. Such an effect, not described before in the literature, is still unclear in its own mechanism, and more refined spectroscopic characterizations and photoluminescent quantum yield measurements are needed in order to investigate this effect.

Acknowledgements

Un sentito ringraziamento va al Professor Turri e alla Professoressa Levi per i consigli e il coordinamento offerti durante tutto lo svolgimento del lavoro di tesi. Desidero inoltre ringraziare il Dott. Brambilla per il prezioso aiuto e per averci gentilmente concesso la disponibilità ad utilizzare la strumentazione per le prove spettroscopiche.

Questo lavoro, però, non avrebbe visto luce se non grazie al costante e straordinario supporto del Dott. Griffini che mi ha aiutato incessantemente, non facendomi mai mancare il suo apporto nella realizzazione di prove e nella stesura del presente scritto. Sei un grande.

Un grazie particolare va a tutti i membri del ChIP Lab, grazie ai quali tutte le giornate, anche le meno positive, avevano qualche cosa per cui farti sorridere. Un grazie speciale va poi a Gilly che con i suoi utilissimi consigli, è sempre stata pronta a risolvere qualsiasi problema si fosse presentato.

I miei genitori si meritano il ringraziamento più grande per tutto ciò di splendido che sono riusciti a fare durante questi anni: siete un esempio impeccabile e non avete mai mancato di sostenermi, nemmeno per un secondo, incitandomi e tranquillizzandomi quando tutto sembrava nero. Questo lavoro è anche un po' vostro. Un po'di merito, però, è anche di mia sorella Paola, sempre pronta a darti aiuto anche se spesso non te lo meriti. A voi tre va un grazie di cuore. I miei nonni, specialmente chi mi ha insegnato le tabelline, meritano invece un immenso abbraccio perché se oggi sono ingegnere, il merito va anche a voi che con la vostra saggezza mi avete sempre guidato verso le scelte più giuste.

Il grazie più speciale va a te, Ila: sei stata fantastica per tutti questi anni in cui sei stata al mio fianco, incoraggiandomi, capendomi, completandomi ma anche sgridandomi… Sei e sarai una persona straordinaria.

Un grande grazie va a tutti gli amici della mia compagnia. In rigoroso ordine alfabetico D, Ele, Ferra, Fra, Henry, Laura, Maggio, Mancu, Marco, Mecca, Meno, Piaia.. Ogni volta con voi è uno spettacolo e vi assicuro che sarebbero stati cinque anni (se non di più per gli amici più vecchi) più lunghi e privi di risate senza la vostra presenza.

Ai miei compagni di università dico grazie perché avete reso bellissimi gli ultimi cinque anni della mia formazione scolastica: le interminabili partite al “due”, le lunghissime giornate spese insieme a studiare…resteranno per sempre un ricordo indelebile nella mia memoria. Per cui grazie a: Albi, Andre, Bea, Cala, Claudio, Dave, Jack, Guido, Marco.

Anche ai miei amici del G.A.P Varese vanno dei ringraziamenti, perché in voi ho trovato delle persone fantastiche con cui crescere e diventare grandi uomini prima che grandi arbitri. Grazie pertanto a Aldo, Davide, Placido, Riky, Sergio, Teo.

Per ultimo, ma non per importanza (e chi mi conosce bene, lo sa) ringrazio l’Inter 2009-2010, quella del Triplete, quella i cui giocatori sono e saranno degli eroi, guidati da una leggenda il cui nome è José Mourinho.